Study of Global Power System Frequency Behavior Based on Simulations and FNET Measurements

by

Shu-Jen Steven Tsai

Dissertation submitted to the faculty of the Virginia Polytechnic Institute and State University in partial fulfillment of the requirements for the degree of

Doctor of Philosophy
in
Electrical Engineering

Approved by:

Dr. Yilu Liu (Chair)
Dr. Virgilio Centeno
Dr. Jaime De La Ree
Dr. Tao Lin
Dr. Amitabh Mishra

July, 2005
Blacksburg, Virginia U.S.A.

Keywords: Power system frequency dynamics, wide area measurement system, FNET, electromechanical wave propagation, visualization, wavelet denoise

Study of Global Power System Frequency Behavior Based on Simulations and FNET Measurements

Shu-Jen Steven Tsai

ABSTRACT

A global view of power system's frequency opens up a new window to the "world" of large system's dynamics. With the aid of global positioning system (GPS), measurements from different locations can be time-synchronized; therefore, a system-wide observation and analysis would be possible. As part of the U.S. nation-wide power frequency monitoring network project (FNET), the first part of the study focuses on utilizing system simulation as a tool to assess the frequency measurement accuracy needed to observe frequency oscillations from events such as remote generation drops in three U.S. power systems. Electromechanical wave propagation phenomena during system disturbances, such as generation trip, load rejection and line opening, have been observed and discussed. Further uniform system models are developed to investigate the detailed behaviors of wave propagation. Visualization tool is developed to help to view frequency behavior simulations. Frequency replay from simulation data provides some insights of how these frequency electromechanical waves propagate when major events occur. The speeds of electromechanical wave propagation in different areas of the U.S. systems, as well as the uniform models were estimated and their characteristics were discussed. Theoretical derivation between the generator's mechanical powers and bus frequencies is provided and the delayed frequency response is illustrated.

Field-measured frequency data from FNET are also examined. Outlier removal and wavelet-based denoising signal processing techniques are applied to filter out spikes and noises from measured frequency data. System's frequency statistics of three major U.S. power grids are investigated. Comparison between the data from phasor measurement unit (PMU) at a high voltage substation and from FNET taken from 110 V outlets at distribution level illustrates the close tracking between the two. Several generator trip events in the Eastern Interconnection System and the Western Electricity Coordinating Council system are recorded and the frequency patterns are analyzed. Our trigger

program can detect noticeable frequency drop or rise and sample results are shown in a 13 month period. In addition to transient states' observation, the quasi-steady-state, such as oscillations, can also be observed by FNET. Several potential applications of FNET in the areas of monitoring & analysis, system control, model validation, and others are discussed. Some applications of FNET are still beyond our imagination.

Acknowledgement

I would like to express my deepest appreciation to Prof. Yilu Liu, my academic advisor, for her consistent encouragement and support throughout my research activities here at Virginia Tech, and her lavishly sharing her technical knowledge had lead me through many obstacles.

Much appreciation goes to Prof. Virgilio Centeno, Prof. Jaime De La Ree, Prof. Tao Lin and Prof. Amitabh Mishra for serving as my committee members; in addition, through communicating with them and attending their lectures not only did I benefit from the knowledge conveyed in the classroom but also I saw great research role models in both academia and industry.

Special thanks to Prof. Arun Phadke and Prof. James Thorp for various consultations in this study. Also, I would also like to thank the contributions from Dr. Liling Huang, Dr. Baofu Gao, and Dr. Jiuping Pan. Thanks to Ian Grant and Travis Sykes of TVA Transmission Planning Department for his assistance with system data issues.

Several members of the Power System Lab and Power IT Lab should be recognized: Dr. Li Zhang, Marcos Donolo, Kevin Zhong, Emily Xu, Ryan Zuo, Mark Baldwin, Keith McKenzie, Dawei Fan, Matt Gardner, Will Kook, Vivian, Liang, Dawei Fan, and Ming Zhou, for their technical support and friendship. Also thanks to Glenda Caldwell and Carolyn Gyunn for their administrative support. I am grateful to have you as staying here at Tech. Also, I am blessed to be surrounded by many warm-hearted Taiwanese friends in Blacksburg.

Part of this work is being supported by NSF, TVA and ABB. Special thanks to Michael Ingram, Sandra Bell, and Lisa Beard of TVA, Dr. Le Tang and Dr. David Lubkeman of ABB for their support and technical guidance. We would like to thank Navin Bhatt, Jerry Jamison, Earl Dooley, Eddie Lambert, and Sanjoy Sarawgi of the American Electric Power Company for providing the testing facility and data, and for the assistance and

expertise of their staff.

I would like to express gratitude to my wife, Yuling Su, for her being with me when I/we encountering difficulties. As both of us pursuing degrees and raising a young baby, the hectic life would not have become easy without her companion. Her loving support has been and always will be my most precious possession on earth. I dedicate this dissertation to her. Moreover, how lucky I am to have such wonderful parents and in-laws who always support what we want to pursue to fulfill our dreams.

Besides all, I thank the almighty power above, God and Jesus Christ, who granted me the wisdom, strength, and perseverance to finish this seemingly impossible work. In addition, I would like thank my house group members, and brothers and sisters of Blacksburg Chinese Christian Fellowship who constantly gave me spiritual support and prayed for our family.

To Yuling, Nathan

and our Parents

Acronyms

AEP: American Electric Power[1]
AGC: Automatic generation control
ECAR: East Central Area Reliability Coordination Agreement
EMTSP: Extended Transient Midterm Stability Program
ERCOT: Electric Reliability Council of Texas, Inc
EST: Eastern Standard Time
EUS: Eastern U.S. interconnected system
FACTS: Flexible alternating current transmission systems
FDR: Frequency disturbance recorder
FFT: Fast Fourier transform
FNET: U.S. national frequency monitoring network
GPS: Global position systems
GUI: Graphical user interface
IPFLOW: Interactive power flow
ITC: International Transmission Company
KR: Kanawha River 345kV substation[2]
MAAC: Mid-Atlantic Area Council
MAIN: Mid-America Interconnected Network, Inc
MF: Matt Funk 345kV substation[3]
MSA: Microsoft Access
NE 39: New England 39 bus system
NERC: North American Electric Reliability Council[4]
PJM: PJM interconnection[5]
PMU: Phasor measurement unit
PSCAD: Power system computer aided design[6]
PSS/E: Power system simulator for engineering[7]
PSAPAC: Power system analysis package
SCADA: Supervisory Control and Data Acquisition

[1] http://www.aep.com/
[2] In AEP's control territory
[3] In AEP's control territory
[4] http://www.nerc.com/
[5] http://www.pjm.com/index.jsp
[6] http://www.pscad.com
[7] http://www.pti-us.com/PTI/software/psse/index.cfm

SERC: Southeastern Electric Reliability Council
std: standard deviation
UTC: Universal Time, also known as GMT, or Greenwich Mean Time
VT: Virginia Tech
WAMS: Wide area measurement system
WECC 127: Western Electricity Coordinating Council 127 bus system

Table of Content

List of Figures

List of Tables

Chapter 1 Introduction

1.1 Scope

In this dissertation, we examine the global frequency dynamic behavior by system simulations and from field measurements. We cover findings of frequency sensitivity of the system, frequency wave propagation and its speed. The global frequency dynamics observation would not be possible without the wide area measurement system (WAMS). Therefore, our underlying assumption for the study is based on WAMS. We use actual power system models where available; in addition, we construct our own uniform system models to get some insights of the frequency wave propagation characteristics. In attempt to find the decrement wave propagation speed, we assumed some conditions in the linearized power flow equation and swing equation to solve for a mathematical model that would be suitable for the wave propagation study. Special data management system and signal processing techniques are developed to be applied to the field measurement data. Based on field measurement data, system frequency statistics, several disturbance events in the systems, and oscillation will be discussed. Lastly, we presented some potential applications for the FNET.

1.2 Wide area measurement system (WAMS) and its importance

Traditionally, measurements in power systems are at local nodes with no common time reference. Local measurements can only provide limited system information. And system-wide synchronous measurement cannot be obtained; therefore, people could hardly get a full picture of system's dynamics. With the invention of GPS (global position

system), it provides one of the ways to obtain system-wide and time-synchronized measurements [1]. Hence we can start unveiling the complex dynamics of the electric power network [2].

GPS was first developed to provide accurate position on the globe. U.S. Department of Defense (DoD) built the first GPS at a cost of 12 billion and intended it for military use. Due to the persuasion from the device manufacturers, who saw enormous potential market of this technology, the Pentagon made the GPS commercially available. As a compromise, only limited signal accuracy is released to civilian users, typically within 100 feet in the original released version. In addition, this incredible new technology was made possible by a combination of scientific and engineering advances, particularly development of the world's most accurate timepieces: atomic clocks that are accurate to within a billionth of a second. The clocks were created by physicists seeking answers to questions about the nature of the universe, with no conception that their technology would some day lead to a global system of navigation [3, 4]. Today, GPS is a constellation of 24 satellites. The spatial distribution of orbits insures that at least eight satellites can be simultaneously seen at any time from almost anywhere on Earth. The GPS satellites circle the Earth at an altitude of about 20,000 km (13,000 miles) and complete two full orbits every day. Each satellite broadcasts radio waves towards Earth that contain information regarding its position and time. We can receive this information by using GPS receivers, which can detect and decode this information. By combining signals transmitted from several satellites and received simultaneously, a GPS receiver can calculate its position on the Earth with an accuracy of 10m or better nowadays. In our application, the GPS 1pps time signal provided by the GPS receiver is used to

synchronize data sampling within 1μs accuracy.

Wide area measurement system (WAMS) is to place sensors/recorders across a wide area to record power system's states, e.g. voltage, current, phasor angle, frequency, power, etc. Of course, to obtain meaningful measurements, the device/sensor has to be accurate enough to extract the desired information from the measured signal(s). Several phasor/frequency calculation methods [5-12] have been proposed over the years to deal with different circumstances, such as the presence of harmonics, transients, etc. And some algorithms have been applied to commercial phasor measurement units (PMUs). The other criterion for WAMS is to have synchronous time stamp for each sensor measurement. The most common way to acquire such synchronous time for wide-area sensors is to receive GPS satellite signals at each sensor and use the atomic clock in the GPS, as discussed previously. In most cases, only the time information is needed for WAMS and position data is required only once during initialization, since we are most concerned about having synchronized-time measurement among different devices.

To illustrate the importance and potential impact to the system control of WAMS, we use the 2003 Northeastern US system blackout as an example.

On Aug. 14, 2003, a wide-area blackout occurred in the northeastern United States and Canada [13, 14]. We compiled the sequence of the events on Aug. 14, 2003 between noon and 16:25 (EST) from various sources publicly available (NERC, AEP, PJM and ITS). Out of the 114 major events (mainly generator tripping, and line openings), 98 events were identified in the Eastern U.S. interconnected system model (EUS). The time line of

events before and after the blackout can be found in Appendix I. Based on the identified events, we performed dynamic simulation in PSS/E (Power system simulator for engineering).

Between noon and 16:08:58 (EST), the simulation time was shrunk into the first 50 seconds proportionally, and the simulation time, after 50 seconds, corresponds to the actual time span until 16:25 (EST). Fig 1-1, Fig 1-2 and Fig 1-3 show the frequencies at selected buses in various part of the system.

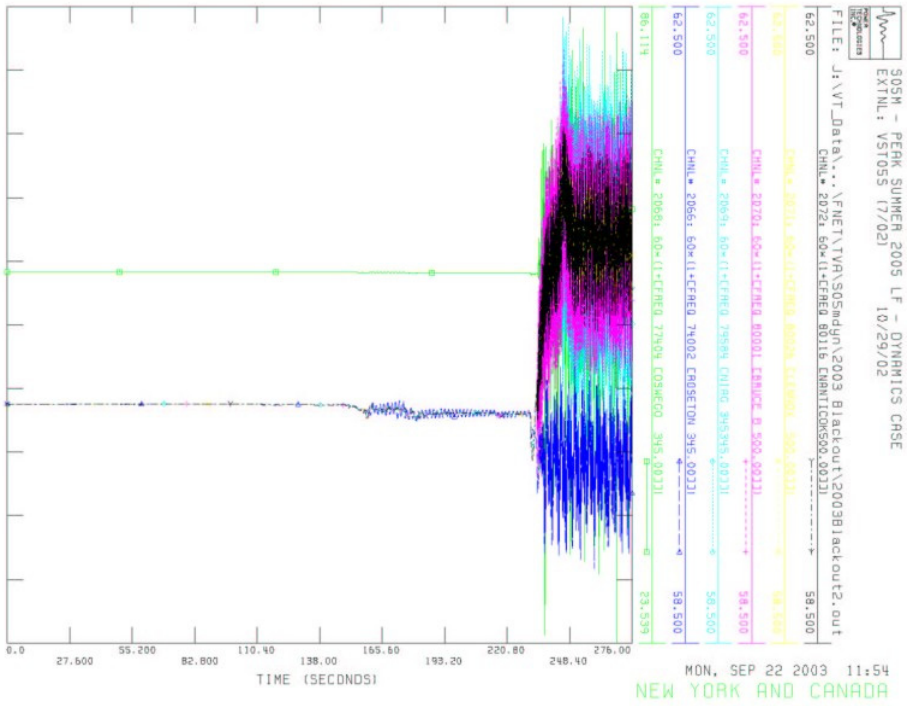

Fig 1-1. Selected bus frequencies in New York and Canada

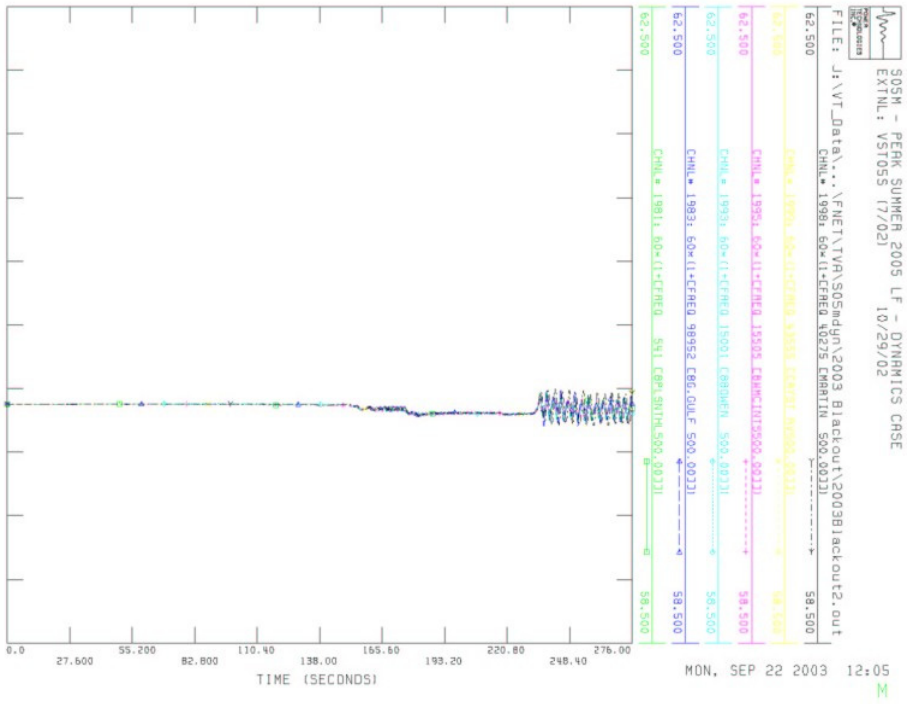

Fig 1-2. Selected bus frequencies in Missouri, Georgia and Florida

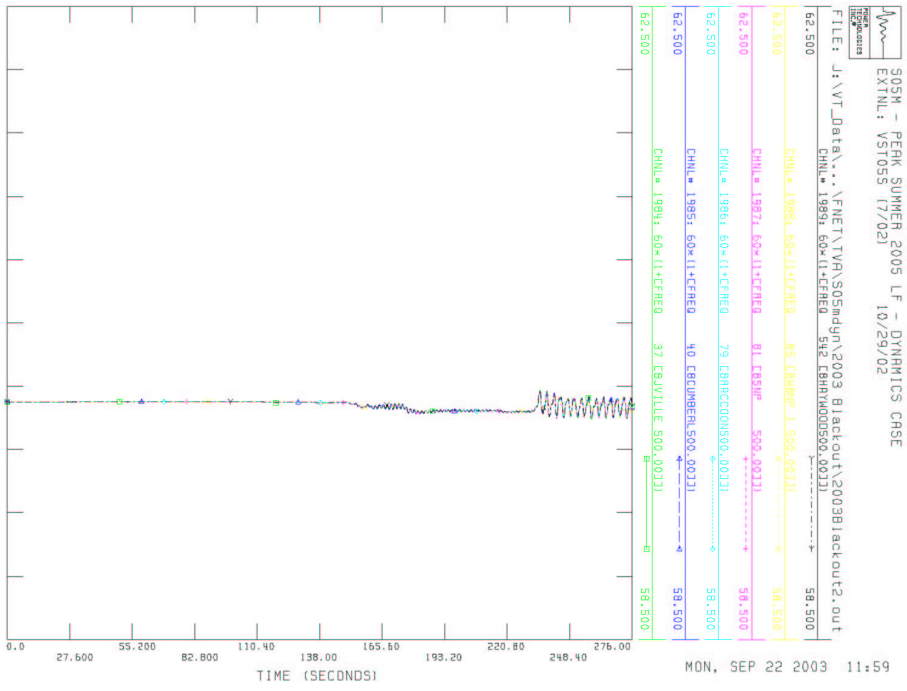

Fig 1-3. Selected bus frequencies in Tennessee

In Fig 1-1, the bus frequencies in New York and Canada become unstable at time mark 228 second, which corresponds to 16:11:57 (EST), where the reported actual wide-area blackout began at 16:10:57 (EST). Note the very slight time difference which could be caused by many factors besides the fact that the system model used here is for summer 2005 projection. From the simulation results, the wild-variation of the bus frequencies indicate that part of the system is not stable and, therefore, those buses eventually suffered blackout. In Missouri, Georgia, Florida and Tennessee, the bus frequencies were still within the operable range as shown in Fig 1-2 and Fig 1-3.

From this example, we can see that WAMS allows us observe the system's dynamics synchronously from various measurement points. In addition, it can provide crucial information that some defensive actions might be devised to reduce massive blackouts.

1.3 WAMS applications

One observation can be made from WAMS's frequency data is the disturbance wave propagation. Field PMU (phasor measurement unit) data, Fig 1-4, Fig 1-5, and Fig 1-6, implicitly show that there is a form of frequency oscillation and wave propagation in the power system when some disturbance occurred, e.g. generation trips in Fig 1-4 and Fig 1-5 and load rejection in Fig 1-6. Although the network is electrically connected, when the disturbance, e.g. generation trip, line open, or load rejection, occurs, frequencies at different points of the network do not deviate from their steady state value all at the same time. So there is a form of wave propagating in the electric power network. This kind of wave is sometimes referred as "electromechanical wave". The wave propagates in a system with the combination of electrical and mechanical components. Some continuum

models have been derived in [15, 16] to simulate some fault events. Other works in [17-20] also discuss the phenomenon and/or models for electromechanical wave propagation.

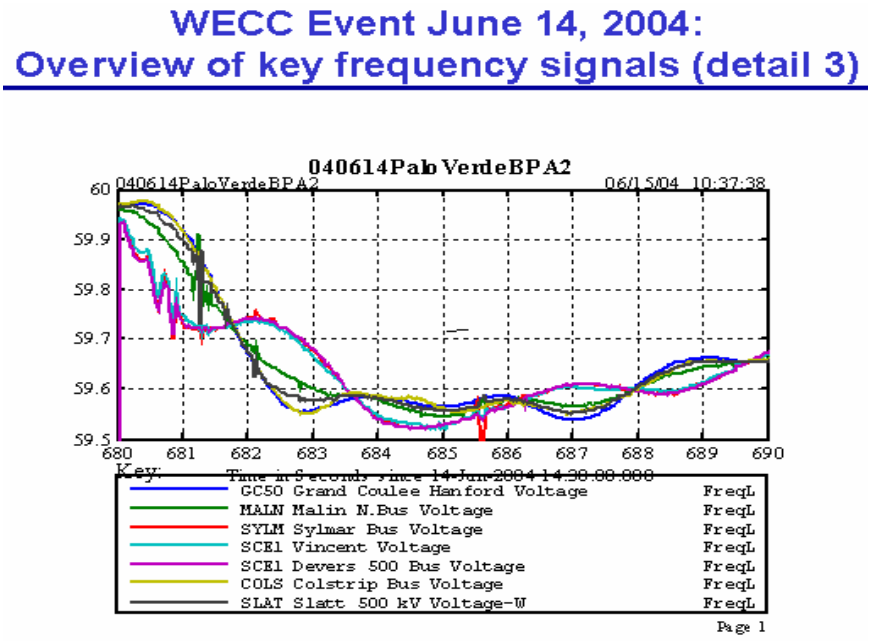

Fig 1-4. Disturbance propagation of a generator trip in WECC on June 14, 2004 [8]

[8] Courtesy of Dr. John F. Hauer, Pacific Northwest National Laboratory

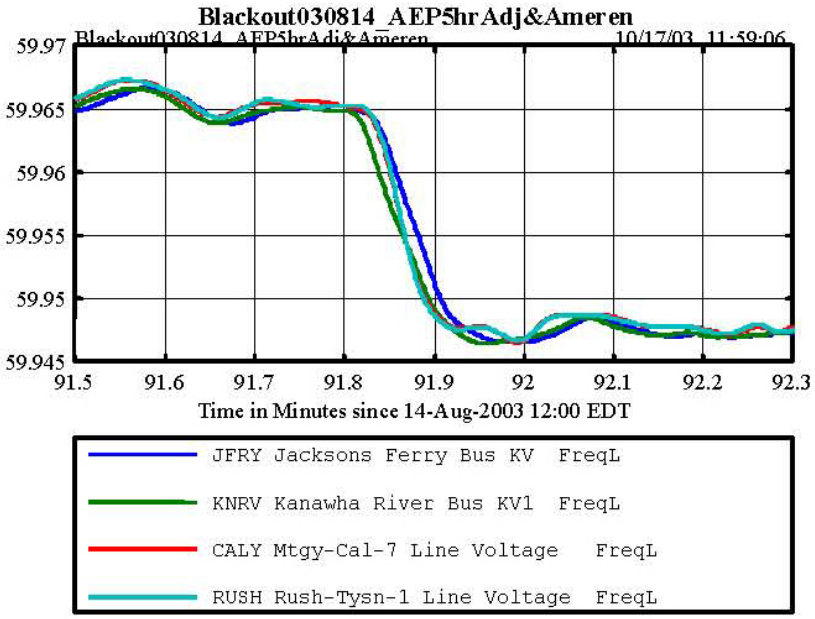

Fig 1-5. Frequency record alignment check: Eastlake #5 trip at 13:31 EDT. (Data have been smoothed with a 0.2 Hz lowpass filter.) [21]

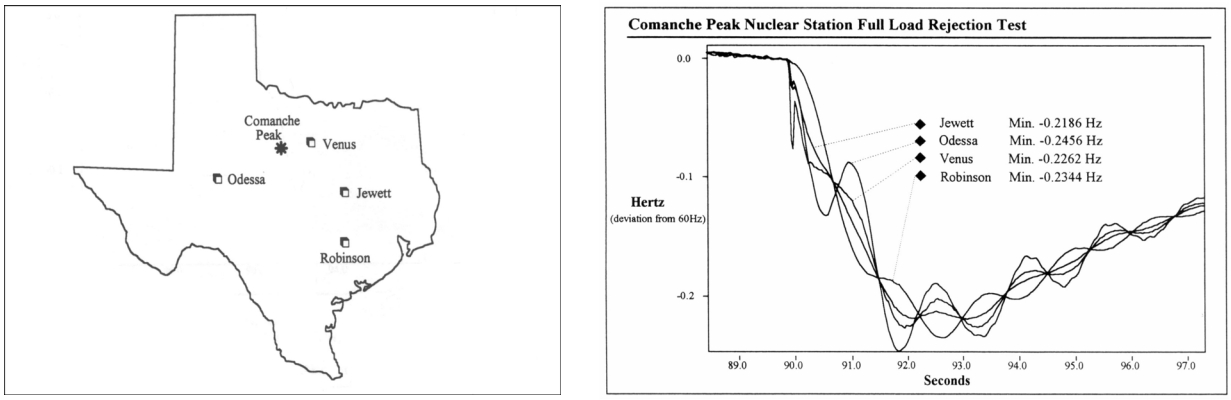

(a) (b)

Fig 1-6. (a) PMU Locations in the Texas System, (b) Comanche Full Load Rejection Test [22]

In addition to observing system's transient events [21, 23-26], WAMS can also be used to observe and study oscillations in power system [27-31]. Damping controls using WAMS with FACTS (flexible ac transmission systems) are discussed in [32-35] and with power system stabilizer are discussed in [36]. System controls, such as dynamic stability control

[37, 38], emergency voltage/stability control [39-42], and relay scheme [43-46] were re-developed to enhance system's stability and reliability under disturbance. Online security analysis provides a quantitative and practical way to determine how far away from system collapse [47-50]. Other control strategies are also being developed using wide area measurement information [51, 52]. WAMS can also be applied to validating system model [53-57]. Matching the computer model to the real system can further enhance our understanding to the system's behavior under different circumstances. Other potential applications can be found in Chapter 7.

1.4 What is FNET?

FNET stands for U.S. national frequency monitoring network. The system implements WAMS in a way that the frequencies of the whole U.S. power grid can be collected and managed in a central server. Power frequencies are currently being measured all over the system for various applications; such information is not shared in large scale for global observation and large system study due to technical and administrative limitations. Continuous synchronized wide area frequency information will provide system operators with near real-time system status. Here, by "near real-time" we mean less than 1-2 seconds delay for most of the data. FNET will help to detect system disturbance, to perform post disturbance scenario reconstruction, to verify system models and parameters used in simulations, and to track the sequence of events leading to an emergency.

FNET has the following special features: (1) Nation-wide system frequency information (and phase angles) can be collected from hundreds of key sites chosen to satisfy observability and controllability criteria. (2) The measurements are taken at 110V single

phase power outlets to avoid costly substation installation. (3) Time stamped frequency data are collected via Internet on a continuous basis in near-real time. (4) Standard frequency disturbance recorders (FDRs) are used in all measurement sites to guarantee convenient data integration and comparison.

The current commercial PMU works best if all 3-phase voltage signals are measured; therefore, it is typically installed at high voltage level buses. The installation cost of PMU at high voltage level substation is high and the wide deployment of PMU has been slow. Therefore WAMS is not available as it should have been. To justify the issues of cost and ease of deployment, the FNET deploys low-cost (~$1000) frequency disturbance recorders (FDR) to measure system frequency all over the U.S. from voltage waveforms taken at 110V outlets. FNET provides close-to-real time frequency information all over the power grid and an opportunity to study the system dynamics globally. Since no substation installations are required, FNET is extremely low-cost and suitable for deployment on a large scale. Fig 1-7 shows the system architecture of FNET.

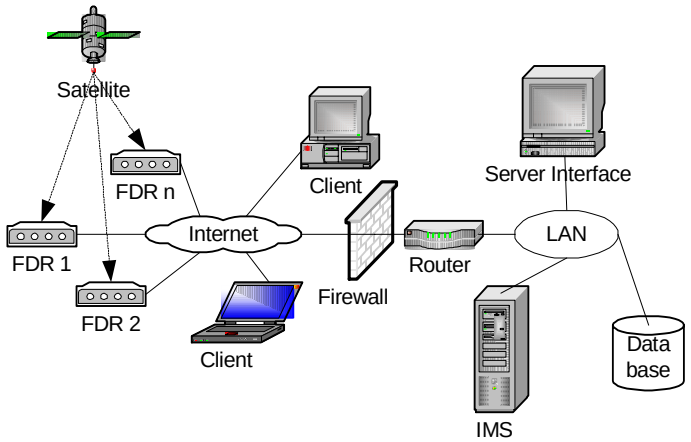

Fig 1-7. Frequency Monitoring Network System Architecture

The FNET system consists of two major components: a) Frequency Disturbance Recorders (FDRs), which perform local frequency measurements and send data to a server through the Internet; b) The Information Management System (IMS), which includes data collection and storage service, data communication service, database operation service, and web service. The Internet provides the wide-area communication network between the FDR units and IMS. Detailed description of the FNET system can be found in [58, 59]

FDR can measure frequency and phase angle from voltage signal at 110 V outlet. The FDR unit consists of a voltage transducer, a low pass filter, an analog to digital (A/D) converter, a GPS receiver, a microprocessor, and the network communication modules. The FDR can quickly calculate the power supply frequency using the phasor algorithms developed at Virginia Tech [10, 60]. All measurements are time-synchronized with GPS signal and are transmitted to central servers via Internet.

As of June of 2005, we have deployed 15 FDRs across U.S., as shown in Fig 1-8. Among them, 4 are in Western Electricity Coordinating Council (WECC), 1 is in Electric Reliability Council of Texas (ERCOT) and 10 are in the Eastern Interconnection System (EUS). Current FDR deployment in the Eastern Interconnection has covered 5 reliability councils. FNET is an ongoing project and we anticipate more FDRs will be placed into the system.

Fig 1-8. FDR locations as of June 2005. FDRs are labeled as red double circle

1.5 Complex system data visualization

The need for visualization of large amount of data is stringent in analyzing the complex system's dynamic behavior [61]. Human beings respond better to the visual data than numeric data [62]. Therefore, developing tools to help visualize data from either simulation or field measurement can help understand the system's dynamics better [63].

Tools can be used to view the system dynamics in many different ways. One is to show several key power system states, such as voltage, load flow, oscillation modes and etc. For power systems, finding the hot-spot in the system is crucial to maintain system's operation. That includes the equipment monitoring and visualization, which helps to reduce the maintenance cost and more importantly to reduce outages. A recent trend for power system modeling has moved from text input to GUI (graphical user interface)

design. For example, PSS/E, PSCAD, and PowerWorld[9] have all incorporated friendly GUI for end users to model and view system's status.

The applications of visualizations are extensive and powerful. First, the data is easy to be understood and explained. They can be also used to perform dynamic and security assessment and contingency analysis for the system. Showing the system model in a graphical way can assist users debugging the model easily. For education purpose, visualization could stimulate student's interest in the subject and help them to understand certain complex system's dynamics [64, 65].

Visualization tools that have been developed are concentrated on showing the system's states, such as voltage[66], load flow [67], oscillation modes [68]. In the study, we developed a systematic way to visualize frequency from simulation data and will discuss some findings from animations.

1.6 Organization of the study

Chapter 1 defines the scope of this study, illustrates the importance of wide area measurements by the 2003 eastern U.S. blackout example, shows the disturbance propagation phenomenon from system measurement, reviews some WAMS applications and introduces the FNET system (national frequency monitoring network). Visualizations of complex system data is needed for better understanding of the system, some advantages of doing so is introduced.

[9] http://www.powerworld.com/

In Chapter 2, we studied the frequency sensitivity for the generation trip in 3 different U.S. power systems based on simulations. In Chapter 3, we presented the detailed frequency wave propagation phenomenon due to generation trip, load rejection and line trip. Visualization examples from these events are provided to help understand the mechanism of this wave propagation. Also the wave propagation can be further understood from uniform single-line system. Chapter 4 presents the findings of the "speed" of this frequency electromechanical wave propagation in Eastern U.S. interconnection systems (EUS) and Western Electricity Coordinating Council 127 bus system (WECC 127). Additionally, discussions of propagation speed on the uniform systems are provided. In Chapter 5, we illustrate a mathematical way to analyze the relationship between active power and frequency and an example is given.

In Chapter 6, comprehensive analyses of FNET data are presented. Signal processing using outlier removal and wavelet denoisng techniques is introduced. Comparisons between FDR and PMU are discussed. System operating frequency statistics are summarized. Several generation trip events were recorded and analyzed. Also, a frequency trigger program was designed and used to record significant frequency drop or rise in a given time frame and detection results for EUS is presented. System oscillation can also be observed from FNET data and examples are given. In Chapter 7, several potential applications of FNET are discussed. Lastly, in Chapter 8, we conclude the work and state the contribution to the professional field and suggest some future works.

Chapter 2 Frequency Sensitivity

2.1 Introduction

Power imbalance between generation and consumption, including load and losses, in the electric power system induces frequency variation. Such variation cannot be always detected if it is below the precision of the measurement device. Several frequency calculation techniques have been proposed and some of them have applied to the practical field [5, 6, 8-10, 12]. The Virginia Tech frequency disturbance recorder (FDR) [59], developed as part of the national frequency monitoring network (FNET) [69] at Virginia Tech, adopted the phasor calculation algorithm reported in [10, 60]. The frequency calculation algorithm allows us to have the frequency sensitivity over 0.0001Hz. This section is to, from simulations, find how much of power drop from generators in the electric power system for the FDR to detect such frequency deviation; in other words, we intend to find how severe of the event can be observed by the FDR. To leave some margins, we select 0.005 Hz as our target frequency sensitivity. This study was performed using system models of the New England 39 bus system, the Western Electricity Coordinating Council 127 bus system, and the Eastern US Interconnected system. We abbreviate these 3 systems as WECC 127, NE 39 and EUS, respectively.

2.2 New England 39 bus system frequency sensitivity

2.2.1 System description

NE 39 is simplified from a large system. The extent of the system is unknown. The system data is extracted from [70] and the one line diagram of NE 39 is shown in Fig 2-1.

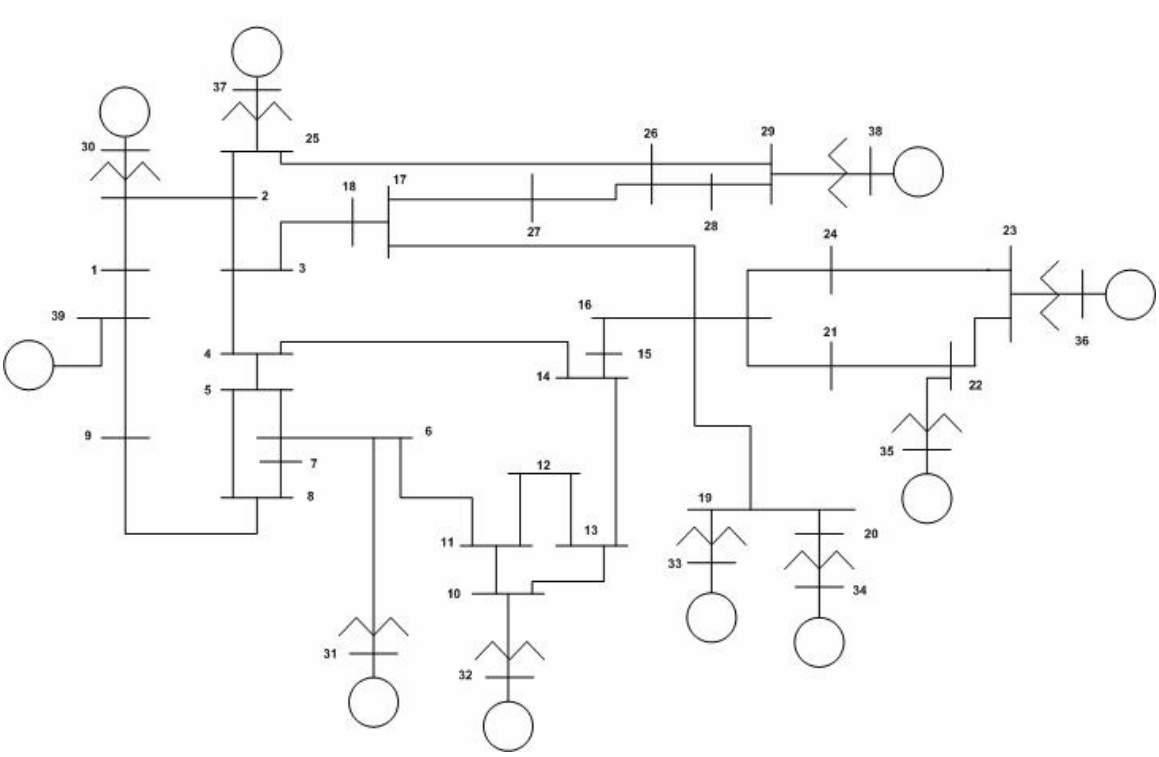

Fig 2-1. New England 39 bus system one-line diagram.

In NE 39, there are 10 generators in the model. The electric generation powers from the generators are shown in Table 2-1.

Bus number	MW	MVAR
29	0.00	117.16
30	250.00	176.30
31	573.98	256.67
32	650.00	250.87
33	632.00	122.80
34	508.00	173.12
35	650.00	226.37
36	560.00	109.09
37	540.00	17.54
38	830.00	19.26
39	1000.00	119.17
Total	6193.98	1588.35

Table 2-1. Generator output active and reactive powers in NE39 system.

This part of the study was simulated in the Interactive Power FLOW (IPFLOW) [71] and Extended Transient Midterm Stability Program (ETMSP) [72] computer programs which are parts of Power System Analysis PACkage (PSAPAC). The system is first solved by the IPFLOW to obtain the power flow solution, or static state solution. Then apply the power flow solution as the system's initial states to simulate dynamic scenarios in ETMSP.

2.2.2 Spliting generator

The electric power system is large and complex; models are often simplified by combining similar devices from the original system into a single model from original system for the ease of system representation and simulation purposes. Therefore at each bus, one generator model may represent several generators and/or it may have only one load for several loads. Smaller generators at one plant are typically aggregated into a single generator model. Sometimes, dynamically-coherent generators can be combined into one generator in the system model [73].

In real system, if only a part of the generation at a bus is tripped from the system, in the model, we would disconnect a portion of generation power from the generator bus. To achieve this, we will need to modify the generator model accordingly to simulate this scenario. To disconnect a portion of generation from a generator bus, a separation of the generator model is firstly done in both power flow and dynamic files. Then in the dynamic simulation, a switching/tripping command can be issued to take a separated generator offline.

To split a generator into smaller power-output ones, in power flow raw data, we first duplicate the data of the generator bus data to be split, modify each duplicated generator by assigning different circuit identification numbers, and change the active and reactive power outputs to the desired values. An example is given below.

In the dynamic data, to split a generator, we again duplicate the data block of the one to be split, modify the circuit identification number to distinguish between different units (which should match the changes made in power flow file), and reduce the MVA base for each unit to represent the corresponding power changes in the power flow data. The MVA base for each split and reduced-powered generator is in proportion to the original non-split power. The impedances in the dynamic raw data are represented in per unit, so modifying the base MVA of each split generator would result in changing the actual impedance of each split generator. Therefore, no changes are needed to modify the impedances. In addition, all the time constants should be intact in each split generator model. As an example, a generator's power flow and dynamic data is shown as follows:

```
38 'BUS38' '1 ' 1 830.00 19.39
```
[10]

```
38    1
0.0000     0.211     0.205     0.030     0.057     0.059     0.057     0.059
4.790    1.9600    0.0000    0.0000
34.50    14.000    100.0000   60.0
```
[11]

The generator outputs 830 MW and 19.39 MVAR, and the base MVA is 100 MVA. To split the generator into 2 smaller power-output generators with one outputting 817.61

[10] Power flow data: Bus number, bus name, machine identifier, status (1: on), active power output and reactive power output

[11] Dynamic data: 1st line – bus name, machine identifier. 2nd and 3rd line – rotor data. 4th line – inertia time constant, damping coefficient, base MVA, base frequency

MW and 16.92 MVAR and the other outputting 12.39 MW and 2.47 MVAR, we first duplicate the data block and modify the power output and machine identification in the power flow data as follows (changes are in bold):

```
38 'BUS38' '1 ' 1 817.61 16.92
38 'BUS38' '2 ' 1 12.39 2.47
```

For the dynamic data, we duplicate the data block and modify the machine identification and the MVA base. The MVA base for machine identification number 1 is calculated as 817.61/830*100 = 98.507 and for machine 2, the MVA base is 12.39/830*100 = 1.492. The dynamic data then becomes (changes are in bold):

```
38   1  100  100
   0.0000    0.211    0.205    0.030    0.057    0.059    0.057    0.059
    4.790   1.9600   0.0000   0.0000
    34.50   14.000   98.507   60.0

38   2  100  100
   0.0000    0.211    0.205    0.030    0.057    0.059    0.057    0.059
    4.790   1.9600   0.0000   0.0000
    34.50   14.000   1.493    60.0
```

Therefore, during the dynamic simulation process, we can trip the generator of desired output power.

2.2.3 Findings and generator tripping simulations

Numerous simulations suggested to us that when the tripping power is at least 6.19 MW and 1.59 MVAR, which correspond to 0.1% of NE 39's total generation, bus frequencies would deviate at least 0.005 Hz at all buses in the system. In the following, we show 4

simulation results of generator trips at bus 30, 35, 38, or 39. The changes of the frequencies at all the generator buses are monitored; in addition, the mechanical torque outputs from generators are also recorded to see how it varies and when governors would have effect on the power output. We simulated the process for 10 seconds with a time step of 0.005 second. Generator disconnection was initiated at 1 second and remained disconnected from the system throughout the simulations.

1. Trip 6.19 MW and 1.59 MVAR from generator bus 30

Frequency

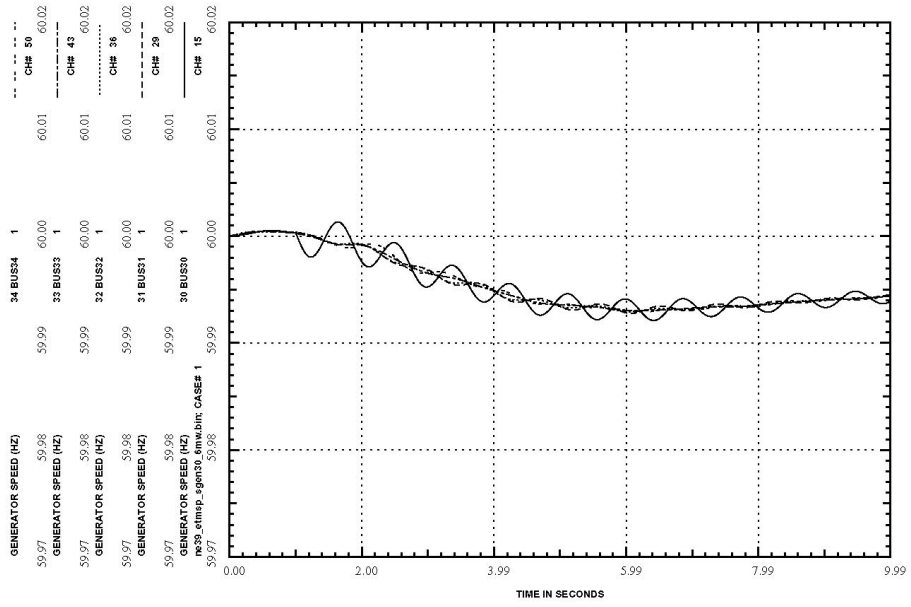

(a)

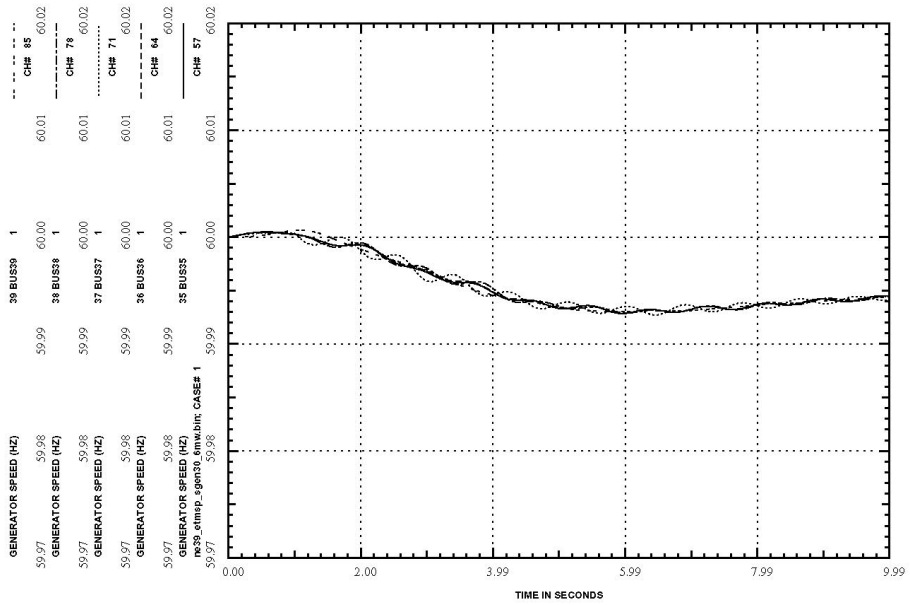

(b)

Fig 2-2. Bus frequencies at generator buses when 6.19MW and 1.59 MVAR is tripped from bus 30. (a) bus 30-34, (b) bus 35-39

Mechanical Torque output

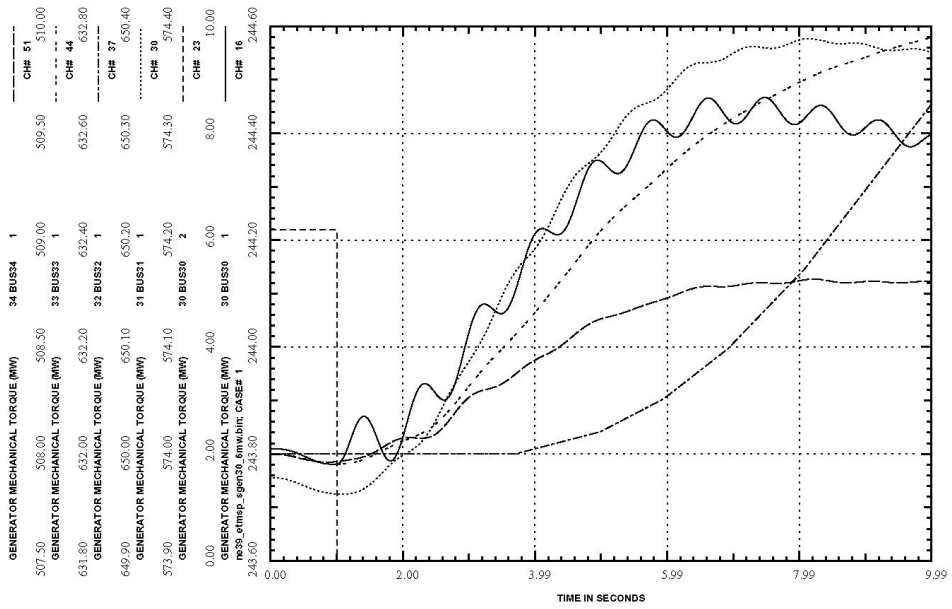

(a)

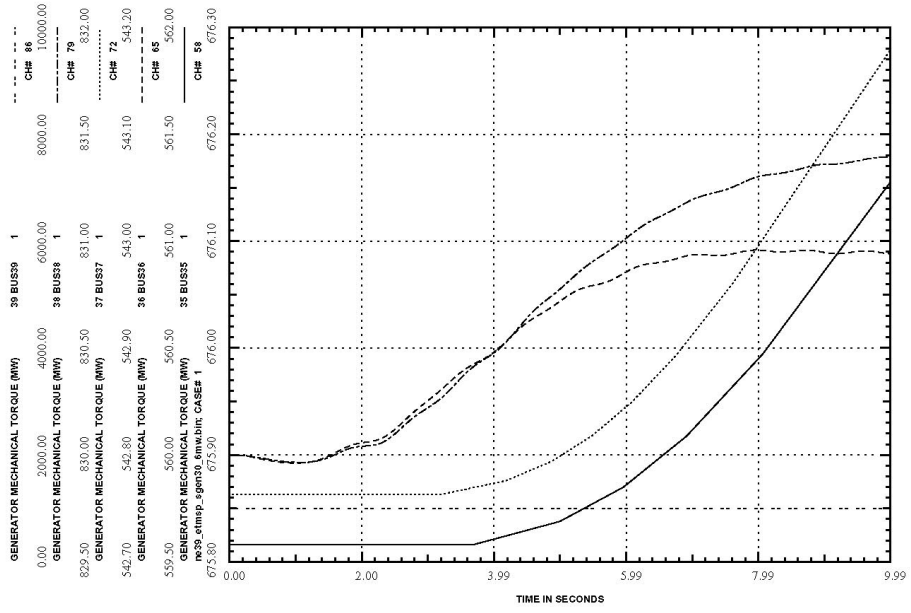

(b)

Fig 2-3. Mechanical torque output from generators when 6.19MW and 1.59 MVAR is tripped from bus 30. (a) bus 30-34, bus 30 is split into 2 buses namely ‘bus30 1’ and ‘bus 30 2’ (b) bus 35-39

2. Trip 6.19 MW and 1.59 MVAR from generator bus 32

Frequency

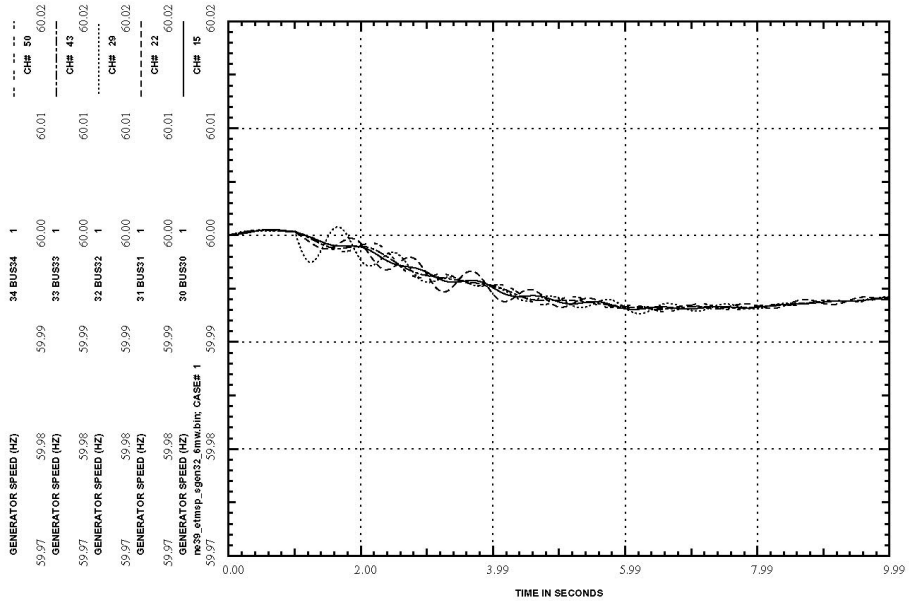

(a)

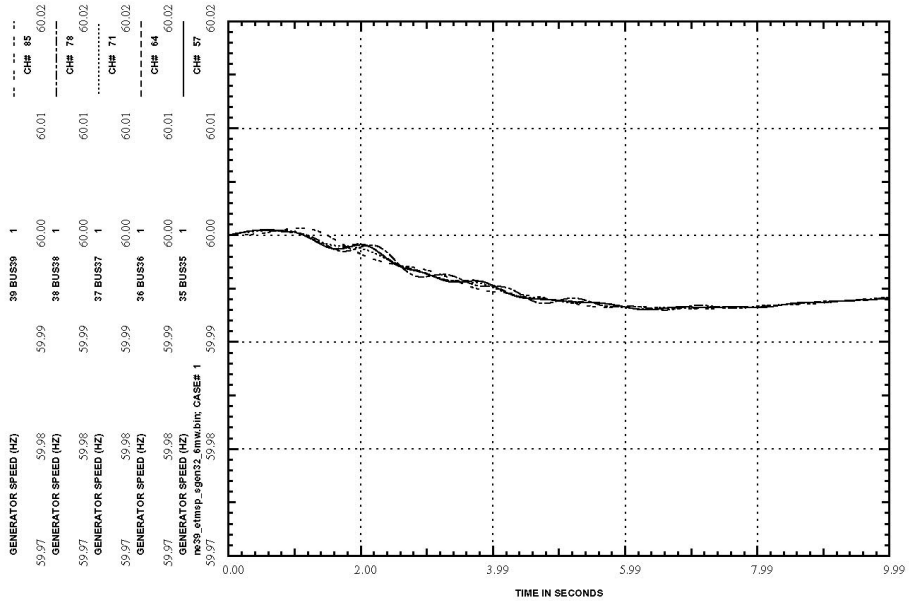

(b)

Fig 2-4. Bus frequencies at generator buses when 6.19MW and 1.59 MVAR is tripped from bus 32. (a) bus 30-34, (b) bus 35-39

Mechanical Torque output

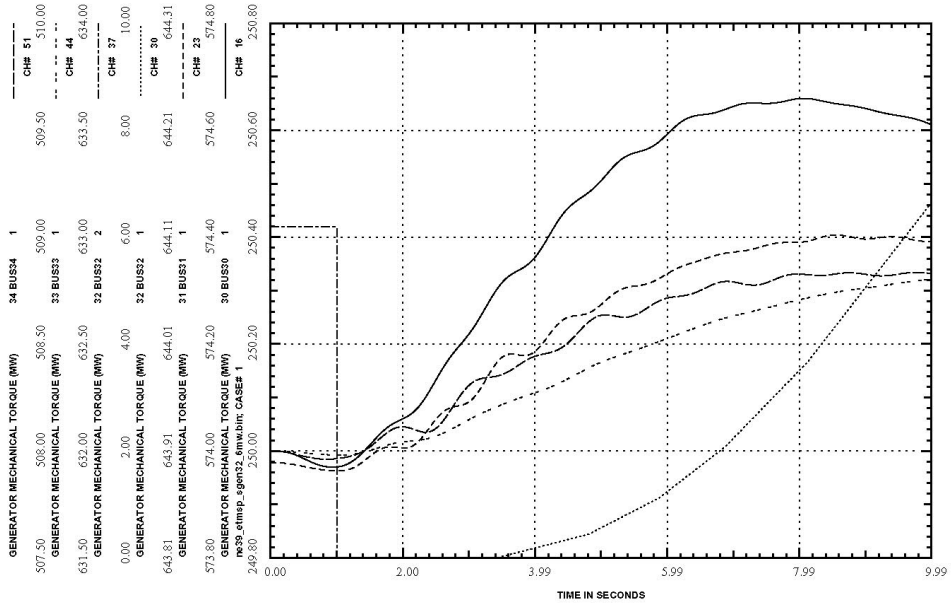

(a)

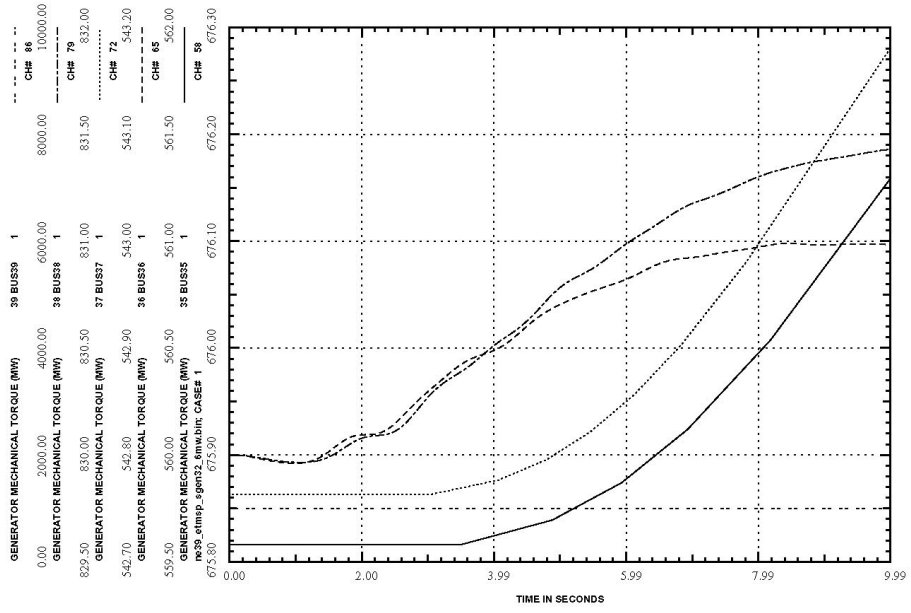

(b)

Fig 2-5. Mechanical torque output from generators when 6.19MW and 1.59 MVAR is tripped from bus 32. (a) bus 30-34, bus 30 is split into 2 buses namely ‘bus32 1’ and ‘bus 32 2’ (b) bus 35-39

3. Trip 6.19 MW and 1.59 MVAR from generator bus 38

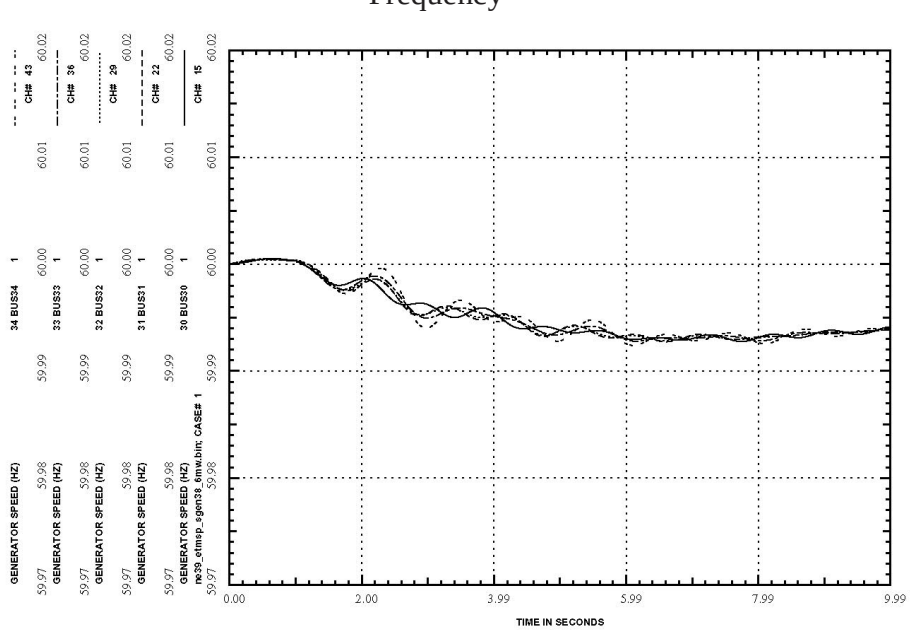

(a)

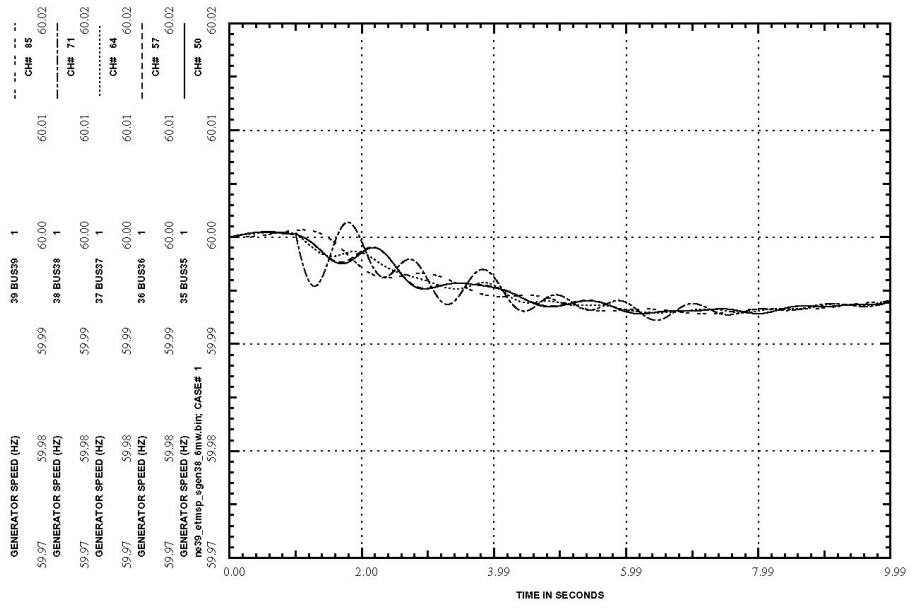

(b)

Fig 2-6. Bus frequencies at generator buses when 6.19MW and 1.59 MVAR is tripped from bus 38. (a) bus 30-34, (b) bus 35-39

Mechanical Torque output

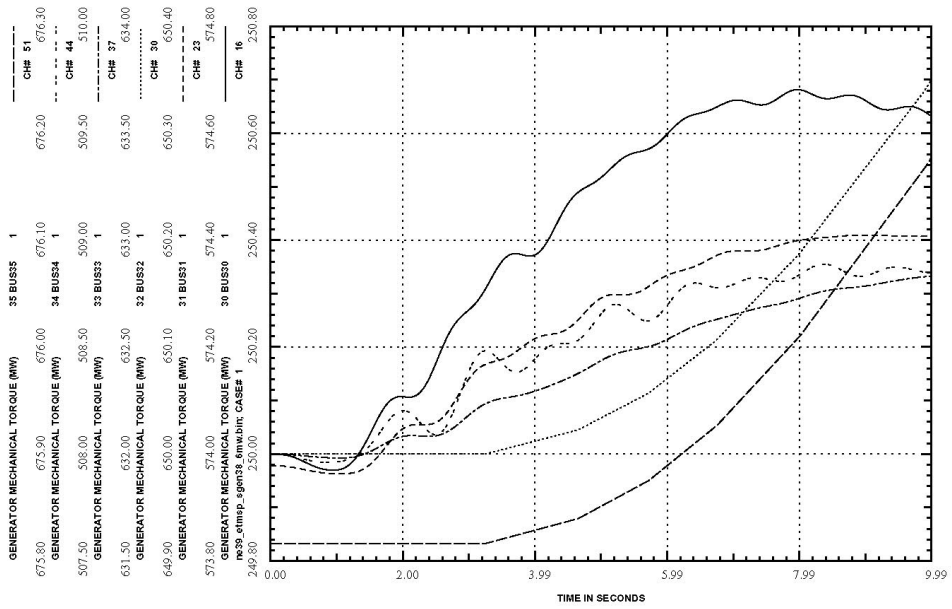

(a)

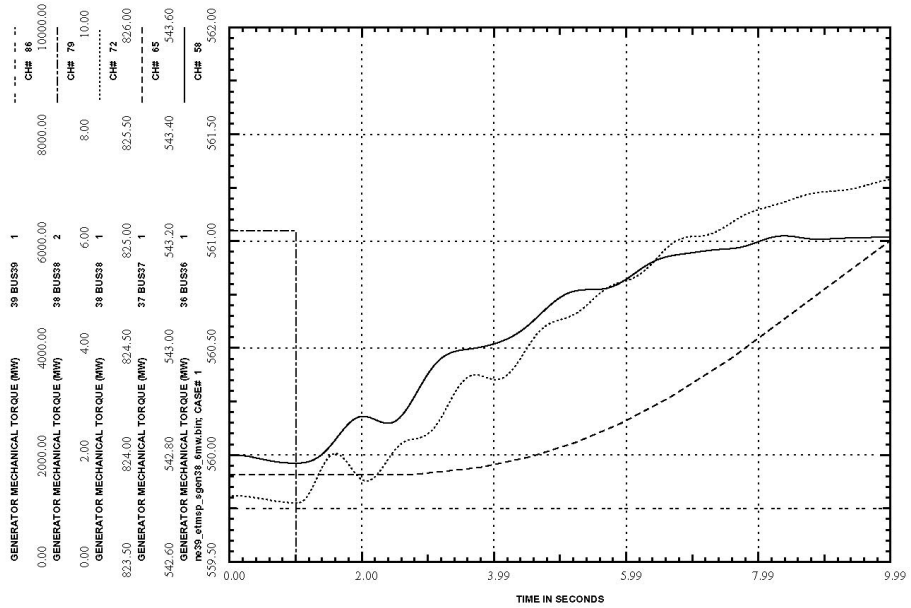

(b)

Fig 2-7. Mechanical torque output from generators when 6.19MW and 1.59 MVAR is tripped from bus 38. (a) bus 30-34, bus 30 is split into 2 buses namely ‘bus38 1’ and ‘bus 38 2’ (b) bus 35-39

4. Trip 6.19 MW and 1.59 MVAR from generator bus 39

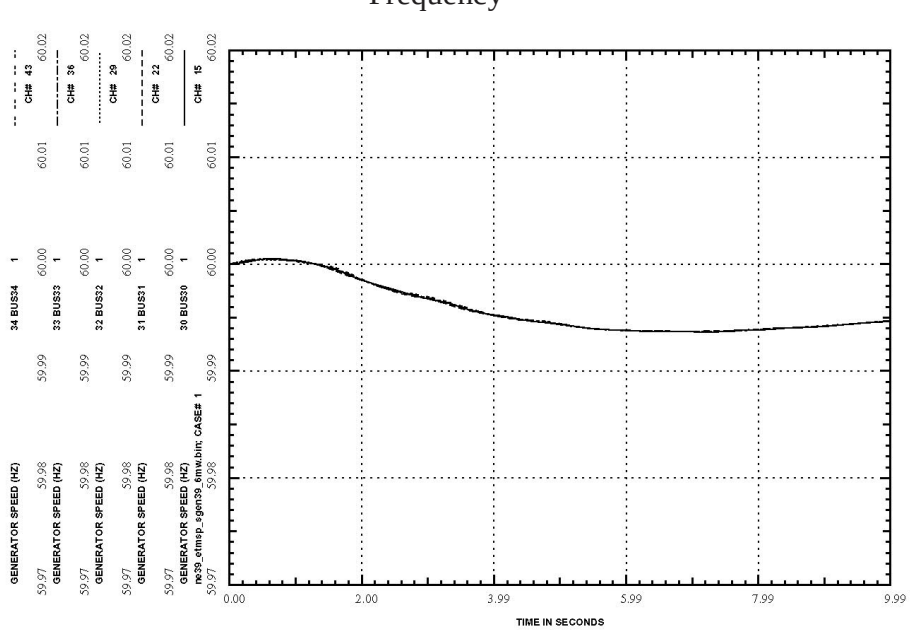

(a)

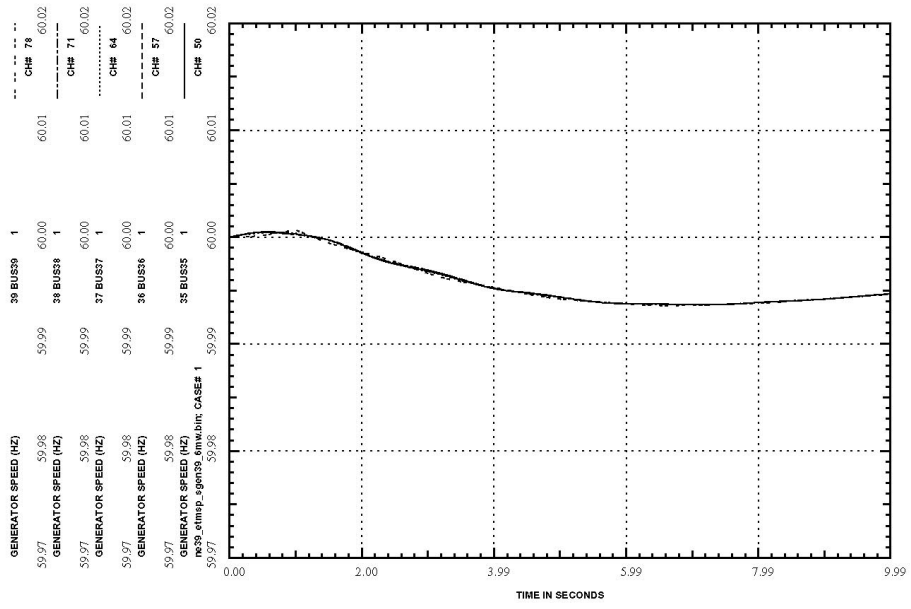

(b)

Fig 2-8. Bus frequencies at generator buses when 6.19MW and 1.59 MVAR is tripped from bus 39. (a) bus 30-34, (b) bus 35-39

From the simulation results, we can observe that when some generation is disconnected from the system bus frequencies would first decrease then increase to a new steady state value. The reason that after the post-transient state bus frequencies do not go back to 60 Hz is that no reference changes have made to governor. That is typically done in the automatic generation control (AGC), which is a supervisory frequency control for the system. The frequency responses also show that at different observing points in the system, we would see different frequency fluctuations. Typically, the most significant fluctuation would occur at the bus where we disconnect generation power. From above figures, we can see that all the frequency responses are similar to each other due to the fact that NE 39 is a tight system. Therefore, not much frequency difference can be observed due to the generator trip.

The frequencies could vary by at least 0.005 Hz when tripping 6 MW and 1.6 MVAR from any generator bus in NE 39 system. The observation implies that for a tripping of the generation, as small as 0.1% of the system's total generation power, the variation of the frequencies would be significant enough to be captured by the FDR to be placed anywhere in the system.

In addition, the governors wouldn't have taken effect in 1~2 seconds after the tripping based on the mechanical torque output at the generators. This result would be useful when we study the WECC 127 bus system.

2.3 WECC 127 system frequency sensitivity

2.3.1 System description

WECC 127 bus system is a simplified model consisting of 127 buses of which 29 buses are connected to generators. The geographical area and the one-line diagram of the system is shown in Fig 2-9. The system data can be found in [74]. In addition, the generators' steady-state powers are listed in Table 2-2:

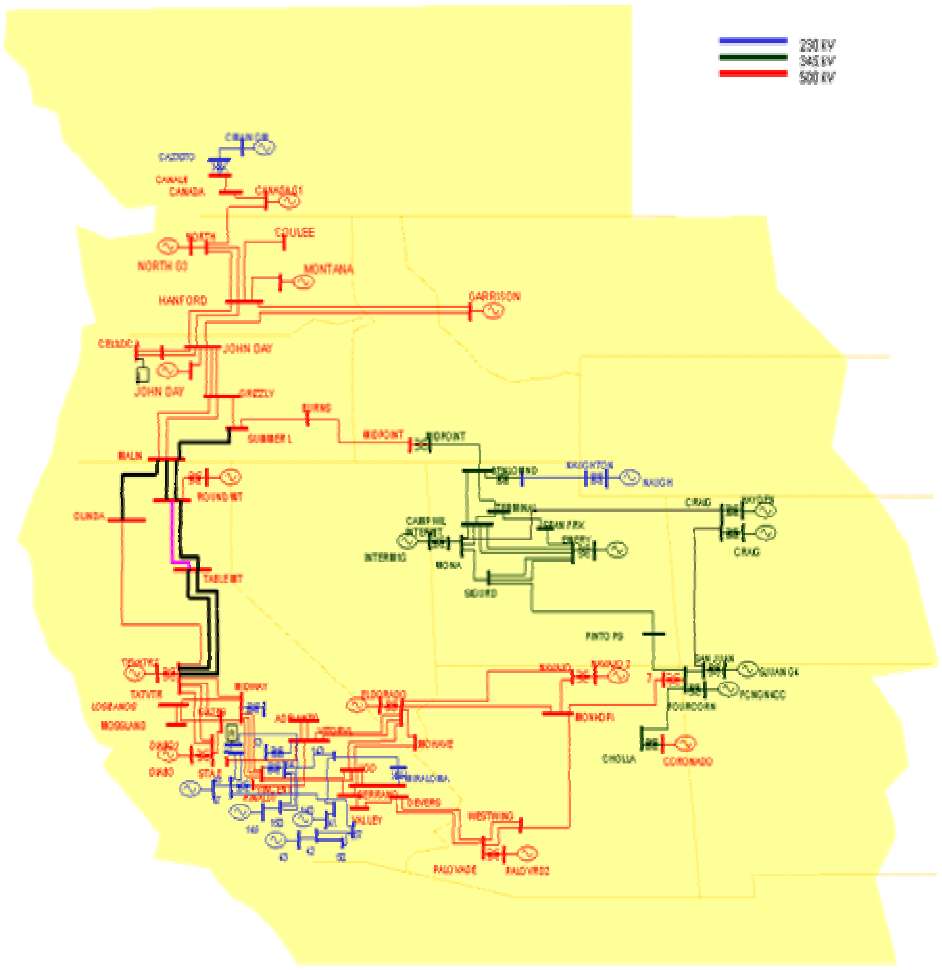

Fig 2-9. WECC 127 system geographical area and one-line diagram

Generator Bus Number	Real Power (MW)	Reactive Power (MVAR)	% of generator real power to the total system real power
1	4480.0	1150.2	7.30%
5	4450.0	1011.1	7.25%
8	9950.0	1854.0	16.20%
13	5174.8	855.2	8.43%
19	1301.0	431.5	2.12%
26	2910.0	953.3	4.74%
28	1640.0	285.7	2.67%
33	445.0	91.7	0.72%
38	1665.0	-31.4	2.71%
44	1780.0	534.6	2.90%
46	1048.0	-132.9	1.71%
47	2050.0	464.8	3.34%
49	962.0	148.8	1.57%
53	2160.0	-30.5	3.52%
56	800.0	123.0	1.30%
60	2640.0	378.1	4.30%
62	1690.0	195.5	2.75%
65	982.7	-128.8	1.60%
67	1680.0	446.6	2.74%
72	1690.0	593.8	2.75%
76	3195.0	1032.5	5.20%
81	2200.0	393.7	3.58%
88	765.0	-206.2	1.25%
91	3467.0	1654.6	5.65%
96	1057.0	25.6	1.72%
102	594.0	192.4	0.97%
113	325.0	68.3	0.53%
119	110.0	29.1	0.18%
126	200.0	-52.2	0.33%
Total:	61411.5	12332.1	100.00%

Table 2-2. WECC 127 system output real and reactive powers from generators and the percentage of the real power to the system's total real generated power.

For this system, we will study the effect of a single drop of generation power on the system's frequency. The generator models of the WECC 127 system do not include governor. We can anticipate that any loss of power from generator(s) would not be compensated by other generators; therefore, the bus frequencies will continue to decrease to overcome the deficiency between the generation and consumption. Due to this reason, the frequency variation from the simulation process would not give us the response of the real system after the first few seconds; we need to set some cut-off time from the results to determine the frequency sensitivity from the drop of generation.

Based on the observation from NE 39 from Fig 2-3, Fig 2-5, and Fig 2-7, the mechanical torque outputs typically would not increase from its pre-fault condition after 1~2 seconds when some generation powers are disconnected from the system. After additional power outputs from generators due to the action of governors, the frequencies would not decrease further, instead they would increase back to some new steady state value. If we assume that the governors of WECC 127 have similar characteristics to that of NE 39, we could set our target time at 2 seconds after generation trip to see if the frequency would vary by at least 0.005 Hz so that the FDR to be placed anywhere in the system would be able capture the variation.

Again, WECC 127 is a simplified system, where one generator model may represent a group of aggregated generators. To split a generator into ones that output less power of the original ones, we use the splitting techniques as stated in 2.2.2.

2.3.2 Findings and generator tripping simulations

The generation drop simulations were performed in PSAPAC on each generator in the system. Some typical frequency responses are presented here. Each plot represents a group of generators in a similar geographic region. For all the cases we tested, we found out that if we drop at least 122.8 MW and 24.7 MVAR, which corresponds to 0.2% of the system's total generation power would make the frequency variation equal or greater than 0.005 Hz across the system 2 seconds after the power being drop.

Bus names, which will be shown as the label in the following plots, and their corresponding bus numbers are listed in Table 2-3.

Generator Bus Number	Generator Bus Name	Generator Bus Number	Generator Bus Name
1	CMAIN GM	60	PALOVRD2
5	CANAD G1	62	NAVAJO 2
8	NORTH G3	65	ELDORADO
13	JOHN DAY	67	MOHAV1CC
19	DALLES21	72	MIRALOMA
26	MONTA G1	76	LITEHIPE
28	BRIDGER2	81	PARDEE
33	NAUGHT	88	DIABLO1
38	EMERY	91	TEVATR2
44	INTERM1G	96	ROUND MT
46	CRAIG	102	TEVATR
47	HAYDEN	113	HAYNES3G
49	SJUAN G4	119	OWENS G
53	FCNGN4CC	126	CASTAI4G
56	CORONADO		

Table 2-3. Recorded bus numbers and their corresponding bus names in WECC 127.

We simulate the process for 10 second with the time step of 0.005 second. Generator disconnection was initiated at the time of 1 second and remained disconnected from the system throughout the simulation. Three tripping examples are given below.

1. Trip 122.8 MW and 24.7 MVAR from generator bus 5

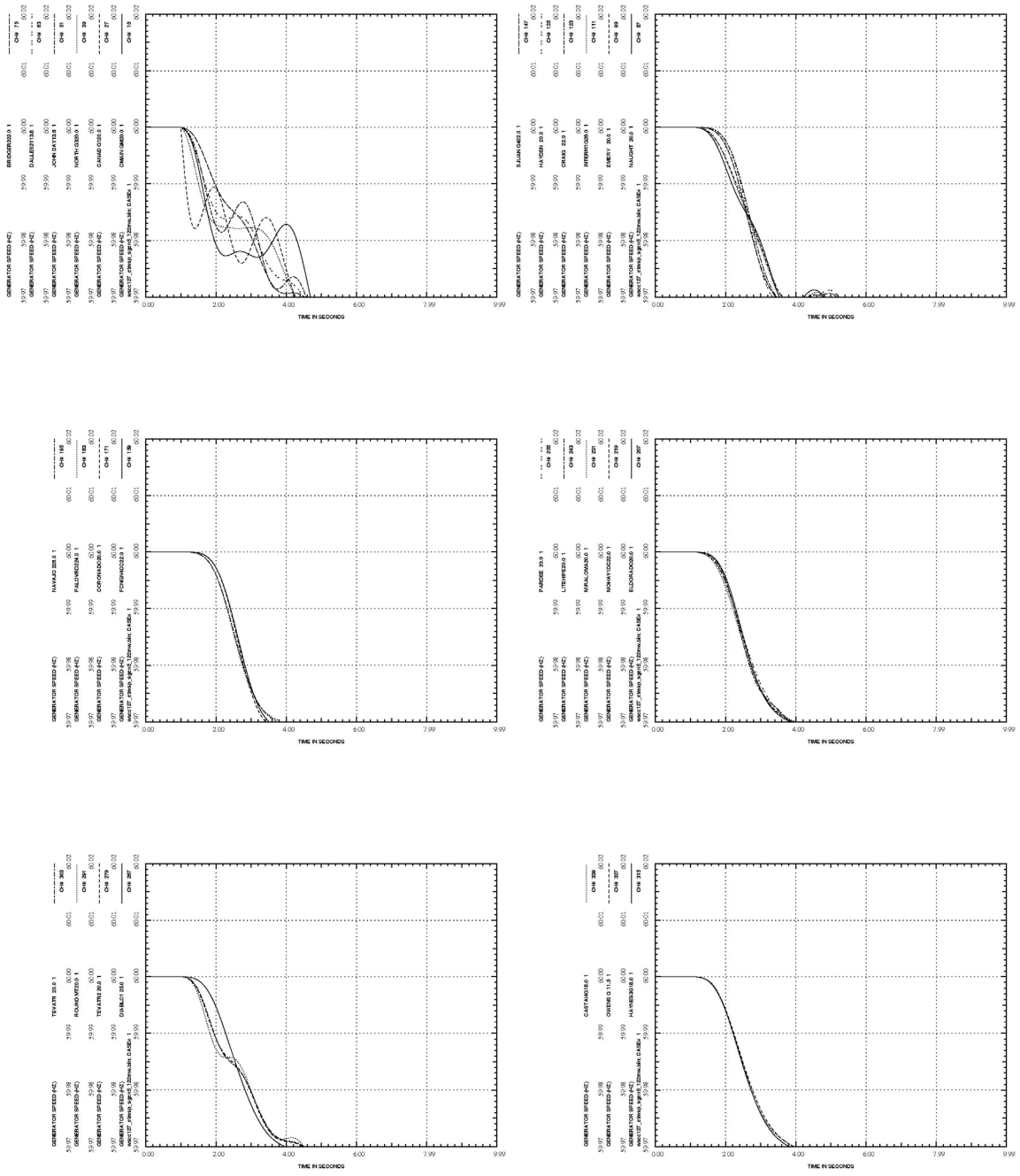

Fig 2-10. Bus frequencies at generator buses when 122.8 MW and 24.7 MVAR is tripped from bus 5

2. Trip 122.8 MW and 24.7 MVAR from generator bus 44

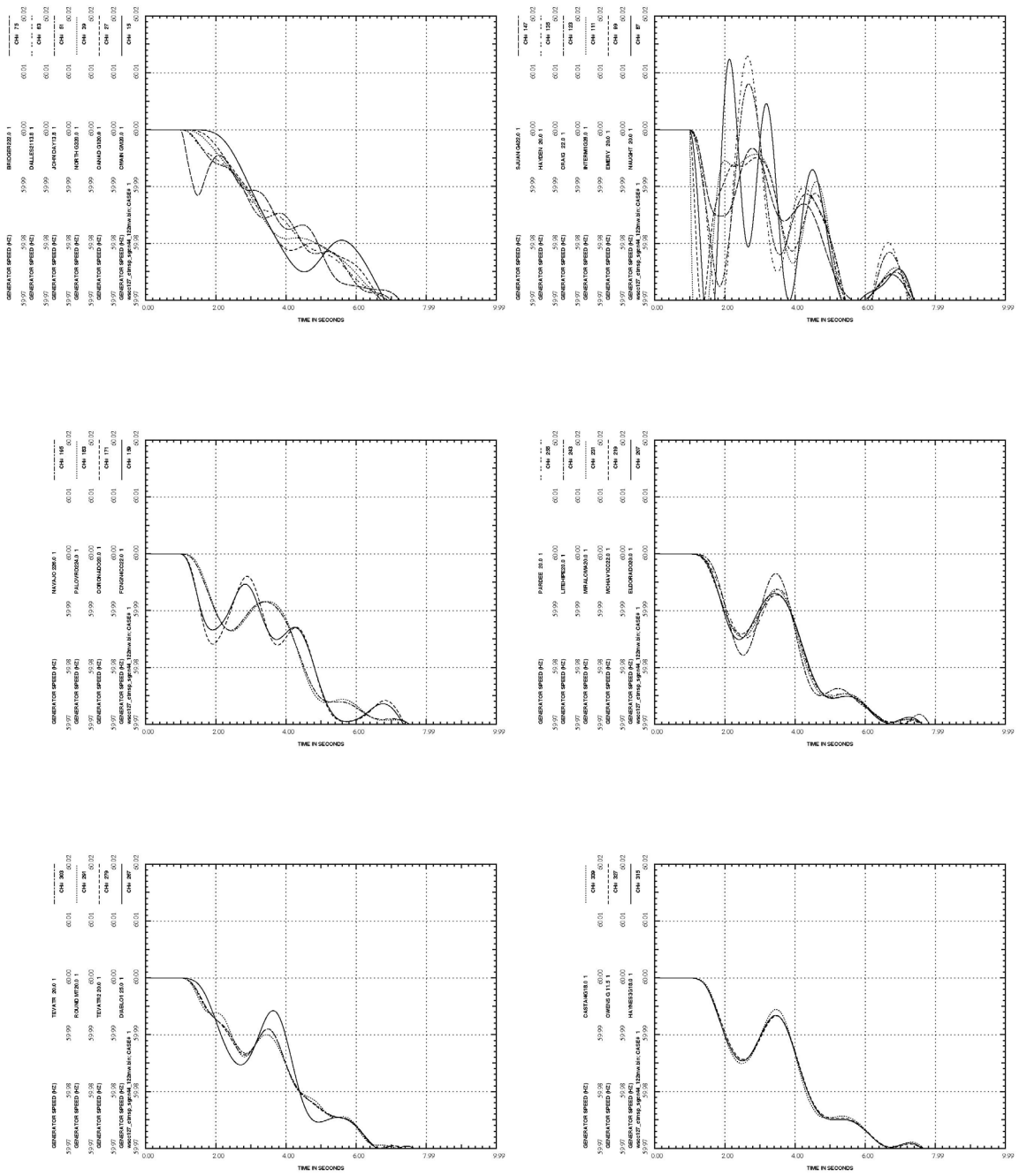

Fig 2-11. Bus frequencies at generator buses when 122.8 MW and 24.7 MVAR is tripped from bus 44

3. Trip 122.8 MW and 24.7 MVAR from generators bus 91

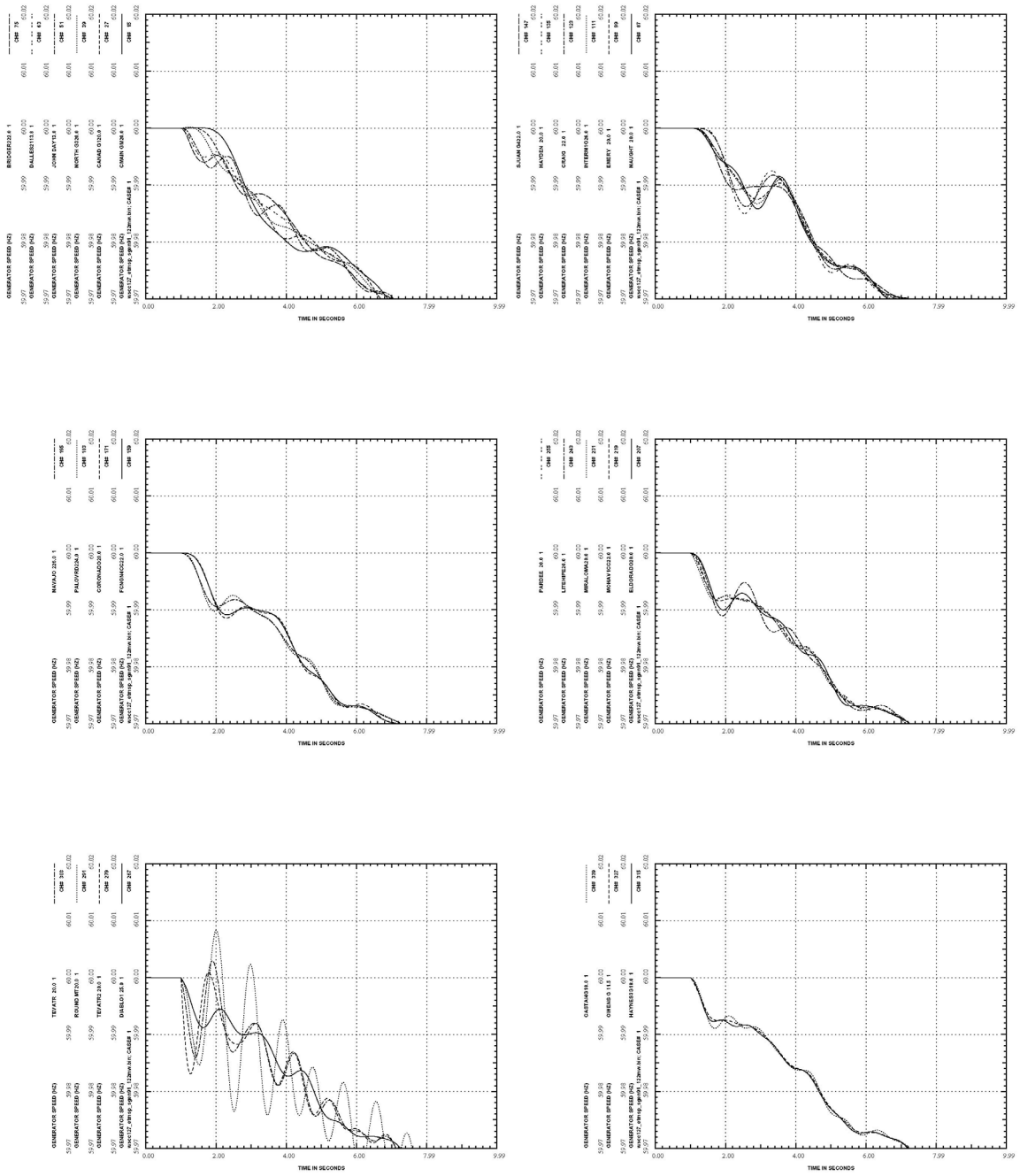

Fig 2-12. Bus frequencies at generator buses when 122.8 MW and 24.7 MVAR is tripped from bus 91

From simulation results we can observe that when some generation is disconnected from the system, the frequencies at all buses will decrease and never come back to steady state due to the lack of power compensation from other generators. Due to this fact, our observation of the frequency variation would need to set a cut-off point. We choose to look at the frequency variation at 2 seconds after the generation trip, based on the assumption that the governor would not have effect on the system's frequency after 2 seconds from the trip time. And when governors do have effect on generator's output power, the frequency will stop declining but start rising.

The frequencies could vary by 0.005 Hz or more in 2 seconds after a generation drop of 122.8 MW and 24.7 MVAR at any generator bus in the WECC 127 system. The observation implies that for a tripping of the generation, as small as 0.2% of the system's total generation power, the variation of the frequencies would be significant enough to be captured by the FDR placed anywhere in the system.

Note that the above findings are only based on the simplified WECC 127 system from simulations. The findings need to be verified with measurements or more realistic system model.

2.4 Eastern US interconnected System

2.4.1 System description

Eastern US interconnected transmission system contains the major portion of the NERC (North American Electric Reliability Council). Fig 2-13 shows the coverage area of the system model in the U.S. with some identified 345 KV and higher voltage lines/buses.

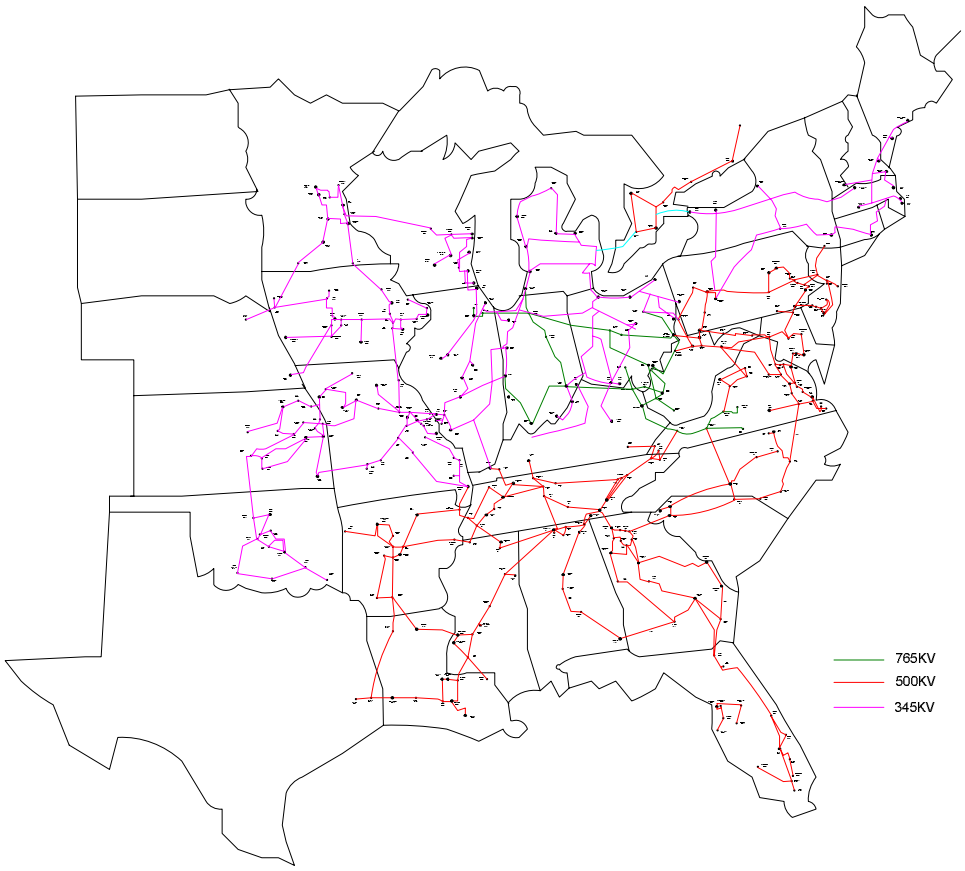

Fig 2-13. Eastern US interconnected transmission system of 345 kV and higher voltage levels

This system model is comprehensive and detailed and contains voltage levels from 765 KV down to the distribution levels. Excluding out-of service buses/units, there are 2287 generators and 16016 buses (only some of them are shown in Fig 2-13). In addition, there are 20093 transmission lines and 7221 branches with transformer(s). At this time of

writing, we have confidentiality agreement with the provider of the system model, therefore, details of the system model cannot be provided.

The data is in the PTI format, so we used Power System Simulator for Engineering (PSS/E) version 29.3 to perform simulations. From the power flow solution, the system's total active generation power is 590476.8 MW and total reactive generation power is 137509.9 MVAR. In this part of study, we drop a generator as a whole unit without splitting it.

2.4.2 Findings and generator tripping simulations

Again, we are to find out how small the generation drop is with the focus on the active power, would cause any bus in the system experience a 0.005 Hz variation therefore this variation can be recorded by the FDR. To search for this minimum generation drop, we tried different amounts of generation drops in the system and examined the bus frequency variations of some selected buses across the system. The simulation results suggest that any generation drop of 500 MW or higher, which is about 0.084 % of the system's total active power, or more would result in a 0.005 Hz variation from its steady state frequency at any bus in the system.

In the following examples, we show frequencies from randomly selected buses. The monitored bus numbers and their corresponding bus names are listed in Table 2-4. Bus names are the names used in the model, and do not necessarily correspond to the actual names that are being used in field.

Bus number	Bus name	Bus number	Bus name
61604	PR ISLD3	29385	20JKSMIT
61695	AS KING3	27008	11MIL CK
62424	SYCAMOR3	31747	SIOUX
64065	COOPER 3	36255	COLLI
57968	STILWEL7	36421	ZION ; R
57972	HAWTH 7	39214	EDG 345
96049	7THOMHL	22655	05COOK
99486	8ANO	28289	18PALISA
98246	8WGLEN	21660	02AVON
98937	8B.WLSN	22703	05CONES
79	8RACCOON	90004	CONEM-GH
52	8BFNP	90021	SUSQHANA
15037	8HATCH	77404	OSWEGO
40275	MARTIN	80116	NANTICOK
11105	8OCONEE	70486	VTYNK345
14903	8CHCKAHM	72692	NWGTN345
14917	8MT STM	90017	CHALK PT
1	8SHAWNEE		

Table 2-4. Recorded bus numbers and the corresponding bus names in the Eastern US interconnected system

The following shows three examples of the bus frequencies at some selected buses when a generator of 500 MW or around is tripped in the system.

1. Trip generator at bus 22600 (05Zelda) (501 MW and -22.6 MVAR)

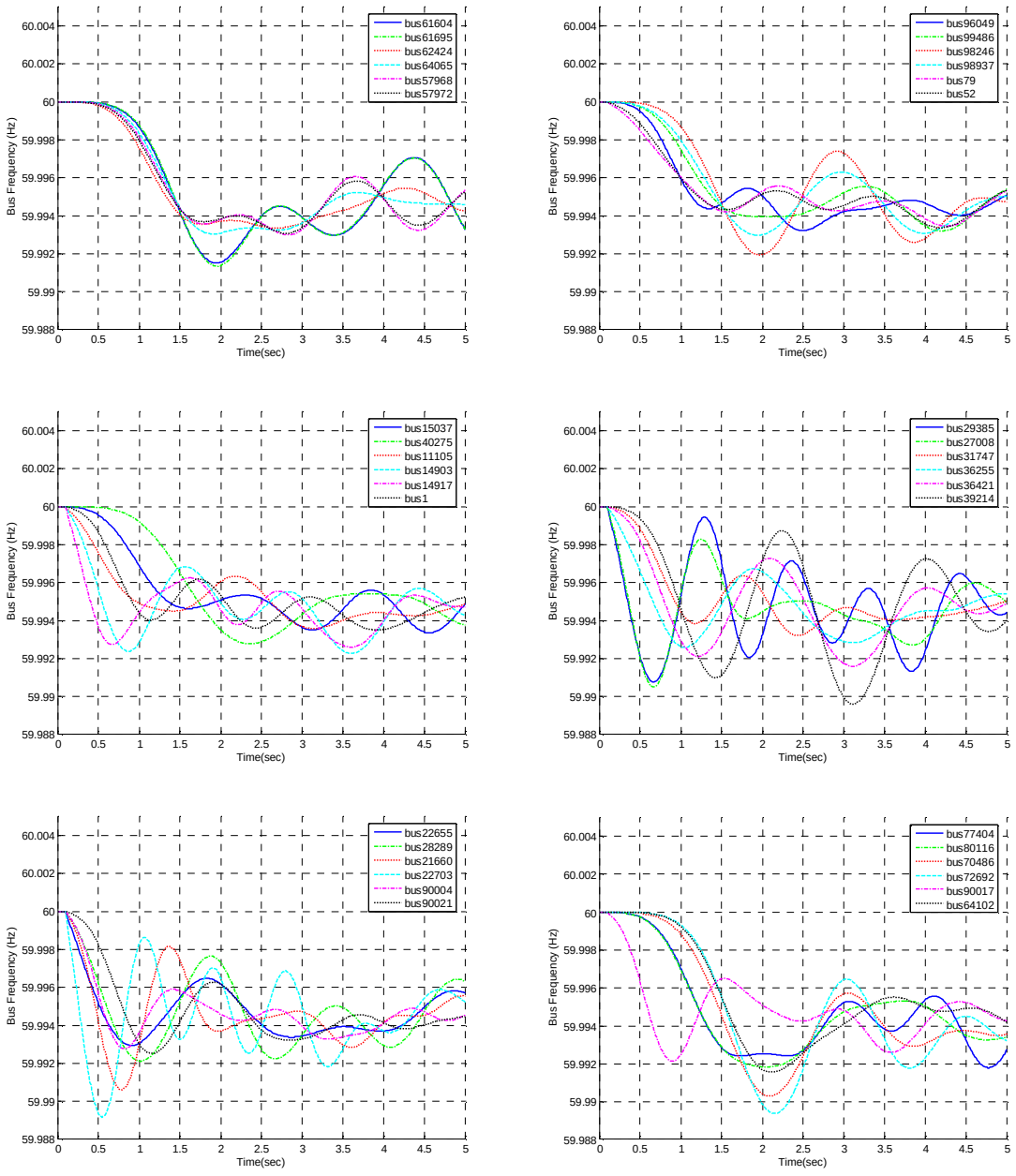

Fig 2-14. Bus frequencies when the generator bus 22600 is tripped

2. Trip generator at bus 79527 (Gilboa #1) (500 MW and 3.3 MVAR)

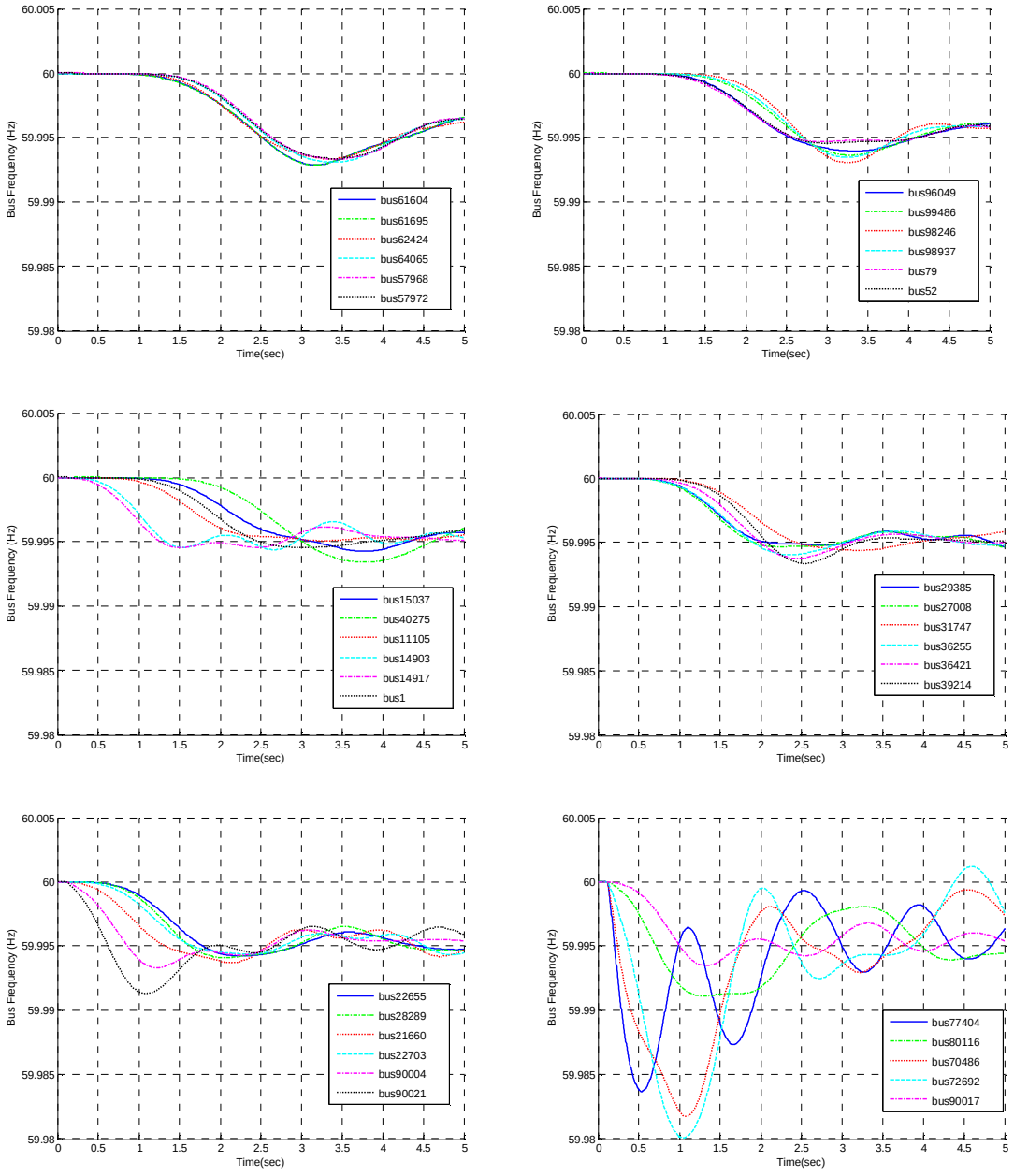

Fig 2-15. Bus frequencies when the generator bus 79527 is tripped

3. Trip generator bus 98243 (G3WGLEN) (500 MW and 55.7 MVAR)

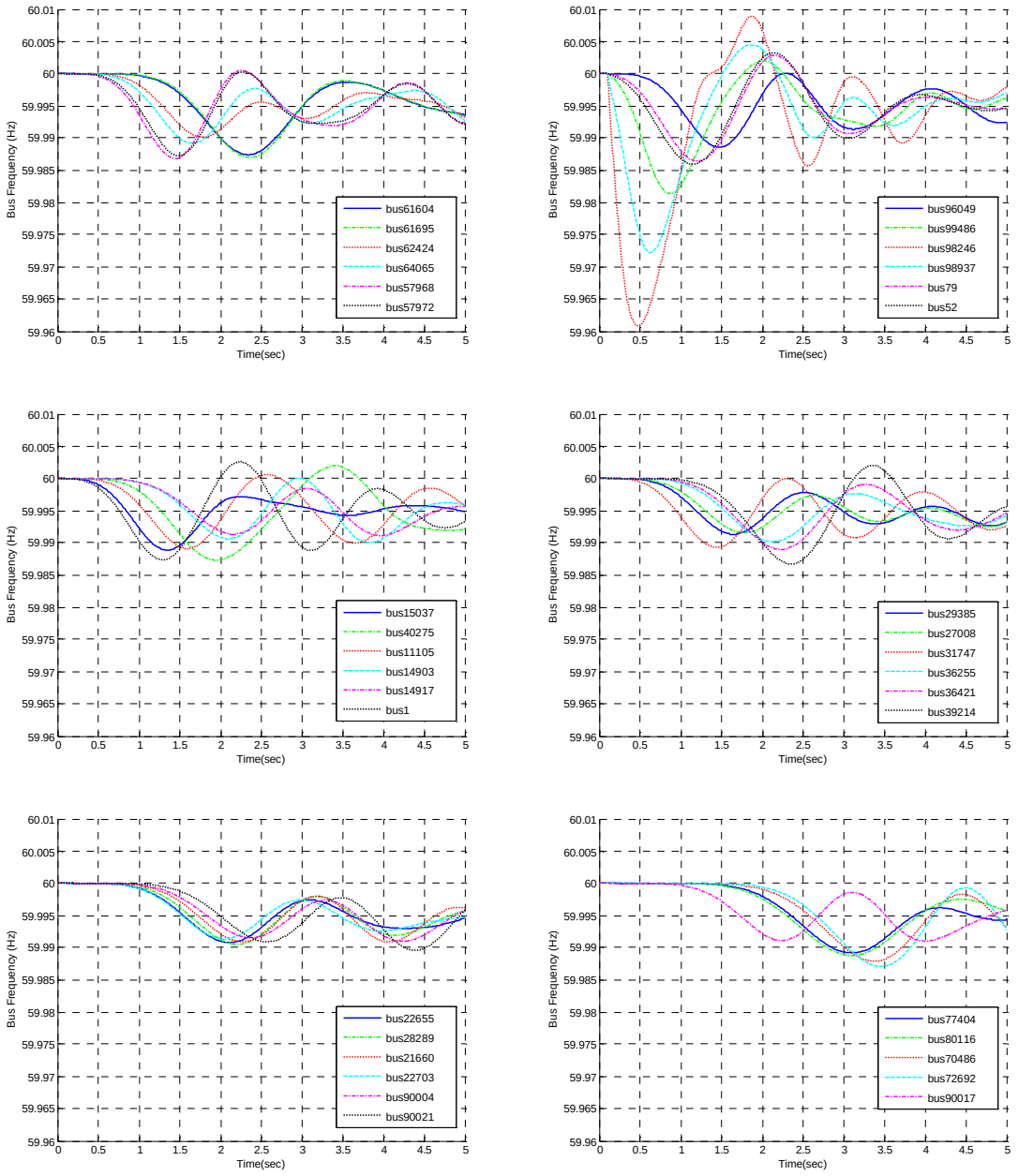

Fig 2-16. Bus frequencies when the generator bus 98243 is tripped

From the above simulation results, we could observe that when there is some generation tripped from the system, bus frequencies would decrease first and oscillatory increaing back to a new steady state; in addition, the frequency variation differs from bus to bus. As

the simulation results suggest, any tripping of 500 MW or greater in the Eastern US interconnected system would result in a 0.005 Hz variation in the bus frequency at any point in the system, and this variation could be captured by the FDR. From the animation, we could also observe that the most influenced buses are the buses that are near to the disturbance points. The disturbance propagates like electromechanical wave to the rest of the system. The farther the electrical distance from the disturbance incipient point, the later it will see the variation.

2.5 Summary

The simulation results suggest that for EUS system, the disconnection of 500 MW, which corresponds to 0.084% of system's total active generation power, or more from any generator would cause the bus frequencies to vary by at least 0.005 Hz. For NE 39 system, the minimum disconnection of 6.19 MW and 1.59 MVAR, which corresponds to 0.1% of the NE system's total generation power, would cause the frequencies to vary by 0.005 Hz or more at all generator buses.

For WECC 127 system, we only looked at the frequency variations during the first 2 second, since the data does not include governor control to compensate the generation drop in the system. This criterion is selected based on the mechanical torque output response of the NE 39 system. From the NE 39 system, we could see that typical mechanical output torques stay as the pre-fault condition and starts to increase 1 second after the generation drop in the system. Also, the frequency starts to increase instead of decreasing after governors are in action. From the study, it is shown that a tripping of 122.82 MW and 24.66 MVAR, which corresponds to 0.2% of the system's total

generation, from any generator would cause 0.005 Hz or more frequency change at all generator buses within the system.

Table 2-5 summarizes the minimal tripping power for the bus frequency varying at least 0.005 Hz at all the buses of the 3 systems we studied.

System	Minimal tripping power for all the buses in the system to see 0.005 Hz deviation	Minimal tripping power as a percentage of system's total power
New England 39	6.19 MW and 1.59 MVAR	0.1%
WECC 127	122.82 MW and 24.66 MVAR	0.2%
Eastern US interconnected	500 MW	0.084%

Table 2-5. Summary of the minimal tripping power for all the buses to experience at least 0.005 Hz deviation

Chapter 3 Frequency Wave Propagation

3.1 Introduction

The frequency disturbance propagation phenomenon is noted in [75-77] and also in our FNET (National Frequency Measurement Network) measurement data, as shown in Fig 3-1 and Fig 3-2. Details of FNET measurement results will be discussed in Chapter 6. Electromechanical wave phenomenon of power system disturbances has been known to power engineers [78, 79]. Not only does actual recording reveal some characteristics of the disturbance propagation, mathematical derivation further illustrates that the disturbance propagation exhibits a form of wave [78, 80]. Data from both phasor measurement unit (PMU) and frequency disturbance recorder (FDR) indicate that the frequency responses are notably delayed from measurement point to point when certain events occur in the system, e.g. generation trip, line trip, load rejection, etc.

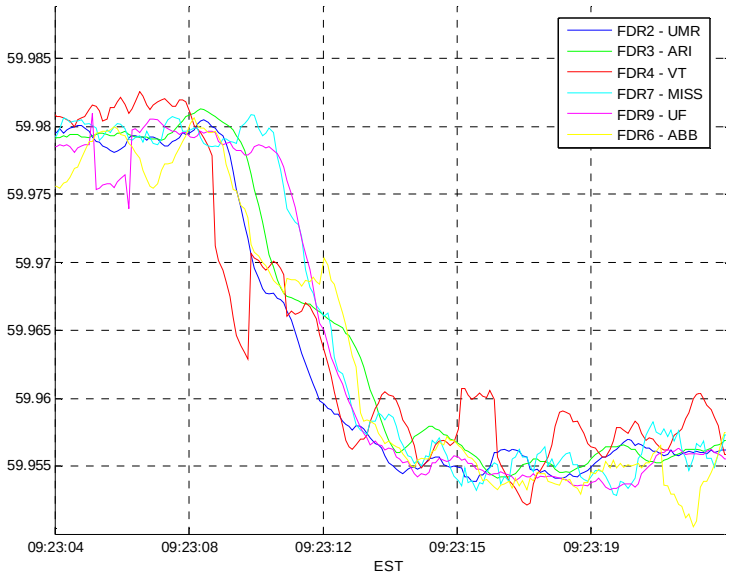

Fig 3-1. 2004/8/4 Bus frequency at various FDR locations when some generation is tripped at Davis Beese in Ohio

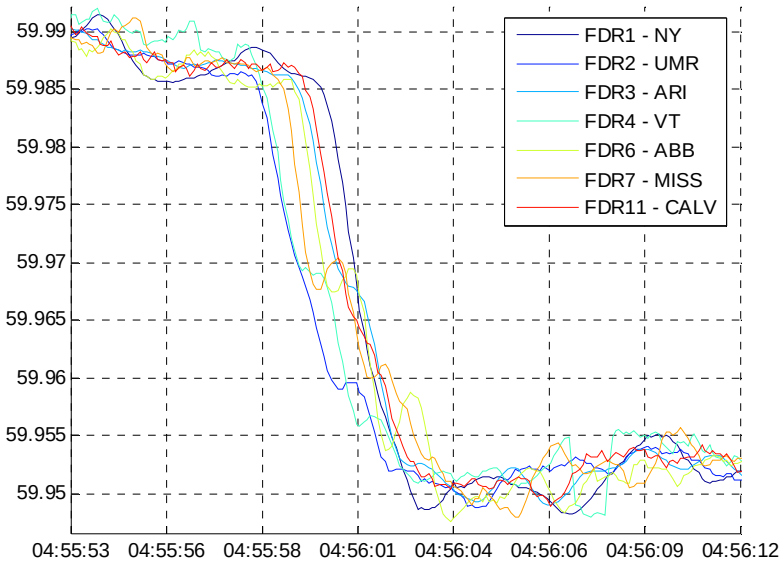

Fig 3-2. 2004/9/19 Bus frequency at various FDR locations when some generation is tripped at Watts Bar in Tennessee

In this chapter, we will study how the frequency disturbance propagates due to generation trip from simulations in 2 major U.S. systems - the Western Electricity Coordinating Council 127 bus system (WECC 127) and the Eastern US interconnected system (EUS). And we will discuss how we define the disturbance propagation as a form of electromechanical wave propagation. In addition to generation trip, we look at the propagation due to line trip and load rejection in EUS. At last, we setup uniform models of single-line, multi-line and mesh system to see how the frequency wave travels in those systems.

In addition to time-series frequency presentations, we created some playback animations from simulation data to visualize the frequency wave propagation phenomenon. We will show how the visualizations were made; and for each visualization result, some findings

will be discussed.

3.2 Generator trip

From generator trip simulations on NE 39, Fig 2-2, Fig 2-4, Fig 2-6, and Fig 2-8, on WECC 127, Fig 2-10, Fig 2-11, and Fig 2-12, and on EUS, Fig 2-14, Fig 2-15, and Fig 2-16, the frequency responses show that at different observing points in the system, we can see different frequency variations. Due to the trip, the frequency always drops from its pre-fault value (60 Hz in simulation). This can be understood by a simplified system, where there are only a generator and a load. The active power injection at the generator bus to the system can be written as the swing equation shown as following:

$$\frac{2H}{\omega_s}\cdot\frac{d\omega_i}{dt} = P_{mi} - P_{ei}$$
$$\frac{d\delta_i}{dt} = \omega_i \qquad \textbf{(3-1)}$$

Where H is the inertia constant, ω_s is the synchronous speed (2*π*60 rad/sec), ω_i is the angular speed at bus i, P_{mi} is the mechanical power from generator and P_{ei} is the electrical power injecting into the system (or power consuming by the load). The units of P_{mi} and P_{ei} are per-unit.

If a generator is tripped from the system, P_{mi} equals to 0 in (3-1) and the right hand side of the first equation of (3-1) becomes $-P_{ei}$. And $d\omega_i/dt$ has to be negative. So the change of frequency will be negative therefore frequency will decrease.

In addition, depending on locations, some buses may experience more oscillatory than others. Typically, the most significant fluctuation would occur at the bus where the

generation power is tripped and nearby buses. If governors exist, which is to regulate the mechanical power output of the generators and compensate the change of frequency, the frequencies would stabilize to a new steady state value, other than 60 Hz. If no governor exists, the frequency will continue going down, given the consumption power does not change.

More importantly, we can see that a noticeable time difference of the beginning of frequency decline due to the trip in WECC 127 and EUS simulations, a duplication of part of Fig 2-15 is shown below. NE 39 is a relatively tight system, therefore, no significant frequency delay between buses can be observed.

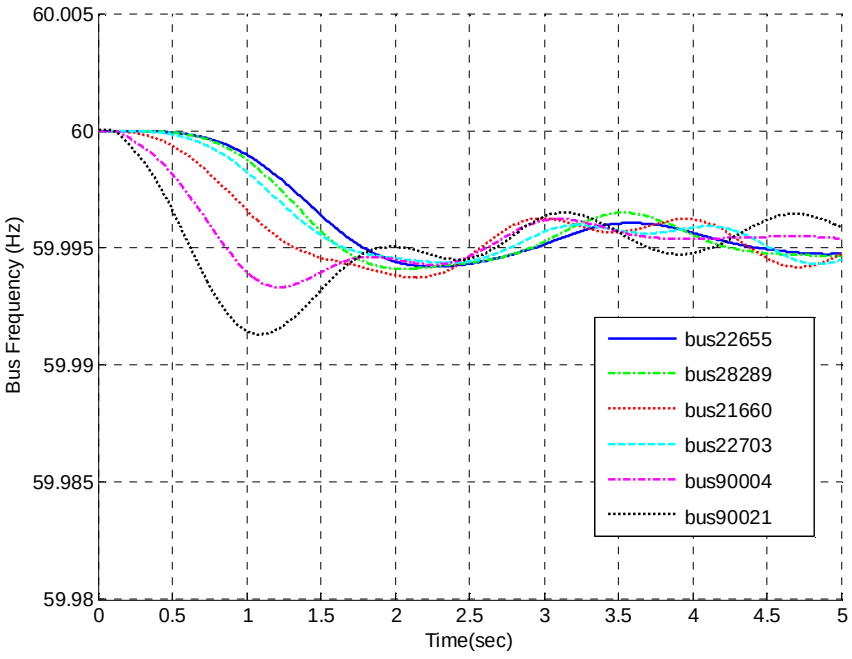

Fig 2-15. Bus frequencies when the generator bus 79527 is tripped (part)

3.3 Load rejection

Similarly to generation trip, load rejection introduces power imbalance in the system. The major difference is that load rejection makes the generation greater than consumption (in majority composing of loads); therefore, we can anticipate that, in contrary to generation trip, the bus frequencies in the system would go up. This can be understood by making P_{ei} be 0 in (3-1) and the change of frequency becomes positive. We chose EUS to simulate several load rejection cases, since EUS is a closer-to-real-system model.

In the EUS, we selected several buses to record frequencies in simulations. These buses are the nearest high-voltage buses to FDRs' location. The bus number and name and the corresponding FDR unit name is listed in Table 3-1. FDR locations can be found in Fig 1-8. We randomly selected buses to trip their loads. Three examples are included here. In the following plots, we will use FDR names with a prime as a representation of the frequency at the nearest high voltage buses to the FDRs.

FDR unit	Nearest high voltage buses to FDRs				
	Bus number	Plot legend	Bus voltage (KV)	Bus Name	Bus Location
NY	78980	NY'	230	ROTRDM.2	RotterDam, NY
UMR	96041	UMR'	345	7FRANKS	Franks,MO
ARI	14053	ARI'	230	6JEFF ST	Jefferson ST.,VA
VT	22567	VT'	345	05M FUNK	Matt Funk, VA

ABB	11107	ABB’	500	8PL GRDN	PleasantGarden,NC
MSSTATE	35	MISS’	500	8W POINT	West Point, MS
UFL	44102	UFL’	230	PKRD	Parker Road, FL
Calvin College	28197	CALV’	345	18ARGENT	Argenta, MI
Tulane	98652	TUL’	230	6MICHO	New Orleans, LA

Table 3-1. Bus number and name of the buses nearest to FDRs

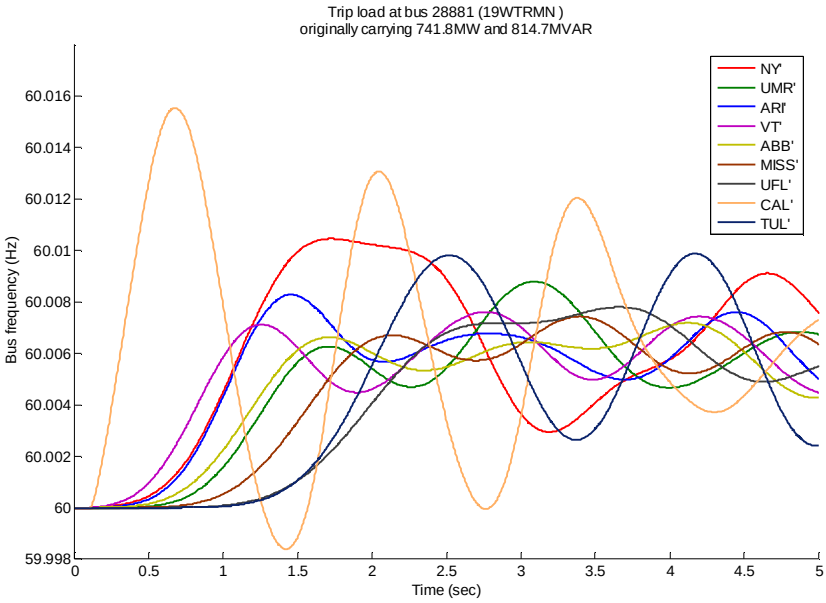

Fig 3-3. Load rejection at bus 28881 with 741.8MW and 814.7 MVAR.

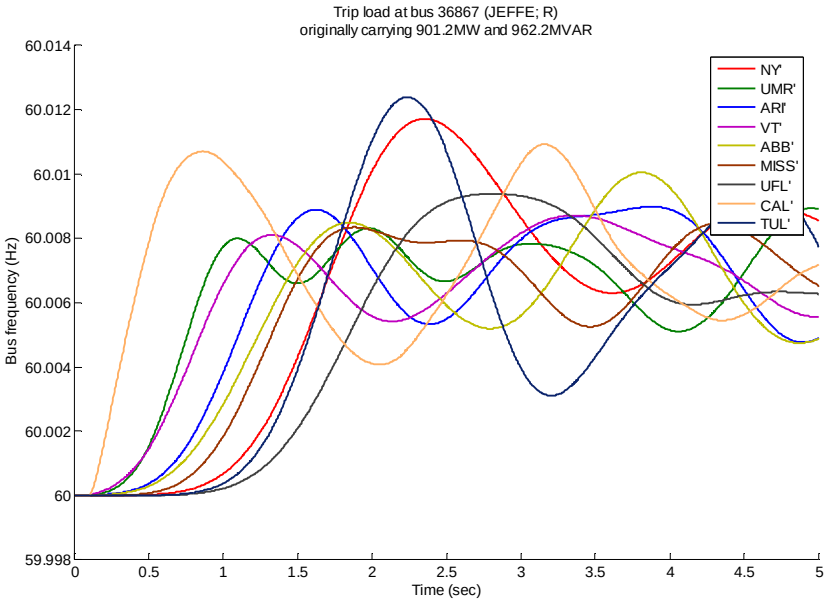

Fig 3-4. Load rejection at bus 36867 with 901.2 MW and 962.2 MVAR

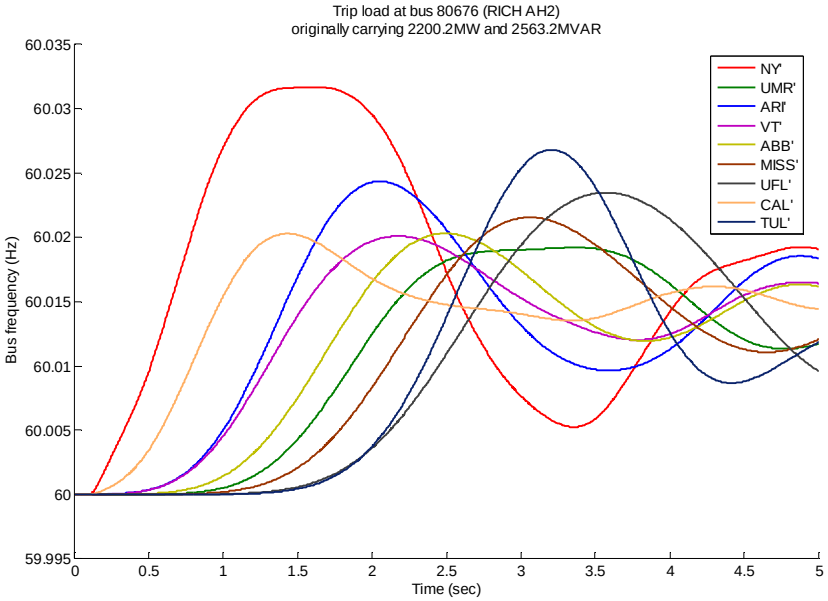

Fig 3-5. Load rejection at bus 80676 with 2200.2 MW and 2563.2 MVAR

As expected, frequencies rise after the load is tripped. Time delay between different units can also be seen. Therefore, the disturbance could propagate throughout the system just

like the generation trip. In other words, from the wide area measurement point of view, we will be able to detect such disturbance. In addition, frequency oscillation is above 60 Hz which indicates that when the system reaches steady state, the frequency will be above 60 Hz, unless proper action is taken by the AGC to correct this bias.

3.4 Line trip

In this section, we investigate the frequency deviation due to a single line trip. Unlike generation trip or load rejection cases, where it is an event at a single node, line trip involves power separation between 2 buses. The frequency responses at different buses would be more complex depending on the type of the tripped line. Tripping a line would typically redistribute the power flow throughout a meshed system; therefore, we can anticipate the frequencies would oscillate around 60 Hz. If the tripped line is a tie line, which means that the 2 ends of the tie line is either a generation center or a load center, tripping such line would make the frequency at the generation center rise because it is just like tripping of loads. On the contrary, at load center buses, the frequencies would decrease because it is like a generation trip.

Numerous cases have been simulated due to the expected more complex frequency response from line trip. Eleven typical line tripping examples are included here, from Fig 3-6 to Fig 3-16.

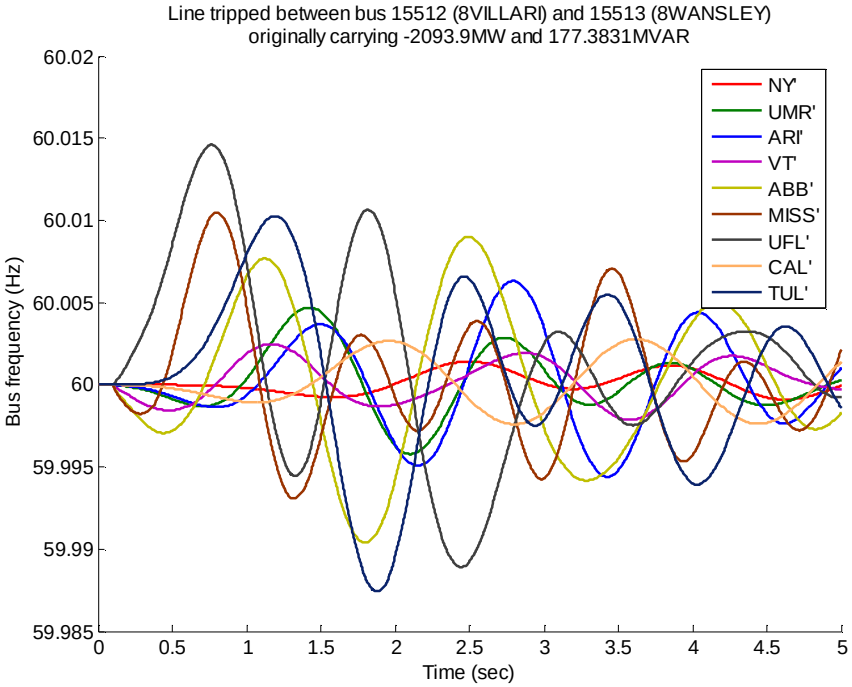

Fig 3-6. Trip line between bus 15512 and 15513

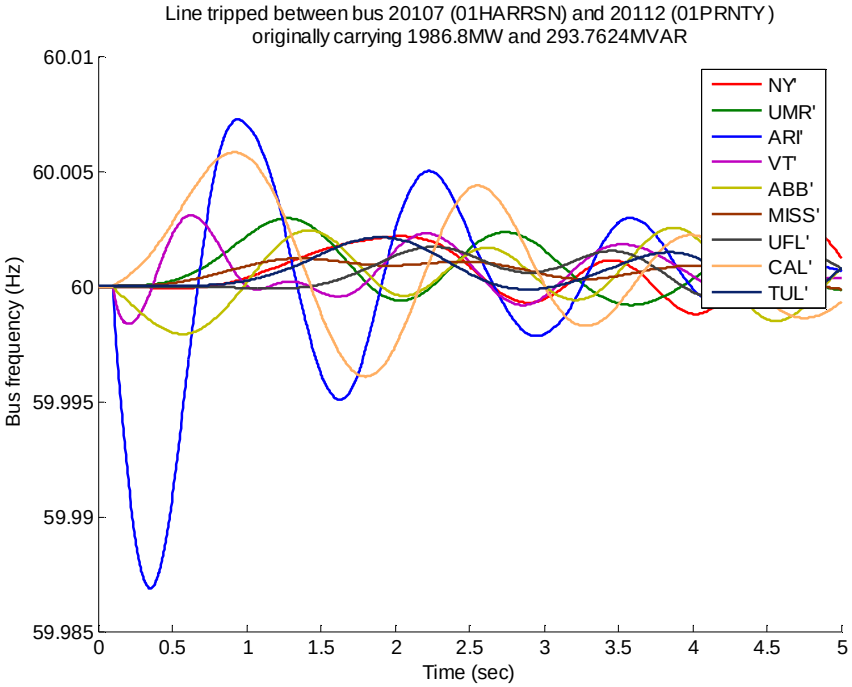

Fig 3-7. Trip line between bus 20107 and 20112

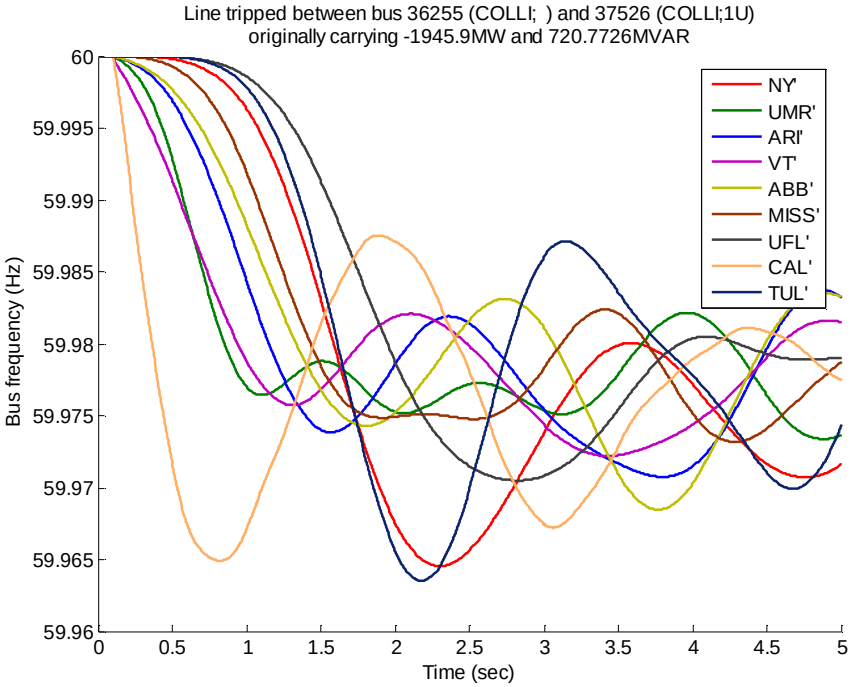

Fig 3-8. Trip line between bus 36255 and 37526

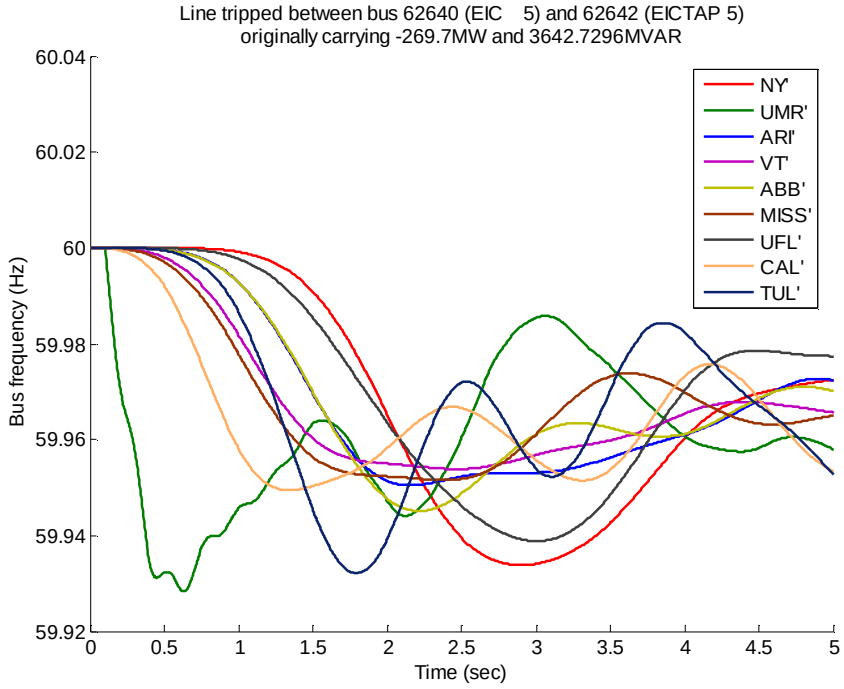

Fig 3-9. Trip line between bus 62640 and 62642

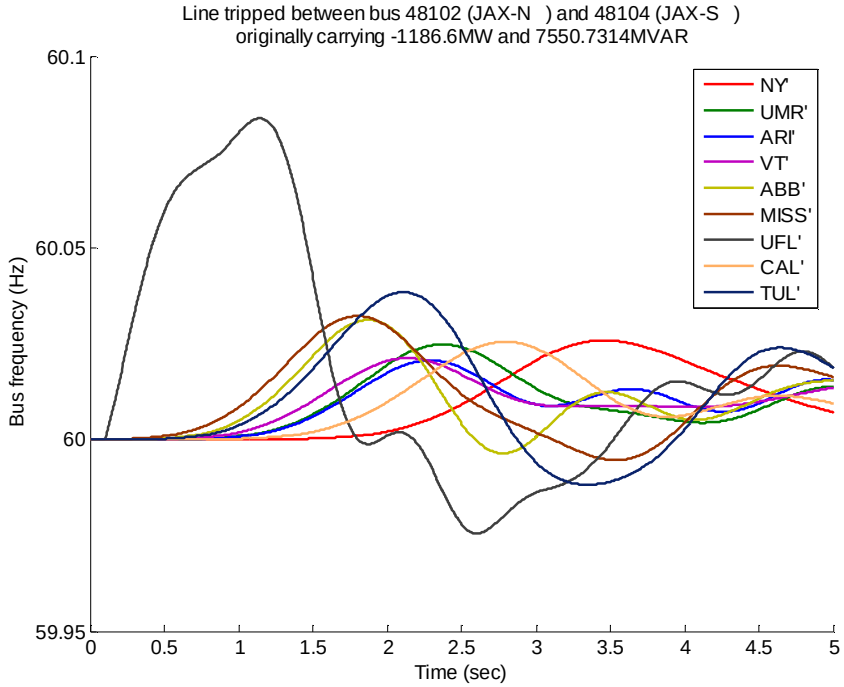

Fig 3-10. Trip line between bus 48102 and 48104

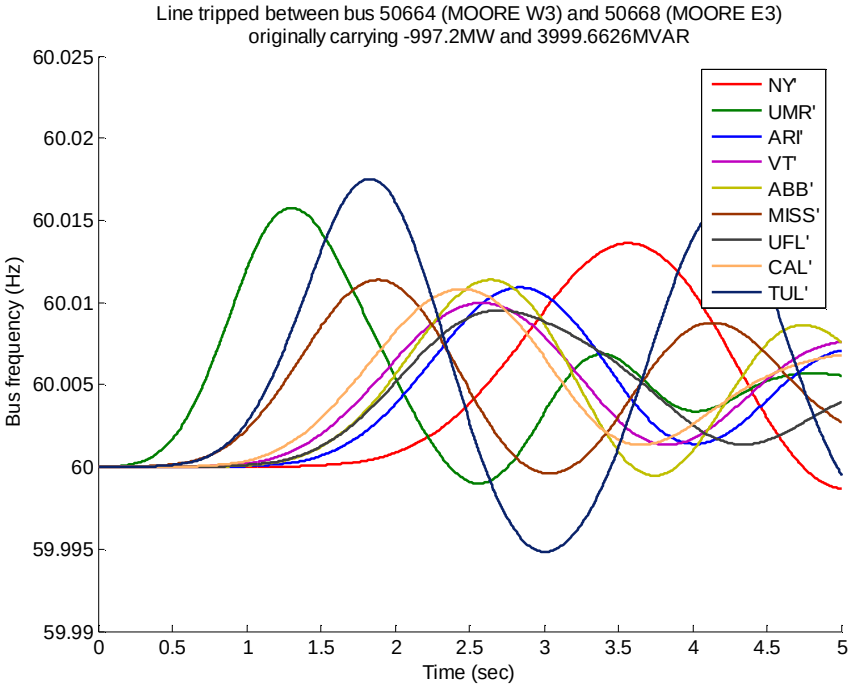

Fig 3-11. Trip line between bus 50664 and 50668

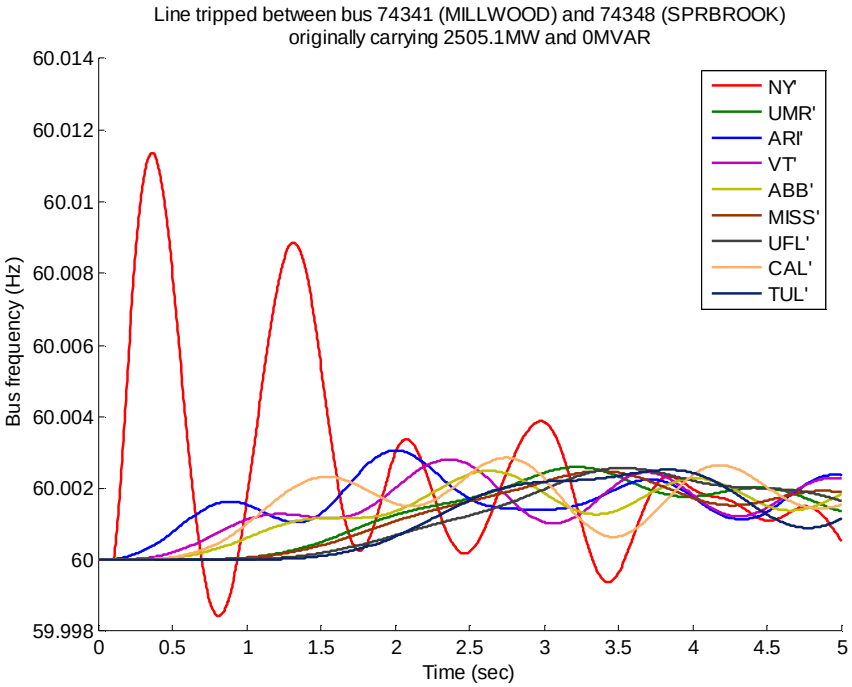

Fig 3-12. Trip line between bus 74341 and 74348

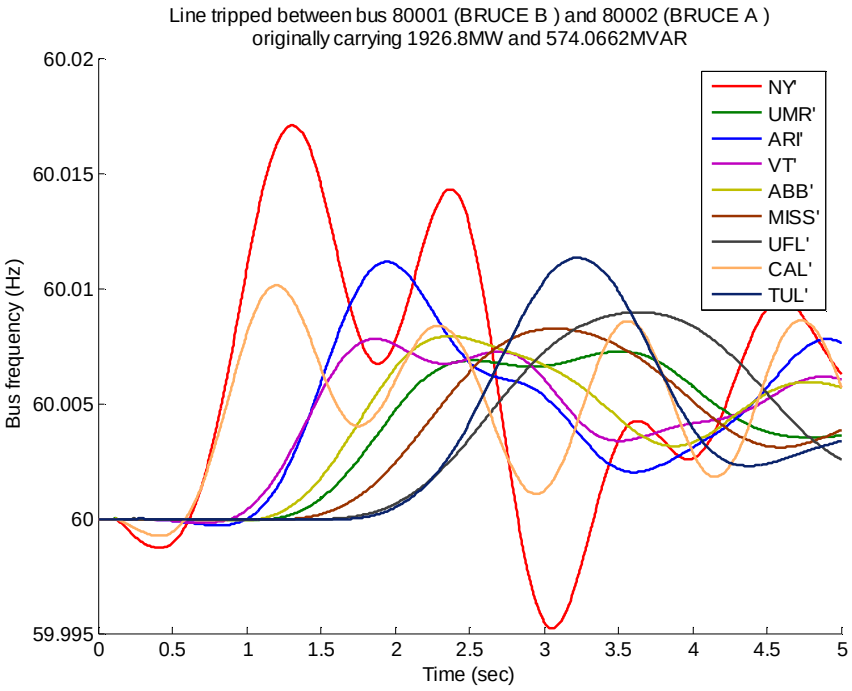

Fig 3-13. Trip line between bus 80001 and 80002

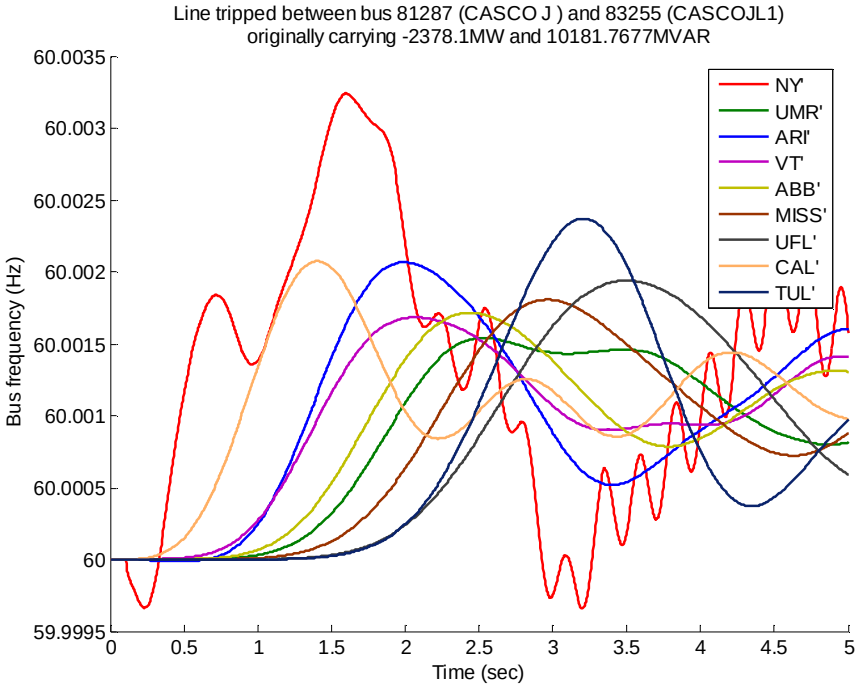

Fig 3-14. Trip line between bus 81287 and 83255

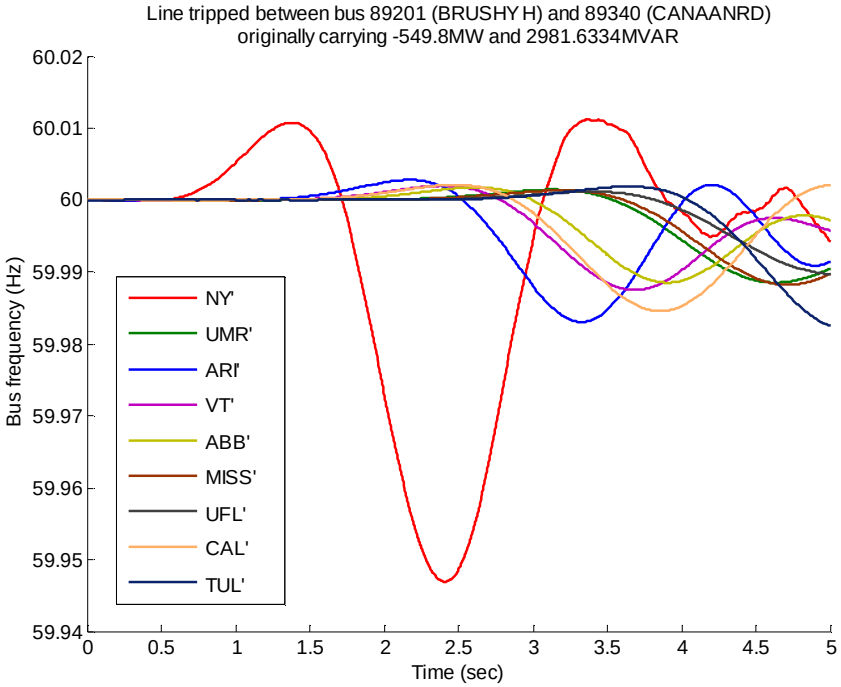

Fig 3-15. Trip line between bus 89201 and 89340

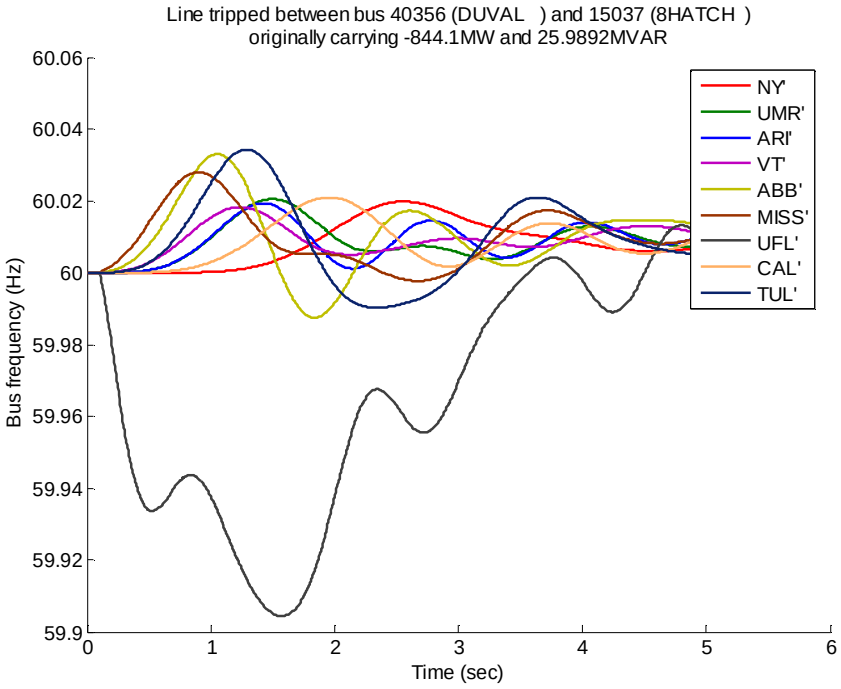

Fig 3-16. Trip line between 40356 and 15037, 15038

From the above simulation results, we can see that frequency responses from a line trip could be mixed. Unlike generation trip or load rejection, where the frequencies at all buses would either all rise or all decline about 60 Hz in the first swing, line trip's frequency response is more complicated. Depending on where we record the frequency, different conclusions can be drawn. Based on the monitored bus frequencies, as listed in Table 3-1, Different types of responses is categorized in Table 3-2.

Frequency response type	Figure number
1. Oscillation about 60 Hz	Fig 3-6, Fig 3-7
2. Like generator trip	Fig 3-8, Fig 3-9
3. Like load rejection	Fig 3-10, Fig 3-11, Fig 3-12
4. Mixed	Fig 3-13, Fig 3-14, Fig 3-15
5. Islanding	Fig 3-16

Table 3-2. Different frequency response types due to line trip

For the first type, the average of monitored bus frequencies is about 60 Hz and the frequencies oscillate about 60 Hz. From the responses, we can conclude that such tripping is within a mesh system and no separation of the system was occurred.

For the second type, the average of monitored bus frequencies is oscillating below 60 Hz. The line is connected to a generation center, relative to the monitored buses, therefore, tripping such line would induce frequency drops in the rest of the system. Additionally, time delay of the frequency drops of the first swing would make such recording look like a generation trip.

For the third type, the average of monitored bus frequencies is oscillating above 60 Hz. The tripped line connects to a large load center relative to the monitored buses; therefore, tripping such line is equivalent to tripping a bus load to the rest of the system, and the frequencies rise in the first swing and oscillate above 60 Hz afterwards. In addition, the time delays of frequencies initial rise can be seen in these cases. If such frequency data set were recorded, it could be concluded as load rejection.

For the fourth type, we can see the frequencies rise and decline about 60 Hz and there is some time-delay of frequency responses between different buses. For these cases, the pattern is unique to all other cases.

For the fifth type, we see a group of bus frequencies oscillate above 60 Hz and one bus frequency oscillates below 60 Hz. This is an indication of islanding, which means that the system is divided into 2 subsystems. One part of the system has more generation than consumption and the frequencies rise; and the other part of the system is lack of generation therefore, the frequencies decline. This case is a combination of type 2 and type 3, where the monitored buses are all within either generation or load center areas, relative to the tripped line.

3.5 Frequency wave propagation visualization

As shown previously, the massive number of frequency plots makes it hard to comprehend how exactly the system responds to different events. To help visualize the frequency variations in the system, we created a replay tool in Matlab® using the simulation data to show the change of bus frequencies. As mentioned in section 1.5, people respond better to visualization results than just numbers or single plots. Therefore, creating such a visualization tool to understand the underlying system global behavior is essential.

The first step to display system's data on a map is to identify where the buses are located geographically. Here we only look at WECC 127 and EUS, since there is no geographical

information of the system for NE 39. For the models (WECC 127 and EUS), although we have the system's coverage area, there is no geographical information available for the bus locations. For a large system, identification of where the bus is on a geographical map can become time-consuming and tedious since the bus names used in the model usually dos not match with the bus names used in the field. Network topology is sometimes used to identify any unknown buses in the system. Sometimes, the map may not show all the buses in the system, so some guess works need to be done first. Then we come back and verify the guessed results.

For WECC 127, the system one-line diagram and geographical area are shown in Fig 2-9. The map was a courtesy of Dr. Arun G. Phadke. We recorded all the frequencies at generation buses for visualization purpose. Recorded bus names and numbers are given in Table 3-3.

number	name	number	name	number	name	number	name
1	CMAIN GM	5	CANAD G1	8	NORTH G3	13	JOHN DAY
19	DALLES21	26	MONTA G1	28	BRIDGER2	33	NAUGHT
38	EMERY	44	INTERM1G	46	CRAIG	47	HAYDEN
49	SJUAN G4	53	FCNGN4CC	56	CORONADO	60	PALOVRD2
62	NAVAJO 2	65	ELDORADO	67	MOHAV1CC	72	MIRALOMA
76	LITEHIPE	81	PARDEE	88	DIABLO1	91	TEVATR2
96	ROUND MT	102	TEVATR	113	HAYNES3G	119	OWENS G
126	CASTAI4G						

Table 3-3. Recorded generators (bus name and number) in WECC 127

For EUS, the system model has 16016 buses from 765 kV down to distribution levels. Among all the buses, we were able to identify all the 765 kV buses and about 70% of the

500 kV buses and about 30% of the 345 kV buses in the system model on the map. Out of these identified buses, we selected 160 buses, mainly the ones that are connected to generators, to record the bus frequency in simulations. The 160 buses are carefully selected to be dispersed enough, yet not over simplified for dense areas, especially mid-west and northeast regions. The dispersion of points gives us a margin to interpolate data to a larger region. For dense areas, more points are needed to represent the frequency variations when scenarios are introduced to the system.

In simulations, the selected buses are listed in Table 3-4 to record the frequency for animation analysis.

Number	Name	Number	Name	Number	Name	Number	Name
61662	SHERCO 3	542	8HAYWOOD	31747	SIOUX	74002	ROSETON
61655	MNTCELO3	85	8WBNP 1	30395	COFFEEN	77404	OSWEGO
61702	BLUE LK3	81	8SNP	36343	KINCA; R	75404	KINTI345
61608	WILMART3	79	8RACCOON	32346	CLINTON	79584	NIAG 345
61604	PR ISLD3	52	8BFNP	33161	DUCK CRK	80116	NANTICOK
61695	AS KING3	15004	8MILLER	36379	POWER; R	80001	BRUCE B
62492	CBLUFFS3	16154	8FARLEY	36255	COLLI;	80026	LENNOX
62424	SYCAMOR3	15001	8BOWEN	36295	CRAWF; R	90013	SALEM
62660	OTTUMWA3	15513	8WANSLEY	36421	ZION ; R	73110	MILLSTNE
62549	ARNOLD 3	15510	8SCHERER	39432	PLS PR1	71551	STNY BRK
62207	LAISA 3	15037	8HATCH	39367	OK CRK	72926	NRTHFLD
36382	QUAD ;	15505	8WMCINTS	39214	EDG 345	70486	VTYNK345
64065	COOPER 3	43555	CRYST RV	38900	PT BCH4	71193	CANAL
56753	JEC 7	40275	MARTIN	39630	KEWAUNEE	70759	MYSTIC
56762	WOLFCRK7	11101	8BAD CRK	39176	SFL 345	72694	SEBRK345
57968	STILWEL7	11102	8JOCASSE	39157	COL 345	72692	NWGTN345
56756	NEOSHO 7	11105	8OCONEE	28268	18LUDING	70088	WYMAN
57982	IATAN 7	11103	8MCGUIRE	30265	CAMPBELL	70086	ME YANK
57972	HAWTH 7	10015	8MAYO 1	28289	18PALISA	90017	CHALK PT
59201	SIBLEY 7	14906	8CLOVER	22655	05COOK	60441	GARRISN4
96049	7THOMHL	14903	8CHCKAHM	28274	18MCV	60519	OAHE 4
30224	CALWY 1	14918	8NO ANNA	28245	18HAMPTO	64102	GENTLMN3
30886	LABADIE	14922	8POSSUM	21630	02DAV-BE	56449	HOLCOMB7

31669	RUSH	14901	8BATH CO	21660	02AVON	40119	TURKEY P
96046	7NEWMAD	14917	8MT STM	21650	02PERRY	40280	FT.MYER2
54803	SONR 7	20106	01FMARTN	22703	05CONES	70027	ORRINGTN
55045	SEMNL7	20107	01HARRSN	22623	05TIDD	65023	DAWSONCT
99486	8ANO	22564	05AMOS	22611	05KAMMER	60604	TIOGA4 4
99818	8ISES 5	22560	05BAKER	22568	05MOUNTN	11269	LOOKOUT
99340	8WH BLF	29385	20JKSMIT	22607	05GAVIN	60635	STEGALL3
99148	8STERL	27013	11TRIMBL	22609	05KAMMER	60633	SIDNEY 3
97916	8NELSON	42	8PARADIS	26648	09STUART	53615	WELSH 7
97301	8CAJUN2	1	8SHAWNEE	27621	15BVRVAL	97691	8CYPRESS
98246	8WGLEN	27665	15AES	20106	01FMARTN	97478	6JACINTO
98539	8WATERFO	22607	05GAVIN	90010	KEYSTONE	51437	TOLK W 6
541	8PLSNTHL	27008	11MIL CK	90004	CONEM-GH		
98937	8B.WLSN	22671	05ROCKPT	90020	SUNBURY		
98952	8G.GULF	26220	08NOBS1	90021	SUSQHANA		
40	8CUMBERL	28011	17SCHAHF	90012	PEACHBTM		
37	8JVILLE	32274	BALDWIN	90023	LIMERICK		

Table 3-4. Recorded Eastern US interconnected system bus numbers and the corresponding bus names

We created two animation versions, namely dot and surface, for different representations,. In the dot animation version, a bus shows a dot when the frequency firstly drops by 0.005 Hz from its steady state – 60 Hz. At each time step, a search is performed to find the buses that frequencies have been deviated by at least 0.005 Hz. The procedure of how to generate the dot-version animation movies is shown in Fig 3-17.

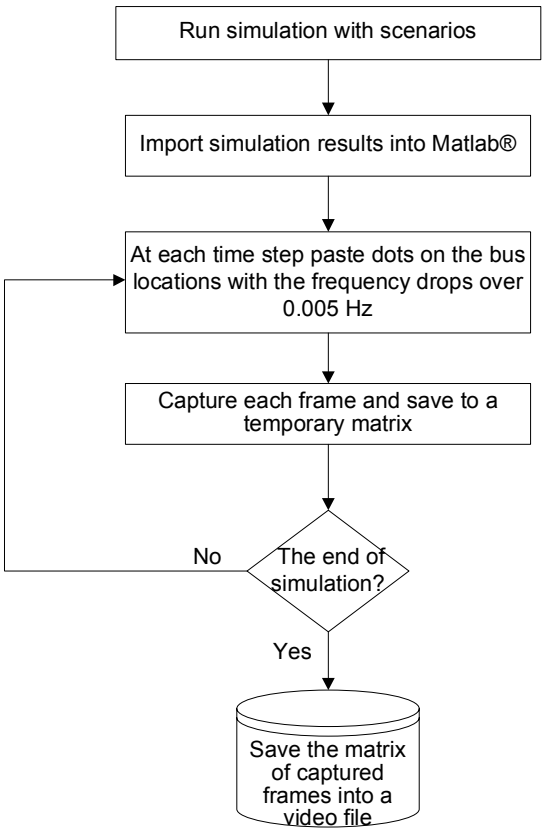

Fig 3-17. Data visualization flow chart for dot version animation

For the surface animation version, the value of each surface point in the system's coverage area is interpolated from recorded bus node frequencies. From the simulation, the time series of frequency is recorded for each bus node. Points are discrete in the coordinate; we then perform a 3-dimensional interpolation in Matlab[12] to create a smooth surface between points. For each time step, a new surface is generated, and the surface is captured to a frame and frames are saved to create a playback movie. The procedure for generating a surface-version animation is shown in Fig 3-18. In this version, visualization results show not only the first swing but also oscillations afterwards, which is indeed illustrate certain characteristics of the frequency disturbance wave propagation.

[12] http://www.mathworks.com

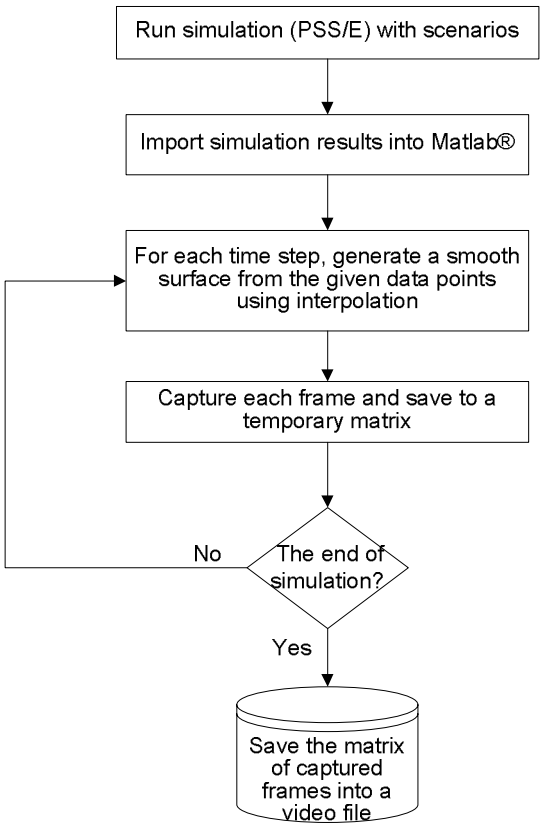

Fig 3-18. Data visualization flow chart for surface version animation

The generated movie file from Matlab® is saved in avi format, which can be played back in most commercial-available video software (e.g. Windows Media Player[13], RealPlayer[14] and etc.). Following are some examples of snapshots from the movies after scenarios are introduced to the system. Here we illustrate examples of generator trips in WECC 127 and EUS, line openings in EUS and load rejections in EUS. For surface version animations, please note that the range of color bar (on the left side of each plot) corresponds to the maximum and minimum of the frequencies of each scenario in the period of simulation time.

[13] http://www.microsoft.com/windows/windowsmedia/mp10/default.aspx
[14] http://www.real.com

3.5.1 WECC 127 generation trip (dot-version)

Fig 3-19, Fig 3-20, and Fig 3-21 show three examples when 122 MW and 24 MVAR were tripped independently from a generator in WECC 127. Fig 3-19 shows the the movie snapshots when the generation trip occurs at bus 5 in Canada, Fig 3-20 shows the movie snapshots when the generation trip occurs at bus 44, and Fig 3-21 shows the movie snapshots when the generation trip occurs at bus 91 in California. The buses experienced the first 0.005 Hz variation from its steady state (60 Hz) show in blue dots. The tripped bus is labeled as a red dot. In addition, the time from the trip initiation when the frequency drops by 0.005 Hz is also labeled beside each bus node.

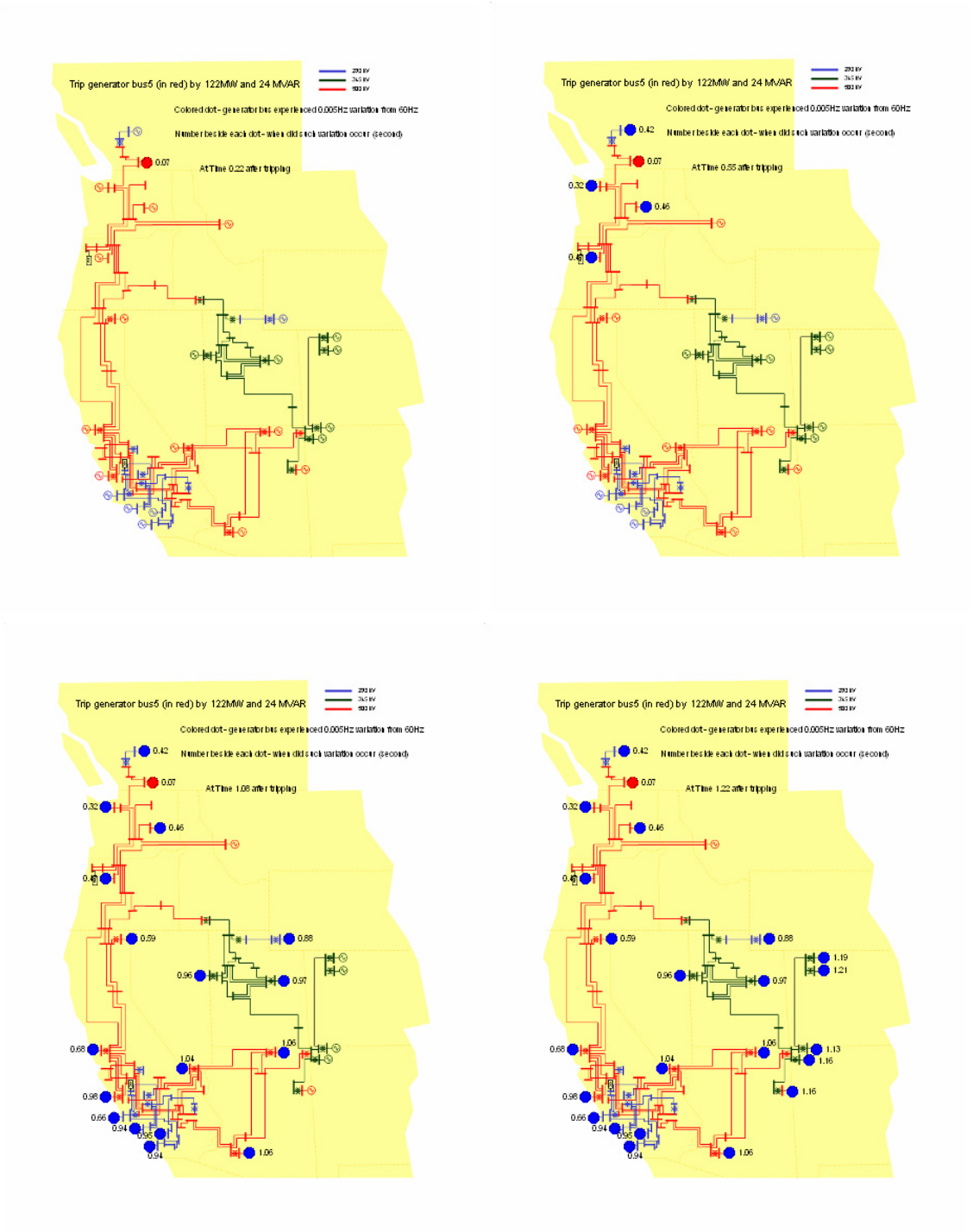

Fig 3-19. Animation snapshots when generator at bus 5 (in British Columbia, Canada) tripped by 122 MW and 24 MVAR. The number beside each bus number is the time when the frequency first drops by 0.005 Hz after tripping.

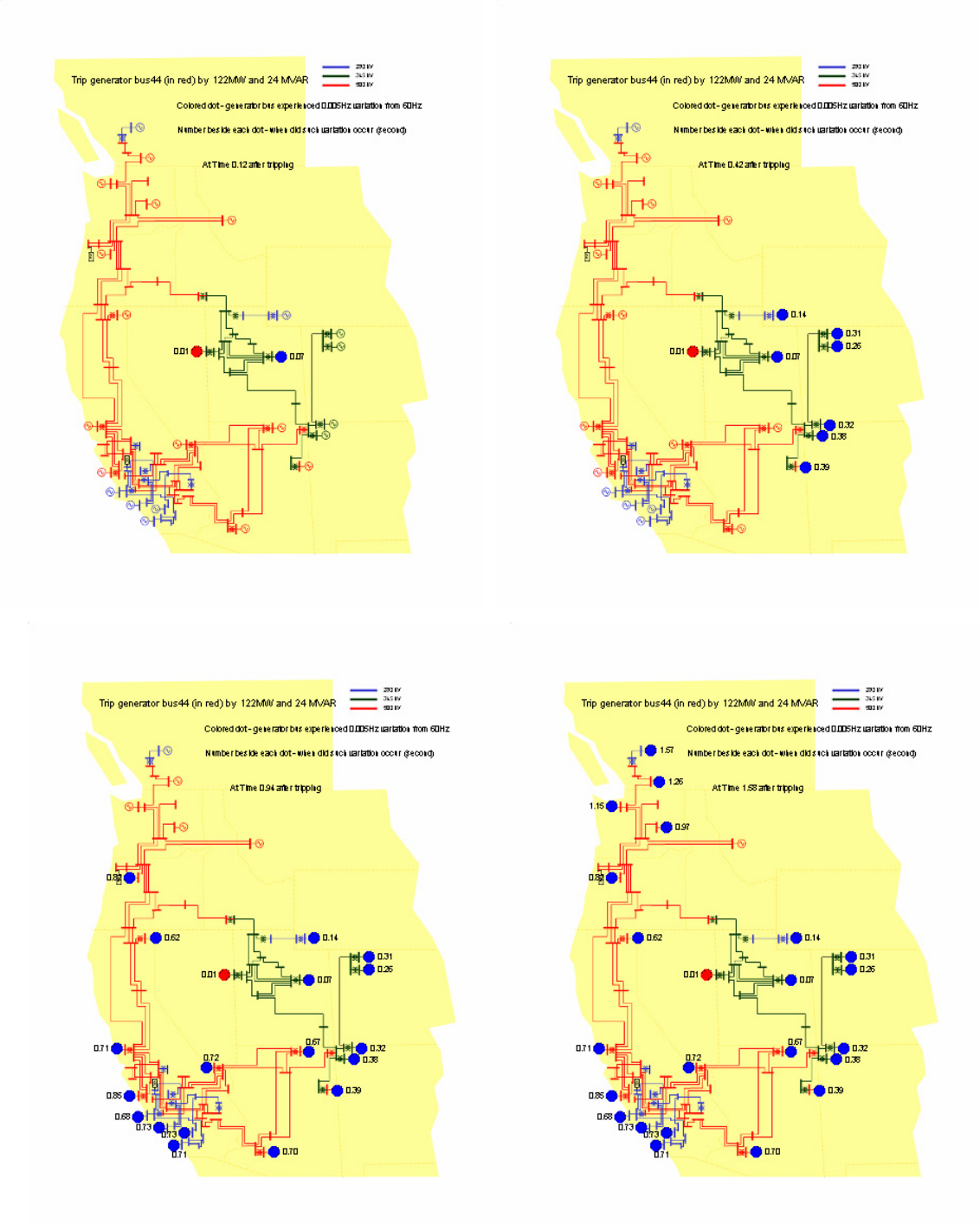

Fig 3-20. Animation snapshots when generator at bus 44 (in Nevada) tripped by 122 MW and 24 MVAR. The number beside each bus number is the time when the frequency first drops by 0.005 Hz after tripping.

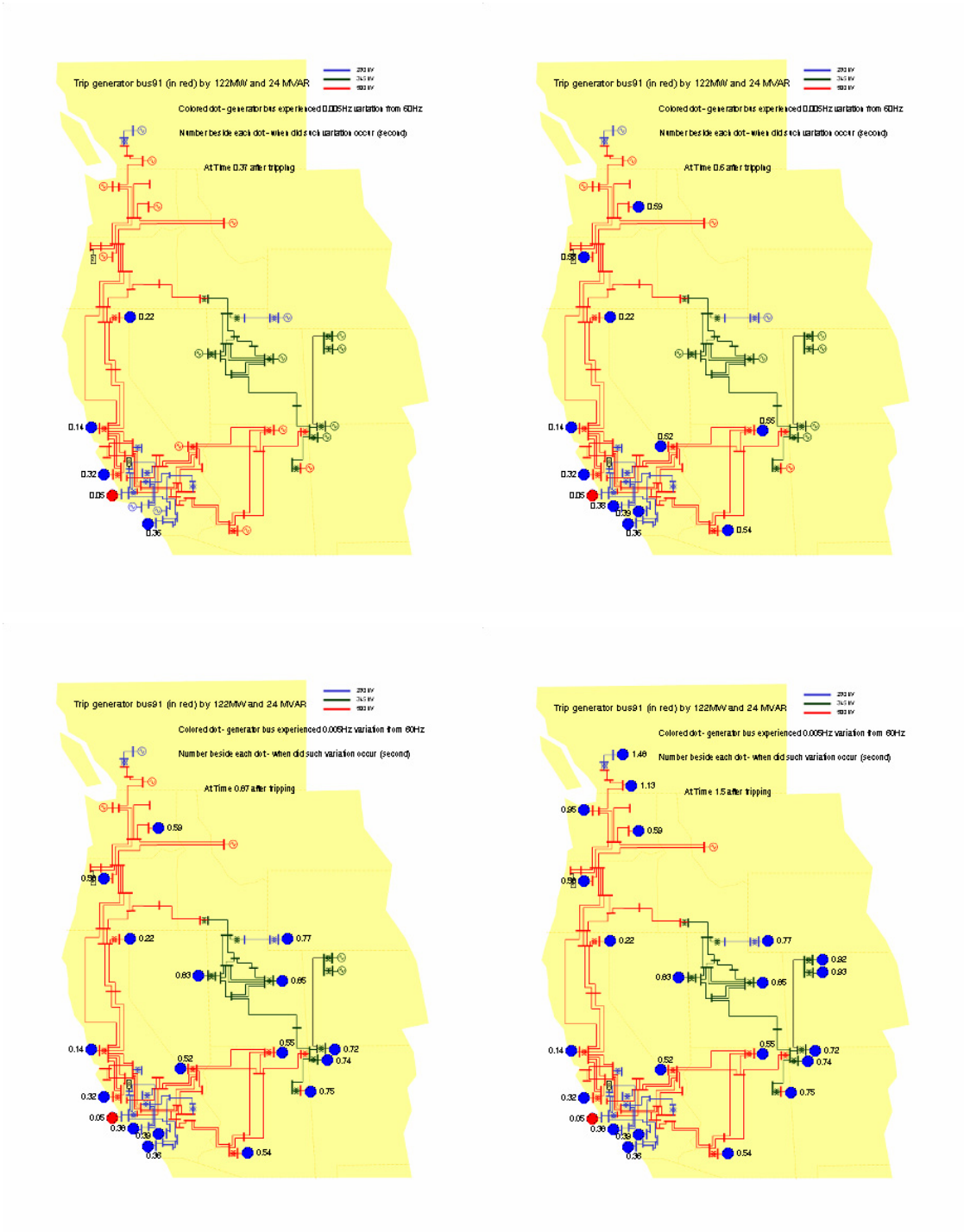

Fig 3-21. Animation snapshots when generator at bus 91 (in California) tripped by 122 MW and 24 MVAR. The number beside each bus number is the time when the frequency first drops by 0.005 Hz after tripping.

3.5.2 EUS generation trip (dot-version)

Fig 3-22, Fig 3-23, and Fig 3-24 show three examples when generators were tripped independently in EUS. Fig 3-22 shows the movie snapshots when the generator trip occurs at bus 22600 in Kentucky, Fig 3-23 shows the movie snapshots when the generator trip occurs at bus 40195 in Florida, and Fig 3-24 shows the movie snapshots when the generator trip occurs at bus 73084 in Massachusetts. The buses experienced the first 0.005 Hz variation from its steady state (60 Hz) show in blue dots. The tripped bus is labeled as a red dot.

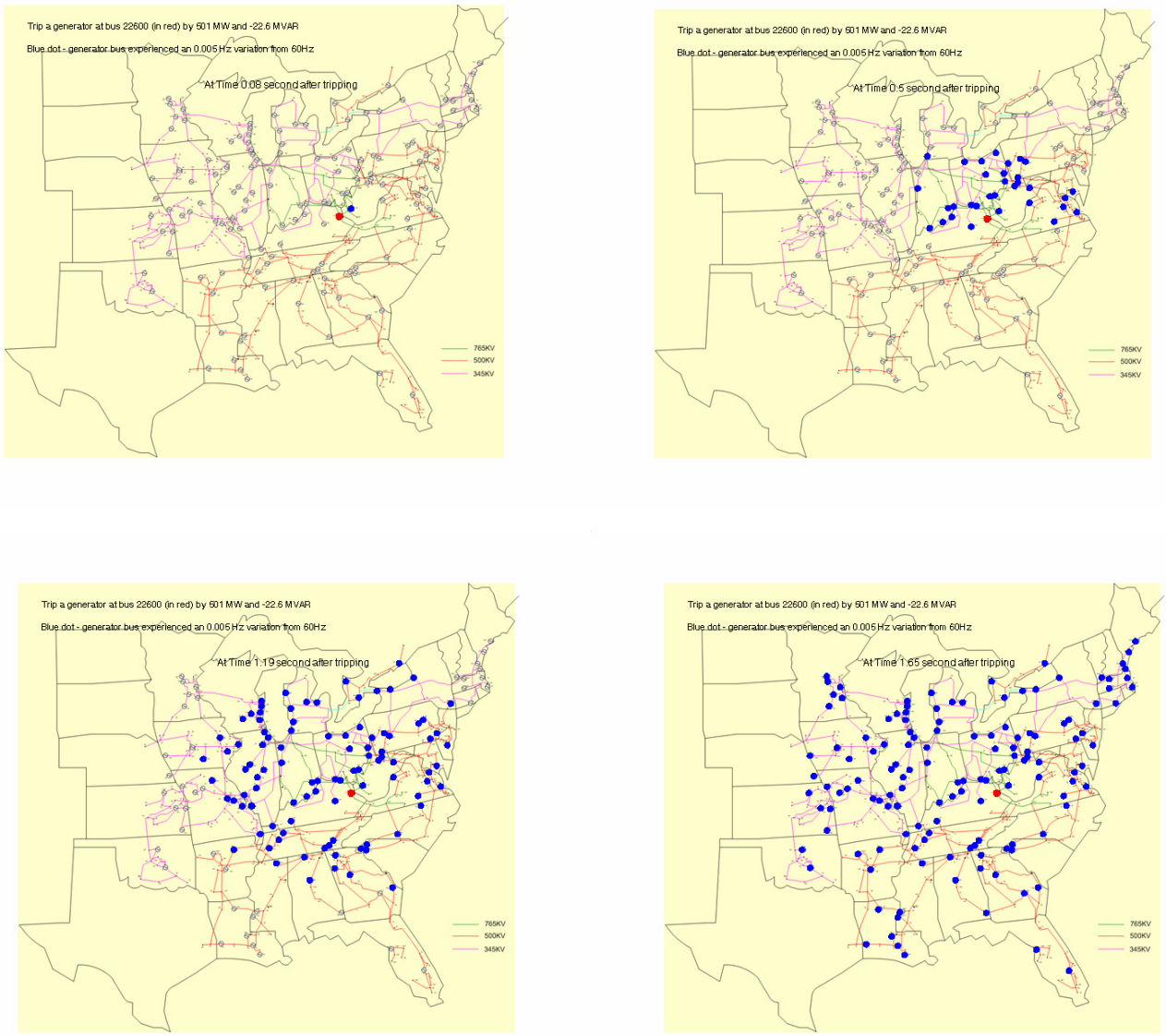

Fig 3-22. Animation snapshots when generator at bus 22600 is tripped.

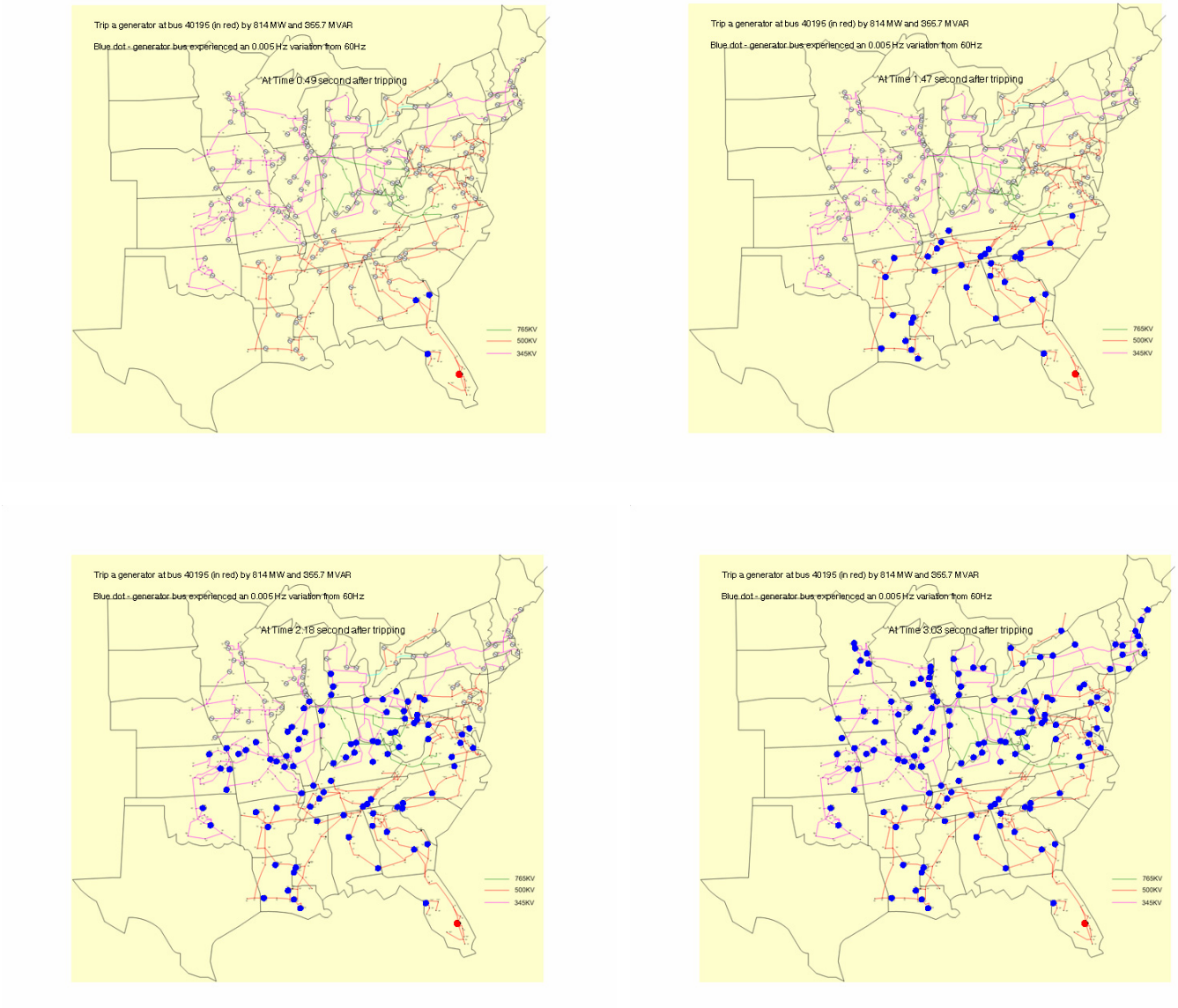

Fig 3-23. Animation snapshots when generator at bus 40195 is tripped

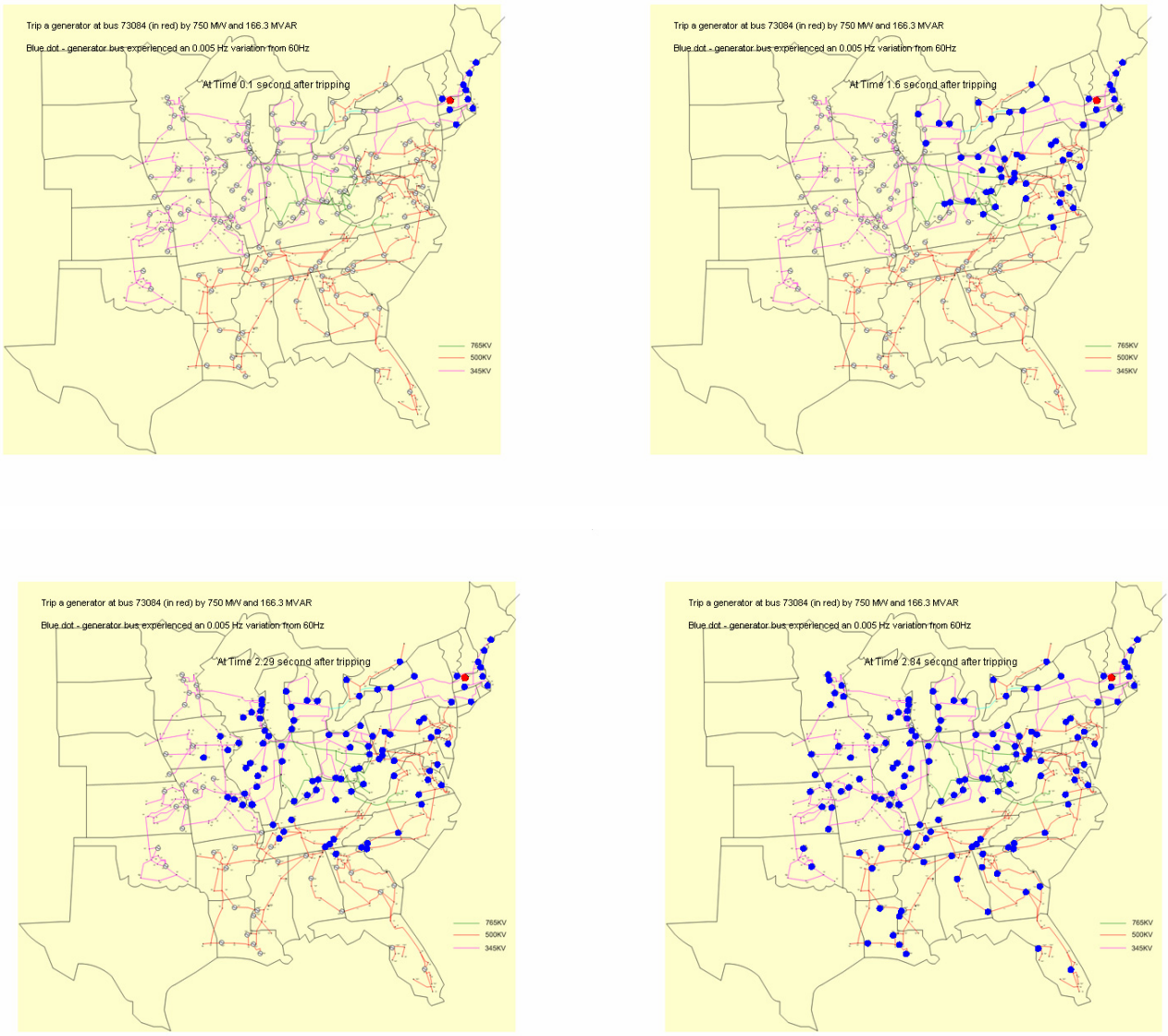

Fig 3-24. Animation snapshots when generator at bus 73084 is tripped

3.5.3 Remark of dot-version animations

From Fig 3-19, Fig 3-20, Fig 3-21, Fig 3-22, Fig 3-23, and Fig 3-24 a generator trip can cause the frequency deviation to propagate throughout the system like a wave. Dots gradually occupied all the buses in the system and the time when the bus experiencing the frequency deviation is at a much lower speed than the speed of light. This observation suggests that there is a form of “electromechanical” wave propagating throughout the system. Discussions of this electromechanical wave propagation can be found in section 3.6. It can be seen that the buses that will experience the fastest decline are the buses where generations are dropped and their nearby buses.

Further, if we compare the frequency drop time of a pair of buses in two different cases, either bus is the tripping generator bus in these 2 cases. The wave arrival time for each bus is not the same compared to the other case, which suggests that the wave may not propagate through the same path between 2 points.

3.5.4 EUS generation trip (surface-version)

Three examples are given below, a generator tripped at bus 22600 in Kentucky, two generators tripped at bus 73084 and 40799 in Massachusetts and Florida, respectively, and a generator tripped at bus 55042 in Oklahoma. The generator output power before the tripping is shown in each plot.

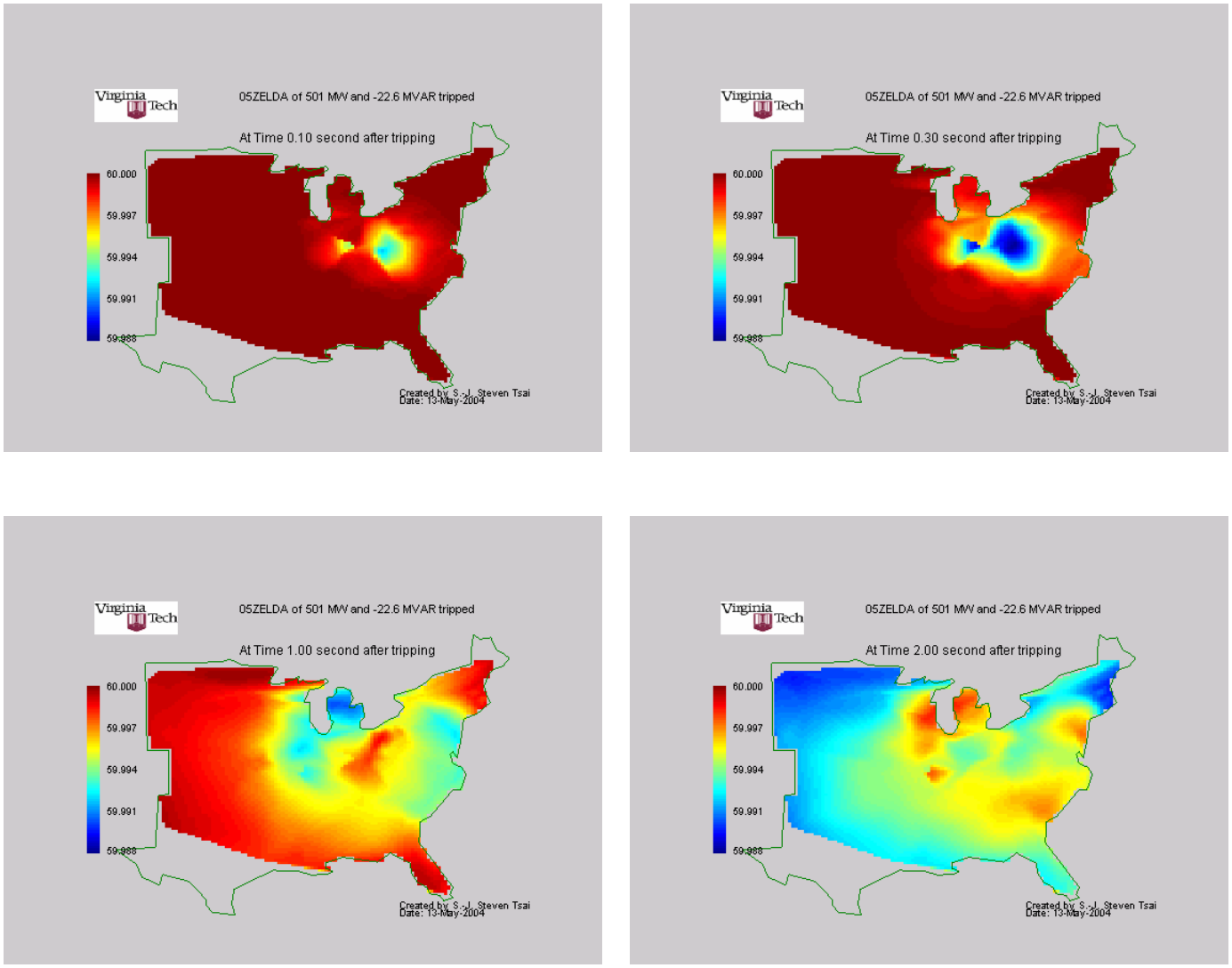

Fig 3-25. Bus frequency animation snapshots when generator at bus 22600 is tripped

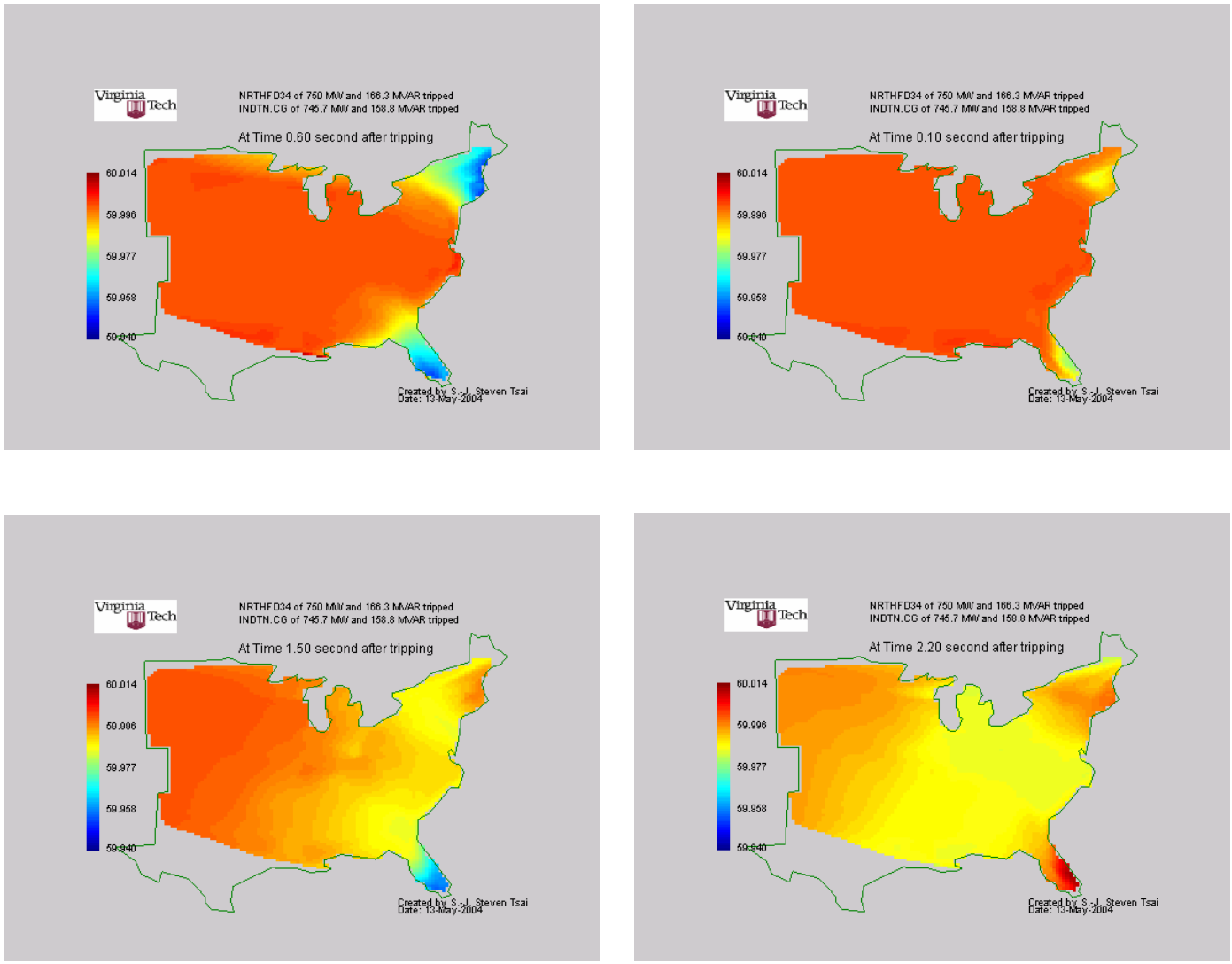

Fig 3-26. Bus frequency animation snapshots when generator at bus 73084 and 40799 are tripped

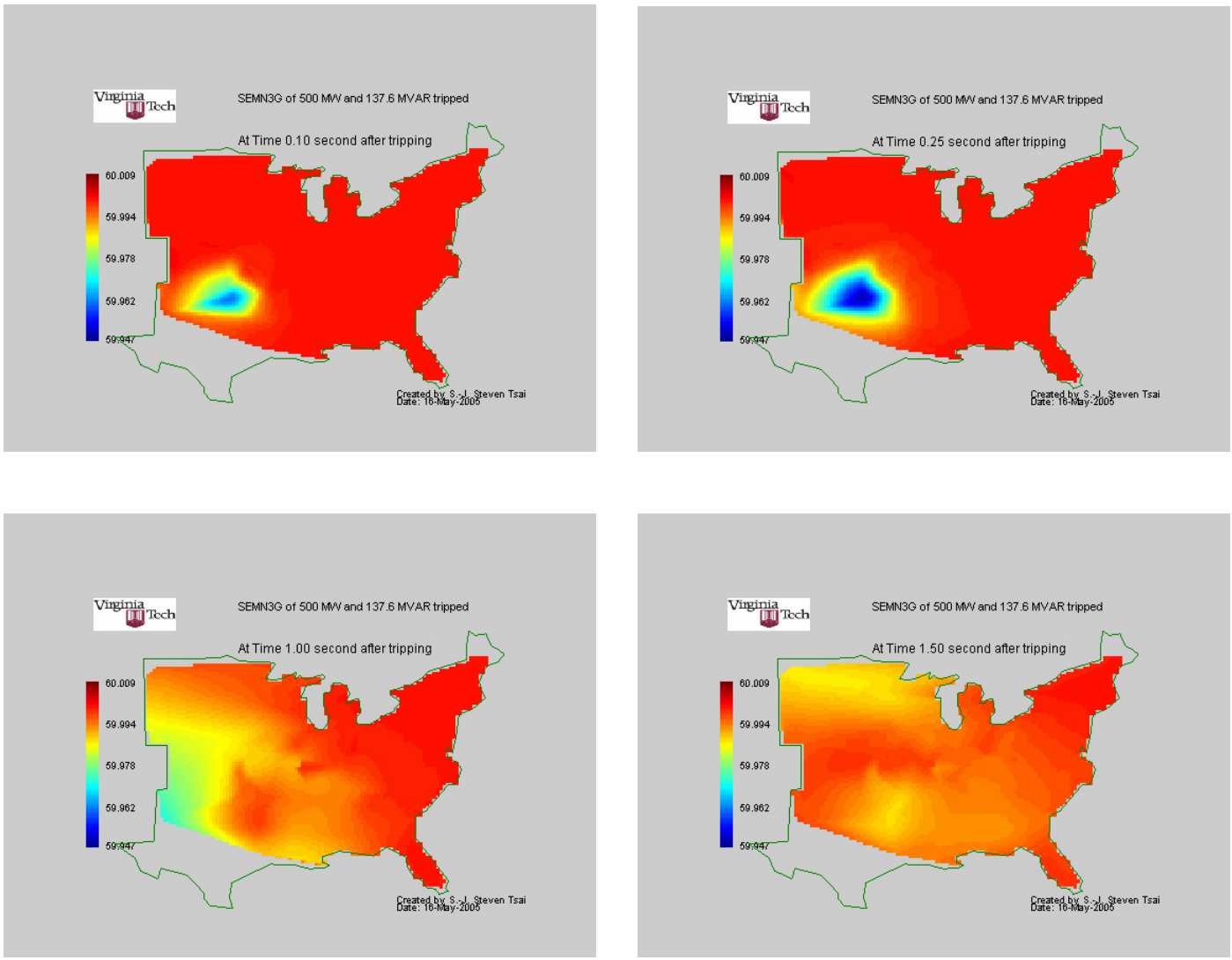

Fig 3-27. Bus frequency animation snapshots when generator at bus 55042 is tripped

3.5.5 EUS load rejection (surface-version)

Two examples are given below, load rejection at bus 28881 in Michigan, Fig 3-28, and load rejection at bus 81615 in New York, Fig 3-29. The active and reactive powers of the load before the tripping are shown in each snapshot plot.

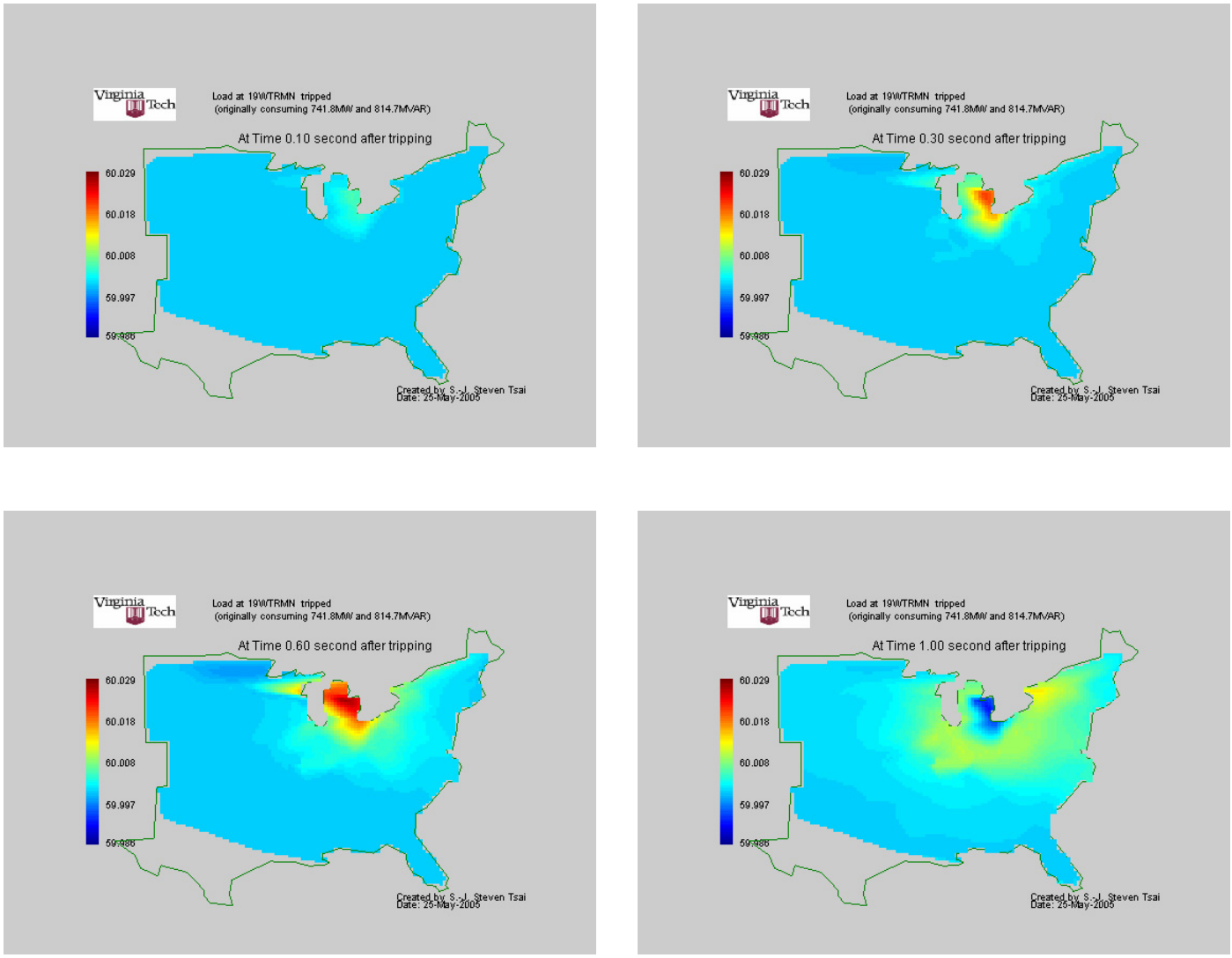

Fig 3-28. Bus frequency animation snapshots when load at bus 28881 is tripped

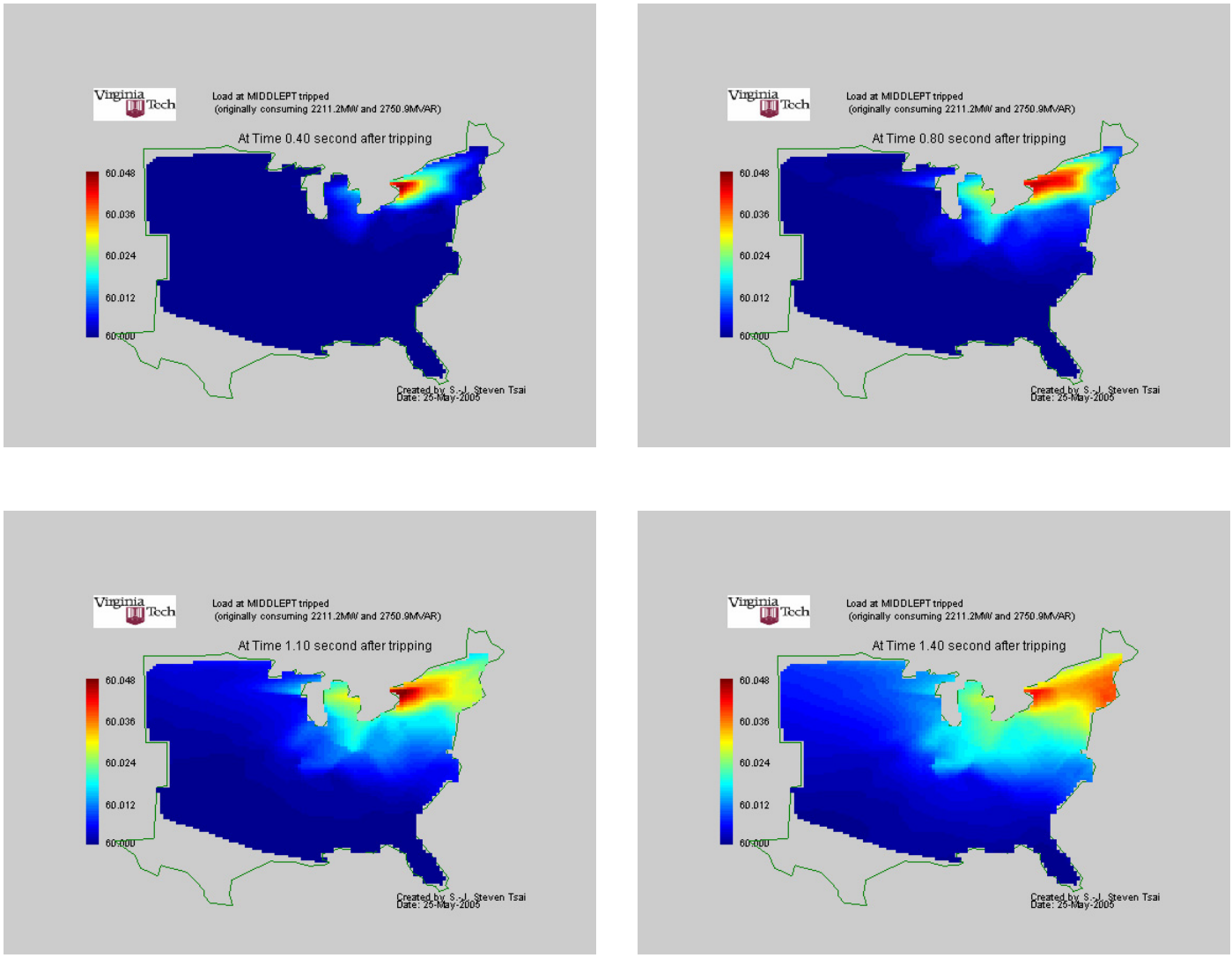

Fig 3-29. frequency animation snapshots when load at bus 81615 is tripped

3.5.6 EUS line trip (surface-version)

The tripping of a line can be categorized into 5 types, as discussed in 3.4. Here we show the animation snapshots of 4 types, namely, oscillation about 60 Hz, generation-trip like, load-rejection like and islanding. They are shown in Fig 3-30, Fig 3-31, Fig 3-32, and Fig 3-33, respectively.

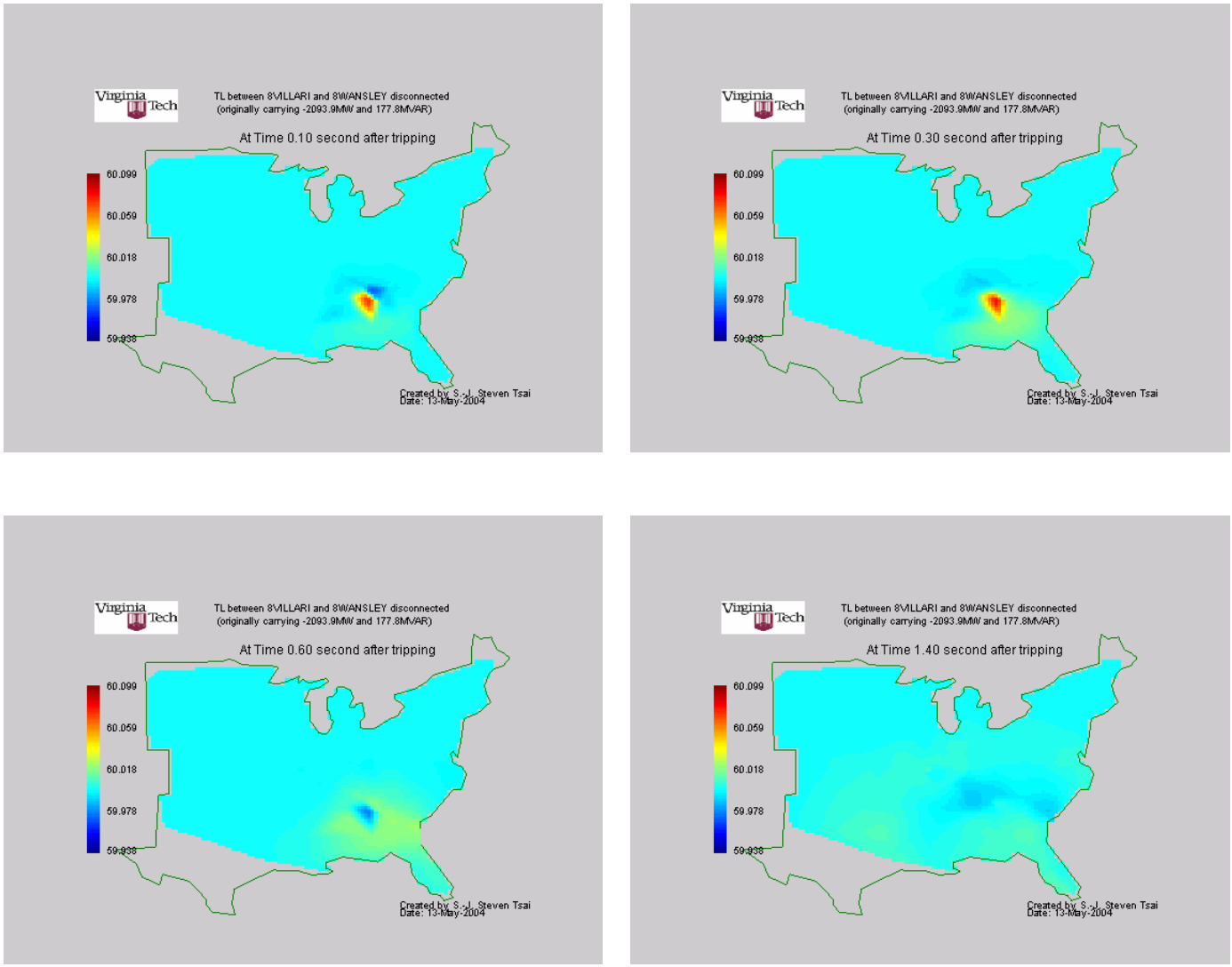

Fig 3-30. Bus frequency animation snapshots when the line between bus 15512 and bus 15513 is opened (oscillation about 60 Hz)

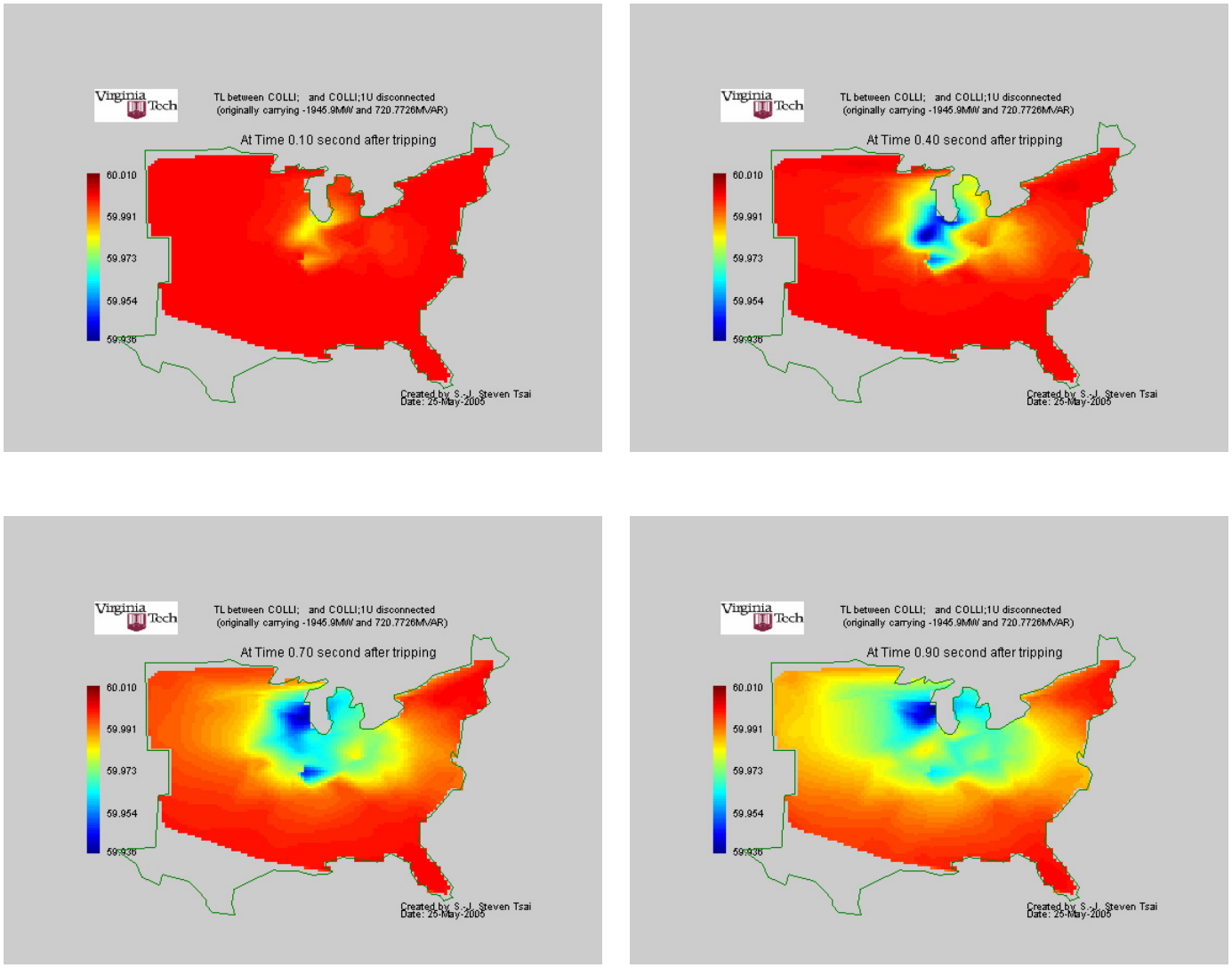

Fig 3-31. Bus frequency animation snapshots when the line between bus 36255 and bus 37526 is opened (generator tripping like)

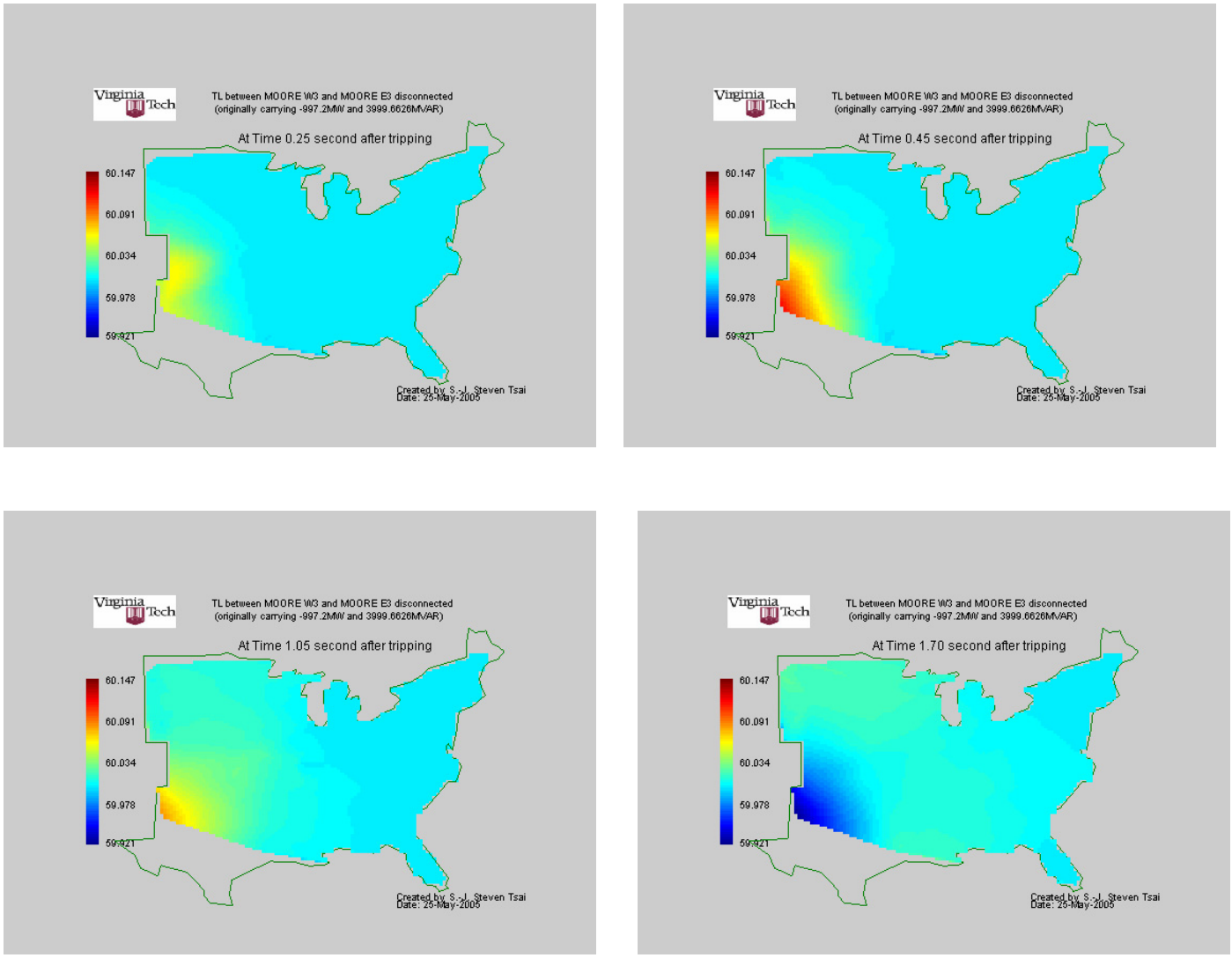

Fig 3-32. Bus frequency animation snapshots when the line between bus 50664 and bus 50668 is opened (load rejection like)

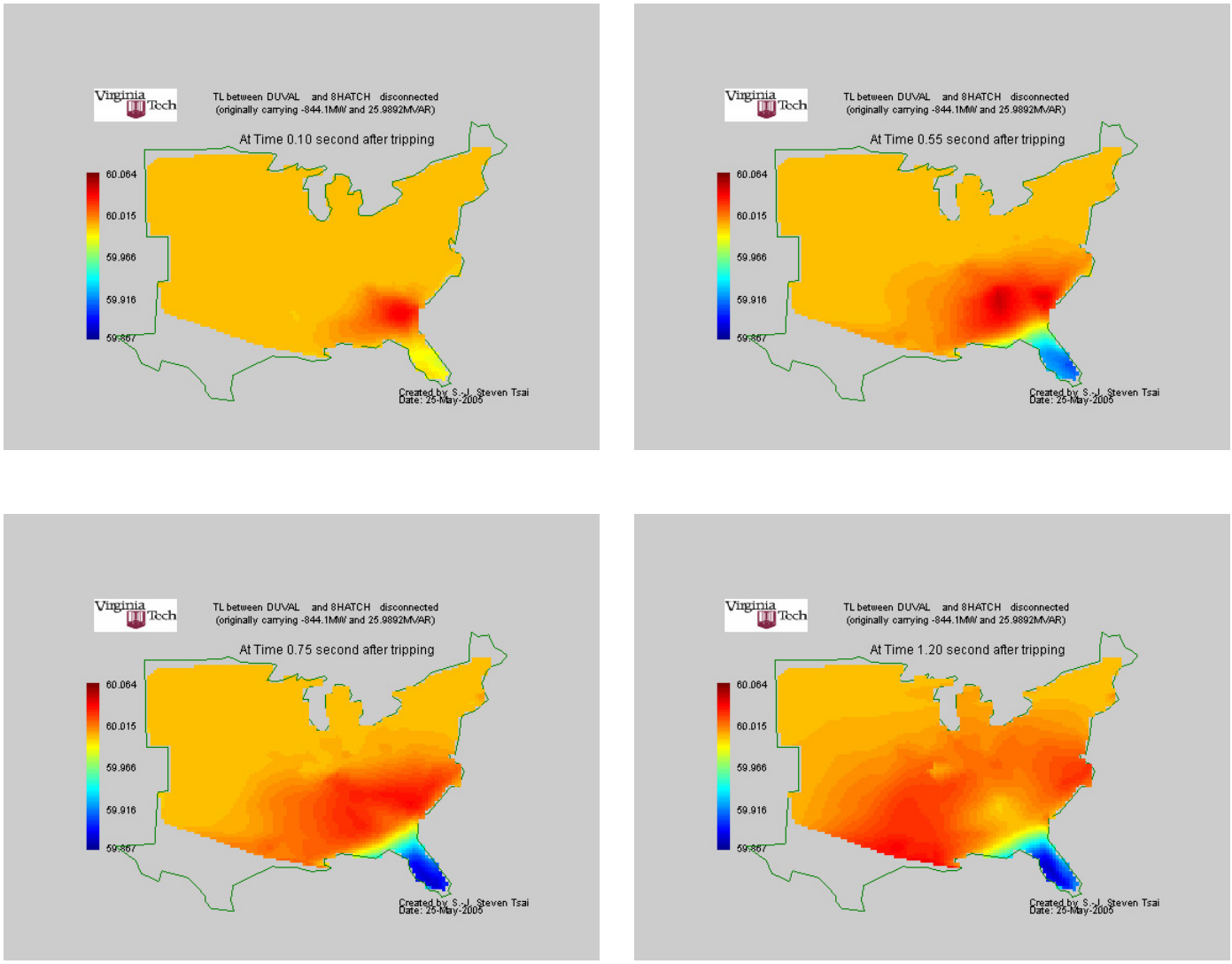

Fig 3-33. Bus frequency animation snapshots when the line between bus 40356 and bus 15037, 15038 (islanding)

3.6 Wave propagation discussion

From the replay snapshots, we can observe that as the time progresses, the dots spread out gradually at a speed much less then the speed of light, which suggests that there is a form of wave propagation from the disturbance origin to the rest of the system. The surface-version snapshots clearly illustrate that there is a kind of wave propagating. We consider this wave as electromechanical wave. References [78, 80] prove mathematically

that the change of the frequency or angle travels in the power system as a form of wave.

The idea of the electromechanical wave can be observed from the delayed bus frequency responses when event(s) (e.g. generation trip) occur in the system. In physics, wave is defined as "A disturbance caused by the movement of energy from some source through some medium. The traveling "hump" produces the appearance of movement that we see as a wave" [15]. Here the source can be considered as the tripped generator or rejected load and the medium is the power systems, including lines, other generators, transformers, loads, etc. The changes of frequencies in the system denote some form of energy exchange in the system.

The frequency is a byproduct of the rotor angle speed of synchronous generator. The rotor is a mechanical mass and is interacting with the electrical power grid via electromagnetic coupling between field and stator windings. By Newton's first law of motion - An object at rest tends to stay at rest and an object in motion tends to stay in motion with the same speed and in the same direction unless acted upon by an unbalanced force. It is the natural tendency of objects to resist changes in their state of motion, which can be described as inertia. The bus frequency is related to the speed of the rotor, so if there is any change of the rotor angle, therefore rotor speed then the bus frequency would change electromechanically. And the disturbance can propagate as an electromechanical wave in the system from the frequency point of view. Here the term "electromechanical" is used due to the unique combination of mechanical and electrical parts in power system.

[15] Quoted from http://lighthouse.tamucc.edu/Waves/WaveDefinition

From the given examples, if there are enough measurement units in the system, we would be able to view this propagation in greater detail. Fast communication may even allow near-to-real-time display. For a relatively small amount of disturbance, the whole system would be able to see the first wave front within 2 seconds after the generator trip. We can anticipate that for large disturbances, the time to see a 0.005 Hz frequency drops throughout the system would be considerably less.

From the above animations, we could observe that the first influenced buses are the buses that are near to the disturbance points. The further the electrical distance or geographical distance from the disturbance incipient point, the later it will see the variation.

The effect of a generator trip or a load rejection is system-wide, whereas a branch trip can be localized or system-wide event. This is due to the fact that when a generator trips or a load rejects, it immediately induces power imbalance between generation and consumption in the system, but when the line trips, the power may be re-dispatched throughout the system or a generator or load center could be tripped from the system. Hence the frequency response from a line trip can be mixed.

3.7 Uniform system

From the previous section, we can visualize how the frequency wave propagates when disturbances were introduced in the power system. The complexity of the large system makes it not possible to analyze the behavior of the frequency electromechanical wave propagation in detail. To look into how this electromechanical wave propagation throughout the system when there is generation trip in detail, we construct 3 simple and

uniform topologies – Single-line, multi-line, and mesh systems to simulate and try to find out the properties of frequency propagating wave. Only the frequency characteristics of the 21-bus single-line system will be described in detail in this section; for other systems, the propagation speed result will be presented in section 4.4.

3.7.1 Single-line system

We construct a uniform single line system which consists of identical transmission lines, generators and loads. Two sizes of systems are created, 21 buses and 41 buses. The system topology for 21-bus system is shown in Fig 3-34.

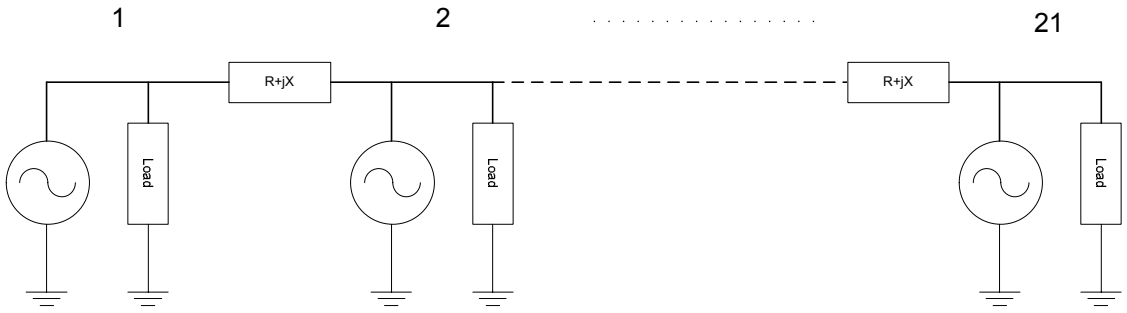

Fig 3-34. Single-line system configuration

The line impedance parameters are taken from one transmission line in EUS. The line connects between '8HATCH' and 'DUVAL', and has the resistance R= 0.0016 (p.u.), and reactance X = 0.0268 (p.u.). Here, we neglect the branch charging susceptance. And the distance between the two buses is roughly 125 miles from estimated measurement on the map.

The generators are rated at 309.2 MW. Only the generator machine itself is modeled for each generator bus and no control components (e.g. exciter, governor, or power system stabilizer) are included. The reason for not modeling the control components associated

with generators is that governors are typically responded to the change of bus frequency after 2~5 seconds, and our aim is to find the wave propagation in the first swing, which is within the first few seconds. The exciter mainly regulates bus voltage which is not our main interest in this study.

Loads are composed of 309 MW and 40 MVAR. In the dynamic simulation, we convert loads into constant impedances.

Three different cases have been studied:

1. Base case: all the parameters in the system are unchanged
2. 2H case: all the generators' inertias are doubled
3. 2Z case: all the line impedances are doubled

For all cases, we tripped 0.3% of total system generation from a selected generator in the system (either from the generator at the first (boundary) bus or from the generator in the middle of the system).

3.7.1.1 Base case

23.7 MW generation power, which corresponds to 0.3% of the system's total generation (7872 MW) is tripped from bus 1. The frequency responses after the tripping of all buses are shown in Fig 3-35.

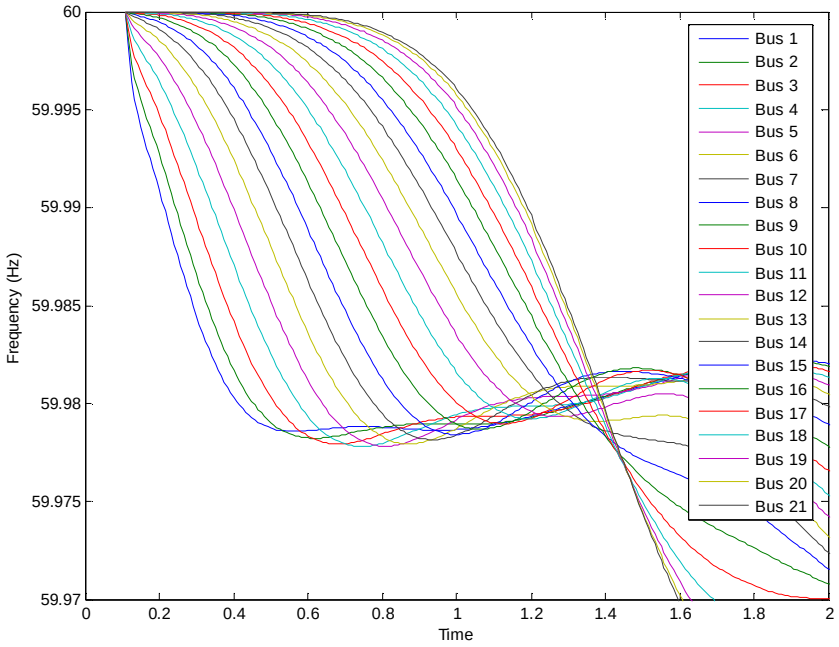

Fig 3-35. Bus frequency responses when 23.7 MW tripped from bus 1 in the single line system

As it is shown, the bus frequency decreases due to the generation insufficiency. After the first swing, some oscillation comes afterwards, which is not shown in the plot. Our aim is to analyze the first swing, where the first propagating wave front is initiated throughout the system. We only look at the bus frequency response to find this electromechanical wave propagation in the system.

We can set a threshold at 59.995 Hz and look at the time when the bus frequency first drops to the threshold. This detection technique enables us to see the wave front in terms of frequency in the system. A calculation of the wave propagating speed will be presented in 4.4.1. From inspection, the time differences between the middle buses are uniform, where at boundary buses (1, 2 or 19, 20, 21), they become smaller. This can be

understood by assuming the system is a spring-mass system, as shown in Fig 3-36. The transmission line may be acting like a spring and generator inertias may be acting like a mass at nodes. Boundaries are free ends.

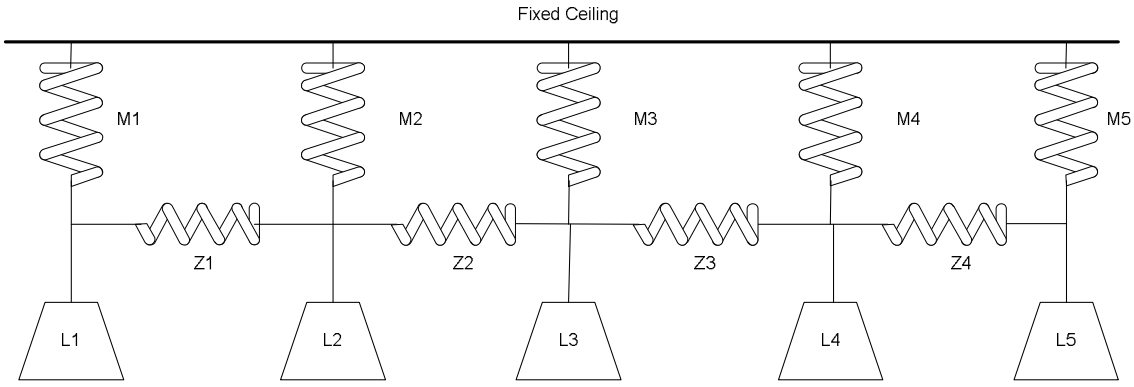

Fig 3-36. Spring-mass system as an analogy of the electromechanical system

The frequency wave propagation may be like any kind of sound or water wave, when there is less obstruction, the wave tends to travel faster; in other words the time difference between adjacent nodes to see the same wave amplitude is less. When the wave reaches free boundary, the less obstruction it will encounter; therefore, from Fig 3-35, at boundary buses the time differences of the same threshold value are smaller.

If 23.7 MW is tripped from bus 11 (the middle bus), the frequency responses of other buses are shown in Fig 3-37. Please note that it seems erroneous to have only 11 lines, instead of 21, showing in Fig 3-37; however, the system is identical and the tripping point is at the center bus of the system so the system is symmetrical about bus 11. Therefore, the frequency responses of the symmetrical pairs, i.e. 1 and 21, 2 and 20, 3 and 19 and so on, are on top of each other in the plot.

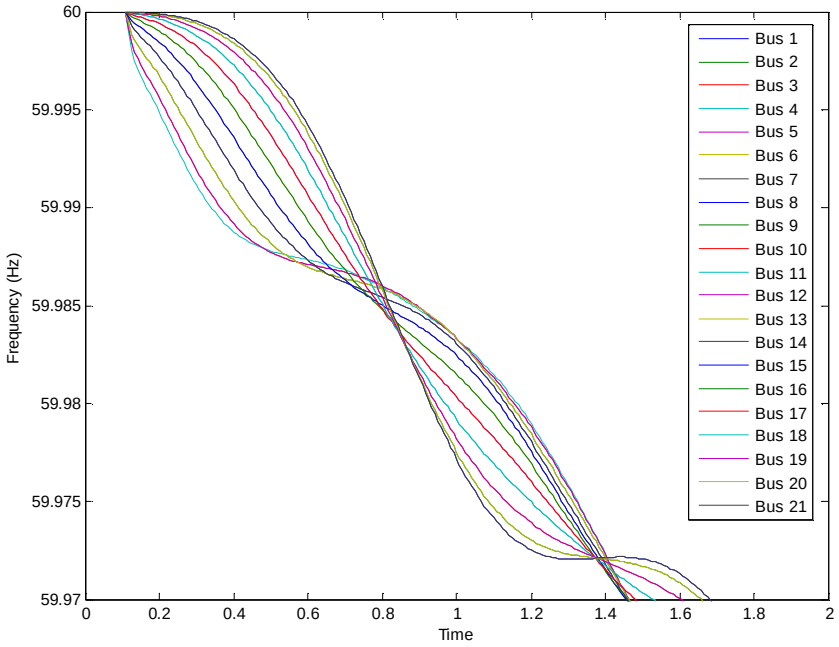

Fig 3-37. Bus frequency responses when 23.7 MW tripped from bus 11 in the single line system

Similarly, we set a threshold at 59.995 Hz and look at the time when bus frequency reaches the threshold at different buses. From inspection, the time differences between the middle buses are uniform, where at boundary buses (1, 2 or 19, 20, 21), the time differences become smaller. This finding is consistent to the previous case.

3.7.1.2 2H case

After doubling the inertia of every generator in the system, the bus frequencies when 23.7 MW is tripped from generator 1 and 11 are shown in Fig 3-38 and Fig 3-39. Comparing to Fig 3-35, the frequency declines less for all buses, and the free-end boundary effect is still in place. The frequencies are less deviated in this case indicating that the increase of inertia makes the wave more difficult to propagate throughout the system.

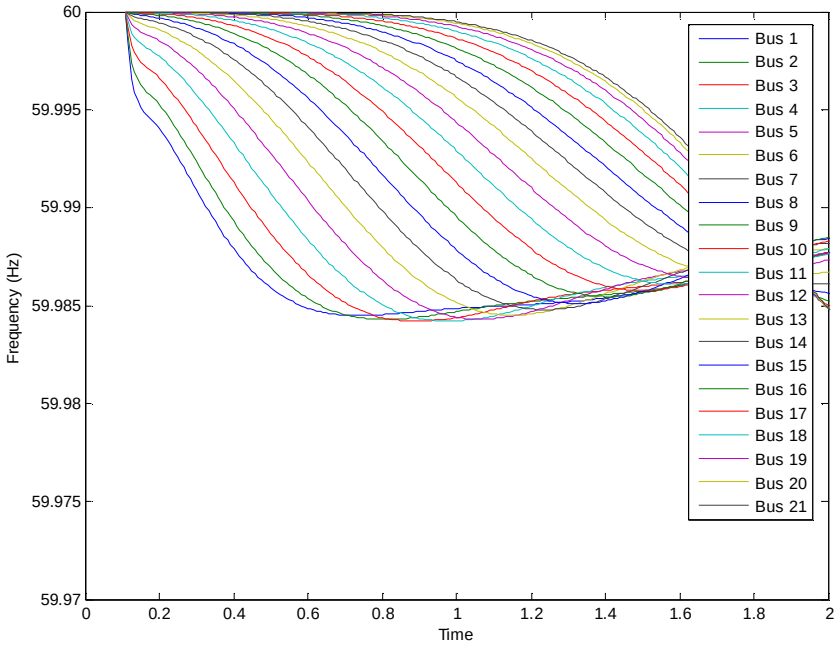

Fig 3-38. Bus frequency responses when 23.7 MW tripped from bus 1 in the single line system. Inertias of all generators are doubled.

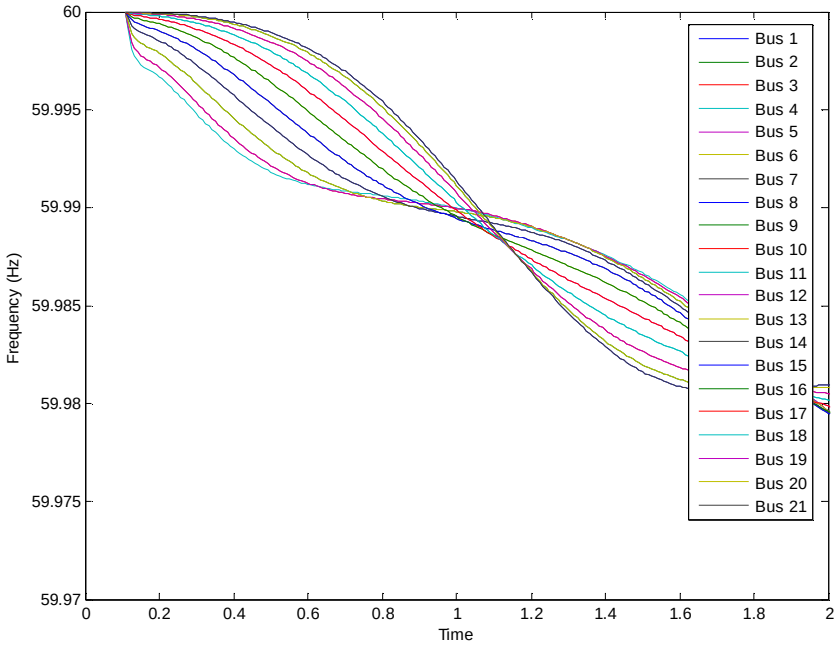

Fig 3-39. Bus frequency responses when 23.7 MW tripped from bus 1 in the single line system. Inertias of all generators are doubled

3.7.1.3 2Z case

Doubling the line impedance of every line presents another interesting phenomenon for wave propagation. Fig 3-40 and Fig 3-41 show the bus frequencies when 23.7 MW is tripped from bus 1 and bus 11, independently. The frequencies drag down to a lower level in the first swing, comparing to Fig 3-35 and Fig 3-37; and the time differences between buses at the threshold value (59.995 Hz) are larger. The free-end boundary effects still exist, especially more dominant between buses 19 and 21. The frequency drag-down phenomenon can be explained by thinking the length of lines are stretched and the disturbance energy takes longer to dissipate to the neighboring node; therefore, the frequency will further decrease before the next node could experience the frequency drop.

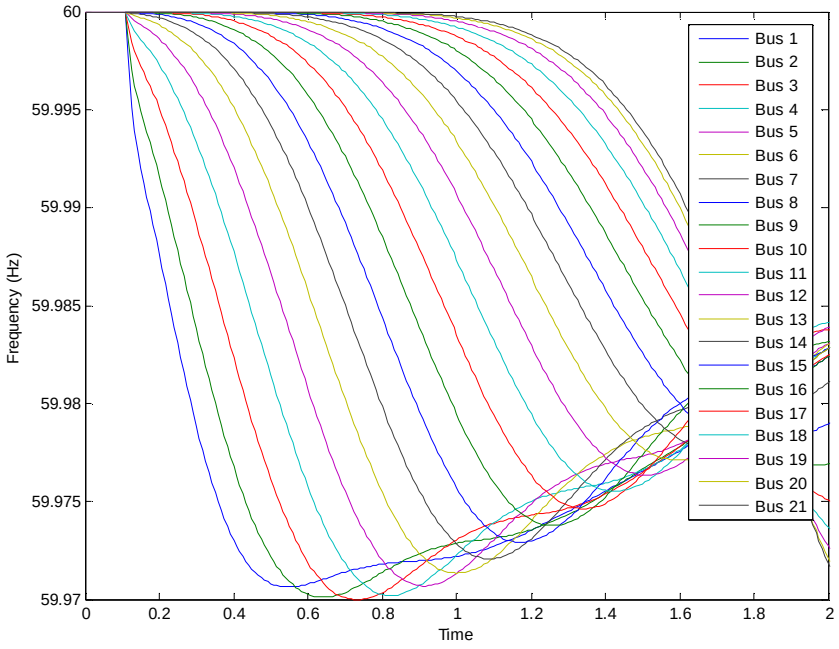

Fig 3-40. Bus frequency responses when 23.7 MW tripped from bus 1 in the single line system. All line impedances are doubled

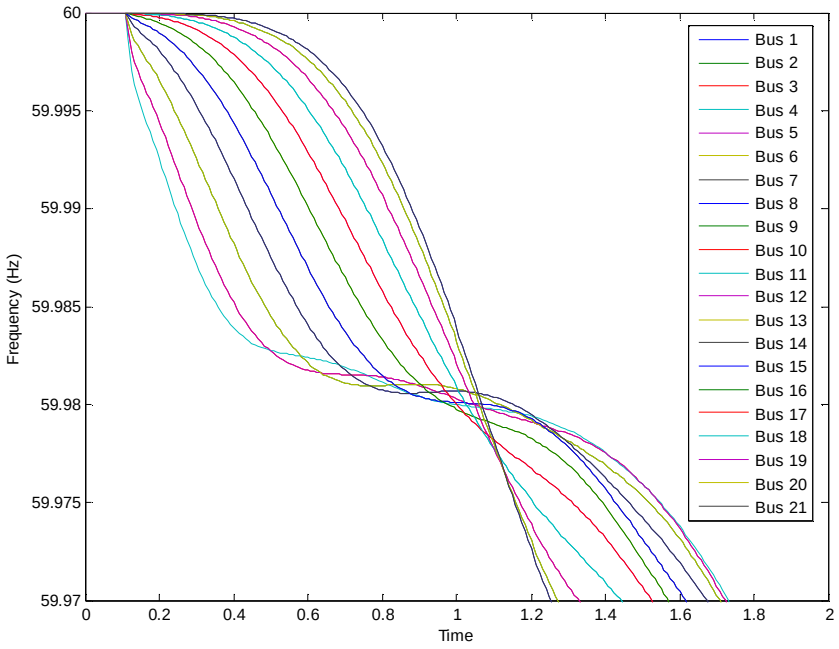

Fig 3-41. Bus frequency responses when 23.7 MW tripped from bus 11 in the single line system. All line impedances are doubled

3.8 Summary

Frequency responses to different disturbances, generation trip, load rejection and line trip are considered in this chapter. Generation trip would result in frequency drops from 60 Hz. Load rejection, conversely, induces frequency rise above 60 Hz. Line trip may result in one of the following cases:

- Oscillation about 60 Hz
- Like generator trip
- Like load rejection
- Mixed
- Islanding

depending on the connection property of the line between 2 buses.

To better understand the system dynamics from the massive amount of data, we created a visualization tool to view the simulation data in Matlab. Two versions were created, namely dot-version and surface-version. Dot-version shows the frequency variation on a map based on pre-selected threshold value, 0.005. Surface-version shows the interpolated surface from the values at the selected points in the system. Both versions illustrate that when some disturbance occurs, some electromechanical waves would initiate and, therefore, anywhere in the system would be able to experience frequency deviation from such disturbance.

Discussion of how we define the frequency electromechanical wave and its propagation, based on basic physics, and from the frequency variation observation in the system, is provided. The frequency is a byproduct of the rotor angle of synchronous generator, and the rotor is a mechanical mass interconnected to the electrical power system via stator windings; therefore, the frequency would vary electromechanically to any disturbance in the system. And disturbance propagates in the system as a form of electromechanical wave.

To better understand how the frequency wave propagates throughout the real system, we construct and investigate how the frequency behaves in a uniform single-line system. The uniform system provides some controllable factors that allow us to view the frequency behavior between adjacent buses and in the overall system. The frequency response changes when network parameters change, such as generator inertia, line impedance, etc.

Chapter 4 Frequency Wave Propagation Speed

4.1 Introduction

The first 2 sub-sections of this chapter attempt to simulate the propagation speed of the electromechanical waves in terms of frequency changes and relate them to the geographical distance with the understanding that the propagation characteristics are mostly determined by the "electrical" characteristics of the system such as line impedance, generator inertial, and others. We studied the frequency wave propagation speed when some generation is dropped in the EUS and WECC. We then look at the cases from the simplified systems – one-line, multi-line, and mesh system in more details.

For large system, we use some approximation method to estimate the speed of frequency wave propagation. For simple system, the wave propagation speed can be calculated in a more accurate way.

4.2 Eastern US interconnected system (EUS)

For EUS system, three generators of roughly equal active power output (~1800MW) across the eastern states are chosen for tripping independently. They are FT MYER3 (40280) in Florida, RAV3 (74702) in New York, and WCEP (28049) in Indiana. The locations of these generators are shown in Fig 4-1. For each case, we picked 4 to 6 buses, which are about 1100 or 550 miles away from the tripping generator geographically, to monitor the bus frequencies when the generator is tripped.

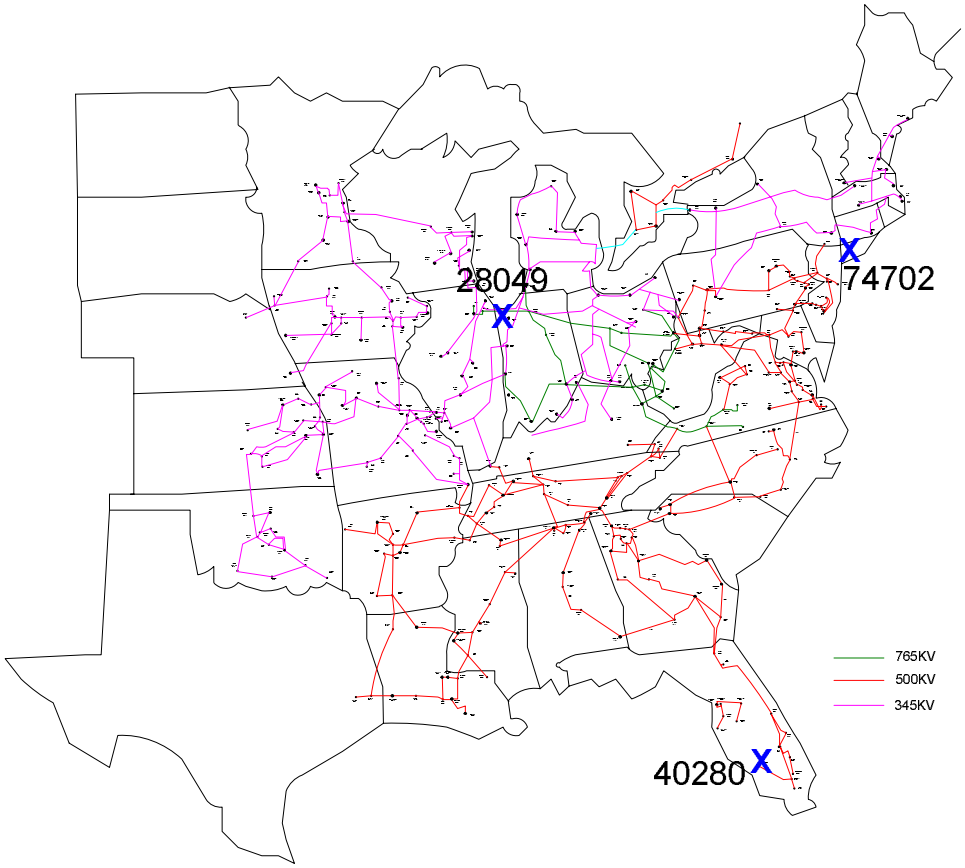

Fig 4-1. Tripping generator geographical locations

In simulations, we initiated the tripping at 0.1 second. To estimate the arriving of the frequency wave, we find the time when the frequency drops below 0.005 Hz from 60 Hz in the first swing (the initial frequency drop). This criterion we choose is based on the capability of our in-house designed FDR as discussed in Chapter 2. Here, we define the frequency wave propagation speed as $v = d/t$, where d is the direct geographical distance between the tripping generator and the measurement bus and t is the time when a 0.005 Hz frequency change is detected after the trip.

The tripped generator and monitored buses for each case are shown in Fig 4-2 (a)-(c). In Fig 4-2 (d), the frequencies at the monitoring buses for case (a) and the time to the threshold (59.995 Hz) from the tripping moment are shown.

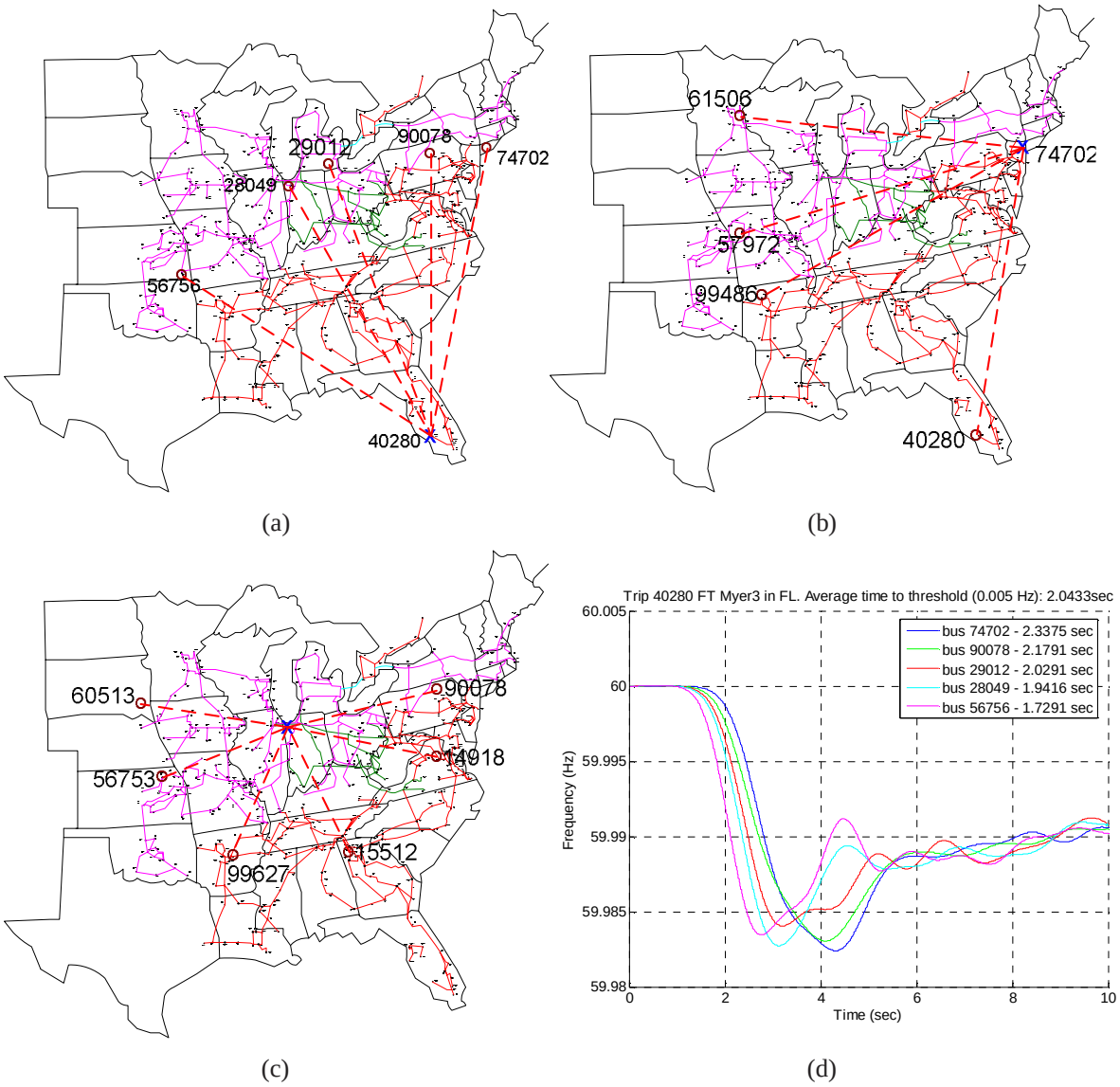

Fig 4-2. (a) Geographical locations of FT MYER3 in Florida, labeled as x, and 5 monitoring buses, labeled as o, (b) Geographical locations of RAV3 in New York, labeled as x, and 5 monitoring buses, labeled as o, (c) Geographical locations of WCEP in Indianna, labeled as x, and 5 monitoring buses, labeled as o, (d) the bus frequencies at monitoring buses for (a)

For each case, we calculated the averaged time when the monitored frequencies drop to 59.995, and then the distance is divided by the averaged time to get the averaged propagation speed. The averaged wave propagation speeds from the above 3 cases are summarized in Table 4-1.

	Case	Averaged Speed (miles/sec)
Eastern US interconnected	a	539
	b	460
	c	663

Table 4-1. Averaged wave propagation speed in Eastern US interconnected system

EUS simulation and calculation results suggest that the frequency wave propagates faster to the western part of the system than to the eastern part of the system. This may be due to the fact that the eastern part has denser generation than the western part, so the wave would experience more “resistance” in the eastern part. The simulation results also show that the wave would propagate slightly faster from the central part of the system than from the rim of the system.

4.3 WECC 127

In the EUS example, we trip roughly 1800 MVA, which is about 0.3% of the EUS’s total generation power, of generation to investigate the wave propagation speeds. In here, we apply the similar fraction of tripping power - 0.3% of the WECC’s total generation power which corresponds to 184.23 MW and 36.996 MVAR, to observe how the propagation speed behaves. We selected 3 generators in the system to trip independently. One is in Washington, one is in New Mexico, and one is in California; and their locations are labeled as red dots in Fig 4-3 (a) – (c). For each case, 2 geographically-equally-distant observing points, labeled as blue stars, are selected to record the bus frequencies.

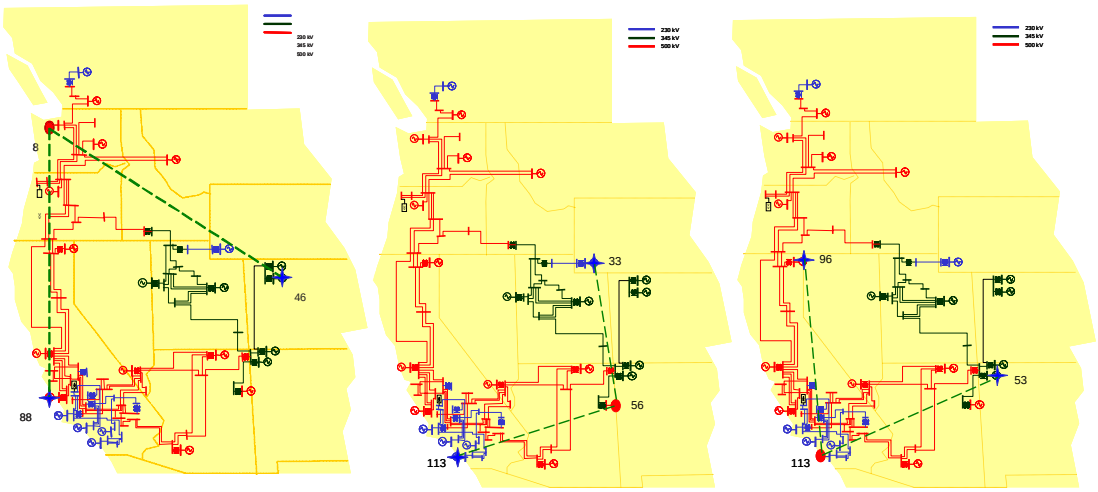

(a) (b) (c)

Fig 4-3. Tripping generators in solid red dot with the corresponding bus numbers for wave propagation study in WECC 127 system. (a) Tripping from a generator in Washington, (b) Tripping from a generator in New Mexico, (c) Tripping from a generator in California

The averaged speeds are calculated in a similar manner as described in EUS system and are summarized in Table 4-2.

	Case	Averaged speed (miles/sec)
WECC 127	a	1144
	b	1144
	c	1301

Table 4-2. Averaged wave propagation speed in WECC 127

For WECC 127 system, the wave propagation speeds for these 3 cases are very similar to each other from our calculation.

4.4 Uniform System

4.4.1 One-line 21 bus

The bus frequency characteristics of one-line 21 bus system are described in 3.7.1. In here, we calculate the frequency wave propagation speed based on the bus frequency deviation. The first wave front is considered arrived when the bus frequency drops to 59.995 Hz in the first swing. Since this is a single line system, and the distance between buses is known, the speed (v) is calculated from the time differences between the wave arrival times of adjacent buses. Here we use $v=d/t$ where d is the distance between adjacent bus and t is the time difference between adjacent buses when the bus frequency drops to 59.995 Hz.

Three different cases have been studied, namely base, 2H and 2Z cases. For the 2H case, we doubled the inertias of every generator, while left other parameters unchanged from the base case; and for the 2Z case, we doubled the line impedance of every lines, while left other parameters unchanged from the base case. Fig 4-4 shows the wave propagation speeds between adjacent buses of the three cases when 23.7 MW is tripped from the generator at bus 1.

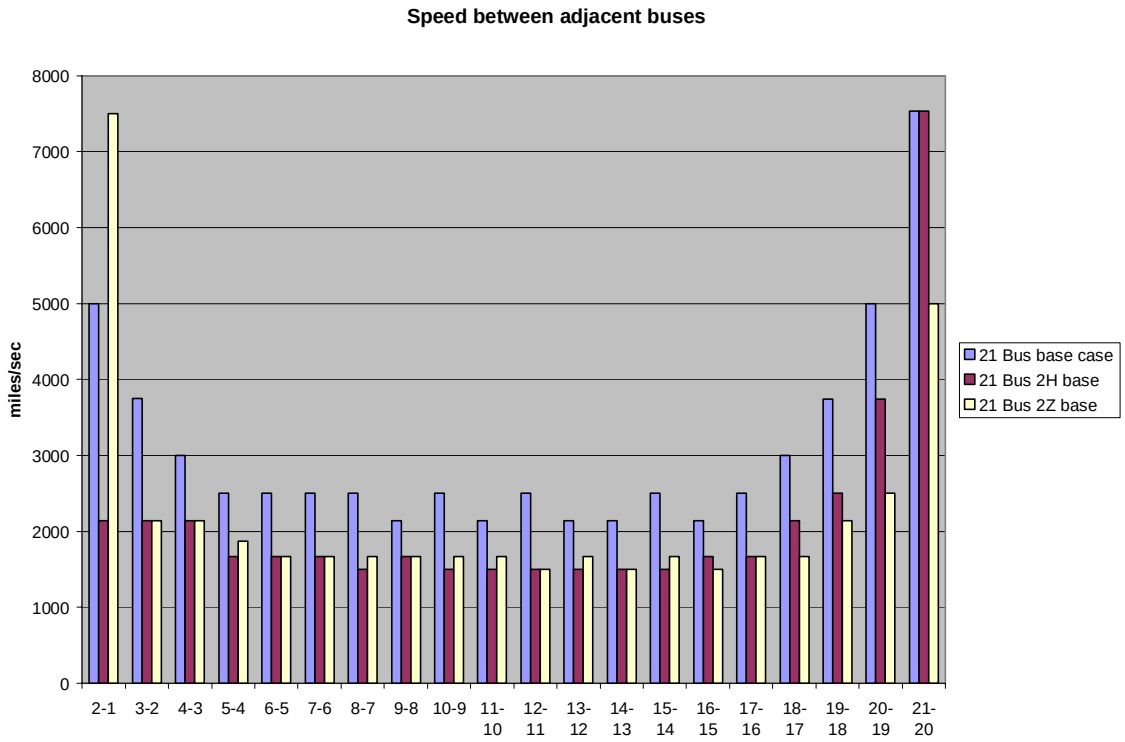

Fig 4-4. Frequency wave propagation speed between adjacent when 23.7 MW is tripped from bus 1 for single-line system

The general trends of the speeds between adjacent buses are that the frequency travels faster at the end buses than that in the middle buses and some speed distribution symmetry is noticed for the base case.

From above, we are able to see that the speeds are considerably reduced in the middle buses when we either double the generator inertias or double the line impedances. This phenomenon can be expected since there are more 'resistances' for the wave to propagate by doubling inertias or line impedances. Between middle buses (2-17), generally speaking, the doubling of inertia or impedance imposes similar effects on speed reduction comparing to the base case. At boundary buses (1-2, or 20-21), the effect of doubling inertia or impedance gives us mixed results. For the 2H case, the speed does not reduce

between bus 20 and 21; on the other hand; for the 2Z case, the speed increases by 50% between bus 1 and bus 2.

If a generation trip of 23.7 MW from the generator at bus 11, the wave propagation speeds between the adjacent buses are shown in Fig 4-5.

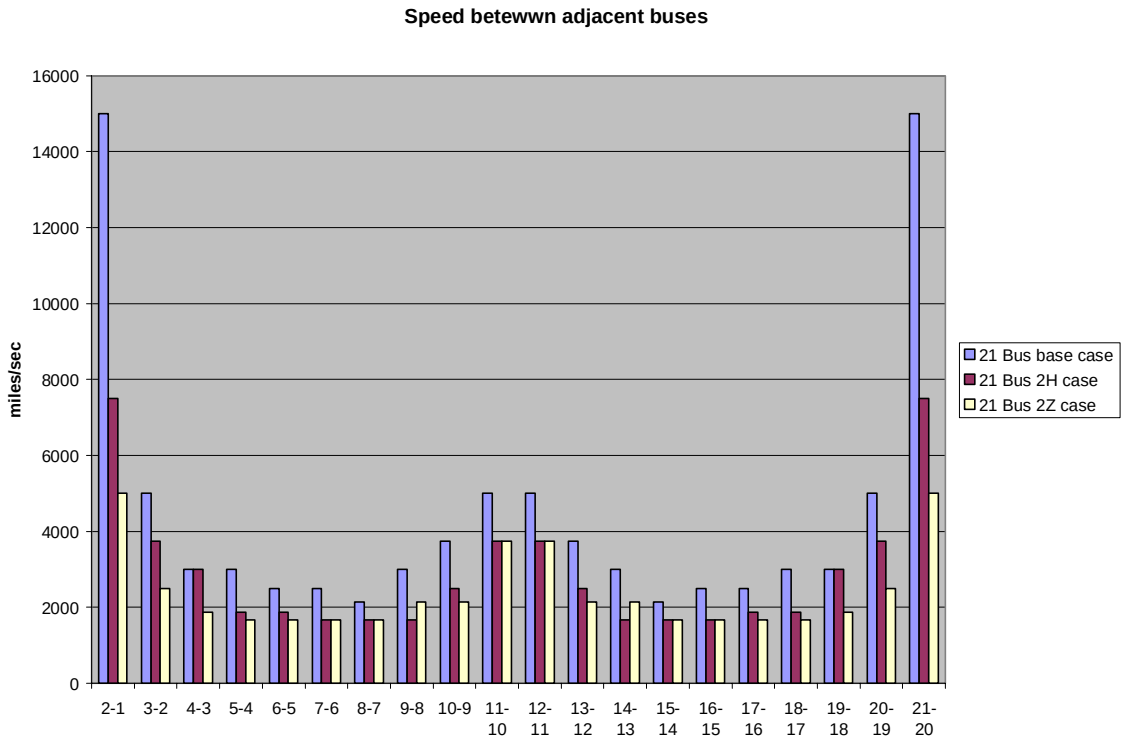

Fig 4-5. Frequency wave propagation speed between adjacent when 23.7 MW is tripped from bus 11 for single-line system

This time, the trip is initiated in the middle bus of the system, bus 11. The first thing we could spot from the speed distribution is that the speeds are symmetrical about bus 11 (the system's middle bus) in all 3 cases (base, 2H and 2Z). Generally speaking, the speed is higher near the tripping bus and becomes much higher at boundary buses. Speeds at everywhere else are in the same ballpark.

The reductions of the propagation speed by doubling either generator inertia or line impedance have consistent effect between bus 4 and 18. At boundary buses (19-21, 1-3), the doubling presents mixed results.

We can also compare the propagation speeds between different numbers of buses of the uniform single-line system. For a 21-bus and a 41-bus system, a generation trip of 0.3% of each system's total generation is introduced at bus 1, Fig 4-6 shows the wave speed between adjacent buses.

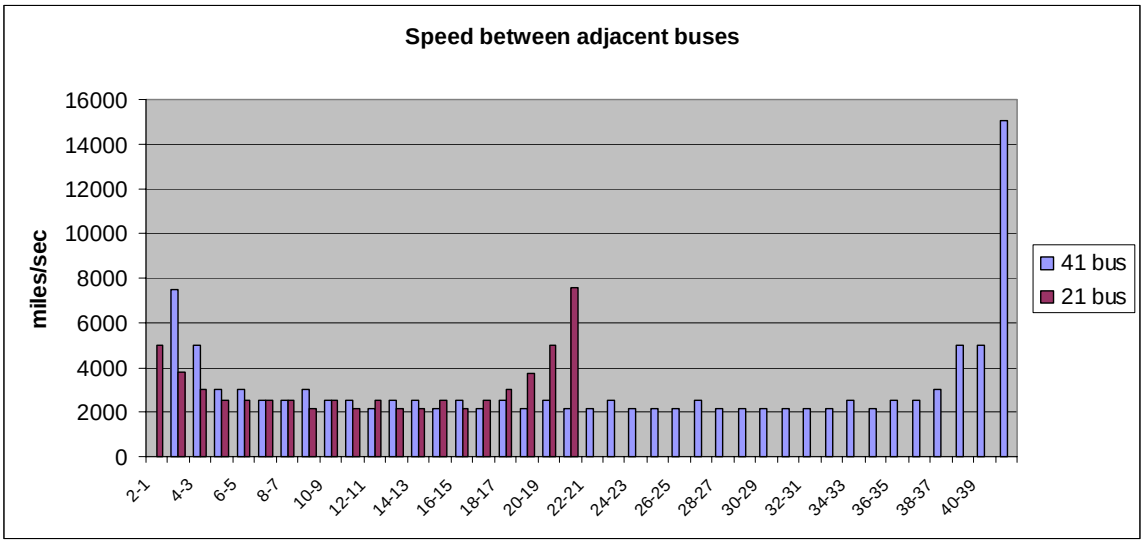

Fig 4-6. Comparison of the speeds between adjacent buses of 21-bus and 41-bus single line system when a tripping is at bus 1

As it is shown, the speeds in the middle buses are within the same ballpark, and the free-end boundary effect presents no matter how small or how large the system is. As explained in section 3.7.1.1, this free-end boundary phenomenon can be understood from a spring-mass model.

4.4.2 Multi-line system

A configuration of a two-line system is shown in Fig 4-7. Similarly, a three-line system is shown in Fig 4-8. Similar to the single-line system, all the generators are identical, so are the loads and line impedances. The middle bus is the only connection point between the other 1 or 2 branches. For the two-line or the three-line system, each line has 11 buses; so there is a total of 21 buses for two-line system; and there is a total of 41 buses for the three-line system.

We introduced a generation trip of an amount of 0.3 % of system's total capacity at the interconnected bus (bus 11) and calculate the wave propagation speeds between adjacent buses in the two-line and three-line system. In Fig 4-9, we only show the wave propagation speed at one branch; the wave propagation speeds at other branch(es) are exactly the same, so only one branch of speed is shown.

From Fig 4-9, we can see that the speeds between adjacent buses are exactly the same except for the speeds between buses 9-10, 10-11, 11-12, 12-13, which are the 4 nearest buses to the tripping point (11). The distribution of the speeds follows the same pattern as discussed in section 4.4.1. It is also interesting to note that the speed between 11-10 and 11-12 doubles and the speeds between 9-10 and 12-13 are slightly increased when an additional line about bus 11. The Thevinin equivalent impedance between bus 11 and adjacent buses becomes half if one branch is added. Therefore, the speed would increase due to the decrease of the impedance. After the wave passing adjacent buses to bus 11, they experience the same Thevinin equivalent impedances and therefore the speeds are the same between the 2 systems.

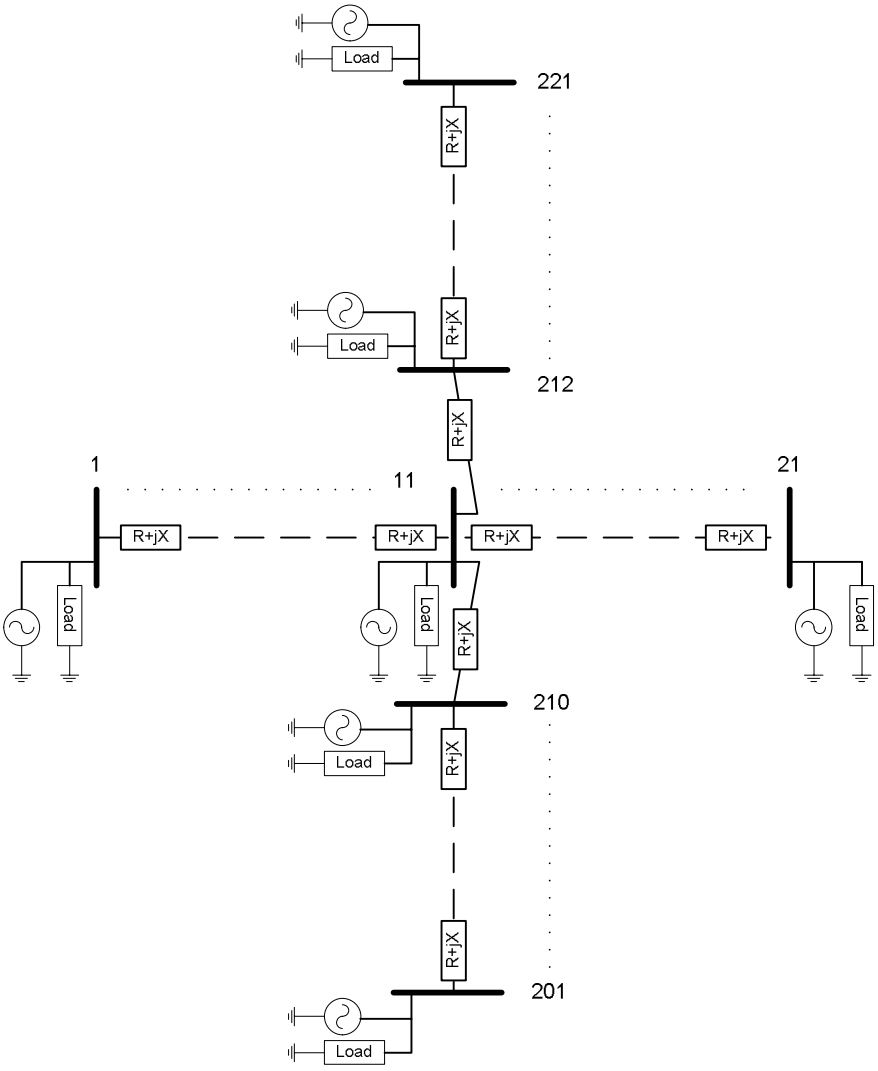

Fig 4-7. Two-line system configuration (bus numbers are labeled besides each bus bar)

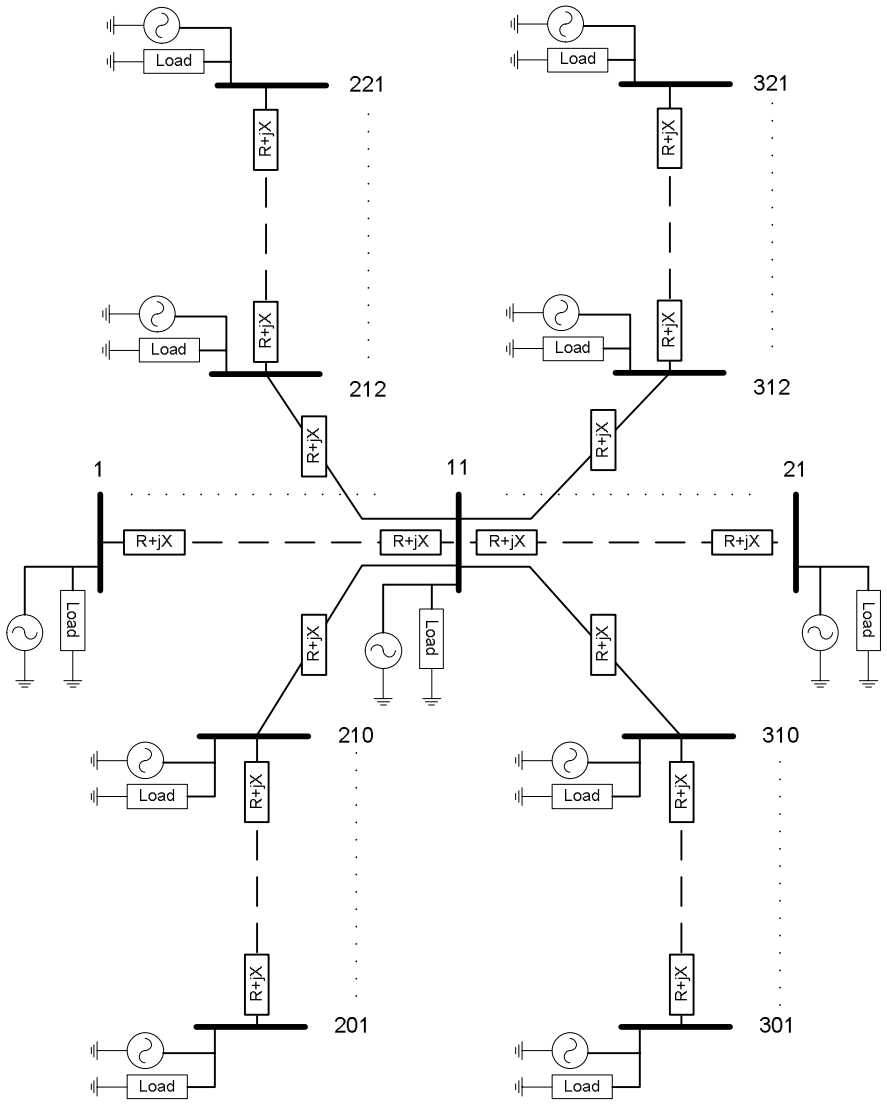

Fig 4-8. Three-line system configuration (bus numbers are labeled besides each bus bar)

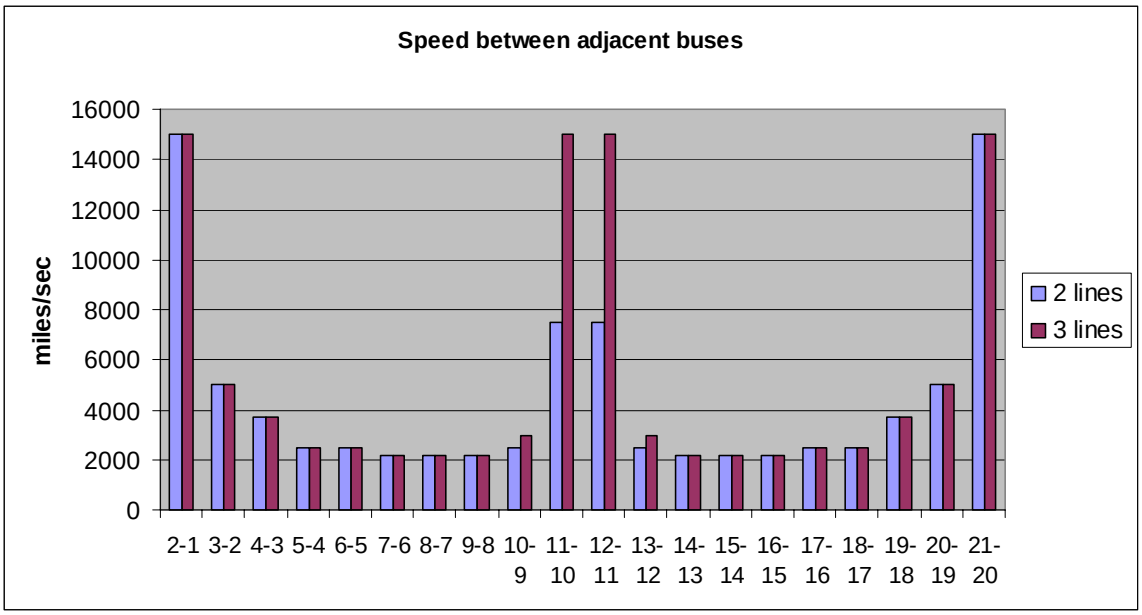

Fig 4-9. Wave speed between adjacent bus for 2-line and 3-line system when 0.3% of system generation was tripped from bus 11

4.4.3 Mesh system

We construct an 11 bus by 11 bus mesh system. Every node has the same generators, loads. The interconnected line impedances are the same across the network. Again, we introduce a 0.3 % of system's total generation trip at the center bus and see how the frequency would change to determine the frequency wave propagation.

Fig 4-10 shows the time plot of each node in the system when the bus frequency drops by 0.005 Hz from the steady state (60Hz). All the times shown below are from 0 second and the trip was initiated at time 0.1 second. The center point with time 0.1958 is the tripping point. Same color represents the same wave arrival time. As we can see from Fig 4-10, the time gradually increases throughout the system in radial direction and reach to the edge of the system at time 0.4625 second after the generation trip.

	1	2	3	4	5	6	7	8	9	10	11	
	0.4625	0.4625	0.4458	0.4375	0.4292	0.4208	0.4292	0.4375	0.4458	0.4625	0.4625	
12	0.4625	0.4542	0.4375	0.4292	0.4125	0.4042	0.4125	0.4292	0.4375	0.4542	0.4625	22
23	0.4458	0.4375	0.4208	0.4042	0.3792	0.3708	0.3792	0.4042	0.4208	0.4375	0.4458	33
34	0.4375	0.4292	0.4042	0.3708	0.3292	0.3042	0.3292	0.3708	0.4042	0.4292	0.4375	44
45	0.4292	0.4125	0.3792	0.3292	0.2708	0.2375	0.2708	0.3292	0.3792	0.4125	0.4292	55
56	0.4208	0.4042	0.3708	0.3042	0.2375	0.1958	0.2375	0.3042	0.3708	0.4042	0.4208	66
67	0.4292	0.4125	0.3792	0.3292	0.2708	0.2375	0.2708	0.3292	0.3792	0.4125	0.4292	77
78	0.4375	0.4292	0.4042	0.3708	0.3292	0.3042	0.3292	0.3708	0.4042	0.4292	0.4375	88
89	0.4458	0.4375	0.4208	0.4042	0.3792	0.3708	0.3792	0.4042	0.4208	0.4375	0.4458	99
100	0.4625	0.4542	0.4375	0.4292	0.4125	0.4042	0.4125	0.4292	0.4375	0.4542	0.4625	110
	0.4625	0.4625	0.4458	0.4375	0.4292	0.4208	0.4292	0.4375	0.4458	0.4625	0.4625	
	111	112	113	114	115	116	117	118	119	120	121	

Fig 4-10. The times (in seconds) when the bus frequency drops by 0.005 Hz in the first swing are shown in different color background. The trip was initiated at 0.1 second. The numbers at the first row and the last row are the bus numbers of the point below or above those numbers. The numbers at the first column and the last column are the bus numbers right or left to those numbers.

In Fig 4-11, we show a 3D plot of the arrival time with the subtraction of the time at the tripping point.

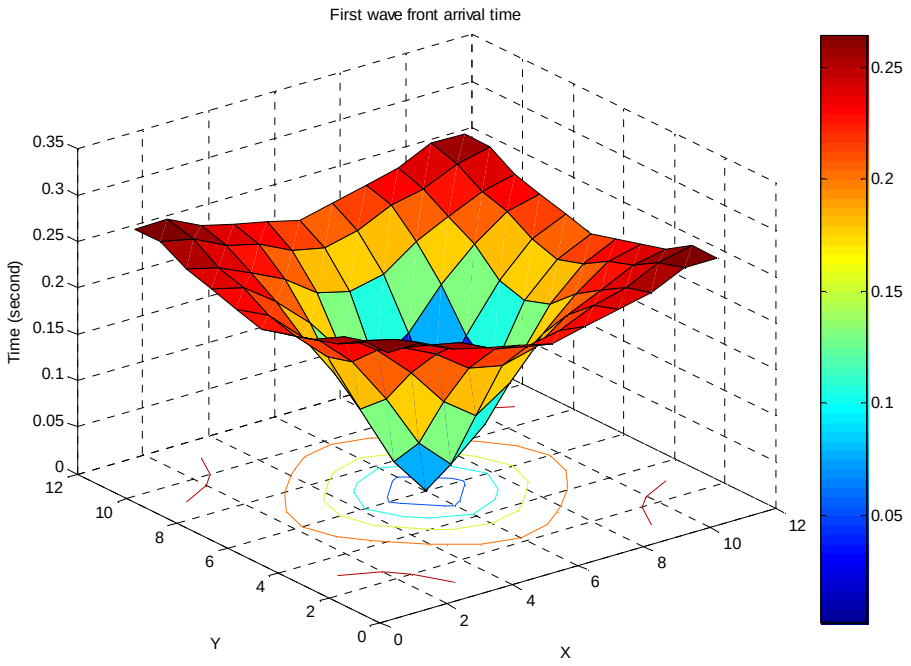

Fig 4-11. Surface plot of first wave arrival time of the uniform mesh network when a tripping initiated in the center bus of the network.

We can visually see from Fig 4-11 how the wave propagation speeds differ from area to area. At the edge of the surface, we can see that the gradient between points becomes smaller compared to that of other areas, this means that the time differences between points are smaller, which implies that the wave is traveling at a higher speed. This is consistent to what we have observed in other single-line and multi-line uniform systems, the free-end boundary phenomenon.

For the mesh network, unlike the previous line systems, we do not know exactly how to determine the distance between points; therefore, only the time of the first wave arrival was shown. In the next section, 4.5, we will attempt to find the relationship between the distance and the Thevinin equivalent impedance in the hope that we can answer the

question: “What is the distance to be used to calculate the speed of the frequency propagation wave?”

4.5 Geographical Distance vs. Thevenin Equivalent Impedance

For the mesh network, we can construct an admittance matrix (Y), which contains the electrical connection information about buses. The inverse of the Y matrix gives us the impedance matrix ($Z=Y^{-1}$). To calculate the Thevenin impedance between any 2 nodes, we can use the following equation [81]:

$$Z_{th,jk} = Z_{jj} + Z_{kk} - 2Z_{jk}$$

where $Z_{th,jk}$ is the Thevenin’s impedance between node j and k, Z_{jj} and Z_{kk} are the driving-point impedance in the impedance matrix, Z_{jk} is the transfer impedance between node j and k.

Fig 4-12 shows the normalized (maximums are normalized to 1) Thevenin equivalent impedance (Zth) and the direct geographical distance (dist) between the tripping bus (61) to other buses.

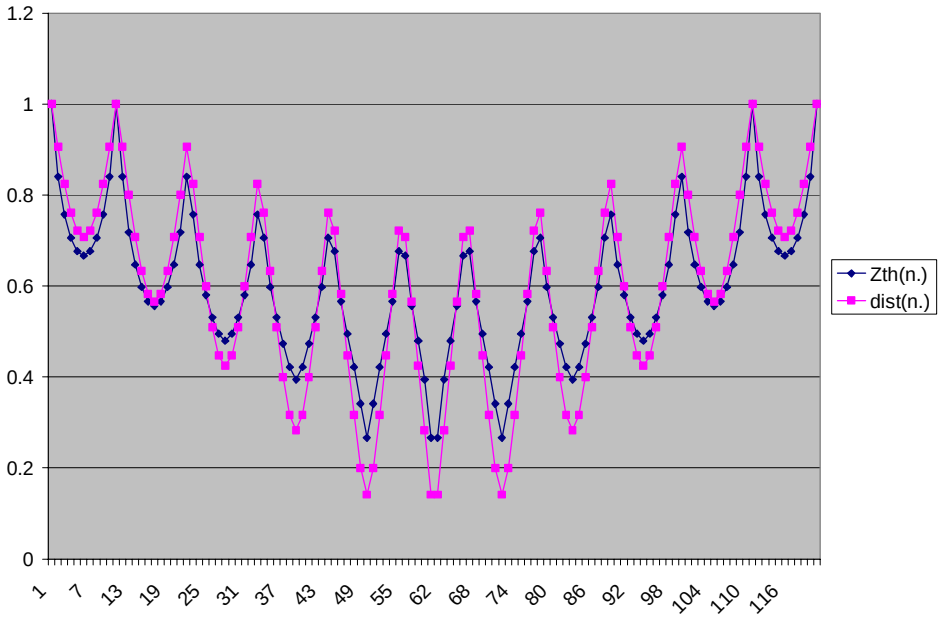

Fig 4-12. Normalized Zth and direct geographical distance between the tripping point and other nodes in the uniform mesh network. The maximums for Zth and dist are normalized to 1

From the plot, it shows that there is a strong correlation between Zth and dist. Some differences occur at some points, indicating that there would be some other parameters (e.g. generator inertia) that should be included in calculating the electromechanical distance.

4.6 Summary

In this chapter, the electromechanical wave propagation speed between 2 buses is defined as the time difference when the frequency drops by 0.005 Hz over the direct geographical distance. For actual power system, the definition becomes an approximation method to estimate the speed of frequency wave propagation. For simple system, the wave propagation speed can be calculated in a more accurate way.

Generally, areas with dense or large generators tend to slow down the electromechanical wave propagation. The wave speed is not the same even between the same two points in opposite directions. For the cases we studied, frequency wave “travels” faster in WECC127 system than in the Eastern U.S. system. For uniform single-line system, doubling generators’ inertia or doubling impedance would decrease the propagation speed except at the boundary buses. From the uniform mesh system, a strong correlation between the Thevenin equivalent impedance and the direct geographical distance can be shown between 2 buses.

Chapter 5 Frequency and Generator Mechanical Power

5.1 Motivation

The derivation of frequency and generator mechanical power stems from the study of the tripping generator power and the bus frequency response. We are primarily interested in finding the relationship between the frequency and the generators' mechanical power, and deriving a way to calculate the effective/equivalent electromechanical distance between points for wave speed calculation. The nonlinear system makes it not possible to find a closed form solution of its states. We can make some assumptions and simplifications on certain variables so that the nonlinear ODEs are solvable using Taylor's series expansion and Laplace transform.

5.2 Problem Description

At any node of the power system, the net injected power can be described as a power flow problem. The net injected power can be written mathematically as:

$$S_i = V_i \cdot I_i^* \qquad \textbf{(5-1)}$$

where S_i, V_i and I_i are the injected apparent power, voltage, injected current at bus i.

I_i can be written as a summation of the current of all other branches:

$$I_i = \sum_{n=1}^{N} Y_{in} V_n \qquad i = 1 \ldots N \qquad \textbf{(5-2)}$$

where N is the total number of buses; and Y_{in} is equal to the negative of the line

admittance between bus i and bus n, if i $\neq$ n and is equal to the sum of all the admittances connecting to bus i if i = n.

If we let $V_i = |V_i| e^{j\delta_i}$ and $Y_{in} = G_{in} + j\, B_{in}$. Combining with (4-1) and (4-2), we will get

$$S_i = \sum_{n=1}^{N} |V_i||V_n| e^{j\delta_{in}} (G_{in} - jB_{in})$$
$$S_i = \sum_{n=1}^{N} |V_i||V_n| (\cos\delta_{in} + j\sin\delta_{in})(G_{in} - jB_{in})$$

The net injected active power and net injected reactive power can be written as

$$P_i = \sum_{n=1}^{N} |V_i||V_n| (G_{in}\cos\delta_{in} + B_{in}\sin\delta_{in})$$
$$Q_i = \sum_{n=1}^{N} |V_i||V_n| (G_{in}\sin\delta_{in} - B_{in}\cos\delta_{in}) \qquad \textbf{(5-3)}$$

As we can see, the power is a function of voltage amplitude, voltage phase angle, and line impedance. To find the solution to these equations, numerical iteration techniques (e.g. Newton, Gauss-Siedel, DC decomposition and etc.) seem to be the only ways. The units of *P*, *Q*, *V*, *G*, *B* and δ are MW, MVAR, kV, 1/Ohm, 1/Ohm, and radian, respectively.

The generator injects active electrical power to the system. To describe the relationship between the generator speed (frequency), and the mechanical and electrical power with neglecting damping and friction effect, we can write two first order equations (known as swing equations) as following:

$$\frac{2H}{\omega_s}\cdot\frac{d\omega_i}{dt} = P_{mi} - P_{ei}$$
$$\frac{d\delta_i}{dt} = \omega_i \qquad \textbf{(5-4)}$$

Where H is the inertia constant, ω_s is the synchronous speed (2*π*60 rad/sec), ω_i is the angular speed at bus i, P_{mi} is the mechanical power from generator i and P_{ei} is the electrical power injecting into the system at bus i. The units of P_{mi} and P_{ei} in (5-4) are per-unit.

Equations (5-3) and (5-4) describe the power system networks statically and dynamically with considering the generator and power network only, where these 2 sets of equations comprise the majority of the system and are our main interests in this study. Computer simulation programs use different integration techniques to solve for the solutions to these equations iteratively due to the nonlinearity nature of these ODEs. At each time step, a predictor is used to calculate the value of the next time step based on the previously calculated values and initial conditions. Therefore, no closed form solutions can be obtained. In the next section, we made some assumptions on some variables to obtain a special closed form solution to (5-3) and (5-4)

5.3 Derivation

The purpose of this section is to derive a relationship between the mechanical powers from the generator to the bus frequencies. For each bus in the network, we assume there are a generator and a load. Load may be represented as a constant power load, constant current load, constant impedance load or combination; we convert loads to constant impedance load for simplicity. This simplification allows us to include load into the

admittance matrix but not as a constraint to the power flow equation (5-3).

In addition, we assume that the voltages are held at constant. By per-unitizing (5-3) to the system's MVA base, we can assume that V_is are equal to 1 per-unit (p.u.). Therefore, (5-3) can be written as

$$P_{ei} = \frac{1}{MVA_{base}} \sum_{n=1}^{N} (G_{in} \cos \delta_{in} + B_{in} \sin \delta_{in}) \qquad \textbf{(5-5)}$$

where MVA_{base} is the system MVA base, which is typically 100, and we change P_i to P_{ei} to represent the electrical power that is injected from the bus to the system. Since only the generator is the electrical power source at each bus, load is combined in the admittance matrix.

(5-5) contains the nonlinear equations of cosine and sine; we then expand the equation about δ_{in} using Taylor series expansion assuming that the phase angle between buses are small, therefore, δ_{in} is small. (5-5) then becomes

$$P_{ei} = \frac{1}{MVA_{base}} \sum_{n=1}^{N} (G_{in}(1 - \frac{1}{2}\delta_{in}^2 + H.O.T.) + B_{in}(\delta_{in} - \frac{1}{6}\delta_{in}^3 + H.O.T.))$$

Since δ_{in} is small between adjacent buses, the 2nd order and higher order terms (*H.O.T.*) of δ_{in} can then be omitted, so the above equation becomes

$$P_{ei} = \frac{1}{MVA_{base}} \sum_{n=1}^{N} (G_{in} + B_{in}\delta_{in})$$

which then becomes a linear equation of δ_{in}.

The above equation is static, which represents the active injected power at a bus at any given time. The variables P_{ei} and δ_{in} can, therefore, be treated as function of time, $P_{ei}(t)$ and $\delta_{in}(t)$, as the power system is continuously changing with time. The line admittances are treated as constants. We can then apply Laplace transform on the above equation and get

$$P_{ei}(s) = \frac{1}{MVA_{base}} \sum_{n=1}^{N} \left(\frac{G_{in}}{s} + B_{in} \Delta_{in}(s) \right) \qquad \textbf{(5-6)}$$

where $P_{ei}(s)$ is the Laplace transform of $P_{ei}(t)$ and $\Delta_{in}(s)$ is the Laplace transform of $\delta_{in}(t)$.

For (5-4), we may also apply the Laplace transform to get an s-domain representation of the swing equation. Here we assume the mechanical power input P_{mi} is constant.

$$\begin{aligned} &\frac{2H}{\omega_s}(s\Omega_i(s) - \omega_i(0)) = \frac{1}{s} P_{mi} - P_{ei}(s) \\ &s\Delta_i(s) - \delta_i(0) = \Omega_i(s) \end{aligned} \qquad \textbf{(5-7)}$$

where $\delta_i(0)$ and $\omega_i(0)$ are the initial condition of phase angle and frequency at bus i.

Special attention should be paid to initial conditions of ω and δ since the differential terms are involved in the swing equation. The initial values of bus voltage angle ($\delta_i(0)$) can be obtained from power flow study. DC decomposition technique can be used to obtain the solution for bus voltage angle ($\delta_i(0)$). Using DC decomposition technique is consistent with the assumption with the previous section where the voltage amplitude is assumed constant. For speed, the initial value of $\omega_i(0)$ is equal to ω_s.

Rearranging (5-6) and (5-7), we can then get

$$\frac{2H}{\omega_s}(s\Omega_i(s)-\omega_i(0))=\frac{1}{s}P_{mi}-\sum_{n=1}^{N}[\frac{1}{s}G_{in}+\frac{1}{s}B_{in}(\Omega_{in}(s)+\delta_{in}(0)]$$

We can substitute $\omega_i(0)$ by ω_s and rearrange the equation by putting Ω terms on one side and other terms on the other side.

$$\frac{2H}{\omega_s}s\Omega_i(s)+\sum_{i=1}^{N}[\frac{1}{s}B_{in}\cdot\Omega_{in}(s)]=2H+\frac{1}{s}P_{mi}-\sum_{i=1}^{N}\frac{1}{s}[G_{in}+B_{in}\delta_{in}(0)] \qquad \textbf{(5-8)}$$

By setting up a system of equations using (5-8), we can then solve a system of algebraic equations in s-domain. The number of equations is equal to the number buses in the system, and the number of unknown is equal to the number of buses, so the system equation is not over or under determinant. After solving for $\Omega_i(s)$, we can apply inverse Laplace transform to get the solution in time domain.

Recap the assumptions for the derivation of (5-8):

1. Each bus has a generator and a load.
2. No damping and friction terms for generators
3. The generator internal angle is assumed to be the same as the connecting bus angle. Therefore, no internal reactance is considered
4. The bus phase angle between adjacent buses is small
5. Bus voltages are assumed to be 1 p.u.
6. Loads are modeled as constant impedance
7. Generator's mechanical power is held constant

5.4 Example

Solving the system of equations (5-8) can be carried out in Maple, which can perform numeric or symbolic calculations. Take the 11 bus single-line system as an example, where the system's parameters are defined in 3.7.1 and the configuration of similar system can be found in Fig 3-34. The system of equations for the 11 bus single-line system to be solved is shown as following:

$$\frac{0.0774\cdot s\cdot\Omega_1}{\pi}+\frac{0.3718091010\cdot(\Omega_1-\Omega_2)}{s}=\frac{Pm_1-0.3542310999}{s},$$
$$\frac{0.0774\cdot s\cdot\Omega_2}{\pi}+\frac{0.3718091010\cdot(\Omega_2-\Omega_1)}{s}+\frac{0.3718091010\cdot(\Omega_2-\Omega_3)}{s}=\frac{Pm_2-0.7045046173}{s},$$
$$\frac{0.0774\cdot s\cdot\Omega_3}{\pi}+\frac{0.3718091010\cdot(\Omega_3-\Omega_2)}{s}+\frac{0.3718091010\cdot(\Omega_3-\Omega_4)}{s}=\frac{Pm_3-0.7045046173}{s},$$
$$\frac{0.0774\cdot s\cdot\Omega_4}{\pi}+\frac{0.3718091010\cdot(\Omega_4-\Omega_3)}{s}+\frac{0.3718091010\cdot(\Omega_4-\Omega_5)}{s}=\frac{Pm_4-0.7045046173}{s},$$
$$\frac{0.0774\cdot s\cdot\Omega_5}{\pi}+\frac{0.3718091010\cdot(\Omega_5-\Omega_4)}{s}+\frac{0.3718091010\cdot(\Omega_5-\Omega_6)}{s}=\frac{Pm_5-0.7045046173}{s},$$
$$\frac{0.0774\cdot s\cdot\Omega_6}{\pi}+\frac{0.3718091010\cdot(\Omega_6-\Omega_5)}{s}+\frac{0.3718091010\cdot(\Omega_6-\Omega_7)}{s}=\frac{Pm_6-0.7045046173}{s},$$
$$\frac{0.0774\cdot s\cdot\Omega_7}{\pi}+\frac{0.3718091010\cdot(\Omega_7-\Omega_6)}{s}+\frac{0.3718091010\cdot(\Omega_7-\Omega_8)}{s}=\frac{Pm_7-0.7045046173}{s},$$
$$\frac{0.0774\cdot s\cdot\Omega_8}{\pi}+\frac{0.3718091010\cdot(\Omega_8-\Omega_7)}{s}+\frac{0.3718091010\cdot(\Omega_8-\Omega_9)}{s}=\frac{Pm_8-0.7045046173}{s},$$
$$\frac{0.0774\cdot s\cdot\Omega_9}{\pi}+\frac{0.3718091010\cdot(\Omega_9-\Omega_8)}{s}+\frac{0.3718091010\cdot(\Omega_9-\Omega_{10})}{s}=\frac{Pm_9-0.7045046173}{s},$$
$$\frac{0.0774\cdot s\cdot\Omega_{10}}{\pi}+\frac{0.3718091010\cdot(\Omega_{10}-\Omega_9)}{s}+\frac{0.3718091010\cdot(\Omega_{10}-\Omega_{11})}{s}=\frac{Pm_{10}-0.7045046173}{s},$$
$$\frac{0.0774\cdot s\cdot\Omega_{11}}{\pi}+\frac{0.3718091010\cdot(\Omega_{11}-\Omega_{10})}{s}=\frac{Pm_{11}-0.3542310999}{s}$$

Fig 5-1. System equations for a 11 bus single-line system

We then solve the equations of Ωs as a function of P_{mi} (i=1..11) and s (laplace domain variable). By applying inverse laplace transform on Ωs, we can get the time functions of ωs as a function of P_{mi}s. As an example of the outcomes, ω_2 is shown as following: (here we only show the dependence to P_{mi} (i=1..11) terms, other terms are too small to have an

effect on ω_2).

$$
\begin{aligned}
\omega_2 = \\
& Pm_1\,(3.689913852\,t + 0.2107522422\,\sin(7.454854940\,t) - 0.6923762838\,\sin(5.871808270\,t) \\
& \quad - 0.05675140002\sin(7.690421698t) - 0.5859658998\sin(3.227577220t) \\
& \quad - 0.4162000864\sin(7.067359406t) + 2.118387856\sin(2.188928107t) \\
& \quad - 0.2103391794\sin(4.200522386t) + 0.6042374876\sin(6.536165443t) \\
& \quad - 6.009303850\sin(1.105718671t) + 0.5926399090\sin(5.087957379t)) \\
+ \\
& Pm_2\,(3.689913852\,t - 0.5653549214\,\sin(7.454854940\,t) + 0.8894434400\,\sin(5.871808270\,t) \\
& \quad + 0.1656553504\sin(7.690421698t) - 0.1814862289\sin(3.227577220t) \\
& \quad + 0.9612870654\sin(7.067359406t) + 1.445814675\sin(2.188928107t) \\
& \quad + 0.03558308746\sin(4.200522386t) - 1.106269324\sin(6.536165443t) \\
& \quad - 5.522465790\sin(1.105718671t) - 0.4239572578\sin(5.087957379t)) \\
+ \\
& Pm_3\,(3.689913852\,t + 0.7404894158\,\sin(7.454854940\,t) + 0.4392190030\,\sin(5.871808270\,t) \\
& \quad - 0.2611352798\sin(7.690421698t) + 0.3482694854\sin(3.227577220t) \\
& \quad - 0.8427742720\sin(7.067359406t) + 0.3142055474\sin(2.188928107t) \\
& \quad + 0.2399026746\sin(4.200522386t) + 0.3149084684\sin(6.536165443t) \\
& \quad - 4.588230398\sin(1.105718671t) - 0.7133105434\sin(5.087957379t)) \\
+ \\
& Pm_4\,(3.689913852\,t - 0.6805607886\,\sin(7.454854940\,t) - 1.014455875\,\sin(5.871808270\,t) \\
& \quad + 0.3354542696\sin(7.690421698t) + 0.6376222584\sin(3.227577220t) \\
& \quad + 0.1424737033\sin(7.067359406t) - 0.9171616236\sin(2.188928107t) \\
& \quad + 0.1637352399\sin(4.200522386t) + 0.8446270422\sin(6.536165443t) \\
& \quad - 3.282283866\sin(1.105718671t) + 0.2209282172\sin(5.087957379t)) \\
+ \\
& Pm_5\,(3.689913852\,t + 0.4045928192\,\sin(7.454854940\,t) - 0.1504801158\,\sin(5.871808270\,t) \\
& \quad - 0.3825896216\sin(7.690421698t) + 0.4868380878\sin(3.227577220t) \\
& \quad + 0.6561799786\sin(7.067359406t) - 1.857336459\sin(2.188928107t) \\
& \quad - 0.1038665291\sin(4.200522386t) - 1.016668469\sin(6.536165443t) - 1.710426213\sin(1.105718671t) \\
& \quad + 0.7761931624\sin(5.087957379t)) \\
+ \\
& Pm_6\,(3.689913852\,t - 0.0001899509013\,\sin(7.454854940\,t) + 1.057286456\,\sin(5.871808270\,t)
\end{aligned}
$$

$$+ 0.3987219218\sin(7.690421698t) + 3.73190998410^{-8}\sin(3.227577220t)$$
$$- 1.001856122\sin(7.067359406t) - 2.207820084\sin(2.188928107t) - 0.2500306290\sin(4.200522386t)$$
$$+ 0.00007340705090\sin(6.536165443t) - 4.2169373301 0^{-9}\sin(1.105718671t)$$
$$- 0.000001060340400\sin(5.087957379t))$$

$+$

$$Pm_7\,(3.689913852\,t - 0.4042744432\sin(7.454854940\,t) - 0.1504489415\sin(5.871808270\,t)$$
$$- 0.3825434494\sin(7.690421698t) - 0.4868380336\sin(3.227577220t)$$
$$+ 0.6559280582\sin(7.067359406t) - 1.857336428\sin(2.188928107t)$$
$$- 0.1038664173\sin(4.200522386t) + 1.016606399\sin(6.536165443t)$$
$$+ 1.710426204\sin(1.105718671t) - 0.7761935396\sin(5.087957379t))$$

$+$

$$Pm_8\,(3.689913852\,t + 0.6804026632\sin(7.454854940\,t) - 1.014464632\sin(5.871808270\,t)$$
$$+ 0.3353661284\sin(7.690421698t) - 0.6376221976\sin(3.227577220t)$$
$$+ 0.1428055571\sin(7.067359406t) - 0.9171616024\sin(2.188928107t)$$
$$+ 0.1637351580\sin(4.200522386t) - 0.8447242110\sin(6.536165443t)$$
$$+ 3.282283860\sin(1.105718671t) - 0.2209262198\sin(5.087957379t))$$

$+$

$$Pm_9\,(3.689913852\,t - 0.7405561904\sin(7.454854940\,t) + 0.4391994748\sin(5.871808270\,t)$$
$$- 0.2610075648\sin(7.690421698t) - 0.3482696988\sin(3.227577220t)$$
$$- 0.8429376576\sin(7.067359406t) + 0.3142056028\sin(2.188928107t)$$
$$+ 0.2399035858\sin(4.200522386t) - 0.3147817578\sin(6.536165443t)$$
$$+ 4.588230392\sin(1.105718671t) + 0.7133077360\sin(5.087957379t))$$

$+$

$$Pm_{10}\,(3.689913852\,t + 0.5657066318\sin(7.454854940\,t) + 0.8894239722\sin(5.871808270\,t)$$
$$+ 0.1654681299\sin(7.690421698t) + 0.1814863547\sin(3.227577220t)$$
$$+ 0.9610739424\sin(7.067359406t) + 1.445814701\sin(2.188928107t)$$
$$+ 0.03558105126\sin(4.200522386t) + 1.106329924\sin(6.536165443t)$$
$$+ 5.522465788\sin(1.105718671t) + 0.4239662488\sin(5.087957379t))$$

$+$

$$Pm_{11}\,(3.689913852\,t - 0.2108388910\sin(7.454854940\,t) - 0.6923942416\sin(5.871808270\,t)$$
$$- 0.05670230404\sin(7.690421698t) + 0.5859656220\sin(3.227577220t)$$
$$- 0.4161680160\sin(7.067359406t) + 2.118387922\sin(2.188928107t)$$
$$- 0.2103388862\sin(4.200522386t) - 0.6042179036\sin(6.536165443t)$$
$$+ 6.009303846\sin(1.105718671t) - 0.5926359436\sin(5.087957379t))$$

We can apply an analysis to the solved ωs. The 'sensitivity' of ωs to each P_ms (i.e. $\partial\omega/\partial P_m$) to have an estimate on each P_{mi}s' influence on ω, can be obtained. As an example, we examine the sensitivity of $\omega 1$ to each P_m

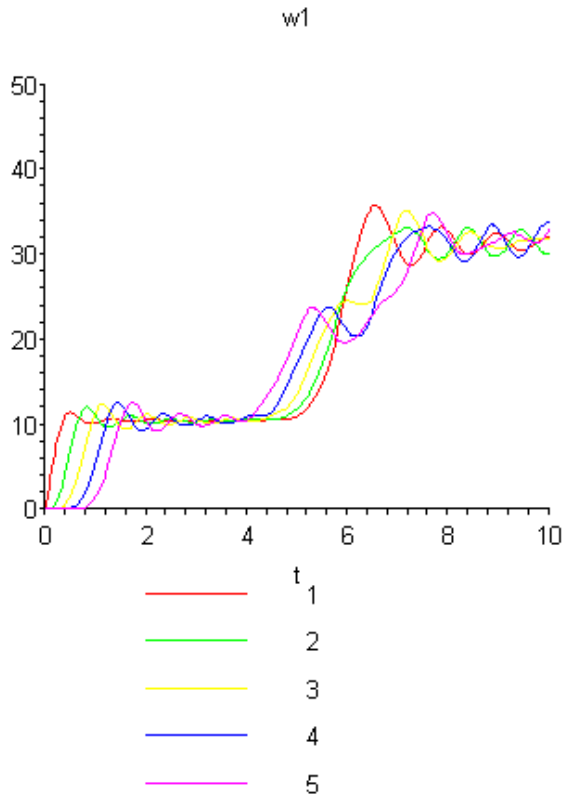

Fig 5-2. Sensitivity of ω_1 to P_{mi} (i=1 to 5)

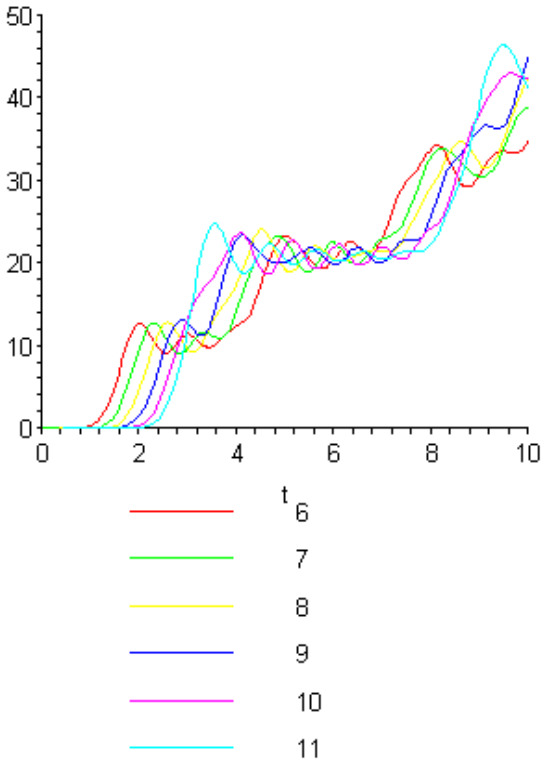

Fig 5-3. Sensitivity of ω_1 to P_{mi} (i=6 to 11)

From Fig 5-2 and Fig 5-3, the delayed response of P_m to ω_1 would explain the delayed response of frequency in system simulation and measurements when generation trips occurred.

Chapter 6 FNET Measurement Data Analysis

6.1 Introduction

FNET continuously collects frequency data from disperse FDRs in the U.S. power grid. The central server archives the data into Microsoft Access (MSA) database files. MSA saves the data into an organized database format, and it is very easy to manage the database. However, if we would like to perform analyses on the data, such as plot data points, signal processing, etc, MSA provides limited or no functionalities of advanced data calculations. Therefore, we convert the data from MSA format into Matlab binary format. Matlab is known for its rich functions for mathematical manipulation and visualization on numeric data. In this chapter, we first show the procedure of converting the data from MSA into Matlab format. During the conversion process, several known data errors can be detected and removed or modified.

The frequency measured at 110 V outlet records not only system's dynamics but also local random load variation. Therefore, the signal sometimes contains noises. To remove such noises, we apply the wavelet denoising technique to extract system's dynamics from FDR measurement data. Since we can extract system's frequency dynamics from FDR measurement, we then compare with PMU data from a 345 kV line with a close-by FDR data to understand how closely the FDR tracks system's frequency.

As we have seen in Chapter 2 and Chapter 3, when disturbance, such as generator trip, load rejection, or line opening, occurred, it would propagate throughout the system as a form of electromechanical wave. From several field recordings, we are able to see such

propagation. In this chapter, some recordings and analysis will be shown. In addition to observing transient events, we would be able to record some oscillation modes in the system. In this chapter, some examples will be provided.

In the following plots, we will represent each FDR in its unit number instead of name. The FDR numbers and the corresponding names are listed in Table 6-1. The FDR locations can be found in Fig 1-8.

Unit number	Unit Name	Area
1	NY	EUS
2	UMR	EUS
3	ARI	EUS
4	VT	EUS
5	Seattle	WECC
6	ABB	EUS
7	MSSTATE (MISS)	EUS
8	EPRI	WECC
9	UFL	EUS
11	Calvin College	EUS
12	Houston	ERCOT
14	ASU	WECC
16	LA	WECC
17	Tulane	EUS
20	TVA	EUS

Table 6-1. FDR unit numbers and names

6.2 FNET server data processing

The collected data from FDRs are stored in database files. The format of the database file is in Microsoft Access (MSA). Each FDR data is stored into a different Table, as shown

in Fig 6-1. For each table, there are 10 different data fields, namely: Index, UnitID, Sample_Date&Time, ConvNum, FirstFreq, LastFreq, VoltageAng, VoltageMag, DateCreated. An example of data section is shown in Fig 6-2:

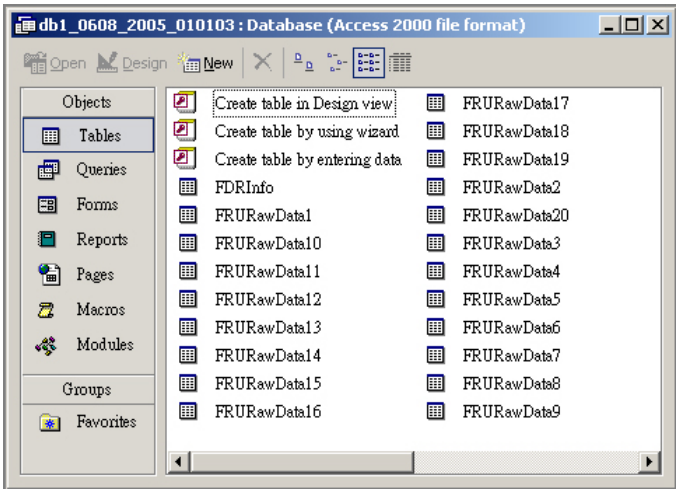

Fig 6-1. Data table in Microsoft Access

FRURawData11 : Table

Index	UnitID	Sample_Date&Time	ConvNum	FirstFreq	FinalFreq	VoltageAng	VoltageMag	DateCreated
1	11	6/8/2005 5:00:52 AM	7	59.9673	59.9699	3.0438	120.743	6/8/2005 1:01:03 AM
2	11	6/8/2005 5:00:52 AM	8	59.9723	59.9749	3.0237	120.7518	6/8/2005 1:01:04 AM
3	11	6/8/2005 5:00:52 AM	9	59.9613	59.9638	3.0004	120.8257	6/8/2005 1:01:04 AM
4	11	6/8/2005 5:00:52 AM	10	59.9633	59.9662	2.9772	120.8689	6/8/2005 1:01:04 AM
5	11	6/8/2005 5:00:53 AM	1	59.9656	59.9683	2.9549	120.8466	6/8/2005 1:01:04 AM
6	11	6/8/2005 5:00:53 AM	2	59.9701	59.9727	2.9335	120.7855	6/8/2005 1:01:04 AM
7	11	6/8/2005 5:00:53 AM	3	59.9666	59.9693	2.9143	120.7854	6/8/2005 1:01:04 AM
8	11	6/8/2005 5:00:53 AM	4	59.9643	59.967	2.8928	120.8505	6/8/2005 1:01:04 AM
9	11	6/8/2005 5:00:53 AM	5	59.9713	59.9739	2.8732	120.7959	6/8/2005 1:01:04 AM
10	11	6/8/2005 5:00:53 AM	6	59.9648	59.9675	2.8516	120.7528	6/8/2005 1:01:04 AM
11	11	6/8/2005 5:00:53 AM	7	59.9677	59.9703	2.8308	120.7231	6/8/2005 1:01:04 AM
12	11	6/8/2005 5:00:53 AM	8	59.9674	59.9703	2.8105	120.7371	6/8/2005 1:01:04 AM
13	11	6/8/2005 5:00:53 AM	9	59.961	59.9635	2.7878	120.766	6/8/2005 1:01:05 AM
14	11	6/8/2005 5:00:53 AM	10	59.9668	59.9694	2.7655	120.7326	6/8/2005 1:01:05 AM
15	11	6/8/2005 5:00:54 AM	1	59.9653	59.9679	2.743	120.758	6/8/2005 1:01:05 AM
16	11	6/8/2005 5:00:54 AM	2	59.9643	59.9668	2.7216	120.7704	6/8/2005 1:01:05 AM
17	11	6/8/2005 5:00:54 AM	3	59.9614	59.9639	2.7012	120.8193	6/8/2005 1:01:05 AM
18	11	6/8/2005 5:00:54 AM	4	59.9631	59.9656	2.6794	120.8703	6/8/2005 1:01:05 AM
19	11	6/8/2005 5:00:54 AM	5	59.9698	59.9724	2.6587	120.8131	6/8/2005 1:01:05 AM
20	11	6/8/2005 5:00:54 AM	6	59.9684	59.971	2.6383	120.7744	6/8/2005 1:01:05 AM
21	11	6/8/2005 5:00:54 AM	7	59.965	59.9677	2.6174	120.7332	6/8/2005 1:01:05 AM
22	11	6/8/2005 5:00:54 AM	8	59.9694	59.972	2.5968	120.7418	6/8/2005 1:01:05 AM
23	11	6/8/2005 5:00:54 AM	9	59.9645	59.9672	2.5751	120.7647	6/8/2005 1:01:06 AM
24	11	6/8/2005 5:00:54 AM	10	59.9657	59.9684	2.5537	120.707	6/8/2005 1:01:06 AM
25	11	6/8/2005 5:00:55 AM	1	59.967	59.9697	2.5322	120.7133	6/8/2005 1:01:06 AM
26	11	6/8/2005 5:00:55 AM	2	59.9615	59.964	2.5101	120.7291	6/8/2005 1:01:06 AM
27	11	6/8/2005 5:00:55 AM	3	59.9675	59.9702	2.4911	120.7739	6/8/2005 1:01:06 AM
28	11	6/8/2005 5:00:55 AM	4	59.9577	59.9603	2.4664	120.8244	6/8/2005 1:01:06 AM
29	11	6/8/2005 5:00:55 AM	5	59.9677	59.9704	2.444	120.7883	6/8/2005 1:01:06 AM
30	11	6/8/2005 5:00:55 AM	6	59.9665	59.9691	2.4233	120.7849	6/8/2005 1:01:06 AM
31	11	6/8/2005 5:00:55 AM	7	59.9677	59.9705	2.4027	120.7468	6/8/2005 1:01:06 AM
32	11	6/8/2005 5:00:55 AM	8	59.9675	59.9702	2.3829	120.7915	6/8/2005 1:01:06 AM

Record: 1 of 863998

Fig 6-2. Sample of stored FDR data

The meaning of each column is stated as follows:

Index: the index number for the data

UnitID: FDR unit identification number

Sample_Date&Time: data sampled time in UTC from GPS.

ConvNum: conversion number

FirstFreq: first calculated frequency from 1440 samples

LastFreq: recalculated frequency from resampled data based on FirstFreq

VoltageAng: voltage angle of the last point from 1 sampling period

VoltageMag: calculated voltage RMS magnitude during 1 sampling period

DateCreated: local server time in EST

MSA provides very good functions in storing and managing the data; however, it has limited data processing functions (such as algebraic calculation on the data). Therefore, we would need to export the saved FDR frequency data into other mathematically-oriented software. Here, we select to use Matlab as our main data processing platform.

Matlab is known for its flexibility of processing numerical data. In addition, it provides easy-to-use plotting functionalities; therefore, the user can visualize the data without much difficulty. The data processing procedure from *.mdb (Microsoft Access data base file) to *.mat (Matlab binary data file) is outlined as follows:

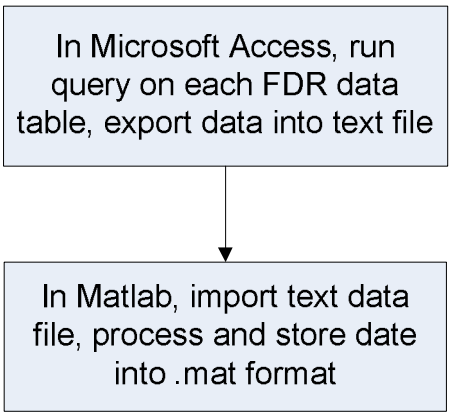

Fig 6-3. Outlined procedure of FDR data processing in Microsoft Access and Matlab

In Microsoft Access operation, detailed steps are as follows:

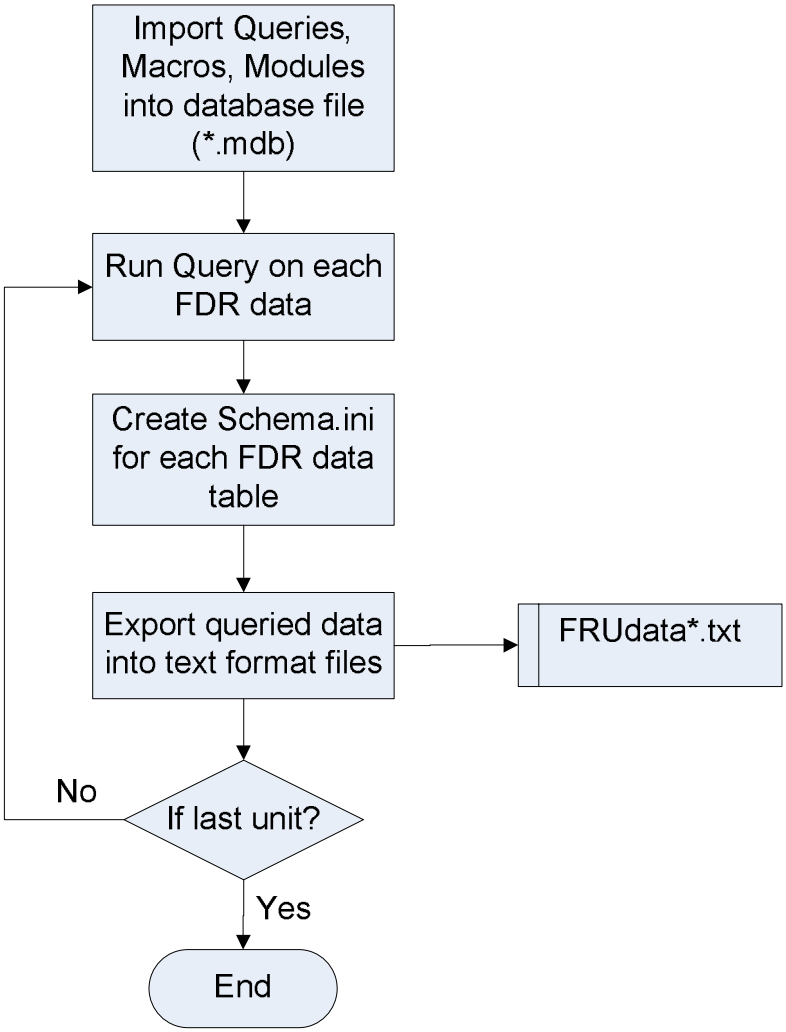

Fig 6-4. Detailed FDR data process procedure in MS Access

The above procedure is written in Visual Basic language in MSA. The script can be found in Appendix I. For each query in MSA, we export only relevant data fields for later processing, namely, Sample_Date&Time, ConvNum, LastFreq, and VoltageAng. A sample of query window is shown in Fig 6-5.

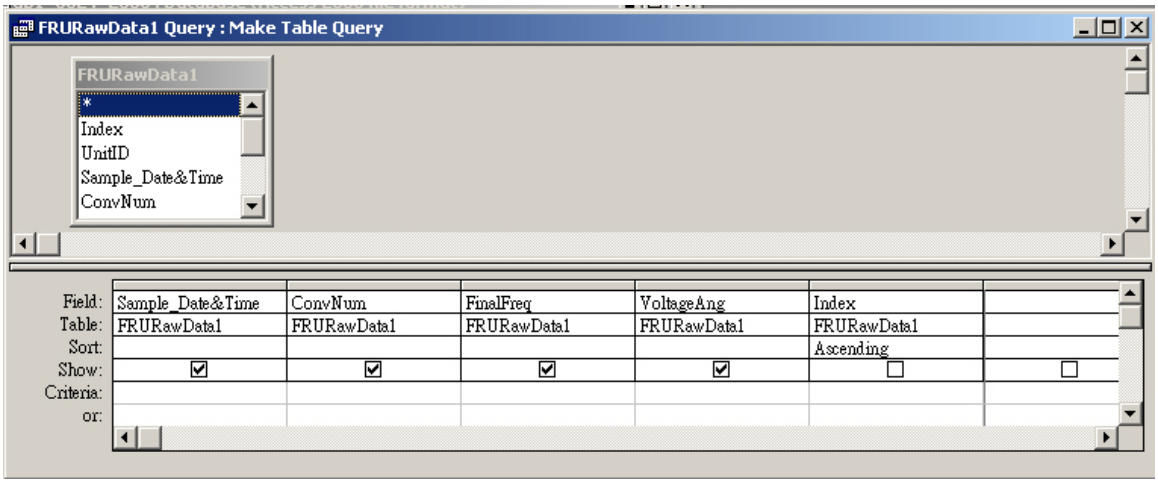

Fig 6-5. A sample query window for FDR data in Microsoft Access

Note that, in order to keep all the digits in the frequency and angle data, we need to export them as LongChar into text files, otherwise MSA, by default, will automatically truncate them into 2 digits. Hence, a new schema.ini file, which is to define the format for the exported text file, is needed for each FDR data export. A typical schema.ini files looks like following:

```
[FRUData20.txt]
ColNameHeader = False
Format = CSVDelimited
Col1=Sample_Date&Time Date
Col2=ConvNum Integer
Col3=FinalFreq LongChar
Col4=VoltageAng LongChar
```

During the operations in MSA, each FDR data is stored into a text file (FRUdata*.txt), where * is the unit number. In Matlab, we can, therefore, import the data from each FRUtdata*.txt file and perform further data processing. In Matlab, the data is handled in the following steps:

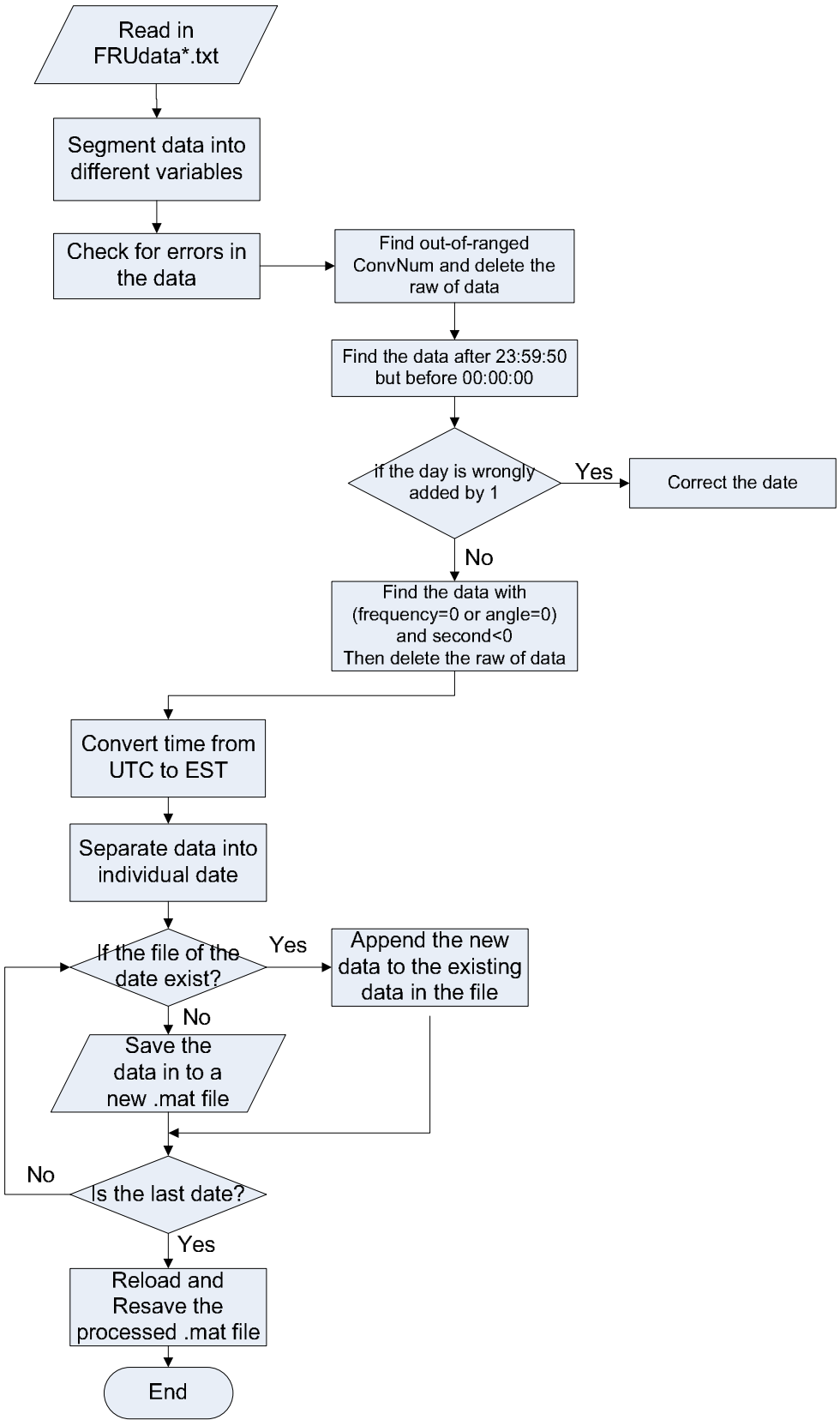

Fig 6-6. Detailed FDR data process procedure in Matlab

The Matlab script of Fig 6-6 is included in Appendix III. Further, each FDR data is stored to an individual structure variable and under each FDR structure variable, 4 fields are created and each store the 4 exported data fields from MSA database file. The data structure for each FDR in Matlab is showns in Fig 6-7.

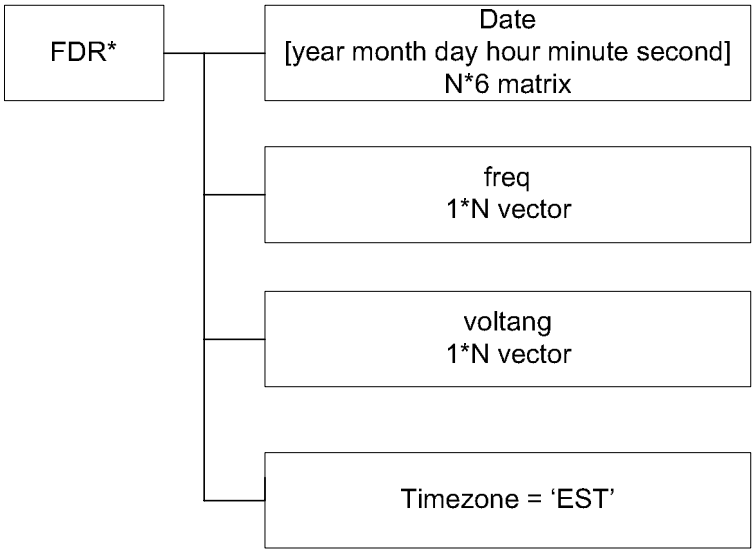

Fig 6-7. FDR data structure in Matlab

A final note, current FDR hardware design buffers 11 GPS pps time in the memory; therefore, when processing FDR date data, we must add 11 seconds to the data to ensure that the time reflects the true UTC time.

6.3 Sample FDR data and signal processing

Samples of different FDR raw data are shown in Fig 6-8 to Fig 6-11. As we can see, there are sharp spikes and noises in the frequency measurement. Since frequency is related to electromechanical properties of the system, it should not vary rapidly in the system. These sharp spikes and noise are, in majority, caused by rapid and random local load changing at the distribution level and/or other unknown noises polluting the measurement

data. In addition to these sharp spikes, sometimes, there are outliers, which the frequency is over 62 Hz or below 58 Hz. These outliers can be caused by measurement errors or other unknown reasons.

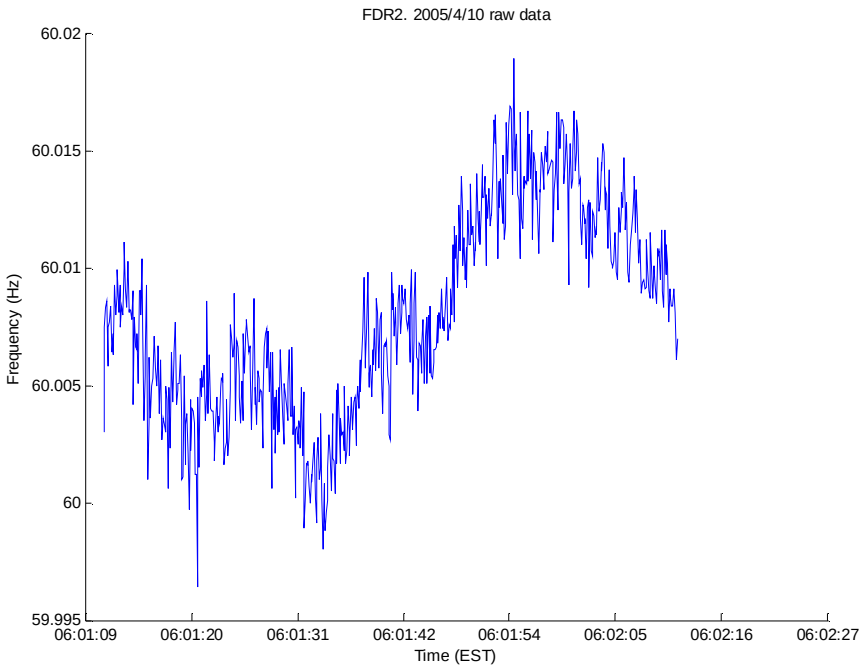

Fig 6-8. Sample FDR2 (UMR) frequency measurement

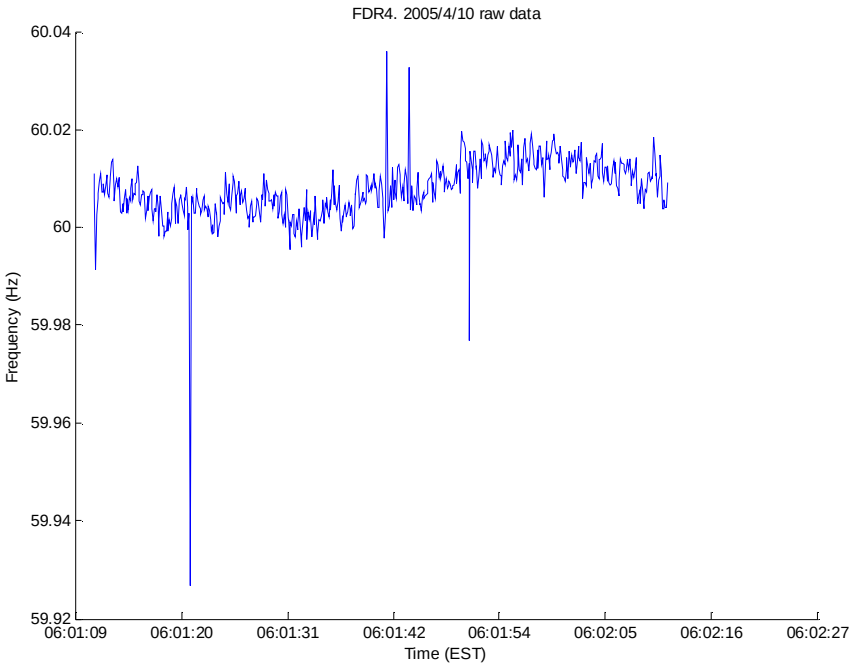

Fig 6-9. Sample FDR4 (VT) frequency measurement

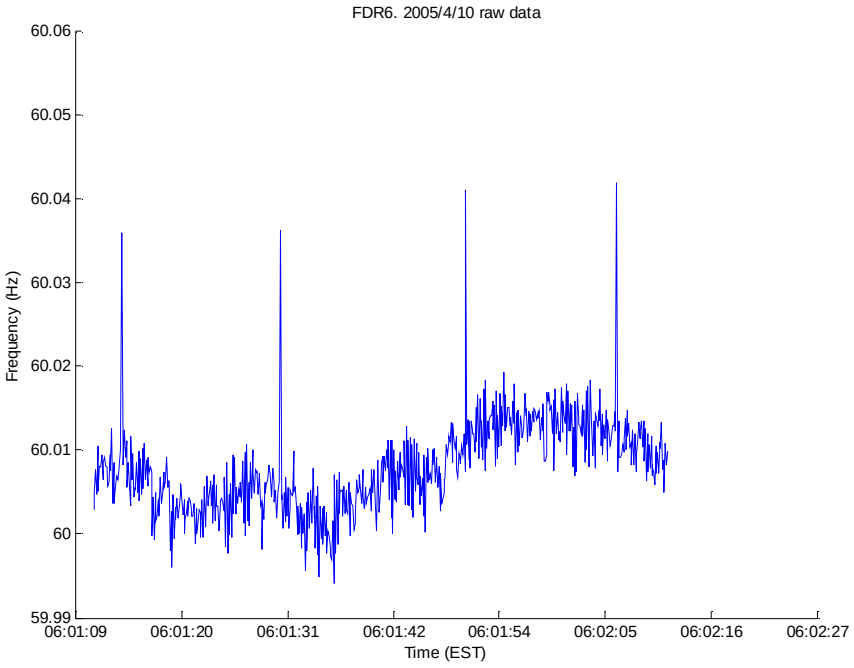

Fig 6-10. Sample FDR6 (ABB) frequency measurement

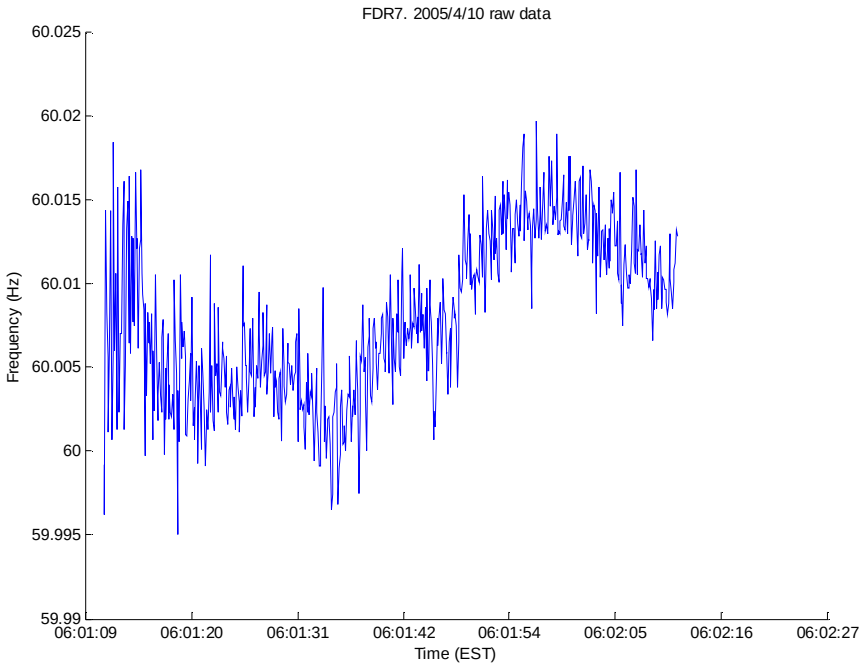

Fig 6-11. Sample FDR7 (MISS) frequency measurement

In this section, we present two signal processing techniques – de-outlier and wavelet denoising to remove outliers, sharp spikes and noise in the measured data. Another possible data processing technique – moving averaging can also be applied to obtain smoothed data. However, the averaging technique is not preferred because it will stretch the data in time depending on how many points of averaging.

6.3.1 De-outlier

In FDR measured frequency signals, there are sometimes outliers, which are over 62 Hz or below 58 Hz. These outliers show as sharp spikes between adjacent points; therefore, they are not related to the power system frequency dynamics. To remove such spikes, we perform the procedure, shown in Fig 6-12, to the signal before the denoising process.

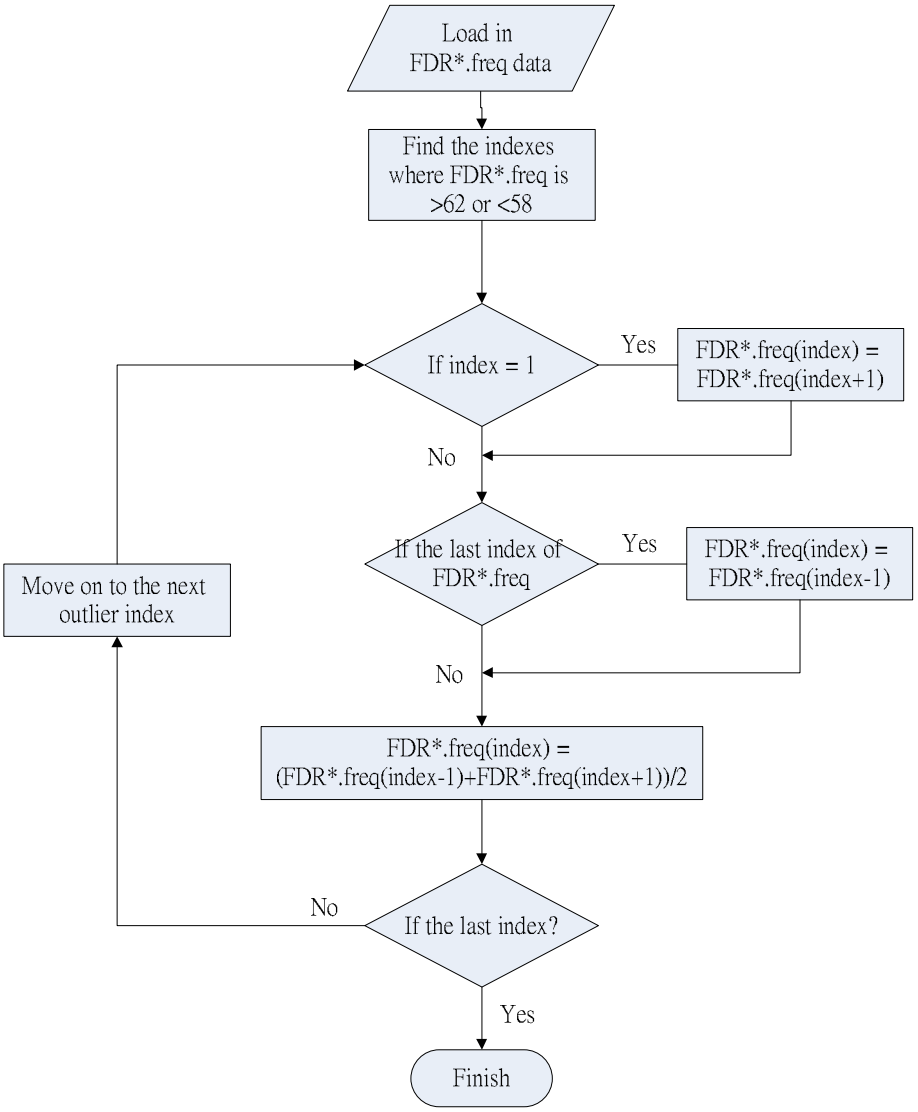

Fig 6-12. Outlier removal process

6.3.2 Denoising based on wavelet decomposition

Here, we only state the rudimentary idea of the denoising technique using wavelet decomposition. For more in-depth description and mathematical formulation, please refer to [82-87].

The wavelet denoising technique allows users to select how detailed information needs to be kept in the output by selecting different levels of decomposition and different types of

threshold. The wavelet decomposition can be illustrated in Fig 6-13.

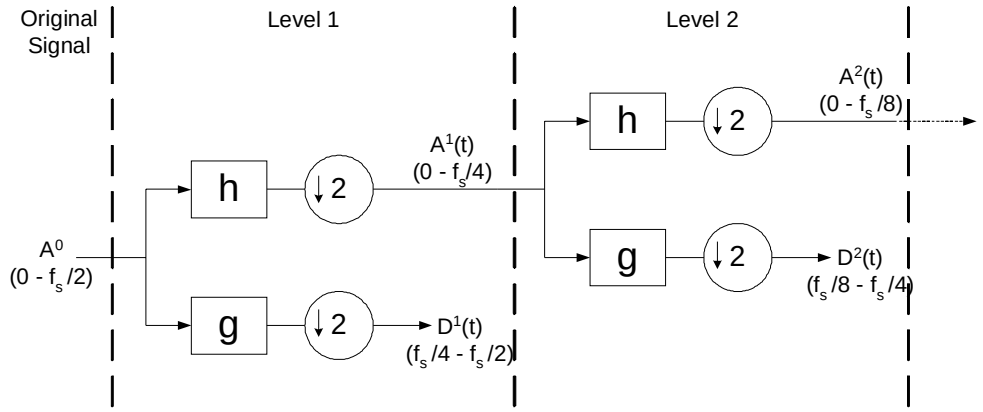

Fig 6-13. Multi-resolution wavelet decomposition. h = low-pass decomposition filter; g = high-pass decomposition filter; ↓2= down-sampling operation. $A^1(t)$, $A^2(t)$are the approximated coefficient of the original signal at levels 1, 2 etc. $D^1(t)$, $D^2(t)$ are the detailed coefficient at levels 1,2. f_s: sampling rate.

Thresholding is a technique used for signal and image denoising. The discrete wavelet transform uses two types of filters: (1) averaging filters (h) and (2) detail filters (g). When we decompose a signal using the wavelet transform, we are left with a set of wavelet coefficients that correlate to the high frequency subbands. These high frequency subbands consist of the details in the data set. If these details are small enough, they might be omitted without substantially affecting the main features of the data set. Additionally, these small details are often those associated with noise; therefore, by setting these coefficients to zero, we are essentially killing the noise. This becomes the basic concept behind thresholding - set all frequency subband coefficients that are less than a particular threshold to zero and use these coefficients in an inverse wavelet transformation to reconstruct the data set.

After performing thresholding on different decomposed levels of the signal, we can then reconstruct the signal back to the time domain. The wavelet reconstruction is illustrated in Fig 6-14.

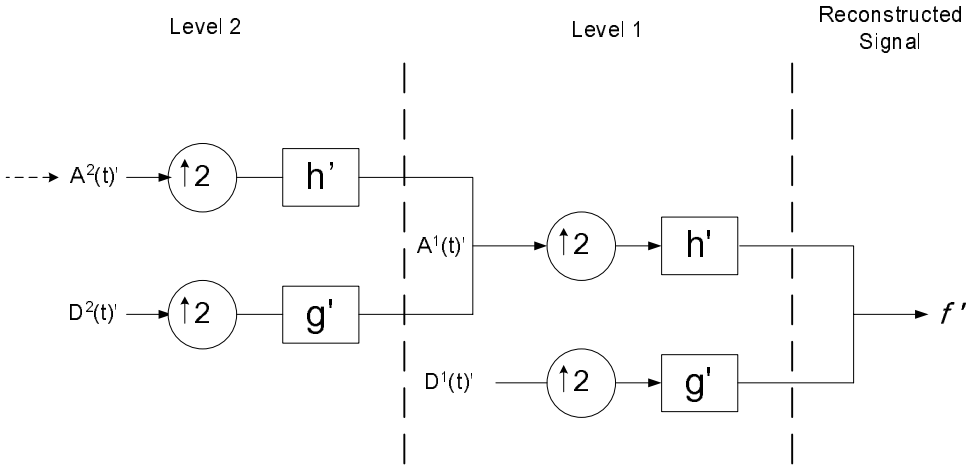

Fig 6-14. Multi-resolution wavelet reconstruction. h' = low pass reconstruction filter; g' = high-pass reconstruction filter; ↑2 = up-sampling operation. $A^1(t)'$, $A^2(t)'$ are the processed or non-processed approximated coefficient of the original signal at levels 1, 2 etc. $D^1(t)'$, $D^2(t)'$ are the processed or non-processed detailed coefficient at levels 1,2. f_s: sampling rate.

Hence, combing the decomposing, thresholding and reconstructing of the noisy signal, a smoother or cleaner signal can be obtained. In the following plots, we present some examples of FDR raw data and the denoised data after applying wavelet denoise technique.

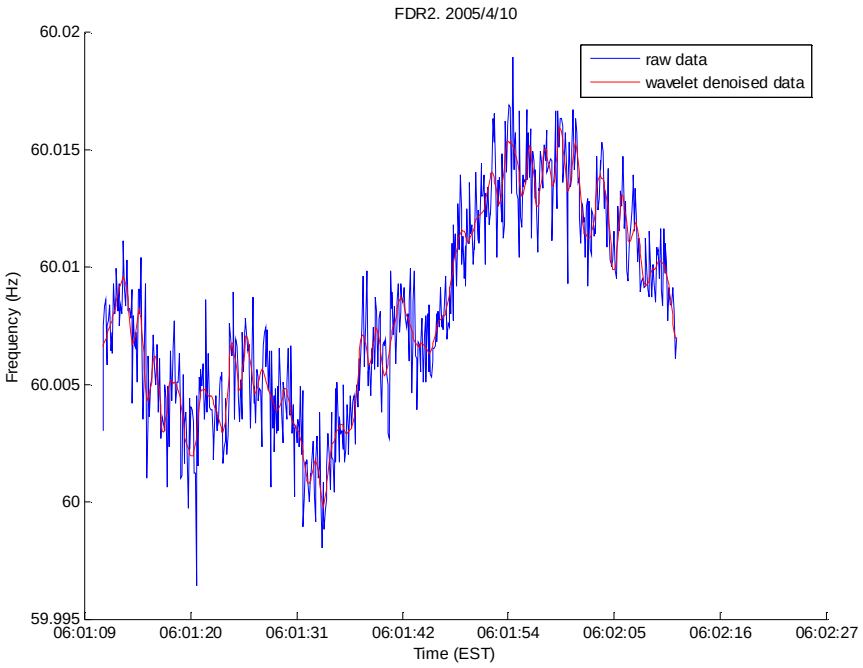

Fig 6-15. Sample FDR2 (UMR) raw and denoised data

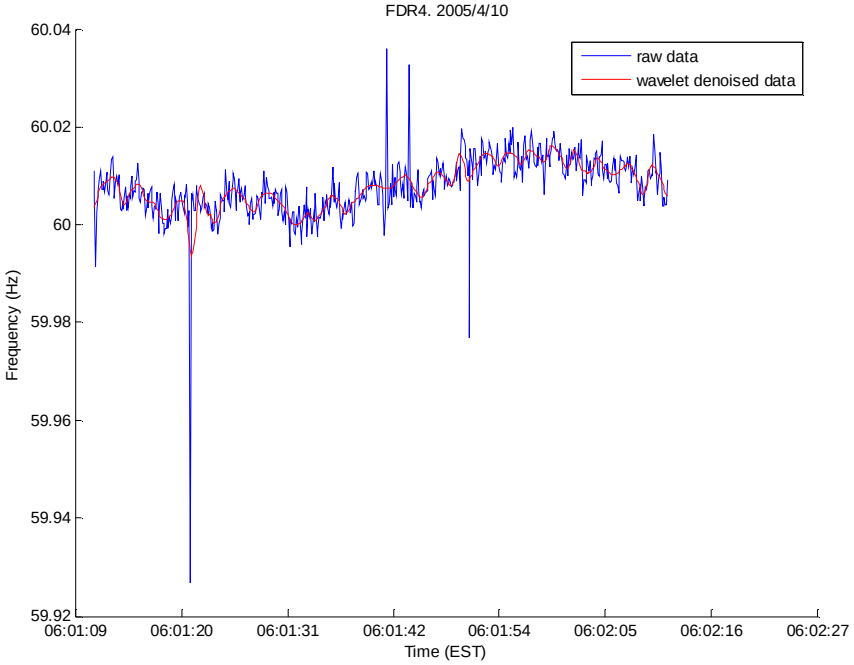

Fig 6-16. Sample FDR4 raw and denoised data

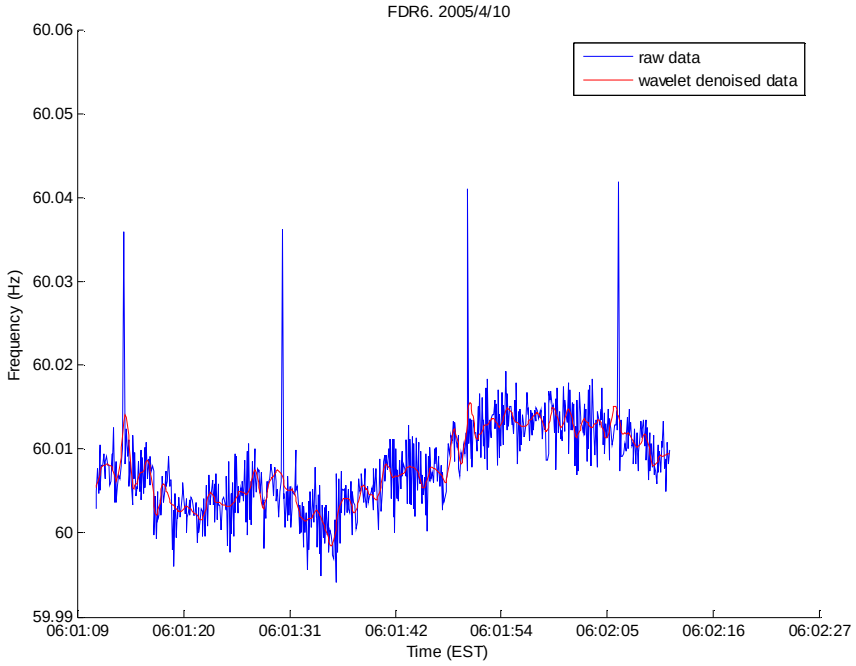

Fig 6-17. Sample FDR6 raw and denoised data

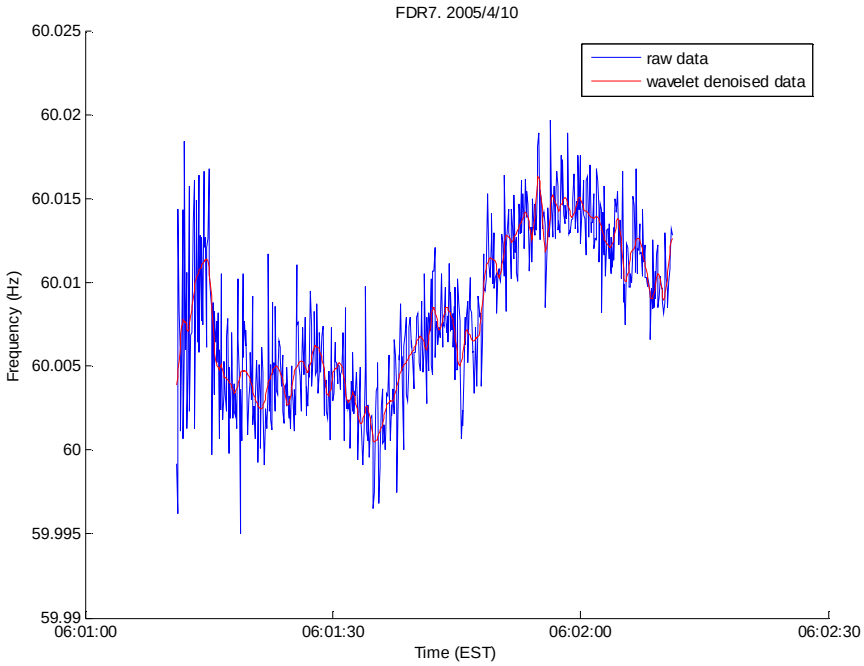

Fig 6-18. Sample FDR7 raw and denoise data

As we can see, wavelet denoising technique can effectively remove sharp spikes as well

as noises from the measured signal.

6.3.3 Remark

The following FDR frequency data will be processed by the de-outlier and the wavelet-based denoising technique to eliminate spikes and unwanted noises to better represent the FDR data.

6.4 PMU vs. FDR

How can we measure frequency at 110 V outlets to observe transmission system's dynamics? The frequency is typically not affected by the voltage transformation, i.e. on the same line with multiple transformers; the frequency stays the same from one point to another. The underlying assumptions of the FNET are that it can observe system's dynamics at the distribution at low cost and the measurement can be separated from local noises. To further prove the above statement, we cooperate with American Electric Power (AEP) to perform measurement tests of FDR in the control room of Matt Funk (MF) 345 kV substation. In addition, we compare the data of the FDR at Virginia Tech with the PMU data at the Kanawha River (KR) 345 kV line.

For the MF test, it was performed between February, 01 2005 and February 15 2005. The MF substation is located in Dixie Caverns, Virginia, which is about 50 miles northwest of Blacksburg, Virginia, where Virginia Tech is located. Based on the available information, Blacksburg is at its distribution supply line. Also it is the nearest high-voltage substation from Blacksburg. One FDR was placed in the control room of the MF 345 kV substation,

where relays, SCADA, back up batteries, and other monitoring and control devices are located. One FDR was plugged into an 110V outlet and a dedicated computer was connected to the FDR to record the frequency data, as shown in Fig 6-20 and Fig 6-19. The GPS antenna was magnetically attached to the outside wall of the control room, which is made of steel, to receive better satellite signal, as shown in Fig 6-21.

Fig 6-19. FDR plugs into 110 V outlet in Matt Funk 345kV substation's control room

Fig 6-20. Matt Funk test setup. Right: computer & monitor, middle (white box): FDR. Left bottom corner: router.

Fig 6-21. GPS antenna placement, circled in red.

During the testing period, 2 generation trip events were recorded. Fig 6-22 shows the frequencies of the generation trip event on 2005/02/09, the trip occurred around 13:48. Fig 6-23 shows the frequencies of the generation trip event 2005/02/11, the trip occurred around 17:29.

Fig 6-22. Matt Funk FDR vs. VT FDR on 2005/2/9 between 13:47:18 and 13:50:07

Fig 6-23. Matt Funk FDR vs. VT FDR on 2005/2/11 between 17:29:12 and 17:30:33

As shown, the frequencies between MF and VT from FDR measurement are very close. This provides evidences that the frequencies in a nearby area are similar. It is interesting

to note that on 2005/2/9, there seems to have been more frequency oscillation in both 2 measurements. If the oscillation were caused by local disturbance, which is dependent on where the measurement is taken, it would not be shown in both data. Therefore, we can conclude that the oscillation is caused by system's dynamics. This further reflects that FDR can measure the system frequency dynamics, which is one of the main FNET assumptions. Additionally, there is a little time advance of the frequency decline at MF comparing to VT. From Fig 6-23, the time delay between the 2 units at 59.99 Hz is 0.5 second.

Further, we obtained several sets of 345 kV PMU measurement data at the KR substation from AEP. We could have compared the PMU data at MF; however, it is found that the PMU data is very noisy. Therefore no useful information can be extracted. The KR substation is located in West Virginia. A geographical map is shown in Fig 6-24. It is estimated that the direct geographical distance between the KR and Blacksburg, VA is about 145 miles[16].

[16] http://gazetteer.hometownlocator.com/PlacesDistance.cfm?ID1=157808&ID2=169726

Fig 6-24. Transmission system one-line diagram around Virginia and West Virginia. The Kanawha River 345 kV substation is red-circled

Seven time periods of KR's PMU are data requested from AEP and compared with VT FDR. The time periods are listed in Table 6-2.

Sample	Date (year/month/day)	Start time (EST) (hour:minute:second)	End time (EST) (hour:minute:second)
1	2005/4/7	21:25:00	21:30:00
2	2005/4/8	05:35:00	05:40:00
3	2005/4/8	07:15:00	07:20:00
4	2005/4/9	10:10:00	10:15:00
5	2005/4/15	01:58:00	02:03:00
6	2005/4/17	07:28:00	07:33:00
7	2005/4/18	21:55:00	22:00:00

Table 6-2. Time periods of frequency measurement comparison between FDR at VT and PMU at KR

Fig 6-25 to Fig 6-31 show the overlaying frequencies between the PMU at KR and the FDR at VT of the time periods in Table 6-2. Frequency data from the FDR at VT have been processed using the signal processing techniques described in section 6.3.2. Frequency data from PMU at KR are not processed.

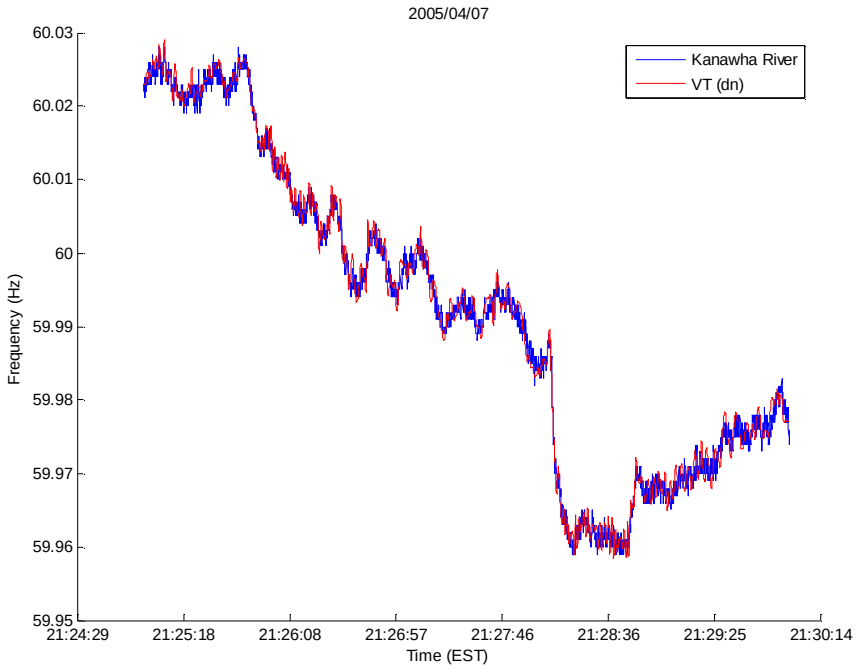

Fig 6-25. FDR (VT) vs. PMU (KR) frequency measurement comparison 1

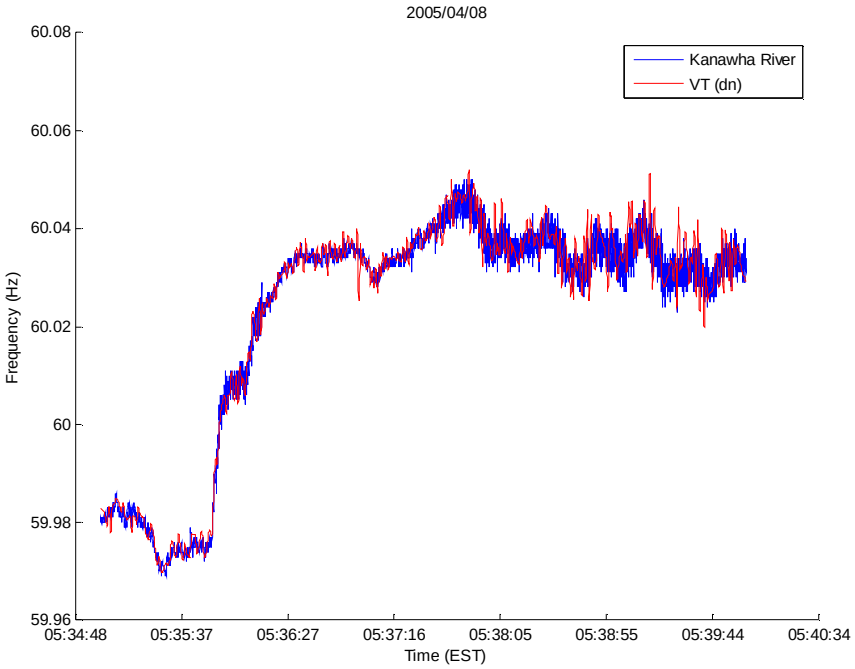

Fig 6-26. FDR (VT) vs. PMU (KR) frequency measurement comparison 2

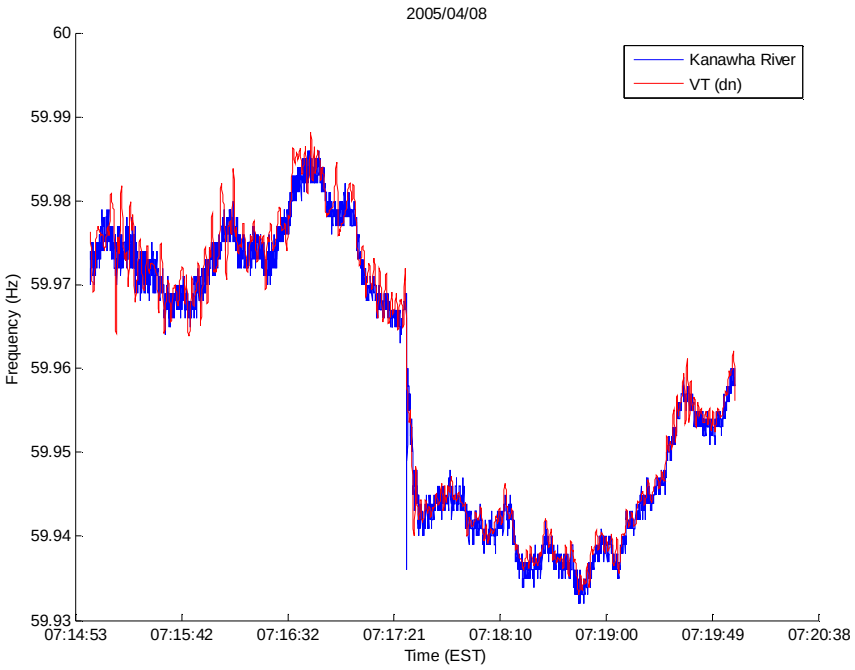

Fig 6-27. FDR (VT) vs. PMU (KR) frequency measurement comparison 3

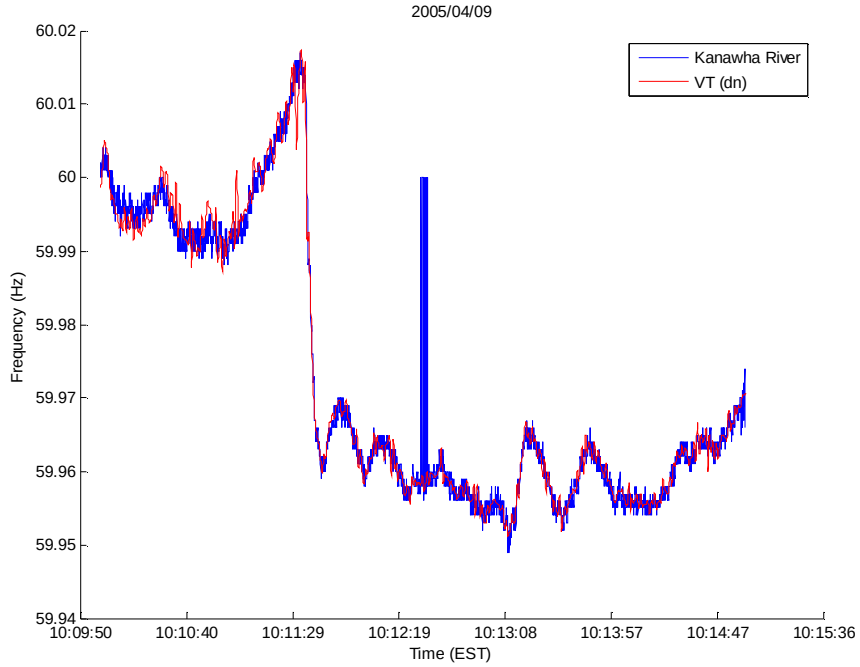

Fig 6-28. FDR (VT) vs. PMU (KR) frequency measurement comparison 4

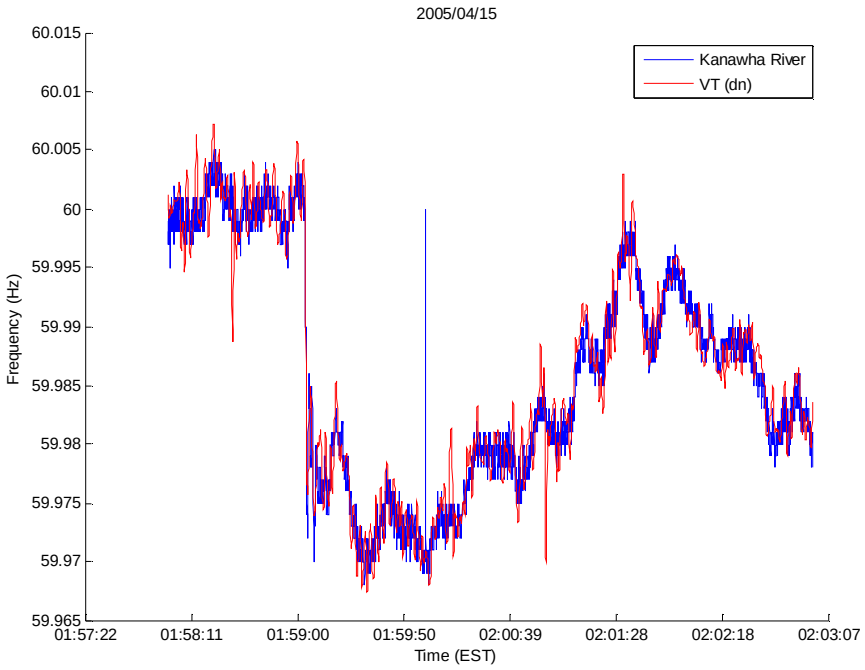

Fig 6-29. FDR (VT) vs. PMU (KR) frequency measurement comparison 5

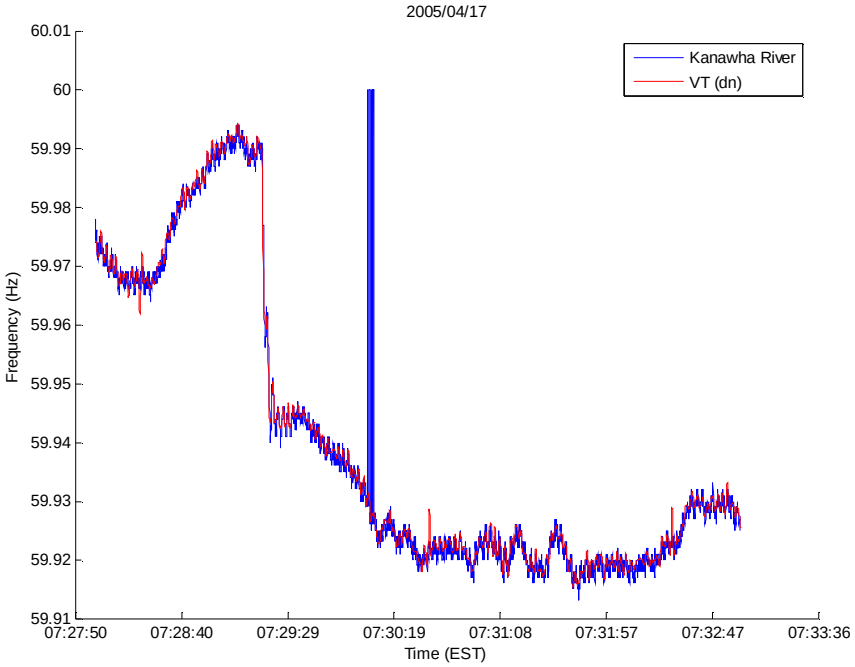

Fig 6-30. FDR (VT) vs. PMU (KR) frequency measurement comparison 6

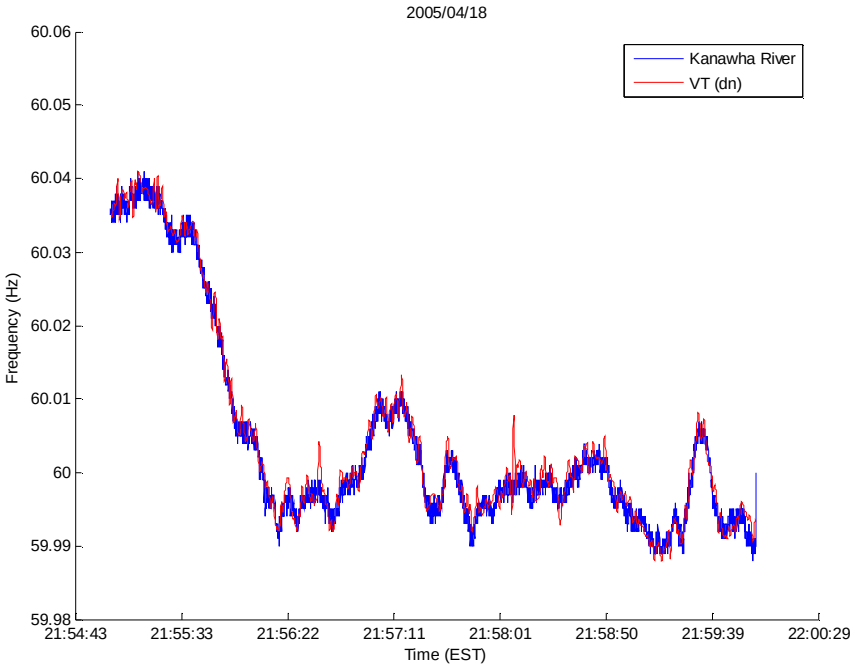

Fig 6-31. FDR (VT) vs. PMU (KR) frequency measurement comparison 7

As shown, FDR frequency measurement matches to PMU frequency measurement very well in either quasi-steady-state, or during transient state, such as tripping or load rejection. Among the comparisons, there are 5 identified generation tripping events, namely 1, 3, 4, 5, and 6. The drop of frequencies from FDR follows closely to the PMU, though there is some time delay due to the electromechanical disturbance propagation as discussed in Chapter 3. The comparisons provide strong evidence that the recording from FDR with signal processing is the frequency of the electric transmission system, using the nearby PMU measurement as the reference. As a side note from the comparison, PMU sets the frequency as 60, if there is any data recording error in PMU, shown as the spikes reaching at 60 in Fig 6-28, Fig 6-29, and Fig 6-30.

6.5 Frequency statistics

From recorded FDR frequency data, we can find its descriptive statistics, such as average, median, standard deviation, maximum, and minimum. The descriptive statistics are a collection of methods for classifying and summarizing numerical data [88]. Here the calculated statistics include normal condition and transient conditions (e.g. generation trip, line opening, load rejection, random event, etc). To eliminate any outliers, the frequency data was first processed by the signal processing techniques presented in 6.3 to remove outliers, sharp spikes and unwanted noises. Then, we find the statistics from frequency data of each FDR for each day. Each day is in the period of time between 00:00:00 to 24:00:00 in EST (Eastern Standard Time). Theorectically we should have 864000 points in a day, sometimes, the data may be missing due to losing GPS signal, network packet loss, manual operation, etc. So we may not the full length of data, therefore when calculating statistics, available frequency data for each FDR are used.

Between April 1, 2004 and April 30, 2005, the frequency statistics of FDRs in 3 US interconnected systems, namely, WECC, EUS, and ERCOT, are calculated. Please note that not all units have the same number of days. Some units may have deployed earlier than others. In addition, units may have their downtimes and, therefore, no frequency data were recorded during these times. We present one FDR statistics for each interconnected system in this section, others can be found in Appendix IV.

In the following, Fig 6-32, Fig 6-33, and Fig 6-34 represent typical frequency statistics for EUS, WECC and ERCOT, respectively.

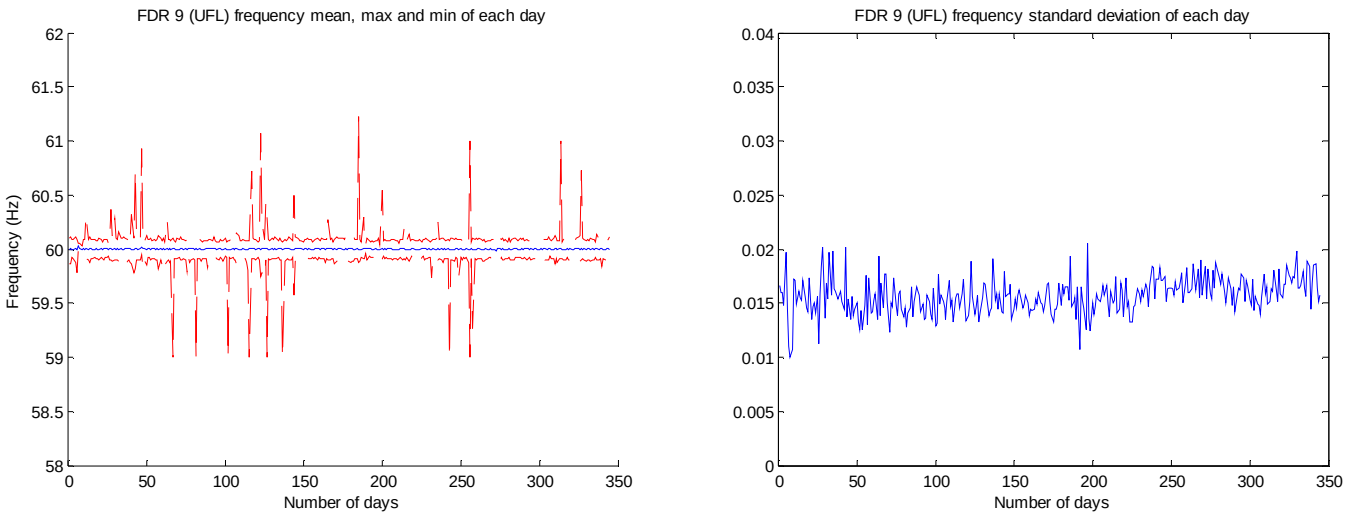

(a) (b)

Fig 6-32. Frequency statistics of FDR 9 (UFL) in EUS (a) maximum, mean and minimum; (b) standard deviation

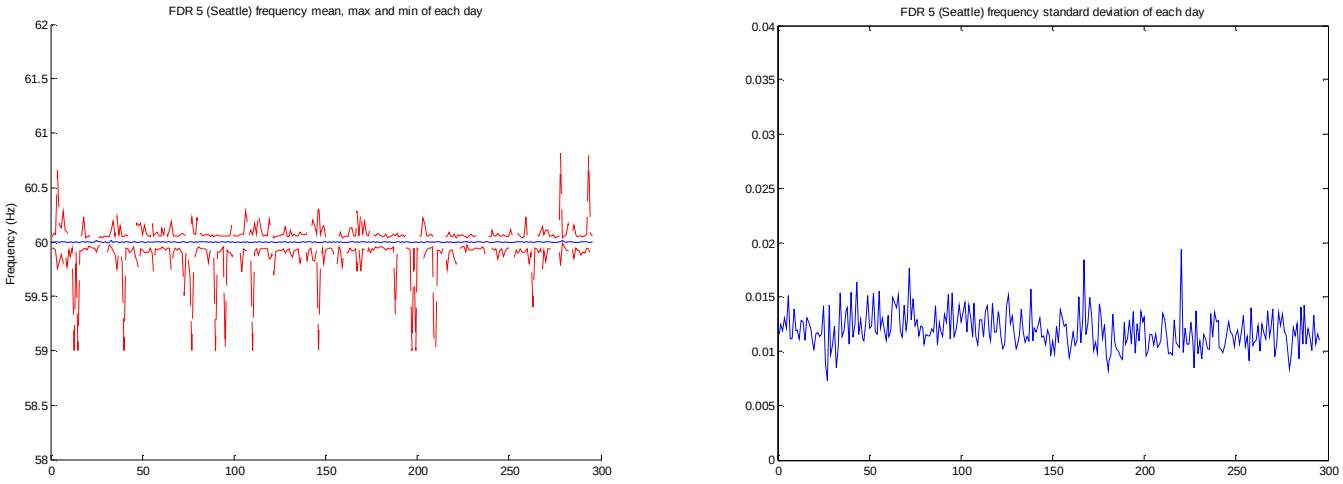

Fig 6-33. Frequency statistics of FDR 5 (Seattle) in WECC (a) maximum, mean and minimum; (b) standard deviation

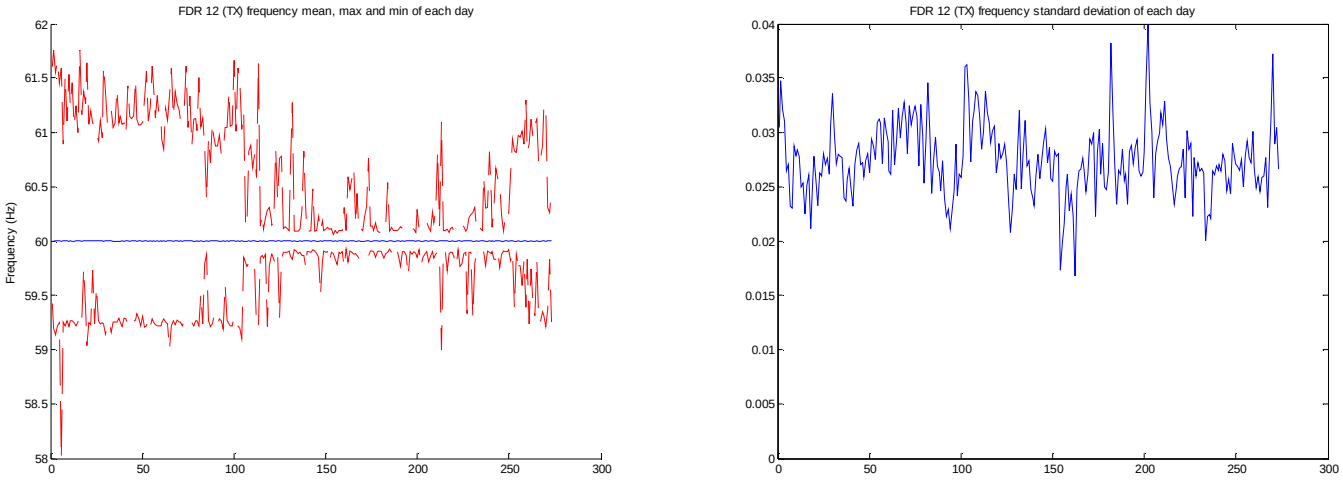

Fig 6-34. Frequency statistics of FDR 12 (Houston) in ERCOT (a) maximum, mean and minimum (b) standard deviation

As we can see from the statistics, the average frequency for each day is close to the scheduled value – 60 Hz, no matter how large the maximum, or how small the minimum would occur in each day. It is, however, interesting to notice that the standard deviation (std) of frequency for each day stays in the same level for each system. For EUS, the std

is about 0.015, for WECC, it is about 0.013, and for ERCOT it ranges from about 0.02 to 0.04. Standard deviation can be used as a measure of the dispersion or variation in a distribution. In other words, it is a measure of how much the data in a certain collection are scattered around the average (mean). A low standard deviation means that the data are tightly clustered; a high standard deviation means that they are widely scattered. From the std value, the frequency in ERCOT is varying at a larger range than that of EUS and WECC. One reason for having larger std, from power system's point of view, could be because ERCORT is not synchronously tied with EUS. A smaller system can be more subject to disturbances. And any slight mismatch between generation and consumption would tend to induce larger frequency variation.

6.6 Generator trip analysis

Based on studies in Chapter 2, any slight power imbalance (even a generation trip as small as 0.1% of system's total generation) in power system between generation and consumption, including loads and losses, will induce frequency variation in the system. As we have seen in the previous section, where simulations on generation trip, line trip and load rejection were discussed, bus frequency can deviate from its steady state if disturbance(s) is introduced to the system. In this section, we will look at and analyze several actual generation trip recordings from FDRs.

6.6.1 Eastern US interconnection (EUS)

From June of 2004 to April of 2005, there are about 10 confirmed generation trips in the Eastern US Interconnection. They are listed in Table 6-3.

No.	Date	Time	Estimated tripped MW	Plant Name	State	NERC region[17]
1	6/22/2004	12:11	700	Limerick	PA	MAAC
2	7/13/2004	16:11	1100	Clinton	IL	MAIN
2	8/4/2004	9:23	900	Davis Besse	OH	ECAR
3	9/19/2004	3:55	800	Watts Bar	TN	SERC
4	11/23/2004	11:01	800-1200	Browns Ferry	AL	SERC
5	1/26/2005	13:31	550	EastBend	KY	ECAR
6	2/11/2005	17:29	1200	Browns Ferry	AL	SERC
7	3/7/2005	15:01	500	Mountaineer	WV	ECAR
8	3/21/2005	11:24	1100	Cumberland	TN	SERC
9	4/2/2005	16:24	400	Eastlake	OH	ECAR
10	4/29/2005	20:53	800	Votgle-Wilson	GA	SERC

Table 6-3. Ten known generation trips in EUS from June 2004 to April 2005. Time, in EST, is rounded to the nearest minute.

For each event, available FDR frequencies around the generator trip time and the zoomed interval of the initial frequency drop are presented in Fig 6-35 to Fig 6-45.

[17] http://www.nerc.com

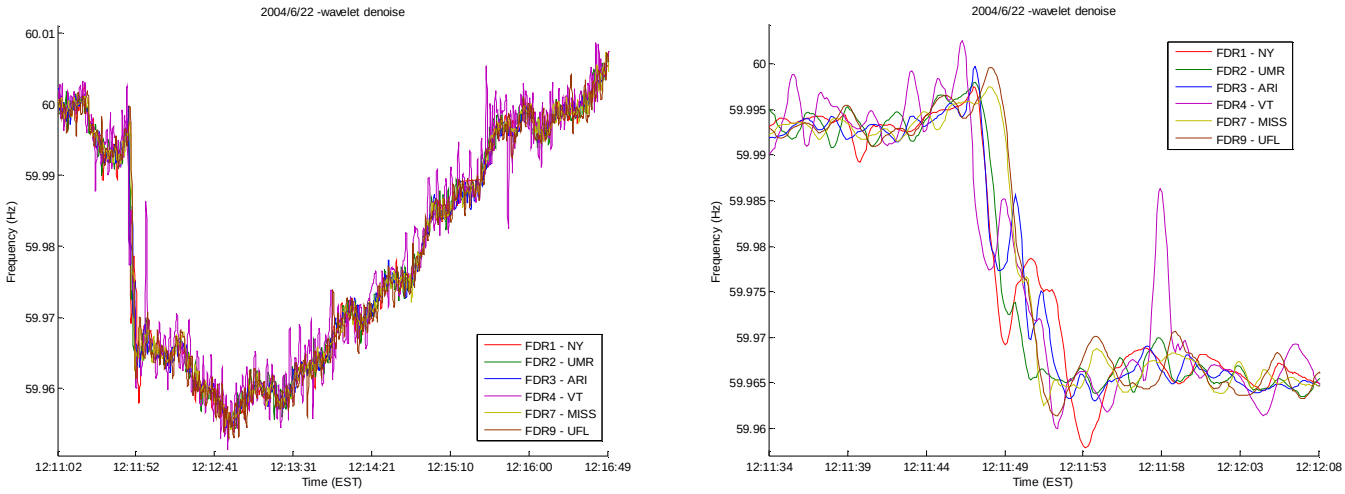

(a) (b)

Fig 6-35. (a) No.1 EUS generation trip on 6/22/2004, (b) zoom on the initial frequency drop

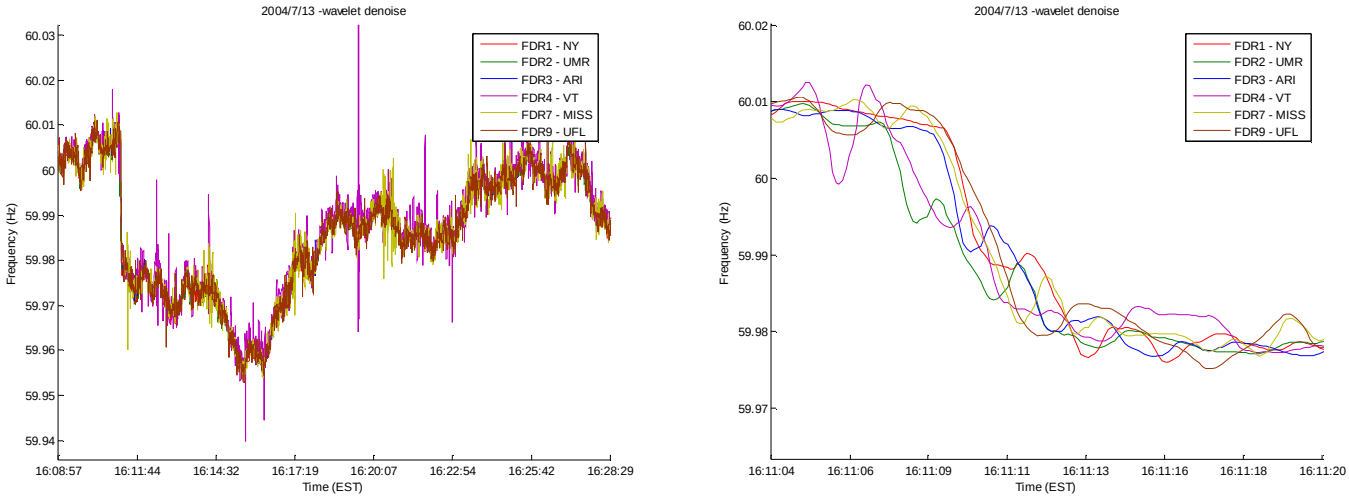

(a) (b)

Fig 6-36. (a) No.2 EUS generation trip on 7/13/2004, (b) zoom on the initial frequency drop

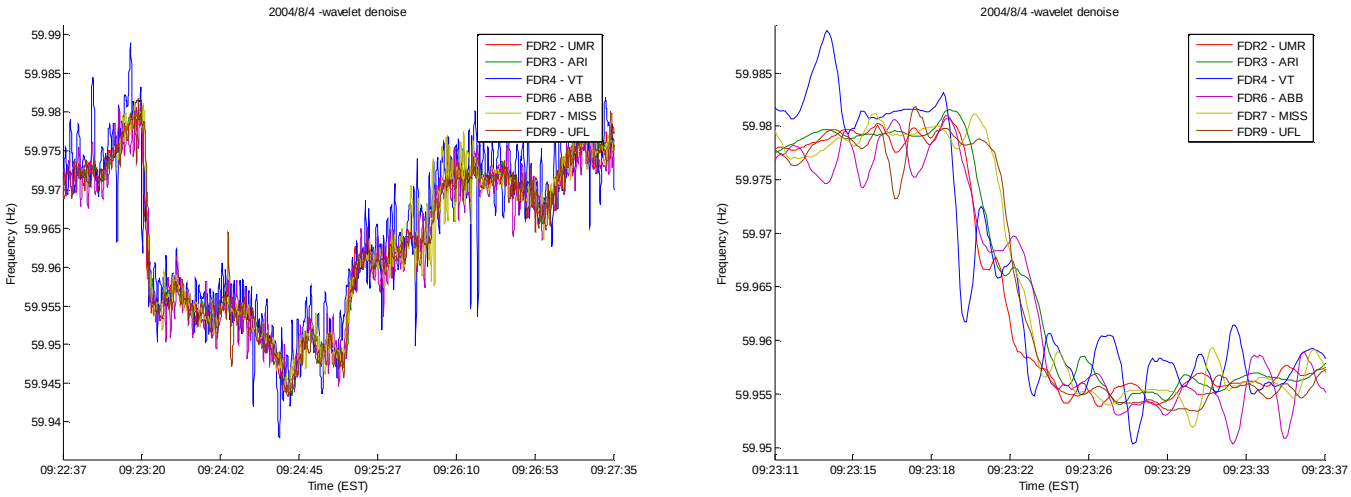

(a) (b)

Fig 6-37. (a) No.3 EUS generation trip on 8/4/2004, (b) zoom on the initial frequency drop

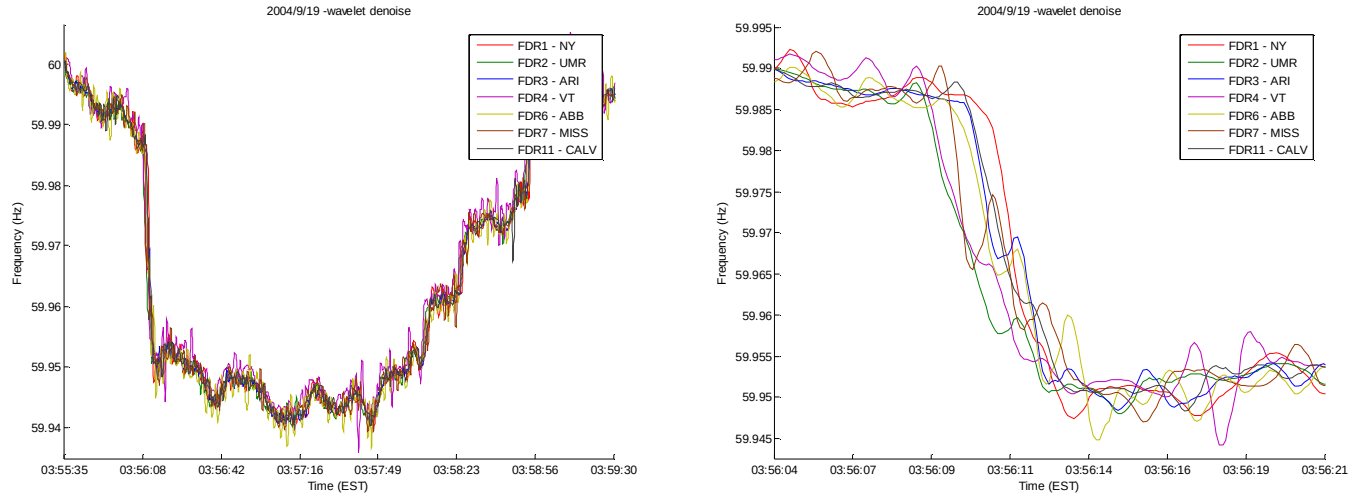

(a) (b)

Fig 6-38. (a) No.4 EUS generation trip on 9/19/2004, (b) zoom on the initial frequency drop

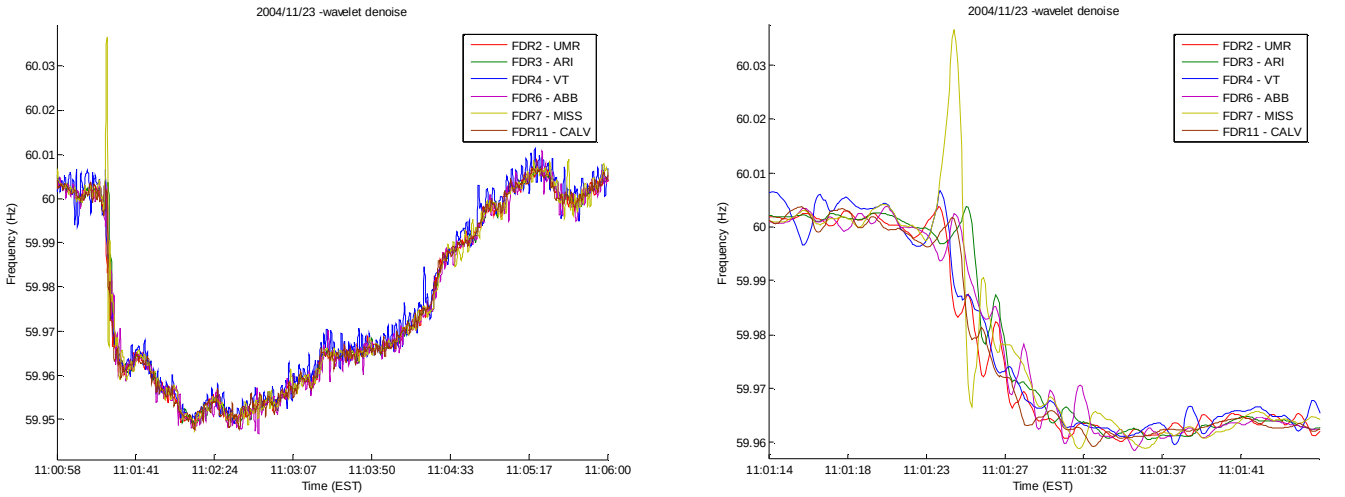

(a) (b)

Fig 6-39. (a) No.5 EUS generation trip on 11/23/2004, (b) zoom on the initial frequency drop

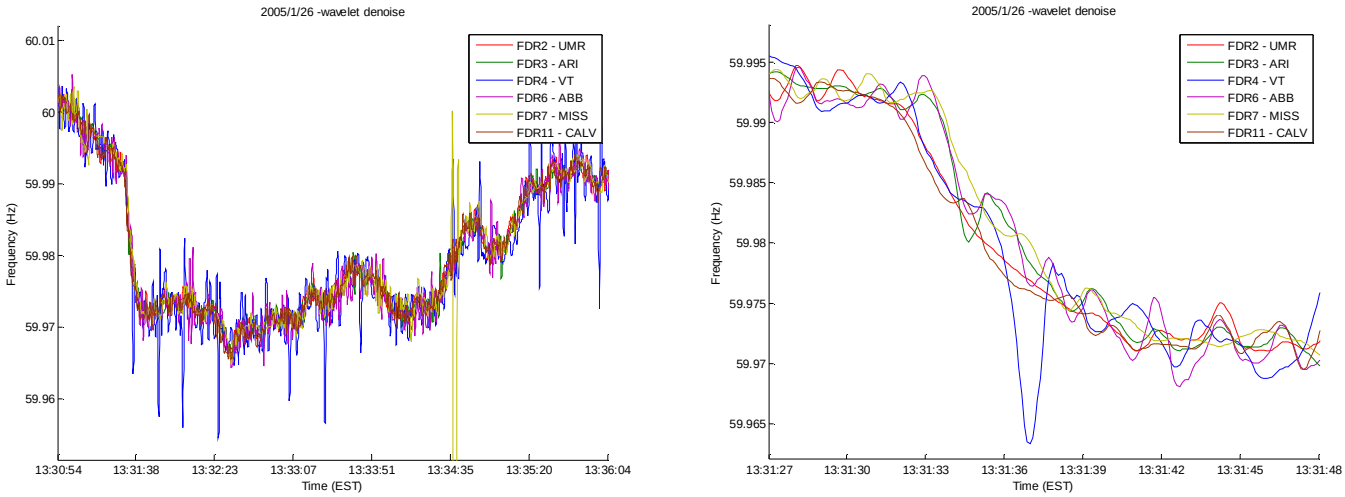

(a) (b)

Fig 6-40. (a) No.6 EUS generation trip on 1/26/2005, (b) zoom on the initial frequency drop

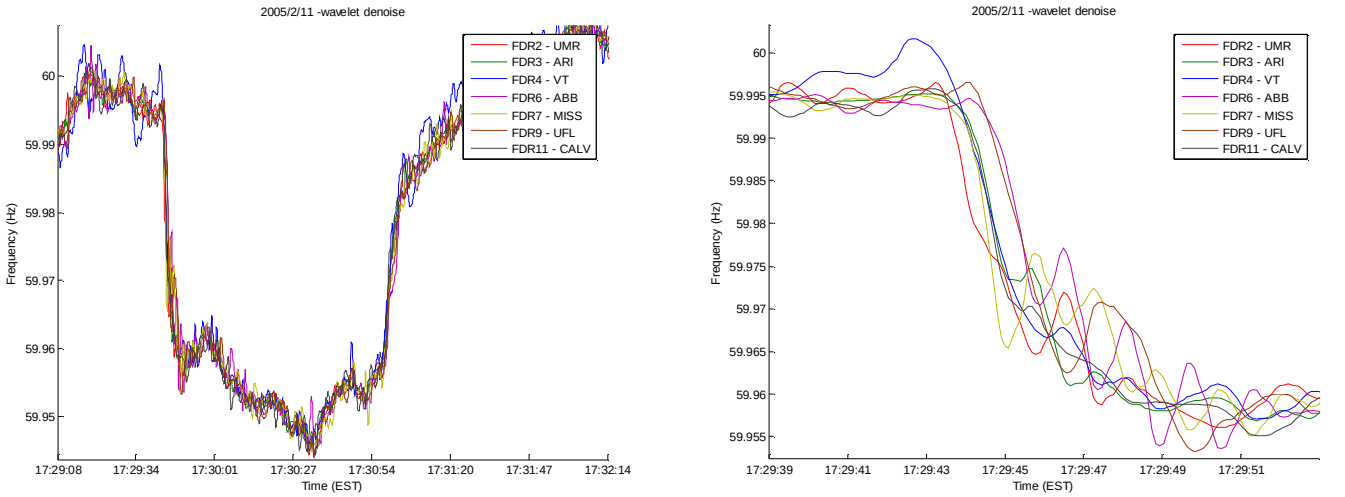

(a) (b)

Fig 6-41. (a) No.7 EUS generation trip on 2/11/2005, (b) zoom on the initial frequency drop

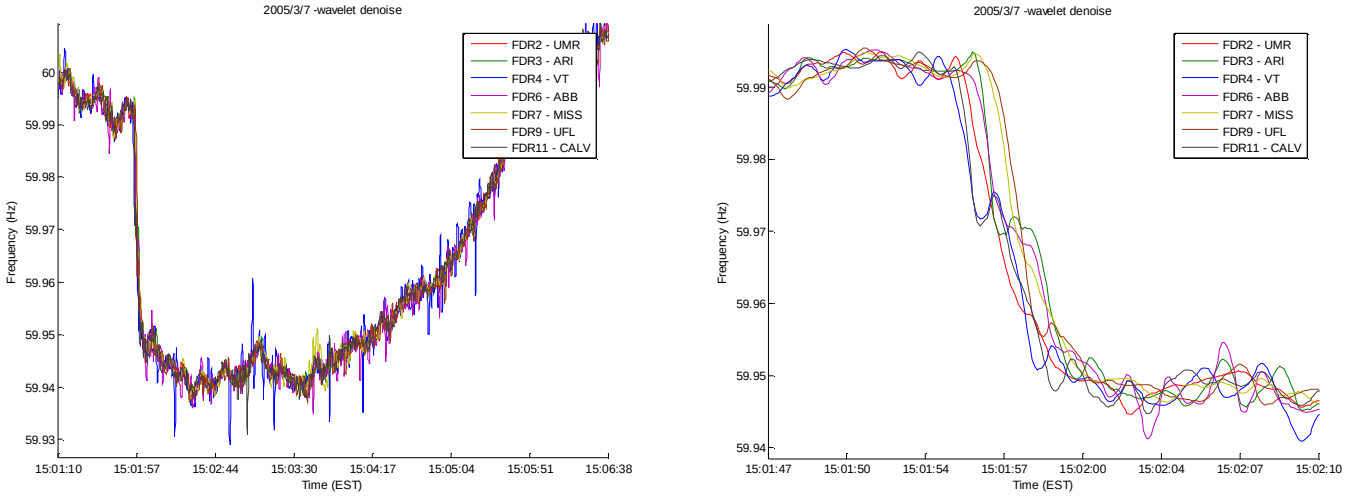

(a) (b)

Fig 6-42. (a) No.8 EUS generation trip on 3/7/2005, (b) zoom on the initial frequency drop

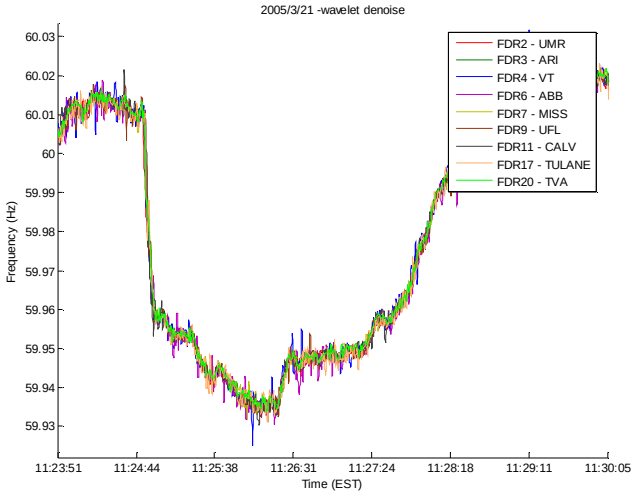

(a)

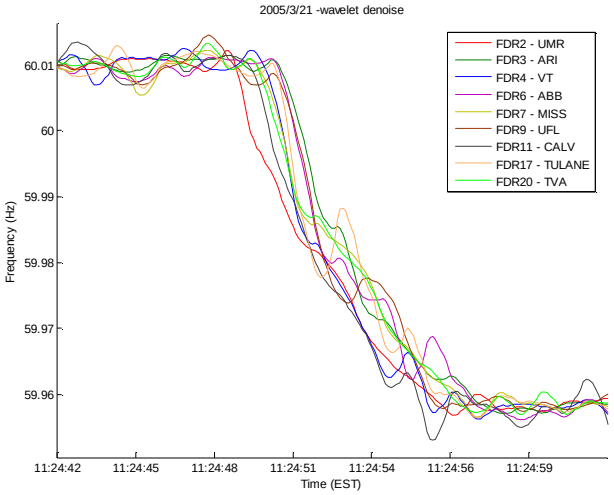

(b)

Fig 6-43. (a) No.9 EUS generation trip on 3/21/2005, (b) zoom on the initial frequency drop

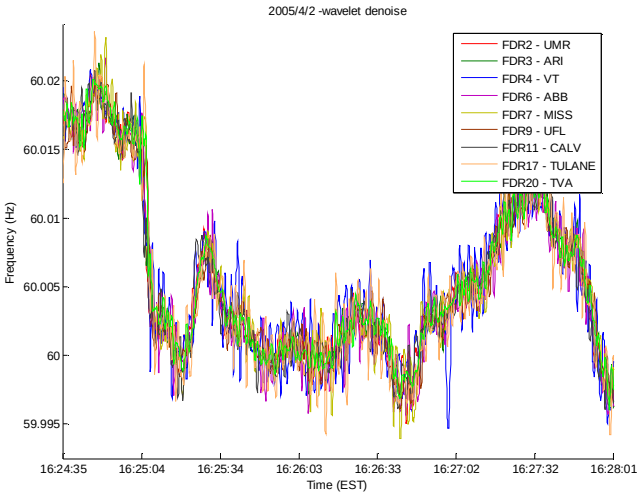

(a)

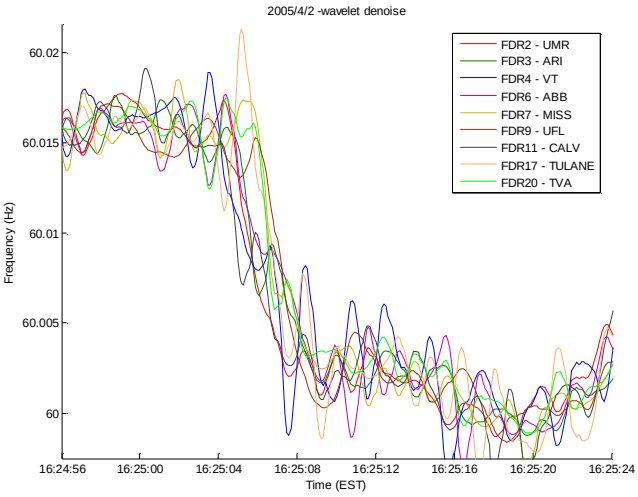

(b)

Fig 6-44. (a) No.10 EUS generation trip on 4/2/2005, (b) zoom on the initial frequency drop

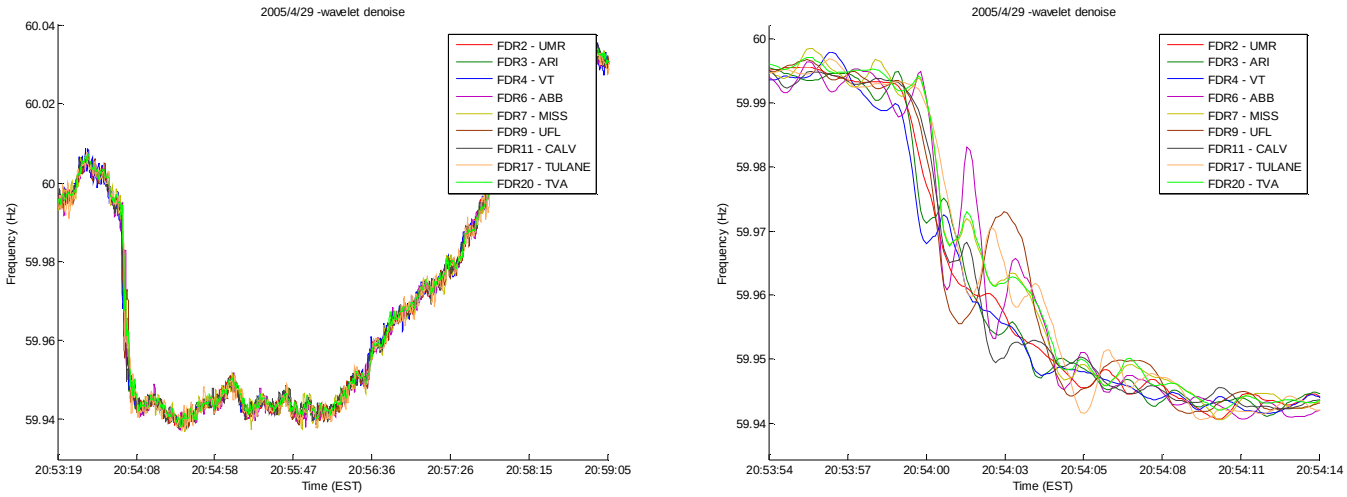

(a) (b)

Fig 6-45. (a) No.11 EUS generation trip on 4/29/2005, (b) zoom on the initial frequency drop

Some characteristics can be found from EUS trip plots:

1. Generation trip induces frequency drops
2. All FDR measured frequencies drop to a common level before going back to 60 Hz level.
3. After the frequency drops to a common level during the first swing, it stays at the level for some time before rising up to 60 Hz.
4. After the trip, we can see that the frequency will gradually rise to 60 Hz or pre-fault value within 3-5 minutes. This is an indication of the AGC's time constant.
5. Time delay of the first frequency drop between units can be observed.
6. Before the generation trip, the frequency between units is on top of each other; after generation trip, frequency starts to show distinct delays between units, which

suggests there is a form of electromechanical wave propagating in the system due to the disturbance.

7. The frequency drop amount and frequency time delay can be very useful to determine how much of the generation tripped, where the trip was and how the disturbance electromechanical waves propagate. Typically, the larger the frequency drops in the first swing, the larger the tripped generation active power.

6.6.2 WECC

In WECC system, we also found 9 known generation tripping events between June 2004 and March 2005, and they are listed in Table 6-4.

No.	Date	Time (EST)	Estimated tripped MW	Plant Name	State	NERC region
1	6/14/2004	9:40	3000	Palo Verde	AZ	WECC
2	8/10/2004	9:08	400	Colstrip	MT	WECC
3	8/15/2004	20:33	500	Colstrip	MT	WECC
4	8/16/2004	15:29	500	Colstrip	MT	WECC
5	11/29/2004	1:32	400	Navajo	AZ	WECC
6	1/7/2005	13:31	800	High Desert	CA	WECC
7	3/27/2005	19:30	700	Four Couners	NM	WECC
8	3/27/2005	14:31	400	Mohave	NV	WECC
9	3/27/2005	15:16	300	Mohave	NV	WECC

Table 6-4. Nine known generation trips in WECC from June 2004 to April 2005. Time is rounded to the nearest minute.

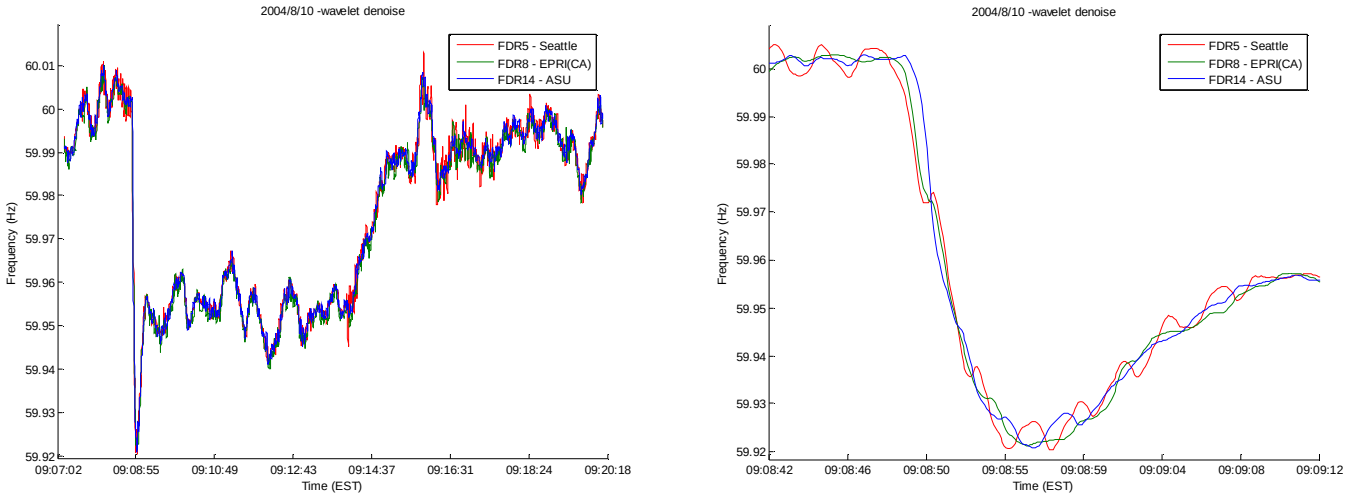

(a) (b)

Fig 6-46. a) No.2 WECC generation trip on 8/10/2004, (b) zoom on the initial frequency drop

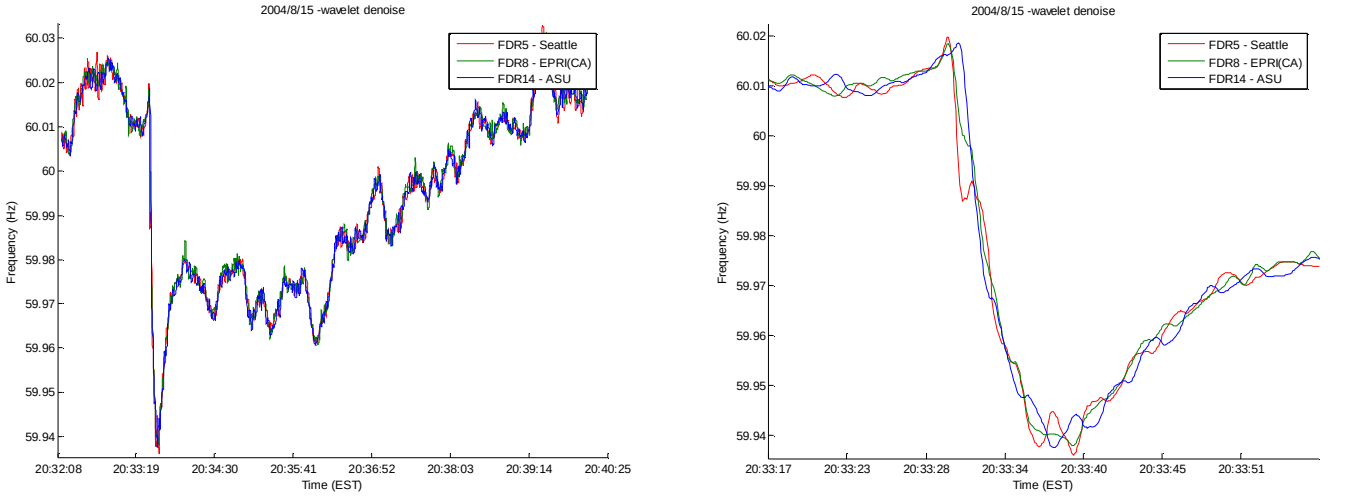

(a) (b)

Fig 6-47. a) No.3 WECC generation trip on 8/15/2004, (b) zoom on the initial frequency drop

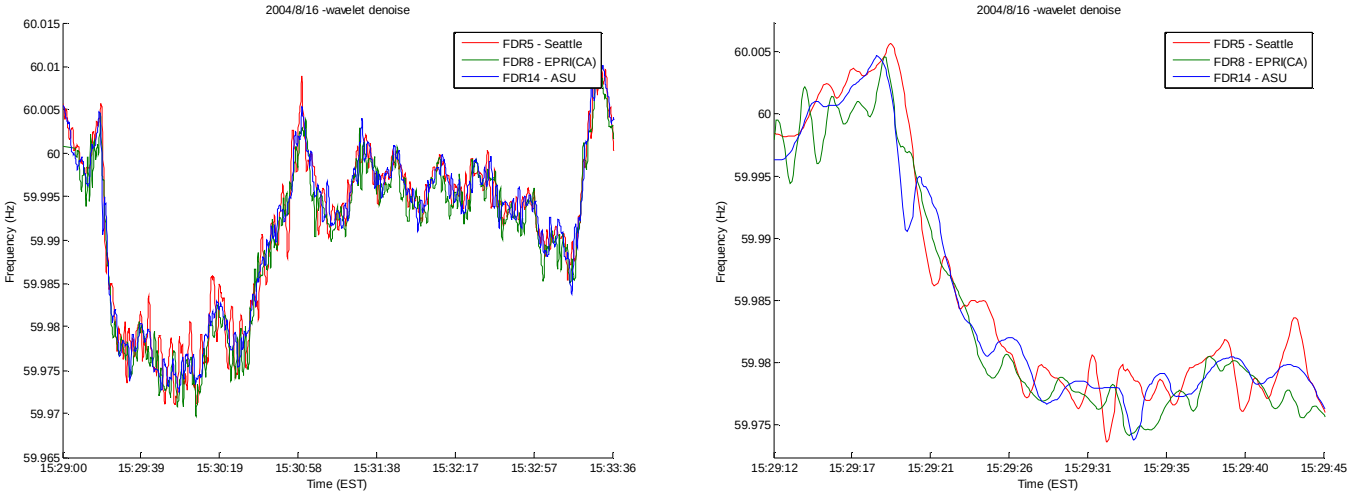

(a) (b)

Fig 6-48. a) No.4 WECC generation trip on 8/16/2004, (b) zoom on the initial frequency drop

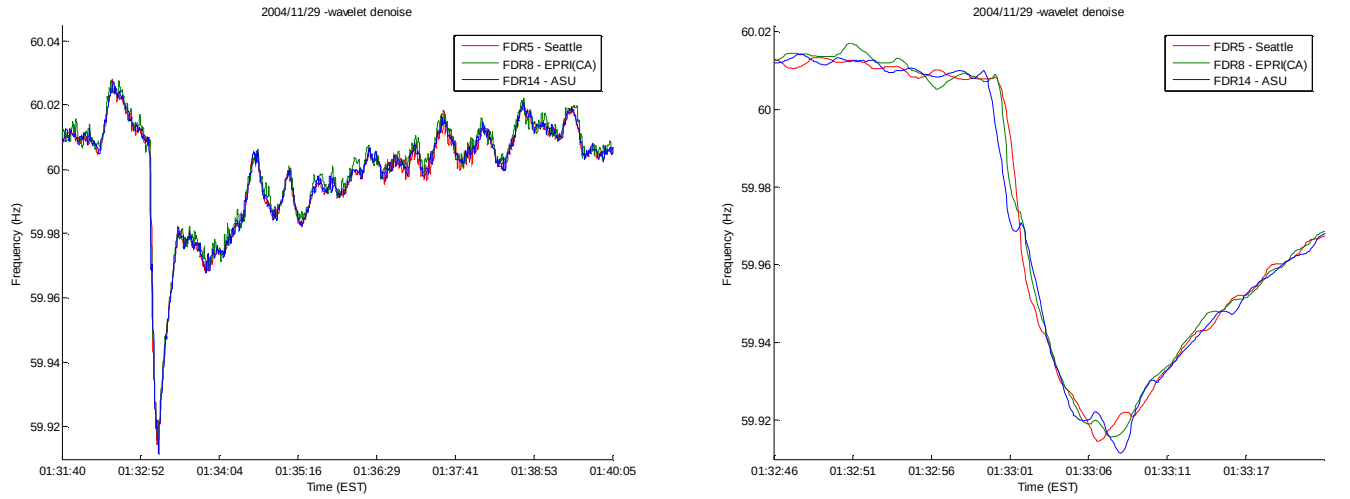

(a) (b)

Fig 6-49. a) No.5 WECC generation trip on 11/29/2004, (b) zoom on the initial frequency drop

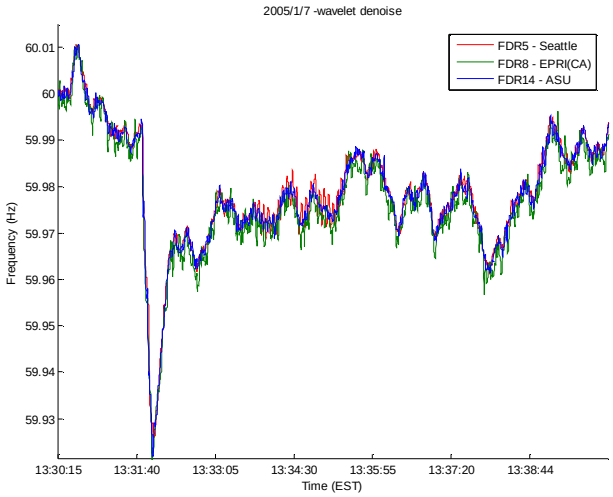

(a)

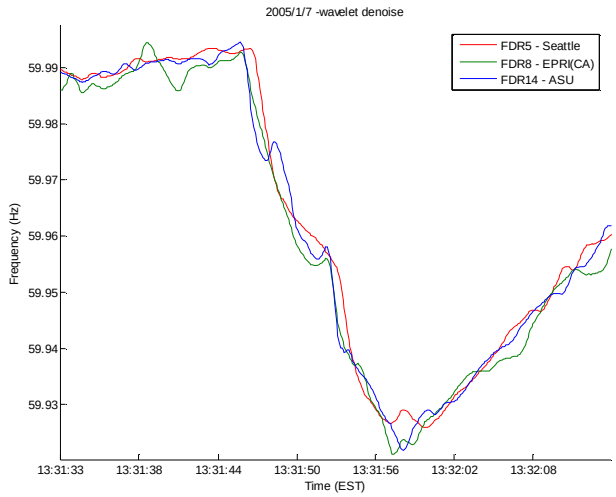

(b)

Fig 6-50. a) No.6 WECC generation trip on 1/7/2005, (b) zoom on the initial frequency drop

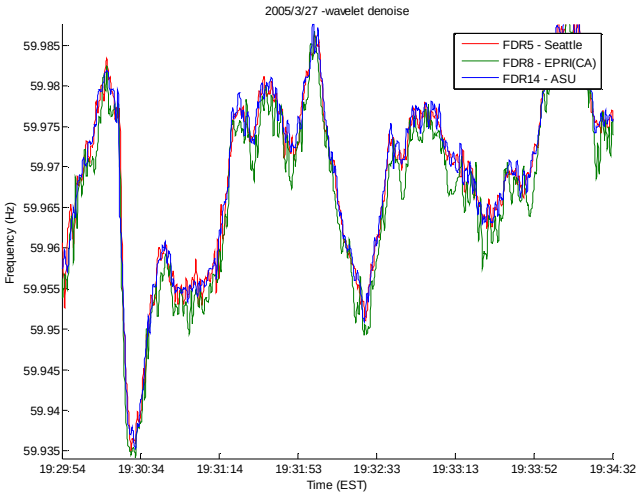

(a)

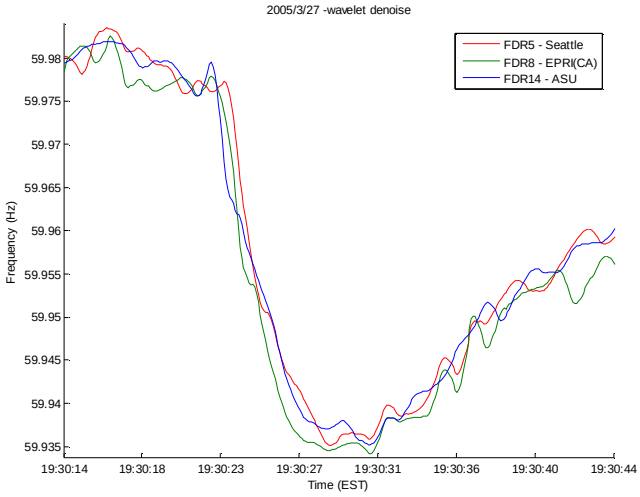

(b)

Fig 6-51. a) No.7 WECC generation trip on 3/27/2005, (b) zoom on the initial frequency drop

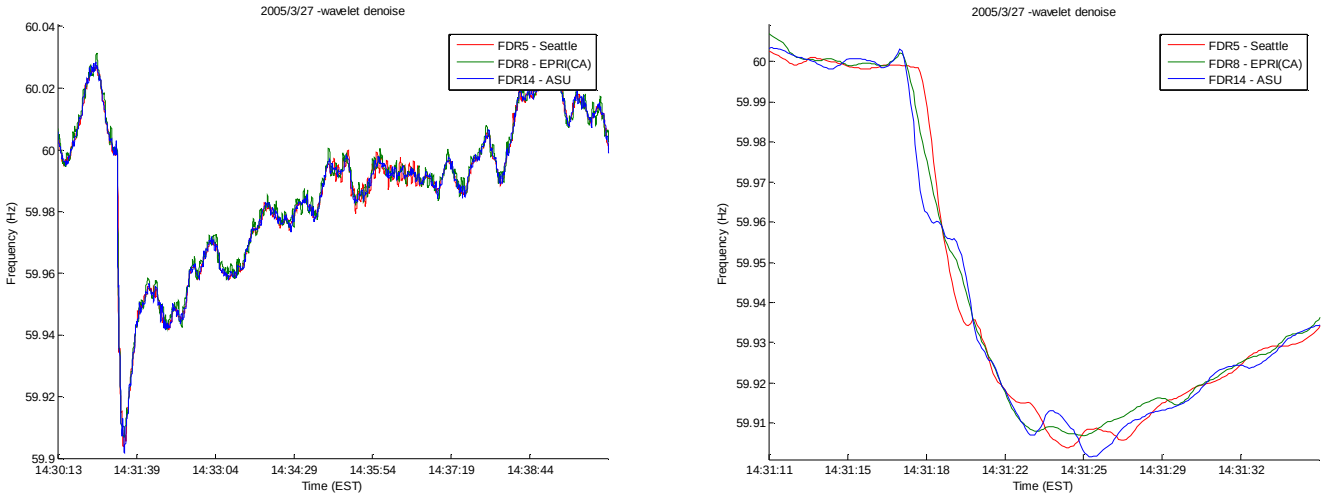

(a) (b)

Fig 6-52. a) No.8 WECC generation trip on 8/10/2005, (b) zoom on the initial frequency drop

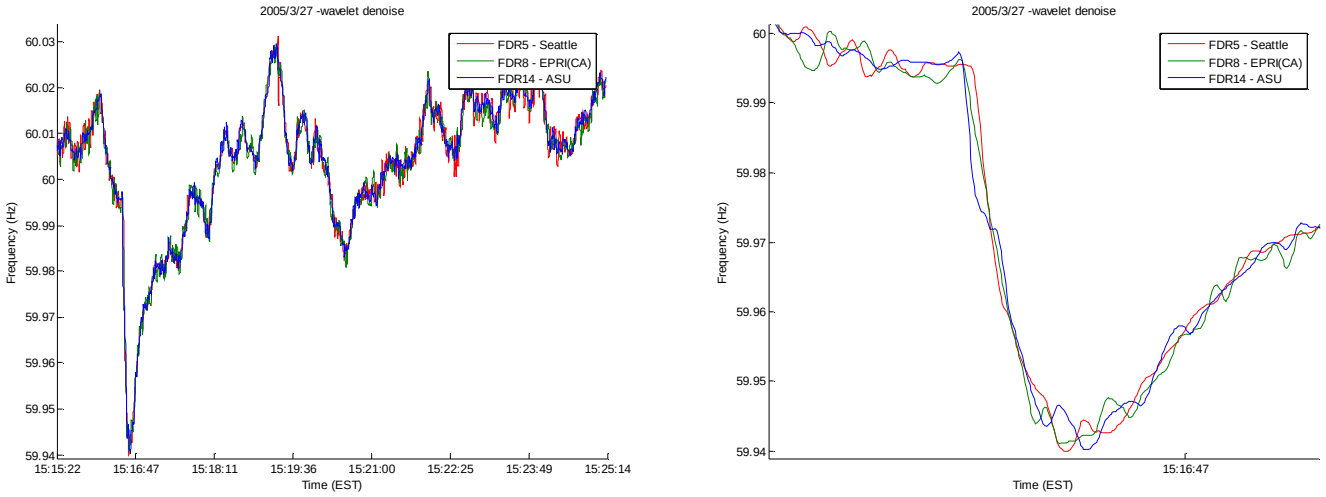

(a) (b)

Fig 6-53. a) No.9 WECC generation trip on 3/27/2005, (b) zoom on the initial frequency drop

Some characteristics can be found from above WECC trip plots:

1. Generation trip induces frequency drops
2. All FDR measured frequencies drop to a common level before going back to 60 Hz level.
3. After the frequency drops to a common level during the first swing, it rises up within 1-2 seconds.
4. After the tripping, we can see that the frequency will gradually rise to 60 Hz or pre-fault value within 2-8 minutes. This is an indication of the AGC's time constant.
5. Time delay of the first frequency drop between units can be observed.
6. Before the generation trip, the frequency between units is on top of each other; after generation trip, frequency starts to show distinct delays between units, which suggests there is a form of electromechanical wave propagating in the system due to the disturbance.
7. The frequency drop amount and frequency time delay can be very useful to determine how much of the generation tripped, where the trip was and how the disturbance electromechanical waves propagate. Typically, the larger the frequency drops in the first swing, the larger the tripped generation active power.

6.7 Noticeable frequency deviation

Generator trip or transmission line open can induce sudden frequency drop. And load rejection or transmission line open can cause sudden frequency rise, as we have seen in the simulation studies in Chapter 3. A frequency trigger program developed by Zhian Zhong (Kevin) and further improved by Jian Zou (Ryan) is designed to detect such events. The flow chart for the program can be found in Appendix V. The detection program can

find significant frequency rise or drop using a 4-second running-average window from 3 FDR measurement data. The main reason for using 3 measurement data instead of 1 is that sometimes we may not record data from a unit at all time; therefore, using the data from 3 units would compensate this deficiency and detect events more precisely. The program can capture and record any frequency difference between the starting point and ending point in the 4-second window that is greater than 0.02 Hz. The 0.02 Hz and 4-second window is chosen, based on our experiences with observation of numerous data from generation trip events. Here, we apply the frequency trigger program to the FDR measurements in EUS to find significant frequency drops or rises between April 1, 2004 and April 30, 2005. All frequency plots can be found in Appendix VI. The list of identified events and their type is listed in Table 6-5. Events are categorized into 4 types:

- Generator-trip-like events (G)
- Load-rejection-like events (L)
- Sharp frequency variation during 2005 Superbowl night (S)
- Misidentified cases (M)

In Table 6-5, four types are abbreviated as G, L, S, and M, respectively.

Date & Time (EST)	Type	Date & Time (EST)	Type	Date & Time (EST)	Type
2004/4/3 3:18:17	G	2004/4/9 11:58:13	G	2004/4/13 6:28:15	G
2004/5/1 7:42:52	G	2004/5/4 3:36:5	G	2004/5/5 13:27:30	G
2004/5/6 11:52:16	G	2004/5/12 2:6:16	G	2004/5/18 18:21:29	G
2004/5/21 18:45:30	G	2004/5/31 2:11:33	L	2004/6/22 12:11:33	G
2004/7/8 22:31:30	G	2004/8/15 4:4:52	G	2004/8/22 10:9:12	G
2004/9/4 11:48:47	G	2004/9/6 10:52:9	G	2004/9/9 0:5:34	G
2004/9/11 9:1:23	G	2004/9/19 3:55:55	G	2004/9/21 18:34:39	G
2004/9/23 6:19:1	G	2004/10/1 7:30:29	G	2004/10/6 8:46:19	M

2004/10/7 11:50:24	G	2004/10/13 23:51:27	M	2004/10/15 8:41:29	M
2004/10/16 10:22:59	M	2004/10/16 10:25:0	M	2004/10/19 5:30:1	L
2004/10/23 12:46:49	G	2004/10/23 14:41:58	G	2004/10/24 17:7:28	G
2004/10/27 23:52:26	G	2004/10/30 9:44:57	G	2004/11/5 5:30:37	M
2004/11/14 14:29:19	G	2004/11/20 11:40:3	G	2004/11/22 14:38:45	G
2004/11/22 19:21:16	G	2004/11/23 11:1:10	G	2004/11/28 23:31:11	G
2004/12/5 20:12:19	G	2004/12/5 21:33:3	G	2004/12/8 19:10:10	G
2004/12/15 4:25:35	G	2004/12/20 8:31:10	G	2004/12/22 14:7:50	G
2004/12/24 7:28:20	G	2005/1/2 17:23:7	G	2005/1/5 0:53:19	G
2005/1/8 9:2:27	G	2005/1/8 23:33:35	G	2005/1/9 1:26:46	G
2005/1/11 7:20:9	G	2005/1/16 18:21:19	G	2005/1/19 13:51:18	G
2005/1/30 9:56:32	G	2005/1/30 21:16:12	G	2005/2/6 19:37:19	S
2005/2/6 19:37:27	S	2005/2/6 19:42:52	L	2005/2/6 20:31:24	S
2005/2/6 20:32:5	S	2005/2/6 20:36:13	L	2005/2/6 21:31:33	S
2005/2/6 22:1:24	S	2005/2/6 22:16:25	S	2005/2/6 22:16:52	S
2005/2/11 17:29:29	G	2005/2/23 21:6:9	G	2005/2/28 6:15:23	M
2005/2/28 6:15:28	M	2005/3/2 0:42:25	M	2005/3/7 15:1:41	G
2005/3/12 14:16:43	G	2005/3/15 10:48:42	G	2005/3/20 9:18:41	G
2005/3/21 11:24:36	G	2005/3/28 13:46:42	G	2005/4/7 12:59:29	G
2005/4/8 5:35:38	L	2005/4/9 10:11:21	G	2005/4/10 16:41:45	G
2005/4/15 1:58:49	G	2005/4/15 18:40:52	G	2005/4/17 7:29:3	G
2005/4/22 7:18:47	G	2005/4/28 12:55:22	G	2005/4/29 20:53:45	G
2005/4/30 10:4:49	G				

Table 6-5. EUS Identified cases' date and type from frequency trigger program (4/1/2004-4/30/2005)

So far, we have identified 91 events during April 01, 2004 and April 30, 2005. Nine misidentified events are detected because of sharp spikes at a unit; by visual inspection, there are no significant frequency rises or drops among others. Excluding those misidentified and sharp frequency variation at 2005 Superbowl night, there were 74

significant frequency variation events (generator-trip like and load-rejection-like) during the time period. The number of significant frequency rise/drop events for each month is shown in Fig 6-54. The majority of those events are generator-trip like (69 out of 74) and for each month, the number of these events is also shown in Fig 6-54.

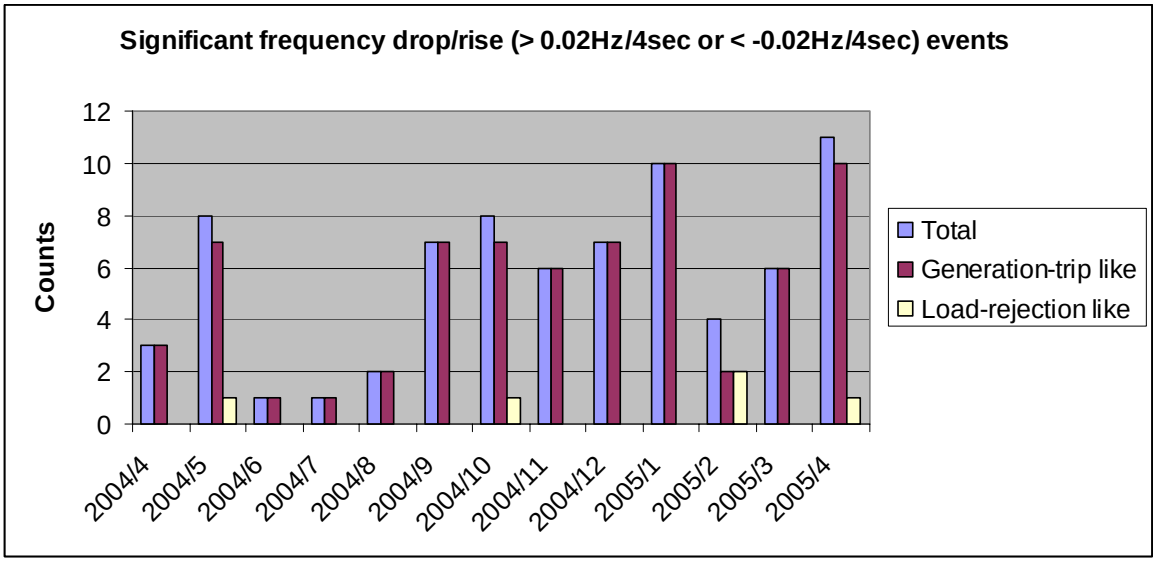

Fig 6-54. Significant frequency drop/rise (>0.02Hz/4sec or <-0.02Hz/4sec) events between 04/01/2004 and 04/30/2005

On an average, about every 5 days (395/74), where 395 is the total number of days and 74 is the total number of identified events during these days, we will see a >0.02Hz/4sec or <-0.02Hz/4sec event in the system, which may be either generator-trip like or load-rejection like event.

6.8 Oscillation observation

In addition to observing transient dynamics in power system, FDR frequency data can also be used to examine the quasi-steady state dynamics. In power system, there exists oscillation modes that may be excited by variations of different system parameters or may

be due to system's configuration. In today's practical power systems, small-signal stability is largely a problem of insufficient damping of oscillation. The oscillation can be generally classified in 4 modes: local modes (machine-system modes), inter-area modes, control modes, torsional modes [89]. Detailed explanation of these modes can be found on page 23 of [89].

From FDR data, we are able to observe electromechanical oscillation modes, namely, local modes, and inter-area modes. Local modes are typically in the 1 to 3-Hz range between a remotely located power station and the rest of the system; and inter-area oscillations are in the range of less than 1 Hz [90]. From our experiences, these oscillation modes only happen once in a while, and the time-series characteristics are not as obvious as those in generation drop, line opening, or load rejection.

In the following, we present an example of frequency oscillations. One case is considered - local-area oscillation. In this case, the oscillation mode(s) can be only observed at 1 unit and such mode(s) do not appear in other units.

The selected example shows the spectrums of frequency measurement on April 02, 2005 between 16:20:30 and 16:24:30. The time series of FDR frequency measurements is shown in Fig 6-55. When calculating the spectrum, the mean of the time period is subtracted, therefore DC component is removed, before FFT (fast Fourier transform) is performed. Some FDR spectrums are shown in Fig 6-56, and Fig 6-57.

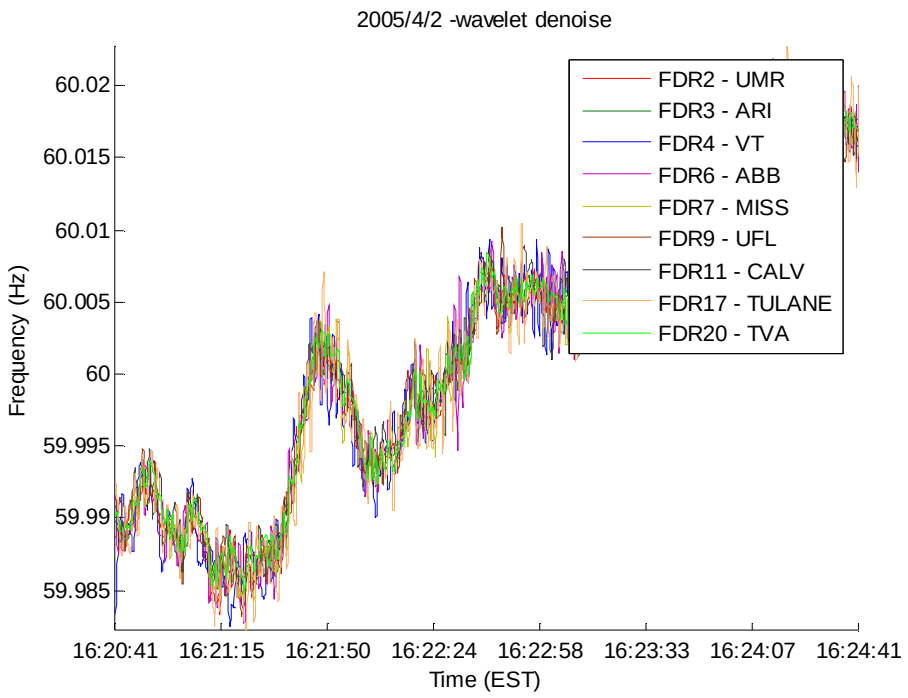

Fig 6-55. FDR frequencies on April 02, 2005 between 16:20:30 and 16:24:30 (EST)

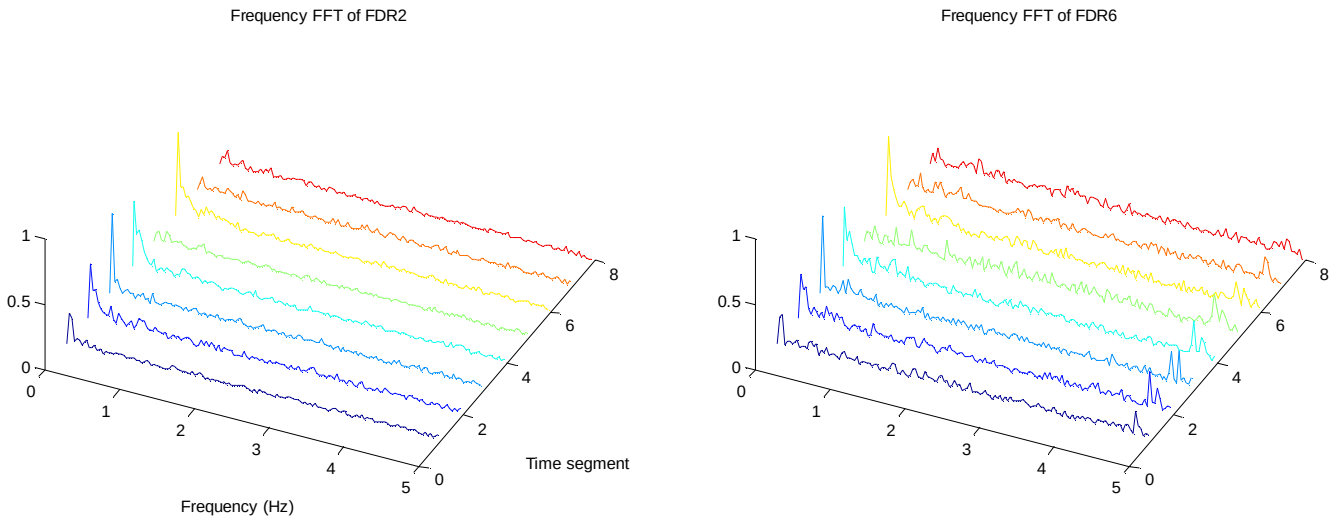

(a) (b)

Fig 6-56. FFT of FDR2 (a) and FDR6 (b) on April 02, 2005 between 16:20:30 and 16:24:30. Each line represents the FFT of a 30-second time segment of the time period.

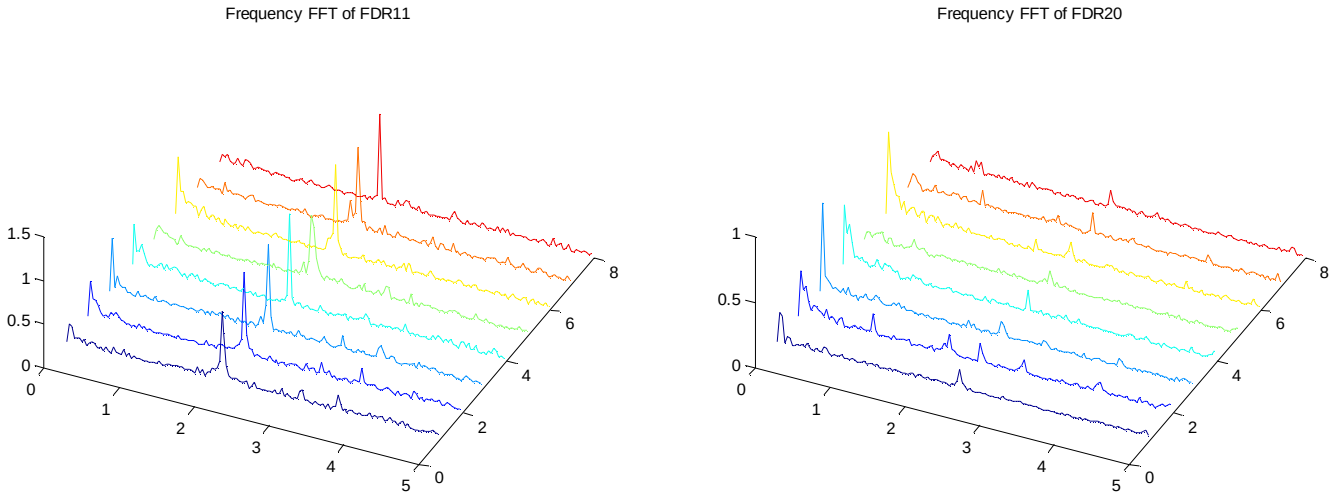

(a) (b)

Fig 6-57. FFT of FDR11 (a) and FDR 20 (b) on April 02, 2005 between 16:20:30 and 16:24:30. Each line represents the FFT of a 30-second time segment of the time period.

As we stated earlier, local modes are typically between 1 to 3 Hz. For FDR2, no modes are found above 1 Hz. For FDR 11, a mode at 2.1 Hz and for FDR 20 a mode at 2.47 Hz show consistently during the time period. These 2 modes are related to the local-area oscillation.

Also we can see for FDR6, there are consistent modes, 4.68 Hz and 4.78 Hz, across the sampled time. Since the 2 modes do not fall into the category of typical local-area and inter-area modes, identification of those modes is required.

6.9 Summary

Frequency is one of the most important parameters in power systems. Using the real-time FDR measurement data can be very useful to observe system's dynamics, such as

disturbance, oscillation, etc. In this chapter, we first discuss the process of converting FNET data from Microsoft Access database into Matlab binary files. In doing so, we have more flexibility to manipulate the data and perform advanced data analyses.

FDR is able to record both system dynamics and local variation dynamics. Local load change and switching typically introduce spikes in frequency measurement. Here, we adopt the de-outlier and denoising technique based on wavelet transform to remove spikes and unwanted noises. A brief introduction of such technique is stated, and examples show that this technique is effective. Therefore, system's dynamics can be better observed.

From the comparisons between a FDR measuring at distribution load and a FDR measuring at a nearby substation's control room, also between a FDR measuring at distribution load and a nearby PMU at a 345 kV transmission line, we can conclude that measuring power frequency at distribution level outlets, with good precision devices and proper signal processing tools, is comparable to that at high voltage line using PMU. System's frequency dynamics can be well tracked by measuring at anywhere-accessible 110 V outlets. The only constraint that we would not be able to record time-synchronized frequency is where GPS antenna cannot receive satellite signals, for example, no access to open sky.

General system operating frequency is examined. For each day, the averaged frequency is close to 60 Hz, no matter how large or how small the frequency may occur in one day. Standard deviation reveals a measure of the dispersion or variation in a distribution. From

the standard deviation calculation, it is found out that EUS and WECC has smaller frequency deviation than that of ERCOT.

Some known generation trip examples in EUS and WECC are illustrated. When a generation trip occurred, frequencies always drop, which is consistent to what we have seen in the simulation studies. Some generation trip characteristics of these 2 systems were discussed in detail. Generally, systems would take about 2-8 minutes to recover to the prefault value or 60 Hz after the trip. The major difference between these 2 systems is that the frequency typically rises right after the first swing of frequency in WECC; however, in EUS the frequency stays at the level for sometime after the first swing before rising up.

Using the frequency trigger program to detect significant frequency drop (> 0.02 Hz/4sec or < -0.02 Hz/4sec) finds 74 events between April 01, 2004 and April 30 2005 in EUS. On an average, about every 5 days, we can see such event. In addition to observing transient states of the system, we can also use the FNET data to observe the system's frequency oscillation. Detection of the oscillation is not trivial though. One example is provided.

Chapter 7 FNET Potential Applications

7.1 Introduction

Frequency measurement provides rich information about system's states as illustrated in previous chapters. FNET can provide close-to real time system wide frequency measurements. Applications of FNET span from fundamental research, such as the electromechanical wave propagation research due to power system perturbation, to immediately-needed applications such as post-mortem analysis right after a system blackout, and to practical applications such as wide area under frequency load shedding and area control error (ACE) calculation improvement. With FNET information, better load shedding schemes can be developed that allow actions taken before frequency drops are experienced locally. Wide-area measurement information should be useful to forecast the inception of a system break-up and recommend remedial actions. Wide-area automatic generation control and tie-line frequency bias control can also be greatly enhanced with the complete picture of system's frequency information. In the following, we look at the potential FNET applications in 4 major areas, namely monitoring and analysis, model validation, system control and other applications; and they are listed below:

- Monitoring and Analysis
    - Information sharing and understanding global frequency dynamics
    - Observing and understanding power system oscillation
    - Study and observe frequency disturbance wave propagation
    - Post-mortem analysis after fault
    - Fault locating

- System Control
    - WAMS based load shedding
    - FACT device control coordination
    - Wide area PSS control
    - Power system restoration
    - Improved ACE calculation
- Model Validation
    - Validation of dynamic load models
    - Validation of or other frequency dependent models
- Other applications
    - Data fusion between FDR, PMU and SCADA
    - Wide area frequency data visualization and graphic user interface

7.2 Monitoring and Analysis

- *Information sharing and understanding global frequency dynamics*

Currently, the frequency information is not shared with different utilities. Therefore, observing and understanding system's frequency dynamics is not accessible. Although a large electric system is divided into sub-regions, they are all interconnected to each other. Sharing one's system states to the neighboring areas can improve the system's reliability. Continuous synchronized wide-area frequency information from FNET will open a new window to the system states; also, system operators at anywhere can observe quasi-real-time system frequency behavior. Such information access capability was never possible before. Through integration of frequency information, one may capture "incremental" angle behavior, thus gaining additional data to devise countermeasure

schemes.

Several examples of visualizing power system frequency dynamics can be found in section 3.5. From the visualizations, we can observe that when certain fault starts in the system, the disturbance will propagate throughout the system. If the disturbance were significant enough, it may cause instability in the system. Having the wide area frequency information, we can detect such instability at early stage and prevent system separation. Using the 2003 US blackout, as shown in section 1.2, we illustrate the importance to have WAMS for observing system's global frequency dynamics.

Also, FNET information can be used to unveil certain operating criteria for system's frequency control. In section 6.5, we illustrate an example of finding the descriptive statistics for frequency for each day. Frequency regulation can be observed from the results.

- *Understanding Power System Oscillations*

Power system oscillations are due to system responses to disturbances. The magnitude and frequency of these oscillations depend on generator rotor inertia, and location. Inter-area oscillations and typical disturbance/load related frequency swings are complicated phenomena. Due to the complexity of the system, the characteristics of dynamics and oscillations are still not well understood. Understanding these characteristics is essential for preventing catastrophic failures and blackouts especially in the deregulated environment. The abundant information from FNET can be applied to study the inter-area mode oscillations, disturbance analysis, and scenario reconstruction.

It could include developing event analysis and pattern recognition algorithms based on frequency measurement information.

From Fig 1-4, Fig 1-5, Fig 1-6 and discussion in Chapter 6, we can see that measurement revealed very complex and interesting frequency excursion patterns. Every measurement point carries area frequency information and exhibits multi-mode behavior. Obviously, more measurement points are needed to further understand the oscillation pattern. FNET can play a unique role in monitoring and understanding patterns and mechanisms of power system electromechanical oscillations.

- *Study and observe frequency disturbance wave propagation*

Power system engineers have long recognized that electromechanical disturbances propagate over the power network with finite speed and exhibit dispersion phenomena. In addition, in Chapter 3, we have extensively discussed the electromechanical wave propagation phenomenon by simulations. FNET will provide field data to validate the wave propagation theory and study desirable wave-reflection conditions to damp system oscillations. It will help investigate power system dynamics from a global approach using the wide area frequency (including df/dt and angle increment derived from the frequency) measurement information.

Visualization examples in section 3.5 have already revealed some characteristics of this electromechanical wave propagation phenomenon. Further investigation may include finding the propagating phenomenon between buses instead of viewing if globally.

- *Post-mortem analysis after system disturbance and fundamental failures of complex system*

FNET information can be used in post-mortem analysis after system disturbance. It can answer questions such as: What happened? Why did it happen? Where did it start? How can we avoid it in the future? When a large blackout occurs, such information will be used to track down the origin and contributing sequential events of the blackout.

- *Disturbance locating*

Using FNET data, we are able to identify the generation trip locations and tripped amount from the various FDR frequency recording [59]. Currently, 10 FDRs are deployed across EUS; and using the frequency data from those units and the triangulation method already can estimate the fault location and the amount of active power tripped with good accuracy. In the future, with the analysis of more events, we can develop algorithms to locate the fault point with better accuracy.

7.3 System control

- *Load shedding based on wide-area frequency information*

The traditional load shedding relays shed load in several steps with the preset tripping frequency and pre-designated feeders derived from assumed system conditions and load distributions. The traditional scheme is a one-size-fits-all compromise of different operation scenarios. With FNET information, especially when combined with existing Energy Management System (EMS) data, better load shedding schemes can be developed. Adaptive load-shedding schemes from global frequency information can be used to shed load based on actual load distribution and power flow constraints.

Since frequency changes propagate as electromechanical waves, rather than passively waiting for local under-frequency relays to shed loads in steps, with FNET information, pro-active approach and overall coordination should be possible to achieve faster system recovery. State estimation and pattern recognition theories can also be used to identify the location of the disturbance and the amount of the generation-load unbalance at a very early stage.

- *FACTS device coordination and control*

FACTS control should not be limited to voltage control and using only local measurement signals. Signals from several remote points (such as remote generators) may be of interest and dynamic frequency is one of the key parameters that can be used as control inputs. If a FACTS device is located in a place where oscillations are not observable locally, it may still be possible for the FACTS device to influence the system behavior by acting upon signals from remote sites where oscillations are seen. An example of using coordinating FACTS with energy storage system to damp inter-area oscillation can be found in [91].

- *Wide-Area power system stabilizer (PSS) control*

The purpose of the PSS is to reduce or eliminate inter-area oscillations; the effective way to control power during the transient state is to damp out the oscillation using remote signals in the feedback control loop. The controller should be designed to act on both local and remote signals to achieve more effective damping of inter-area oscillations.

- *Improvement in area control error (ACE) calculation*

FNET information could be used to improve the accuracy of area control error calculation with multiple point frequency inputs. This is especially true when the system is experiencing some disturbances and the frequencies at different points, even within a relatively small system, are not the same. Further, we can use the more accurate ACE to design more advanced load shedding schemes to achieve faster system recovery. More details can be found in [58].

- *Power system restoration*

During restoration, the system may be split into several islands. The islanding process of the power system after a large disturbance may not be forecast ahead of time. It is important to monitor every part of the remaining system during restoration and hence enhance system's observability. Prompt and accurate identification of the location of faults in a large transmission system is a critical first step in the system restoration. The locating procedure can use the GPS time-stamped FDR data following the disturbance to pinpoint the outage region. Therefore, a possible restoration topology of the system can be created.

FNET system can provide valuable data during power system restoration phase. Additional monitoring and analytical capability based on FNET added to the EMS can certainly further assist system operators during restoration.

7.4 Model validation

- *Validation of dynamic load models*

It has been recognized that the load characteristics play an important role in system stability. The load models, together with the other system element models, are the key elements in the design and operation of power system. Hence, the development of reliable load models is paramount for accurate calculation of system stability limits in both existing systems and in a process of system planning. Different load models can have significant impact on the overall stability analytical results. Various aggregate load models have been proposed and used in small-disturbance, transient stability and voltage stability studies. Different ranges of parameters were recommended for the different types of load.

However, a survey of literature indicates that less work has been conducted in modeling the load than the generators. This is in part due to the difficulties involved in deriving a general-purpose model for loads in large-scale stability analysis. These difficulties include the stochastic nature of load, the number of load nodes in a system and the lack of data surrounding the load. The load model to be employed had to characterize global features of demand and not just local phenomena.

There are two approaches in load modeling, the component based approach and the measurement based approach. The measurement based approach is a method of validation of the load model accuracy, as well. How does dynamic load model based on the measured data affect the veracity of the power system simulation? The answer can be obtained only by being used in the actual power system calculation, and comparing the

results to the recordings in the site.

Because the load characteristics play an important role in system stability, system dynamic characteristics are heavily affected by the characteristics of the load in the system. The load model definition is a mathematical representation of the relationship between a bus voltage (magnitude and frequency) and the power (active and reactive) or current flowing into the bus load. The term “load model” may refer to the equations themselves or the equation plus specific values for the parameters of the equations. The load model can play the same important role in the power system simulation or calculation as the load is in the real power system. From another point of view, the accuracy of the simulation results will reflect the accuracy of the load model and the associated parameters, which is known as the load model validation. The less the difference between the simulation and measurement results is, the more accurate the load model is.

As we mentioned above, the measured dynamic frequency process of the whole power system appears like a fluctuating water surface. At each specific moment, it appears like a static curved surface. It will be the same with the dynamic frequency simulation results. Visually comparing the two fluctuating curved surface will offer the power system engineers a new window of understanding the behavior of power system and clue to modify the existing models used.

The comparison can be from the point of view of the whole system during a period of time, which is to compare the two fluctuating curved surfaces for a period of time. The

comparison can be for the specific moment, which is to compare the two static curved surfaces. Things will be the same when comparisons are from the point of view of electrical geographical line or a specific location.

- *Validation of other system models*

Validation of system models such as governor, generator, transformer, is of vital importance to the system study using the simulation as a tool. References [92, 93] demonstrate the validation of governor models in WECC using staged wide-area measurement data. Numerous works have been concentrated on generator model and its validation. System wide model validation is not yet much in discussion. FNET can provide important frequency data in either steady state or transient state; and using such data will be beneficial to understand the system's dynamics more. Therefore, validation of the system model could be possible.

7.5 Other application areas

- *Data fusion between FDR, PMU and SCADA*

Fusion between measurement data could further enhance the usability of FNET. An important spirit of FNET is to promote the data sharing between different platforms. Such information fusion may seem to be redundant in observing system's states; however, on the other hand, having more probes can reduce inaccurate system measurements. Each measurement scheme exhibits certain characteristics that others don't have, therefore, taking the step towards building a system that can incorporate the advantages of each measurement scheme can greatly enhance the observability of the system dynamics, further control scheme can be designed to prevent system failure in the future.

- *Wide area frequency data visualization and graphic user interface*

As we have illustrated in section 3.5, visualization provides a tool for human beings a direct and quick way to view the system dynamics. Developing different visualization tools using FNET real-time frequency data can help the operator to catch any slight changes in the system; therefore, proper control action might be taken. Easy-to-use visualization tools can be also of great value to the research field. As mentioned, FNET can provide some understandings of the complex dynamics of power systems. Visualization tools can further enhance the usability of such frequency data.

7.6 Remark

As it was pointed out, “one doesn’t really know what one will see till you measure!” More application areas will surface after a large number of FDRs are deployed and measurement results are analyzed. Some of the potential applications are still beyond our imagination at this stage.

Chapter 8 Conclusions and Implications

8.1 Conclusions

Based on simulations on New England 39-bus, Western Electricity Coordinating Council 127-bus and Eastern U.S. interconnection systems, a drop of 0.1% of system's total generation or greater would induce at least 0.005 Hz deviation anywhere in the system, which will be detectable by our in-house design Frequency Disturbance Recorder (FDR). The criteria comes from the fact that FDR is sensible to 0.0001 Hz of accuracy, to leave some margins, we choose 0.005 Hz as the target frequency sensitivity.

Simulation results showed that different location would have different frequency response after a disturbance, e.g. generation trip, load rejection or line trip. Generation trip or load rejection would induce frequencies declining below or rising above 60 Hz. Line trip would induce mixed frequency variation. At selected monitoring buses, the frequency response from line trip can be generation-trip-like, load-rejection-like, oscillation about 60 Hz, islanding or mixed.

From the simulation replay, we could observe that there is an electromechanical wave propagation throughout the system. When a generator trips or load rejects, the wave propagates from the tripping point to the rest of the system. When a line trips, depending on the line criticality, it would either induce power redistribution of the system, which causes minor frequency change, or induce power imbalance between areas, in which frequency in one area would go down and the other would go up. From the frequency map characteristics we may infer which type of event has occurred. The frequency

visualization provides end-users a quick way to capture the state of the system. It helps the user to understand the complex dynamics of power system.

From the uniform single line system, we can deduct a spring-mass model for the frequency propagation study. Changing generators' inertia or line impedances would influence the frequency response.

Generally, areas with dense or large generators tend to slow down the propagation. The wave speed is not the same even between the same two points in opposite directions. For the case we studied, frequency wave "travels" faster in WECC127 system than in the Eastern U.S. system. For uniform single-line system, doubling generators' inertia or doubling impedance would decrease the propagation speed except at the boundary buses. From uniform mesh system, it can be shown a strong correlation between the Thevenin equivalent impedance and the direct geographical distance between 2 buses.

Derivation between frequency and generation power with assumptions provides insights to the delayed frequency response due to generation trip. Based on two govern equations of power system: power flow, swing equations, the sensitivity of bus frequency to generation mechanical power has the delayed response if the generator is away from the bus. Therefore, it is proved that the delayed frequency response can illustrate the disturbance wave propagating phenomenon in real system.

A procedure to convert FNET database file in Microsoft Access into Matlab is provided to better analyze the measured data. FDR is able to record both system dynamics and

local variation dynamics. Local load change and switching typically introduce spikes in frequency measurement. The signal processing including de-outlier and denoising technique based on wavelet transform can effectively remove spikes and unwanted noises. Therefore, system's dynamics can be better observed. From the comparisons between a FDR measuring at distribution load and a FDR measuring at a substation's control room, also between a FDR measuring at distribution load and a PMU at a 345 kV transmission line, we can conclude that measuring power frequency at distribution level outlets with good precision devices and proper signal processing tools is comparable to that at high voltage line using PMU. System's frequency dynamics can be well tracked by measuring at anywhere-accessible 110 V outlets.

General system operating frequency is examined. For each day, the averaged frequency is close to 60 Hz, no matter how large or how small the frequency may occur in one day. Standard deviation reveals a measure of the dispersion or variation in a distribution. From the standard deviation calculation, it is found out that EUS and WECC has smaller frequency deviation than that of ERCOT.

Frequency characteristics from generation trip recordings in EUS and WECC are studied. Generally, frequency swings down to a common level before rising up to 60 Hz. For WECC frequency would start increasing right after the first swing; however, in EUS, frequency would stay at the level for some time before starting to rise. An in-house design frequency trigger program can detect significant frequency drop (> 0.02 Hz/4sec or < -0.02 Hz/4sec). Between April 01, 2004 and April 30 2005, it found 74 events in EUS. On an average, about every 5 days, we can see such event. In addition to observing

transient states of the system, we can also use the FNET data to observe system's frequency oscillation.

8.2 Contributions

This dissertation work provides several unique findings:

- Find the frequency sensitivity of the system for knowing the severity of the event we might expect from measurement.
- Discuss in detail the frequency response and propagation characteristics due to different disturbances (generation trip, load rejection, line trip).
- Create a visualization tool to observe the disturbance propagation and system dynamics.
- Define a way to estimate the frequency electromechanical wave propagation speed.
- Generalize the system frequency operating statistics.
- Summarize several known generation trip data and analyzing the frequency response characteristics.
- Illustrate the close tracking of frequency between frequency disturbance recorder (FDR) and phasor measurement unit (PMU).
- Introduce the in-house design frequency trigger detector and demonstrate examples.

8.3 Future works

Some of the future works have already been stated in detail in Chapter 7 - FNET potential applications. Here we provide the list and other suggested future works:

- Understanding global frequency dynamics
  - Find the electromechanical distance dependences and equation
  - Find the wave propagation speed equation for increment segment
  - Verify the wave speed equation in large system
  - Power system oscillation analysis
- Post-mortem analysis after fault
- WAMS based load shedding, FACTS control coordination, PSS control
- Power system restoration and fault-locating
- Improved ACE calculation
- Validation of dynamic load model and other frequency related models
- Data fusion between FDR, PMU and SCADA
- Implement frequency trigger program on-line
- Design an oscillation detection program

References

[1] A. G. Phadke, "Synchronized phasor measurements in power systems," *IEEE Computer Applications in Power*, vol. 6, pp. 10-15, 1993.

[2] A. G. Phadke, "Application of global positioning systems to electrical systems synchronized phasor measurements techniques and uses," *IEE Colloquium (Digest)*, pp. 4/1-4/2, Feb 1994.

[3] G. Taubes, "GPS: The role of atomic clocks."

[4] "GPS history, chronology, and budgets."

[5] K. E. Martin, G. Benmouyal, M. G. Adamiak, M. Begovic, R. O. Burnett, Jr., K. R. Carr, A. Cobb, J. A. Kusters, S. H. Horowitz, G. R. Jensen, G. L. Michel, R. J. Murphy, A. G. Phadke, M. S. Sachdev, and J. S. Thorp, "IEEE standard for synchrophasors for power systems," *IEEE Transactions on Power Delivery*, vol. 13, pp. 73-77, Jan 1998.

[6] A. G. Phadke, J. S. Thorp, and M. G. Adamiak, "New Measurement Technique for Tracking Voltage Phasors, Local System Frequency, and Rate of Change of Frequency," *IEEE Transactions on Power Apparatus & Systems*, pp. 1025-38, May 1983.

[7] J. S. Thorp, A. G. Phadke, and K. J. Karimi, "Real Time Voltage-Phasor Measurements for Static State Estimation," *IEEE Transactions on Power Apparatus & Systems*, pp. 3098-3107, May 1985.

[8] P. K. Dash, A. K. Panigrahi, H. P. Khincha, and A. M. Sharaf, "New Algorithms for Computer Based Power System Measurements for Relaying," *Electric Machines & Power Systems*, vol. 14, pp. 179-193, 1988.

[9] M. M. Begovic, P. M. Djuric, S. Dunlap, and A. G. Phadke, "Frequency tracking in power networks in the presence of harmonics," *IEEE Transactions on Power Delivery*, vol. 8, Apr. 1993.

[10] J. Chen, "Accurate Frequency Estimation with Phasor Angles," M.S. Thesis, Dept. of Electrical Engineering, Virginia Tech, Blacksburg, 1994.

[11] Z. Salcic and R. Mikhael, "New method for instantaneous power system frequency measurement using reference points detection," *Electric Power Systems Research*, vol. 55, pp. 97-102, 2000.

[12] M.-H. Wang and Y.-Z. Sun, "DFT-based method for phasor and power measurement in power systems," *Automation of Electric Power Systems*, vol. 29, pp. 20-24, Jan 2005.

[13] North American Electric Reliability Council, "August 14, 2003 Power Outages - Announcement," 2003.

[14] Power Systems Engineering Research Center, "Resources for Understanding the Blackout of 2003," 2003.

[15] L. Huang, "Electromechanical Wave Propagation in Large Electric Power Systems," Dissertation, Electrical and Computer Engineering, Virginia Polytechnic Institute and State University, Blacksburg, VA, 2003.

[16] M. Parashar, "Continuum Modeling of Power Networks," Dissertation, Electrical Engineering, Cornell University, Ithaca, NY, 2003.

[17] A. G. Phadke and J. S. Thorp, *Computer relaying for power systems*. Taunton, Somerset, England: Research Studies Press; Wiley, 1988.

[18] F. Saccomanno, *Electric power systems: analysis and control*. Piscataway, NJ: IEEE Press, 2003.

[19] A. Semlyen, "Analysis of Disturbance Propagation in Power systems Based on a Homogeneous Dynamic Model," *IEEE TRansactions on Power Apparatus and System*, vol. PAS-93, pp. 676-84, Mar.-Apr. 1974.

[20] J. S. Thorp, C. E. Seyler, and A. G. Phadke, "Electromechanical wave propagation in large electric power systems," *IEEE Transactions on Circuits & Systems I-Fundamental Theory & Applications*, vol. 45, pp. 614-622, 1998.

[21] J. F. Hauer, N. B. Bhatt, K. Shah, and S. Kolluri, "Performance of "WAMS East" in providing dynamic information for the North East blackout of August 14, 2003," in Power Engineering Society General Meeting, pp. 1685-90, 2004.

[22] R. J. Murphy, "Power System Disturbance Monitoring," in Proceedings of the International Symposium on Signal Processing and its Applications, ISSPA, pp. 282-5, 1996.

[23] S. H. Horowitz and A. G. Phadke, "Boosting Immunity to Blackouts," in *IEEE Power & Energy Magazine*, vol. 1, 2003, pp. 47-53.

[24] K. Newberry, "Wide Area Reliability Monitoring - TVA," Eastern Interconnect Phasor Project (EIPP), 2004.

[25] C. Q. Liu, "A discussion of the WSCC 2 July 1996 outages," *IEEE Power Engineering Review*, vol. 18, pp. 60-1, 1998.

[26] C. W. Taylor and D. C. Erickson, "Recording and analyzing the July 2 cascading outage Western USA power system," *IEEE Computer Applications in Power*, vol. 10, pp. 26-30, 1997.

[27] J. F. Hauer and D. J. Trudnowski, "Using the coherency function in measurement based small-signal analysis of large power systems," *Proceedings of the IEEE*

Power Engineering Society Transmission and Distribution Conference, vol. 2, pp. 809-811 (IEEE cat n 00CH37134), 2000.

[28] X. Jinyu, X. Xiaorong, H. Yingduo, and W. Jingtao, "Dynamic tracking of low-frequency oscillations with improved Prony method in wide-area measurement system," in IEEE Power Engineering Society General Meeting, pp. 1104-9, 2004.

[29] J. Xiao, X. Xie, Y. Han, and J. Wu, "Dynamic tracking of low-frequency oscillations with improved prony method in wide-area measurement system," *IEEE Power Engineering Society General Meeting*, vol. 1, pp. 1104-1109, 2004.

[30] T. Hashiguchi, M. Yoshimoto, Y. Mitani, O. Saeki, and K. Tsuji, "Oscillation mode analysis in power systems based on data acquired by distributed phasor measurement units," in Circuits and Systems, 2003. ISCAS '03. Proceedings of the 2003 International Symposium on, pp. III-367-70, May 2003.

[31] I. Kamwa, "Using MIMO system identification for modal analysis and global stabilization of large power systems," in Power Engineering Society Summer Meeting, pp. 817-22, 2000.

[32] Q. Gu, A. Pandey, and S. K. Starrett, "Fuzzy logic control schemes for static VAr compensator to control system damping using global signal," *Electric Power Systems Research*, vol. 67, pp. 115-22, 2003.

[33] X. Xie, J. Xiao, L. Tong, and Y. Han, "Inter-area damping control of interconnected power systems using wide-area measurements," *Automation of Electric Power Systems*, vol. 28, pp. 37-40, 2004.

[34] B. Chaudhuri, R. Majumder, and B. C. Pal, "Wide-area measurement-based stabilizing control of power system considering signal transmission delay," *IEEE Transactions on Power Systems*, vol. 19, pp. 1971-1979, 2004.

[35] J. Xiao, X. Xie, Z. Hu, and Y. Han, "Power systems wide-area damping control based on online system identification," *Automation of Electric Power Systems*, vol. 28, pp. 22-27, 2004.

[36] A. F. Snyder, N. Hadjsaid, D. Georges, L. Mili, A. G. Phadke, O. Faucon, and S. Vitet, "Inter-area oscillation damping with power system stabilizers and synchronized phasor measurements," in 1998 International Conference on Power System Technology (POWERCON '98), New York, NY, USA, pp. 790-4, Aug. 1998.

[37] M. Smith, "Improved dynamic stability using FACTS decices with phasor measurement feedback," M.S. Thesis, Electrical Engineering, Virginia Polytechnic Institute and State University, Blacksburg, 1994.

[38] I. Kamwa, R. Grondin, and Y. Hebert, "Wide-area measurement based stabilizing control of large power systems-a decentralized/hierarchical approach," *IEEE Transactions on Power Systems*, vol. 16, pp. 136-53, 2001.

[39] J. Peng, Y. Sun, and L. Cheng, "Novel approach for transient stability emergency control based on perturbed trajectory," *Automation of Electric Power Systems*, vol. 26, pp. 17-22, 2003.

[40] C. Rehtanz and J. Bertsch, "Wide area measurement and protection system for emergency voltage stability control," in IEEE Power Engineering Society Winter Meeting, pp. 842-7, 2002.

[41] L. Teng, W.-S. Liu, Z.-H. Yun, G.-C. Li, B. Yu, and Y. Teng, "Study of real-time power system transient stability emergency control," *Zhongguo Dianji Gongcheng Xuebao/Proceedings of the Chinese Society of Electrical Engineering*, vol. 23, pp. 64-69, 2003.

[42] C. Rehtanz and J. Bertsch, "Wide area measurement and protection system for emergency voltage stability control," *Proceedings of the IEEE Power Engineering Society Transmission and Distribution Conference*, vol. 2, pp. 842-847 (IEEE cat n 02ch37309), 2002.

[43] D. J. Sobajic, "Advanced control strategies for interconnected power systems," *10th International Conference on Power System Automation and Control*, pp. 26-31, 1997.

[44] D. Andersson, P. Elmersson, A. Juntti, Z. Gajic, D. Karlsson, and L. Fabiano, "Intelligent load shedding to counteract power system instability," *IEEE/PES Transmision and Distribution Conference and Exposition*, pp. 570-4, 2004.

[45] F. Chunju, L. Shengfang, Y. Weiyong, and K. K. Li, "Study on adaptive relay protection scheme based on Phase Measurement Unit(PMU)," in IEE Conference Publication Eighth IEE International Conference on Developments in Power System Protection, pp. 36-39, 2004.

[46] A. Guzman, D. Tziouvaras, E. O. Schweitzer, and K. Martin, "Local and Wide-Area Network Protection Systems Improve Power System Reliability," Eastern Interconnect Phasor Project (http://phasors.pnl.gov/resources_standards/WAPS_WPRC04.pdf), 2004.

[47] D. Li, F.-K. Han, Z.-M. Guo, L. Zhang, S.-K. Lu, X.-W. Wei, M. Tian, X.-X. Zhang, C.-Y. Liu, J.-Y. Xiao, X.-R. Xie, J.-T. Wu, L.-D. Wang, D. Yang, and X.-C. Xiao, "Wide-area real time dynamic security monitoring system of North China power grid," *Power System Technology*, vol. 28, pp. 52-56, 2004.

[48] J.-Y. Xiao, X.-R. Xie, J. Li, T. Zhang, J.-Y. Luo, X.-Y. Wang, and Y.-L. Wu,

"Wide-area dynamic security monitoring system for power network and its dynamic simulation," *Power System Technology*, vol. 28, pp. 5-9, 2004.

[49] K. K. Yi, J. B. Choo, S. H. Yoon, T. S. Lee, B. C. Park, H. K. Nam, S. G. Song, and K. S. Shim, "Development of wide area measurement and dynamic security assessment systems in Korea," *Proceedings of the IEEE Power Engineering Society Transmission and Distribution Conference*, vol. 3, pp. 1495-1499 (IEEE cat n 01CH37262), 2001.

[50] S.-K. Xu, X.-R. Xie, and Y.-Z. Xin, "Present application situation and development tendency of synchronous phasor measurement technology based wide area measurement system," *Power System Technology*, vol. 29, pp. 44-49, 2005.

[51] C.-C. Liu, "Strategic power infrastructure defense (SPID): a wide area protection and control system," in IEEE/PES Transmission and Distribution Conference and Exhibition, pp. 500-2, 2002.

[52] G. T. Heydt, C. C. Liu, A. G. Phadke, and V. Vittal, "Solution for the crisis in electric power supply," *IEEE Computer Applications in Power*, vol. 14, pp. 22-30, 2001.

[53] D. N. Kosterev, C. W. Taylor, and W. A. Mittelstadt, "Model validation for the August 10, 1996 WSCC system outage," *IEEE Transactions on Power Systems*, vol. 14, pp. 967-79, 1999.

[54] J. H. Kehler, "Synchronous unit testing and model validation in the WSCC," in IEEE Power Engineering Society Winter Meeting, pp. 169-71, 1999.

[55] L. Pereira, J. Undrill, D. Kosterev, D. Davies, and S. Patterson, "A New Thermal Governor Modeling Approach in the WECC," *IEEE Transactions on Power Systems*, vol. 18, pp. 819- 829, May, 2003.

[56] L. Pereira, D. Kosterev, and D. Davies, "New Thermal Governor Model Selection and Validation in the WECC," *IEEE Transactions on Power Systems*, vol. 19, pp. 517-523, Feb. 2004.

[57] R. P. Schulz, "Modeling of governing response in the Eastern Interconnection," in Power Engineering Society 1999 Winter Meeting, IEEE, pp. 561 - 566, 1999.

[58] B. Qiu, "Next Generation Information Communication Infrastructure and Case Studies for Future Power Systems," Ph.D. Dissertation, Electrical and Computer Engineering, Virginia Tech, Blacksburg, 2002.

[59] Z. Zhong, C. Xu, B. J. Billian, L. Zhang, S.-J. S. Tsai, R. W. Conners, V. A. Centeno, A. G. Phadke, and F. Yilu Liu, "Power System Frequency Monitoring Network (FNET) Implementation," *IEEE Transactions on Power Systems*, 2005

(accepted).

[60] X. Zhang, "High Precision Dynamic Power System Frequency Estimation Algorithm Based on Phasor Approach," Thesis, Electrical Engineering, Virginia Polytechnic Institute and State University, Blacksburg, 2004.

[61] T. J. Overbye and J. D. Weber, "Visualizing the electric grid," *IEEE Spectrum*, vol. 38, pp. 52-8, 2001.

[62] T. J. Overbye, D. A. Wiegmann, A. M. Rich, and S. Yan, "Human factors aspects of power system voltage contour visualizations," *IEEE Transactions on Power Systems*, vol. 18, pp. 76-82, 2003.

[63] Y. Min and X.-j. Sun, "Investigation on application of visualization in power system dynamics," *Power System Technology*, vol. 25, pp. 23-6, 2001.

[64] Q. H. A. Arsalan, A. Filbeck, and T. W. Gedra, "Application of virtual instrumentation in a power engineering laboratory," in 2002 45th Midwest Symposium on Circuits and Systems. Conference Proceedings (Cat. No.02CH37378). IEEE. Part vol.1, 2002, pp.I-675-8 vol.1. Piscataway, NJ, USA., pp. 2002.

[65] A. Mota Ad, L. T. M. Mota, and A. Morelato, "Teaching power engineering basics using advanced web technologies and problem-based learning environment," *IEEE Transactions on Power Systems*, vol. 19, pp. 96-103, 2004.

[66] J. D. Weber and T. J. Overbye, "Voltage contours for power system visualization," *IEEE Transactions on Power Systems*, vol. 15, pp. 404-9, 2000.

[67] N. Kobayashi, T. Yamada, H. Okamoto, Y. Tada, A. Kurita, and Y. Sekine, "Visualization of results of load flow calculation and dynamic simulation," *Electrical Engineering in Japan (English Translation of Denki Gakkai Ronbunshi)*, vol. 116, pp. 35-48, 1996.

[68] N. Suzuki, T. Hiyama, and T. Funakoshi, "Real time FFT based on-line identification of power system oscillation modes," *Transactions of the Institute of Electrical Engineers of Japan, Part B*, vol. 120-B, pp. 134-40, 2000.

[69] B. Qiu, L. Chen, V. Centeno, X. Dong, and Y. Liu, "Internet based frequency monitoring network (FNET)," in IEEE Power Engineering Society Winter Meeting, pp. 1166-71, 2001.

[70] "Extended Transient-Midterm Stability Program (ETMSP): Version 3.1 User's Manual," Electric Power Research Institute, May 1994.

[71] "Interactive Power Flow Version 2.1," Electric Power Research Institute, May 1994.

[72] "Extended Transient-Midterm Stability Program (ETMSP): Version 3.1," Electric

Power Research Institute, May 1994.

[73] L. Wang, M. Klein, S. Yirga, and P. Kundur, "Dynamic reduction of large power systems for stability studies," *IEEE Transactions on Power Systems*, vol. 12, pp. 889-95, 1997.

[74] H. Liling, "Electromechanical Wave Propagation in Large Electric Power Systems," Ph.D. dissertation, Dept. of Electrical Engineering, Virginia Polytechnic Institute and State University, Blacksburg, 2003.

[75] D. Faulk and R. J. Murphy, "Comanche peak unit no.2 100% load rejection test-underfrequency and system phasor measured across TU electric system," in Proceeding Annual Conference Protective Relay Engineerings, College Station, TX, pp. 1994.

[76] L. Huang, M. Parashar, A. G. Phadke, and J. S. Thorp, "Impact of electromechanical wave propagation on power-system reliability," in 39th CIGRE Conference, Paris, France, pp. August 25-30 2002.

[77] S. S. Tsai, L. Zhang, A. G. Phadke, Y. Liu, M. R. Ingram, S. C. Bell, I. S. Grant, D. T. Bradshaw, D. Lubkeman, and L. Tang, "Study of global frequency dynamic behavior of large power systems," in IEEE PES Power Systems Conference and Exposition, New York, pp. 328 - 335, Oct. 2004.

[78] J. S. Thorp, C. E. Seyler, and A. G. Phadke, "Electromechanical wave propagation in large electric power systems," *IEEE Transactions on Circuits & Systems I-Fundamental Theory & Applications*, vol. 45, pp. 614-22, 1998.

[79] L. Huang, M. Parashar, A. G. Phadke, and J. S. Thorp, "Impact of Electromechanical Wave Propagation on Power System Protection and Control," in CIGRE conference, pp. 2001.

[80] M. Parashar, J. S. Thorp, and C. E. Seyler, "Continuum modeling of electromechanical dynamics in large-scale power systems," *IEEE Transactions on Circuits & Systems I-Fundamental Theory & Applications*, vol. 51, pp. 1848-1858, 2004.

[81] J. J. Grainger and W. D. Stevenson, *Power system analysis*. New York: McGraw-Hill, 1994.

[82] I. Daubechies, *Ten lectures on wavelets*. Philadelphia, PA: Society for Industrial and Applied Mathematics, 1992.

[83] J. S. Walker, *A primer on wavelets and their scientific applications*. Boca Raton, FL: Chapman & Hall/CRC, 1999.

[84] A. Mertins, *Signal analysis: wavelets, filter banks, time-frequency transforms, and applications*. New York: J. Wiley, 1999.

[85] D. B. Percival and A. T. Walden, *Wavelet methods for time series analysis*. Cambridge; New York: Cambridge University Press, 2000.

[86] G. Strang and T. Nguyen, *Wavelets and filter banks*. Wellesley, MA: Wellesley-Cambridge Press, 1996.

[87] S. Qian, *Introduction to time-frequency and wavelet transforms*, 1 ed. Upper Saddle River: Prentice Hall, 2002.

[88] D. Hinkle, W. Wiersma, and S. G. Jurs, *Applied Statistics for the Behavioral Sciences*, 4th ed. Boston, MA: Houghton Mifflin Company, 1998.

[89] P. Kundur, *Power System Stability and Control*: McGraw-Hill, Inc., 1994.

[90] P. W. Sauer and M. A. Pai, *Power System Dynamics and Stability*. Upper Saddle River, New Jersey: Prentice Hall, 1998.

[91] L. Zhang, Y. Liu, M. R. Ingram, D. T. Bradshaw, S. Eckroad, and M. L. Crow, "Bulk Power System Low Frequency Oscillation Suppression By FACTS/ESS," in Power System Conference & Exposition, New York, NY, pp. Oct. 2004.

[92] L. Pereira, D. Kosterev, and D. Davies, "New Thermal Governor Model Selection and Validation in the WECC," *IEEE Transactions on Power Systems*, vol. 19, pp. 517-523, Feb 2004.

[93] D. M. Cabbell, S. Rueckert, B. A. Tuck, and M. C. Willis, "The new thermal governor model used in operating and planning studies in WECC," *IEEE Power Engineering Society General Meeting*, vol. 2, pp. 1784-9, Jun 2004.

Appendix I 2003 Eastern US Blackout Event Time Line

Each event is reported from various sources. The source of information is identified in color as following:

Black: Commonwealth Associate Inc.
Blue: AEP
Green: NERC
Pink: ITC
Orange: PJM

The second column is the simulation time we defined for this study. Please note that between noon and 16:08:58 (EST), the simulation time was shrunk into the first 50 seconds proportionally, and the simulation time span, after 50 seconds, corresponds to the actual time span until 16:25 (EST).

The bracket after each bus name is the bus number in the EUS model. If we cannot identify the bus name in the model, a question mark is placed.

Time (EDT)	Simulation time (sec)	Events
Precondition	0	Davis-Besse (870MW) [21630] is down for maintenance. In the model change the power output from 2550 MW to 1680 MW
12:05:44	0	Conesville Unit 5 (rating 375 MW) [22703] trips
13:14:04	0	Greenwood Unit 1 (rating 785 MW) [29023] trips
13:31:34	0	Eastlake Unit 5 (rating 597 MW) [21600] trips
14:02	0	Stuart [26648] – Atlanta 345 kV. In the data the nearest point to Atlanta is Beaty [22648]
15:05:41	0+	Harding [22153] – Chamberlain [21832] 345 kV
15:32:03	5	Hanna [21350] – Juniper [22156] 345 kV
15:41:33	10	Star [21961] 138 KV* – South Canton [22619] 345 kV
		Demand of about 600 MW disconnected in the northern Ohio from industry customer. Distribution level customers who were disconnected from the 138 and 69

		kV transmission system.
15:42:53	15	Cloverdale [21430] – Torrey [23243] 138 kV
15:44:12	20	East Lima [23132] – New Liberty [23184] 138 kV
15:45:33	25	Canton Central [23123] – Colverdale [21430] 138kV
15:45:33	25	Canton Central [22601] – Tidd [22623] 345 kV
15:51:41	30	East Lima – North Findlay 138 kV [23132 – (23184,23193) – 23186]
16:05:55	35	Dale –West Canton 138 kV (unknown connection in the model)
16:06:03		Sammis – Star 345 kV (can't find the connection)
15:42:49 - 16:08:58		Multiple 138kV line across northern Ohio disconnected themselves
		Start with the real time span
16:08:58	50	Galion [21868] 138kV* – Ohio Central[22618] – Muskingum [22616] 345kV
16:09:06	58	East Lima [22603] – Fostoria Central [22606] 345 kV
16:09:22	74	Cloverdale [21430] – East Wooster [23140] 138 kV
16:09:23 – 16:10:27		Kinder Morgan (500 MW to 200 MW). Can't find the generator [96403???]
16:09		Demand loss of 700-950 MW, which represents a frequency rise of 0.020 – 0.027 Hz at the Eastern Interconnection
16:10		Harding [22153] – Fox ? 345kV
16:10:00	112	Armstrong [20567, 20569] trip
16:10:04 - 16:10:45	116-157	20 generators along Lake Erie in northern Ohio (loaded to 2174 MW). We pick Avon [21665], Lakesmith [22671, 22672, 22670], but these 4 don't make up 2167 MW drop.
16:10:37	149	West-East Michigan 345 kV. We pick the trip of Vergennes [28317] to Thetford [28309] and Tittabawassee [28312]; and Argenta [28197] to Magestic [28790] and Battle [28201] 138kV
16:10:38	150	MCV (1265 MW) [28276]
164:10:38	150	Transmission system separates northwest of Detroit. We pick Hampton [28245] – Thetford [28309]
16:10:38	150	Perry [21650] – Ashtabula – Erie West [90064] 345 kV

16:10:40	152	Homer City [90102] – Watercure Road 345. The nearest node to Watercure is OakDL [75405]
16:10:40	152	Homer City [90102] – Stolle Road [75507] 345kV
16:10:40	152	East Towanda [90078] – Grover [90080] 230kV
16:10:41	153	South Ripley [76501] – Dunkirk [76500] 230kV
16:10:41	153	Fostoria Central [22606] 345kV – Galion [21868] 138kV*
		Perry 1 (1252MW) [21650] trips
		Avon Lake 9 unit (616MW) [21660] trips
		Beaver – Davis Beese 345kV ?
16:10:42	154	Campbell unit 3 (820 MW) [28339] trips
16:10:43	155	Keith [82591] – Waterman [28882] 230kV
16:10:44	156	East Towanda [90078] – Hillside [75413] 230kV
16:10:45	157	Wawa [81970] – Marathon [82280 1,2] 230kV
16:10:45	157	Branchburg 500kV [90001] – Ramapo 345kV [74347]. The 500kV of Ramapo does not exist in the model 230 and 138 kV lines ties in New Jersey are disconnected along with the 500 kV disconnection. We do not know what they are so ignore for now.
16:10:46	158	During the next minute the following Michigan generators trips: St. Clair 7 [29015] Judd ? Monroe 1 [29031] ,2 ?, and 3 ? Greenwood (already tripped at 1:14:04) St. Clair 2 ?,4 [29017] and 6 [29016] Trenton 7 [29029], 8 ? and 9 [29030]
16:10:48	160	New York transmission splits east-west. From the map, we pick Frasor [75403] and Oak Dale [75405]; and Cooper Corners [75400] and Marcy [79583]
16:10:49	161	Tosco []trips
16:10:49	161	Tosco Unit 1. Can't find it.
16:10:50	162	Athenia – Clifton 230kV. Can't find it Athenia #2 transformer (230/138 kV). Don't know.
16:10:52	164	Athenia – Clifton 230 kV. Can't find it.

16:10:46 – 16:10:55	158-167	Ties between New York – New England transmission lines disconnect. From the map, we pick Alps [78700] to Northfield [72926] and Berkshire [72952]; and Rotterdam [78980] to Brswamp [72385] to be disconnected
16:10:50	162	Ontario system just west of Niagara Falls and west of St. Lawrence separates from New York. We pick Sir Adam Beck [81690] and Alanburg [81680] an Decew [81700]. St. Lawrence has yet to be determined
16:11	172	Midway138kV* [22105] – Lemoyne 138 kV*[21470[- Foster 345 kV [25513]
16:11	172	FitzPatrick near Oswego N.Y. [74913]
16:11:03	175	Various western PA generators trip. We pick New Castle [21510], Beaver Valley [27621], Elrama [27624 (1,2), 27625-6], Hatefield [20580-2]
16:11:07	179	Homer City Unit 3. In the model we have 2 generators related to Homer City namely C1 [90114] and C2 [90115]. C1 is 620 MW and C2 is 1264 MW. Probably pick C2 for severity.
16:11:14	186	Erie West [90064] 345 kV – Wayne [90063] 115 kV*
16:11:22	194	Long Mountain – Plum Tree 345kV. We pick Frost Bridge [73202] – Pleasant Valley [74344]
16:11:24	196	Athenia – Cook Raod. Can't find it.
16:11:44	216	Hudson Unit 2 [90427] trips
16:11:45	217	Seneca [90069] trips
16:11:57	229	Ontario and eastern Michigan separates. We pick Chatham [82555] – Keith [82591]; and Scott[82645] - 28998
16:12	231	Bruce [80327] trips
16:12	231	Ginna [79940] trips
16:12	231	Nine Mile Point [77950] trips
16:12	231	Various Northern New Jersey generators trip. We pick Essex [90415]
16:12:29	260	-Athenia [90377] – Belleville. We guess Belleville as [90392] HDSN7-12 -Linden [90395] – Bayway [90379]

		-Cedar Grove – Jackson. Can't find it -New Milford – Maywood. Can't find it
16:12:45	276	Bergen [90435] trips Linden [90418] trips Newark Bay trips. Can't find it
16:16	471	Oyster Creek [90209] trips
16:17	531	Enrico Fermi [29012] trips
16:25	1011	Indian Point [74701] trips
16:38:02		Academia – Howard 138kV. Unknown connection in the model
	End	

Appendix II Visual Basic Scripts for FNET Data Processing

Visual Basic script for exporting data from Access database file to text files for each FDR.

```
'-------------------------------------------------------------
' Query_ExportFormatedText_DeleteQuery
'
'-------------------------------------------------------------
Function Query_ExportFormatedText_DeleteQuery(startFDRindx As Integer, numofFDRs
As Integer, sPath As String)
Dim i As Integer
Dim a As Double
Dim temp As String

On Error GoTo Query_ExportFormatedText_DeleteQuery_Err

Perform_query_export:
    For i = startFDRindx To numofFDRs
        DoCmd.OpenQuery "FRURawData" & i & " Query", acViewNormal, acEdit
        Call CreateSchemaFile(False, sPath, "FRUData" & i & ".txt")
        temp = sPath & "FRUData" & i & ".txt"
        DoCmd.TransferText acExportDelim, "", "FRURawData" & i & "_query", temp,
False, ""
        DoCmd.DeleteObject acTable, "FRURawData" & i & "_query"
    Next i

    'Beep
    'MsgBox "Export formatted text is done", vbInformation, "Text Export"

Query_ExportFormatedText_DeleteQuery_Exit:
    Exit Function

Query_ExportFormatedText_DeleteQuery_Err:
    'DBEngine.CompactDatabase dbPath & "db1-1009-2004.mdb", dbPath &
"db1-1009-2004.mdb"
    'Resume Perform_query_export
    'MsgBox Error$
    Resume Query_ExportFormatedText_DeleteQuery_Exit

End Function
```

Visual Basic script for generating schema.ini file for each data exporting in MS Access:

```
Function CreateSchemaFile(bIncFldNames As Boolean, sPath As String, sSectionName
As String) As Boolean
        Dim Msg As String ' For error handling.
        On Local Error GoTo CreateSchemaFile_Err
        Dim Handle As Integer
        ' ------------------------------------------------
        ' Open schema file for append.
        ' ------------------------------------------------
        Handle = FreeFile
        Open sPath & "schema.ini" For Output Access Write As #Handle
        ' ------------------------------------------------
        ' Write schema header.
        ' ------------------------------------------------
        Print #Handle, "[" & sSectionName & "]"
        Print #Handle, "ColNameHeader = " & _
                        IIf(bIncFldNames, "True", "False")
        Print #Handle, "Format = CSVDelimited"
        ' ------------------------------------------------
        ' Get data concerning schema file.
        ' ------------------------------------------------
        Print #Handle, "Col1=Sample_Date&Time Date"
        Print #Handle, "Col2=ConvNum Integer"
        Print #Handle, "Col3=FinalFreq LongChar"
        Print #Handle, "Col4=VoltageAng LongChar"
        CreateSchemaFile = True
CreateSchemaFile_End:
        Close Handle
        Exit Function
CreateSchemaFile_Err:
        Msg = "Error #: " & Format$(Err.Number) & vbCrLf
        Msg = Msg & Err.Description
        MsgBox Msg
        Resume CreateSchemaFile_End
End Function
```

Appendix III Matlab Script for FNET Data Processing

Matlab FDR data processing script

```
function fdrraw2mat_direct2divide_date(dbfiledate,numofmeasures,fdrfileno,fdrfilenoend)
%function fdrraw2mat_direct2divide_date(dbfiledate,numofmeasures,fdrfileno,fdrfilenoend)
%Inputs:
%'dbfiledate' in the format of [year month day]
%'numofmeasures': the number of FDR measurements
%
% Created by S.-J. Steven Tsai @ Virginia Tech


numofmeasures = numofmeasures;
dbfiledate = dbfiledate;

maxdates_range = 10; % maximum number of dates allowed in 1 Access database file
if nargin==2
    fdrprocess = [1:numofmeasures];
elseif nargin==3
    fdrprocess = fdrfileno;
elseif nargin==4
    fdrprocess = [fdrfileno:fdrfilenoend];
else
    disp(['Insufficient inputs']);
    return;
end

for fdrno=fdrprocess

    %t0 = clock;
    %=========================================================================
    % read the text file data into 'textdata' matrix
    clear FDRdata FDRtemp
```

```
close all, pack
eval(['fid = fopen(''FRUData'',num2str(fdrno),'.txt'',''r'');']);
textdata = fscanf(fid,'%d/%d/%d %d:%d:%d,%d,"%f","%f"');
fclose(fid);
disp(['Finished FRUData',num2str(fdrno),' loading!']);
textdata_r = reshape(textdata,9,length(textdata)/9);
clear textdata
pack

month = textdata_r(1,:);
day = textdata_r(2,:);
year = textdata_r(3,:);
hour = textdata_r(4,:);
minute = textdata_r(5,:);
second = textdata_r(6,:);
conv = textdata_r(7,:);
finalfreq = textdata_r(8,:);
voltang = textdata_r(9,:);
clear textdata_r
pack

% conv number data error, usually happens at data retransmission
conv_outrangeindx = union(find(conv>10),find(conv<0));
disp(['number of conv error: ',num2str(length(conv_outrangeindx))]);
for j=1:length(conv_outrangeindx)
    finalfreq = [finalfreq(1:conv_outrangeindx(j)-1),finalfreq(conv_outrangeindx(j)+1:end)];
    voltang = [voltang(1:conv_outrangeindx(j)-1),voltang(conv_outrangeindx(j)+1:end)];
    year = [year(1:conv_outrangeindx(j)-1),year(conv_outrangeindx(j)+1:end)];
    month = [month(1:conv_outrangeindx(j)-1),month(conv_outrangeindx(j)+1:end)];
    day = [day(1:conv_outrangeindx(j)-1),day(conv_outrangeindx(j)+1:end)];
    hour = [hour(1:conv_outrangeindx(j)-1),hour(conv_outrangeindx(j)+1:end)];
    minute = [minute(1:conv_outrangeindx(j)-1),minute(conv_outrangeindx(j)+1:end)];
    second = [second(1:conv_outrangeindx(j)-1),second(conv_outrangeindx(j)+1:end)];
    conv = [conv(1:conv_outrangeindx(j)-1),conv(conv_outrangeindx(j)+1:end)];
    conv_outrangeindx = conv_outrangeindx-1;
end
```

```
second = second + ((conv-1)/10);
date = [year' month' day' hour' minute' second'];

%-------------------------------------------------------------
% Store the data into 'FDRdata' structure
FDRdata.date = date;
FDRdata.freq = finalfreq;
FDRdata.voltang = voltang;

clear month day year hour minute second conv date finalfreq voltang;
pack
%=============================================================================================
% detect data error
%-------------------------------------------------------------
% 1st error: date was added wrongly by 1 at 23:59:58 (some case 23:59:59)
%          pull out all the record after 23:59:50 and detect if there is any date error
lastminsecindx = find(FDRdata.date(:,4)==23 & FDRdata.date(:,5)==59 & FDRdata.date(:,6)>50);

for j=1:length(lastminsecindx)
    if datenum(FDRdata.date(lastminsecindx(j),1:3)) ~= datenum(FDRdata.date(lastminsecindx(j)-200,1:3))
        if FDRdata.date(lastminsecindx(j),3) > 1
            FDRdata.date(lastminsecindx(j),3) = FDRdata.date(lastminsecindx(j),3)-1;
        elseif FDRdata.date(lastminsecindx(j),2) > 1
            mo = FDRdata.date(lastminsecindx(j),2);
            FDRdata.date(lastminsecindx(j),3) = max(max(calendar(FDRdata.date(lastminsecindx(j),1),mo-1)));
            FDRdata.date(lastminsecindx(j),2) = mo-1;
        else
            FDRdata.date(lastminsecindx(j),1) = FDRdata.date(lastminsecindx(j),1)-1;
            FDRdata.date(lastminsecindx(j),2) = 12;
            FDRdata.date(lastminsecindx(j),3) = 31;
        end
    end
end

clear lastminsecindx j mo
pack
```

```
%-------------------------------------------------------
%2nd error: when retransmitting the data, it all starts with convolution number 0
%          and the frequency and the angle are 0
freq0indx = find(FDRdata.freq==0);
ang0indx = find(FDRdata.voltang==0);
sec_minus1_indx = find(FDRdata.date(:,6)<0);
f0_I_a0 = intersect(freq0indx,ang0indx);
f0_I_a0_U_sec_minus1 = union(f0_I_a0,sec_minus1_indx);
disp(['number of freq0:',num2str(length(freq0indx)),' ;ang0:',num2str(length(ang0indx)),...
    ' ;f0 U a0:',num2str(length(f0_I_a0)),' (f0 U a0) I -1sec:',num2str(length(f0_I_a0_U_sec_minus1))]);
% remove the error data
pack, memory
for j=1:length(f0_I_a0_U_sec_minus1)
    FDRdata.freq = [FDRdata.freq(1:f0_I_a0_U_sec_minus1(j)-1),FDRdata.freq(f0_I_a0_U_sec_minus1(j)+1:end)];
    FDRdata.voltang = [FDRdata.voltang(1:f0_I_a0_U_sec_minus1(j)-1),FDRdata.voltang(f0_I_a0_U_sec_minus1(j)+1:end)];
    FDRdata.date = [FDRdata.date(1:f0_I_a0_U_sec_minus1(j)-1,:);FDRdata.date(f0_I_a0_U_sec_minus1(j)+1:end,:)];
    f0_I_a0_U_sec_minus1 = f0_I_a0_U_sec_minus1-1;
end
clear freq0indx ang0indx sec_minus1_indx f0_I_a0 f0_I_a0_U_sec_minus1 j
pack


month = [1  2  3  4  5  6 7  8  9  10 11 12];
days = [31 28 31 30 31 30 31 31 30 31 30 31];

dT_UTC2EST = -5; % time advance from UTC to EST (Eastern Standard Time)

FDRdata.date(:,4) = FDRdata.date(:,4)+dT_UTC2EST;

% find the hours that is less than 0, which means that the dates have to substract by 1 and the hours have to add 24
substractdateindx = find(FDRdata.date(:,4) < 0);
FDRdata.date(substractdateindx,3) = FDRdata.date(substractdateindx,3)-1;
FDRdata.date(substractdateindx,4) = FDRdata.date(substractdateindx,4)+24;
day0dateindx = find(FDRdata.date(:,3)==0);
if length(day0dateindx)>0
    FDRdata.date(day0dateindx,2) = FDRdata.date(day0dateindx,2)-1;
    for j=1:length(day0dateindx)
```

```
        if FDRdata.date(day0dateindx(j),2)==0
            FDRdata.date(day0dateindx(j),1)=FDRdata.date(day0dateindx(j),1)-1;
            FDRdata.date(day0dateindx(j),2)=12;
            FDRdata.date(day0dateindx(j),3)=31;
        else
            mo = FDRdata.date(day0dateindx(j),2);
            FDRdata.date(day0dateindx(j),3) = days(mo);
        end
    end

end
clear substractdateindx day0dateindx mo
pack
%-------------------------------------------------------------
% exlcude dates that are out of range
% exclude the data that is greater than the 'maxdates_range'
outrange_dates_indx = find(datenum(FDRdata.date) > datenum(dbfiledate)+maxdates_range | ...
    datenum(FDRdata.date) < datenum(dbfiledate)-maxdates_range);

for j=1:length(outrange_dates_indx)
    FDRdata.freq = [FDRdata.freq(1:outrange_dates_indx(j)-1),FDRdata.freq(outrange_dates_indx(j)+1:end)];
    FDRdata.voltang = [FDRdata.voltang(1:outrange_dates_indx(j)-1),FDRdata.voltang(outrange_dates_indx(j)+1:end)];
    FDRdata.date = [FDRdata.date(1:outrange_dates_indx(j)-1,:);FDRdata.date(outrange_dates_indx(j)+1:end,:)];
    outrange_dates_indx = outrange_dates_indx-1;
end
%-------------------------------------------------------------
clear outrange_dates_indx;
pack
%=============================================================================================
% seperate each date's data and save into individual file of each date
if length(FDRdata.date)>0
    % sorts dates, still thinking if necessary??
    [sorted_date,orig_indx] = sort(datenum(FDRdata.date));
    %figure,plot(orig_indx,'-x');
    %title(['FDR',num2str(fdrno)]);
    FDRdata.date = FDRdata.date(orig_indx,:);
    FDRdata.freq = FDRdata.freq(orig_indx);
```

```
FDRdata.voltang = FDRdata.voltang(orig_indx);
clear sorted_date orig_indx
pack
%-------------------------------------------------------
% Store the data into each date's file
mindate = min(datenum(FDRdata.date(:,1:3)));
maxdate = max(datenum(FDRdata.date(:,1:3)));
if fdrno==1 & nargin == 2
   resavemindate = mindate; resavemaxdate = maxdate;
else if nargin ==2 & exist('resavemindate')
       if resavemindate > mindate
          resavemindate = mindate;
       end
       if resavemaxdate < maxdate
          resavemaxdate = maxdate;
       end
   else
       resavemindate = mindate; resavemaxdate = maxdate;
   end
end
if nargin==4 & fdrno == fdrfileno
   resavemindate = mindate; resavemaxdate = maxdate;
elseif nargin == 4
   if resavemindate > mindate
       resavemindate = mindate;
   end
   if resavemaxdate < maxdate
       resavemaxdate = maxdate;
   end
end

for dateindx = mindate:1:maxdate
   samedateindxes = find(datenum(FDRdata.date(:,1:3))==dateindx);
   if length(samedateindxes) > 0
       eval(['FDR',num2str(fdrno),'.freq = FDRdata.freq(samedateindxes);']);
       eval(['FDR',num2str(fdrno),'.voltang = FDRdata.voltang(samedateindxes);']);
       eval(['FDR',num2str(fdrno),'.date = FDRdata.date(samedateindxes,:);']);
```

```
timezone = 'EST';
savefilename = ['fdr-',datestr(dateindx,29),'-EST.mat'];
%end
eval(['FDR',num2str(fdrno),'.timezone = timezone;']);
clear samedateindxes
pack

%savefilename = ['fdr-',datestr(dateindx,29),'-EDT.mat'];
if exist(savefilename,'file')
    eval(['FDRtemp = FDR',num2str(fdrno),';']); % if file exist, first save the processed FDR data to a temp
                                                %variable (FDRtemp)
    eval(['clear FDR',num2str(fdrno),';']);     % then clear FDRx structure
    warning off
    eval(['load ',savefilename,' FDR',num2str(fdrno)])  % try to load the FDRx structure data
    warning always
    if exist(['FDR',num2str(fdrno)],'var')
        eval(['saveddatelen = length(FDR',num2str(fdrno),'.date);']);
        if saveddatelen>0
            eval(['savedstartdatenum = datenum(FDR',num2str(fdrno),'.date(1,:));']);
            eval(['savedenddatenum = datenum(FDR',num2str(fdrno),'.date(end,:));']);
        else
            savedstartdatenum = 0;
            savedenddatenum = 1;
        end
        processedstartdatenum = datenum(FDRtemp.date(1,:));
        processedenddatenum = datenum(FDRtemp.date(end,:));
        if savedenddatenum < processedstartdatenum
            eval(['FDR',num2str(fdrno),'.freq = [FDR',num2str(fdrno),'.freq, FDRtemp.freq];']);
            eval(['FDR',num2str(fdrno),'.voltang = [FDR',num2str(fdrno),'.voltang, FDRtemp.voltang];']);
            eval(['FDR',num2str(fdrno),'.date = [FDR',num2str(fdrno),'.date; FDRtemp.date];']);
            eval(['FDR',num2str(fdrno),'.timezone = timezone;']);
            eval(['save ',savefilename,' FDR',num2str(fdrno),' -append;']);
            disp(['Date ',datestr(dateindx,29),' - FDR',num2str(fdrno),' is completed']);
        elseif savedstartdatenum > processedenddatenum
            eval(['FDR',num2str(fdrno),'.freq = [FDRtemp.freq, FDR',num2str(fdrno),'.freq];']);
            eval(['FDR',num2str(fdrno),'.voltang = [FDRtemp.voltang, FDR',num2str(fdrno),'.voltang];']);
            eval(['FDR',num2str(fdrno),'.date = [FDRtemp.date ; FDR',num2str(fdrno),'.date];']);
```

```
    eval(['FDR',num2str(fdrno),'.timezone = timezone;']);
    eval(['save ',savefilename,' FDR',num2str(fdrno),' -append;']);
    disp(['Date ',datestr(dateindx,29),' - FDR',num2str(fdrno),' is completed']);
elseif savedenddatenum == processedenddatenum & savedstartdatenum==processedstartdatenum
    disp(['Date ',datestr(dateindx,29),' - FDR',num2str(fdrno),...
        ' data is the same as saved data. Processed data is not saved']);
else
    disp(['Date ',datestr(dateindx,29),' - FDR',num2str(fdrno),...
        ': Date ranges are overlap! Processed data are combined with saved data!'])
    % find out date duplications in 2 structure: FDRx, and FDRtemp
    eval(['[dupdates,FDRtempdupindx,FDRdupindx] = intersect(datenum(FDRtemp.date), ...
       datenum(FDR',num2str(fdrno),'.date));']);

    if length(FDRtempdupindx) > 0 % some duplicates
        % exclude duplicates
        [junk,diffindx] = setdiff(datenum(FDRtemp.date),datenum(FDRtemp.date(FDRtempdupindx)));
        clear junk;
        FDRtemp.date = FDRtemp.date(diffindx,:);
        FDRtemp.freq = FDRtemp.freq(diffindx);
        FDRtemp.voltang = FDRtemp.voltang(diffindx);

        eval(['[junk,diffindx] = setdiff(datenum(FDR', ...
                num2str(fdrno),'.date),datenum(FDR',num2str(fdrno),'.date(FDRdupindx)));'])
        clear junk;
        eval(['FDR',num2str(fdrno),'.date = FDR',num2str(fdrno),'.date(diffindx,:);'])
        eval(['FDR',num2str(fdrno),'.freq = FDR',num2str(fdrno),'.freq(diffindx);'])
        eval(['FDR',num2str(fdrno),'.voltang = FDR',num2str(fdrno),'.voltang(diffindx);'])
    end

    % combine
    eval(['FDR',num2str(fdrno),'.freq = [FDR',num2str(fdrno),'.freq, FDRtemp.freq];']);
    eval(['FDR',num2str(fdrno),'.voltang = [FDR',num2str(fdrno),'.voltang, FDRtemp.voltang];']);
    eval(['FDR',num2str(fdrno),'.date = [FDR',num2str(fdrno),'.date; FDRtemp.date];']);
    eval(['FDR',num2str(fdrno),'.timezone = timezone;']);
    %sort
    eval(['[sorted_date,orig_indx] = sort(datenum(FDR',num2str(fdrno),'.date));']);
    eval(['FDR',num2str(fdrno),'.date = FDR',num2str(fdrno),'.date(orig_indx,:);']);
```

```
                    eval(['FDR',num2str(fdrno),'.freq = FDR',num2str(fdrno),'.freq(orig_indx);']);
                    eval(['FDR',num2str(fdrno),'.voltang = FDR',num2str(fdrno),'.voltang(orig_indx);']);
                    clear sorted_date orig_indx
                    % save
                    eval(['save ',savefilename,' FDR',num2str(fdrno),' -append;']);
                end
            else
                eval(['FDR',num2str(fdrno),'=FDRtemp;']);
                eval(['save ',savefilename,' FDR',num2str(fdrno),' -append;']);
                disp(['Date ',datestr(dateindx,29),' - FDR',num2str(fdrno),' is completed']);
            end
            clear FDRtemp;
            pack
        else
            eval(['save ',savefilename,' FDR',num2str(fdrno)]);
            disp(['Date ',datestr(dateindx,29),' - FDR',num2str(fdrno),' is completed']);
        end
        eval(['clear FDR',num2str(fdrno)]);
    end
  end
end
clear FDRdata
pack
end

% reload and save files to enable compression
for dateindx = resavemindate:1:resavemaxdate
    clear FDR*
    savefilename = ['fdr-',datestr(dateindx,29),'-EST.mat'];
    disp(['Resaving ',savefilename]);
    eval(['load ',savefilename]);
    eval(['save ',savefilename ,' FDR*']);
end
clear FDR*
```

Appendix IV System Frequency Statistics

Between April, 1, 2004 and April, 30, 2005, the frequency statistics of FDRs in 3 US interconnected systems, namely, WECC, EUS, and ERCOT, are calculated. Please note that not all units have the same number of data points. Some units may have deployed earlier than others. In addition, units may have their downtime, and, therefore no frequency data were recorded. In the following, for each row of plots, the left plot represents the maximum (upper envelope), mean (blue line), and minimum (lower envelope) for each day and the right plot represents the standard deviation for each day.

EUS

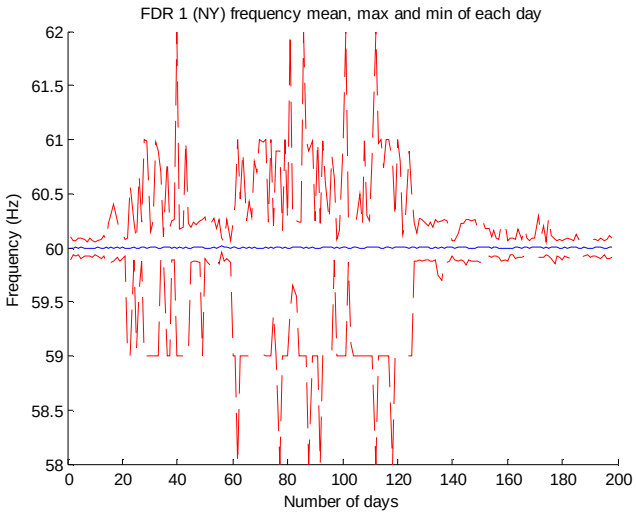

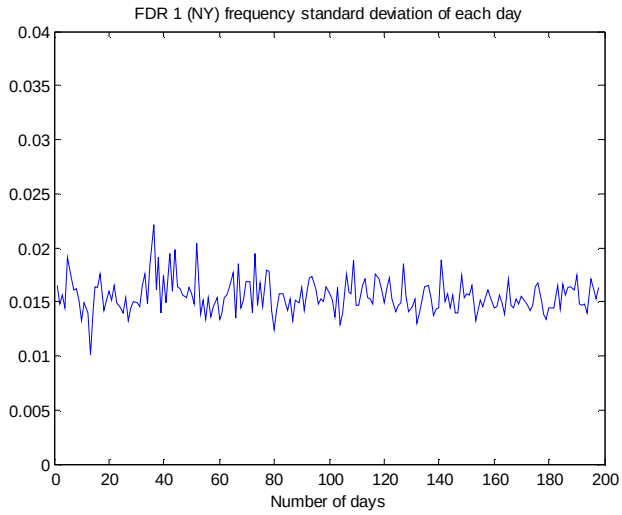

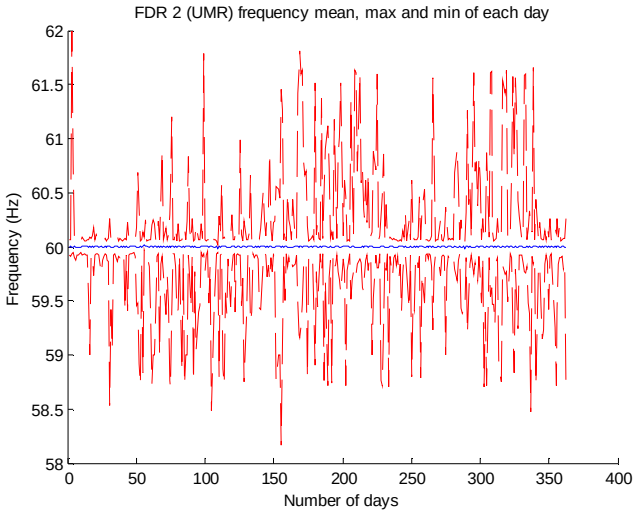
FDR 2 (UMR) frequency mean, max and min of each day
Frequency (Hz)
Number of days

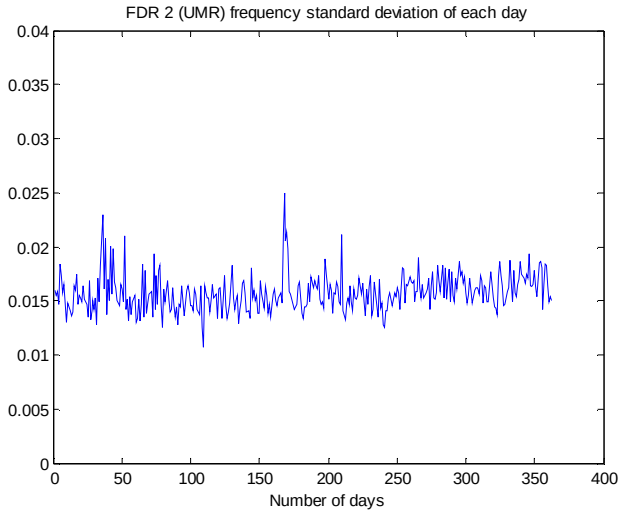
FDR 2 (UMR) frequency standard deviation of each day
Number of days

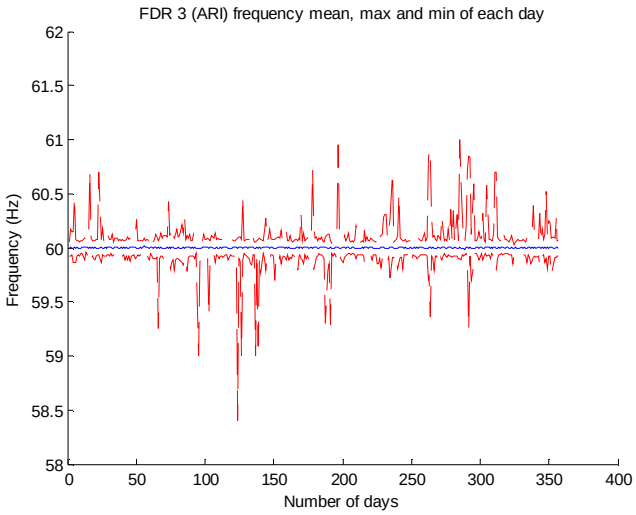
FDR 3 (ARI) frequency mean, max and min of each day
Frequency (Hz)
Number of days

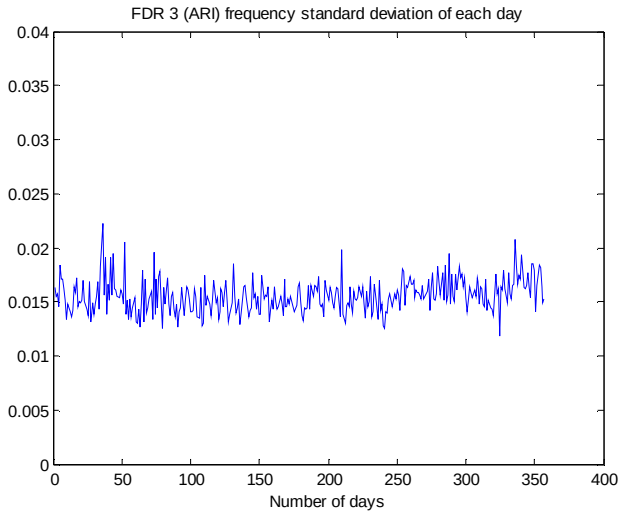
FDR 3 (ARI) frequency standard deviation of each day
Number of days

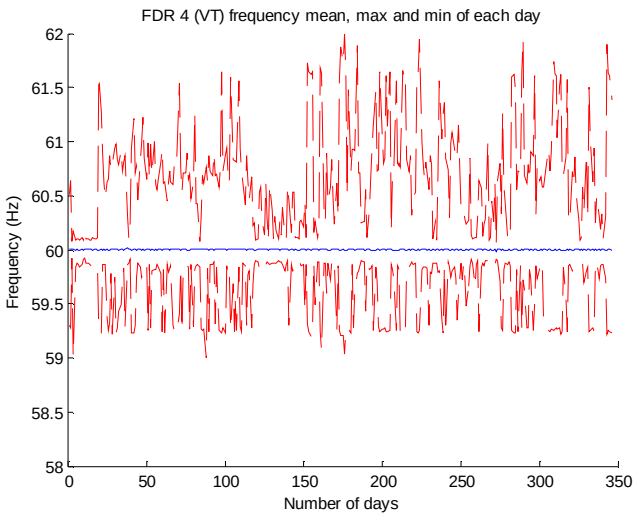
FDR 4 (VT) frequency mean, max and min of each day
Frequency (Hz)
Number of days

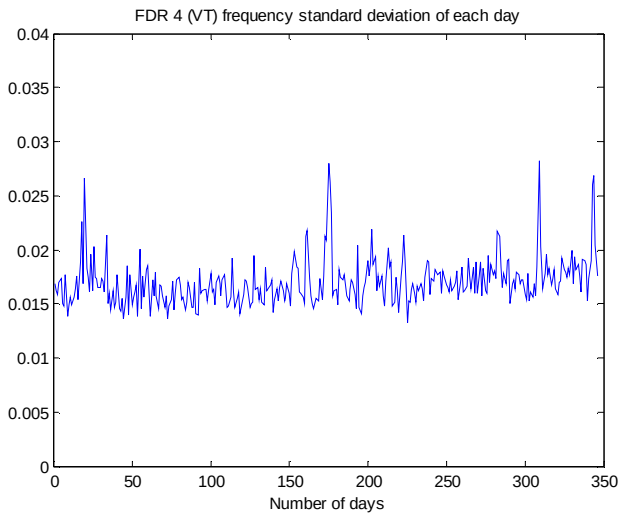
FDR 4 (VT) frequency standard deviation of each day
Number of days

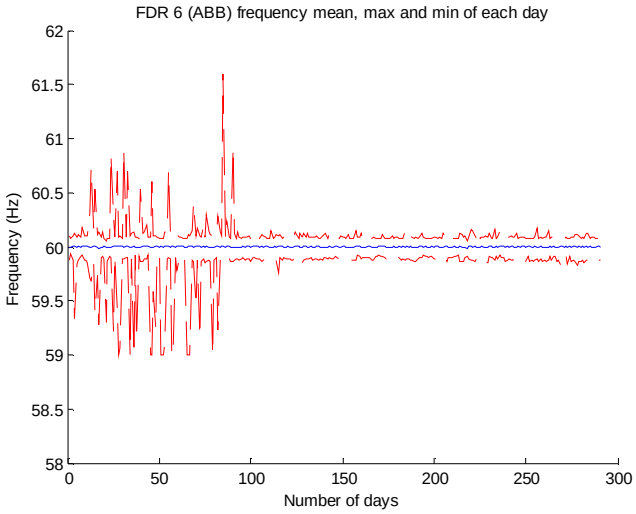
FDR 6 (ABB) frequency mean, max and min of each day
Frequency (Hz)
Number of days

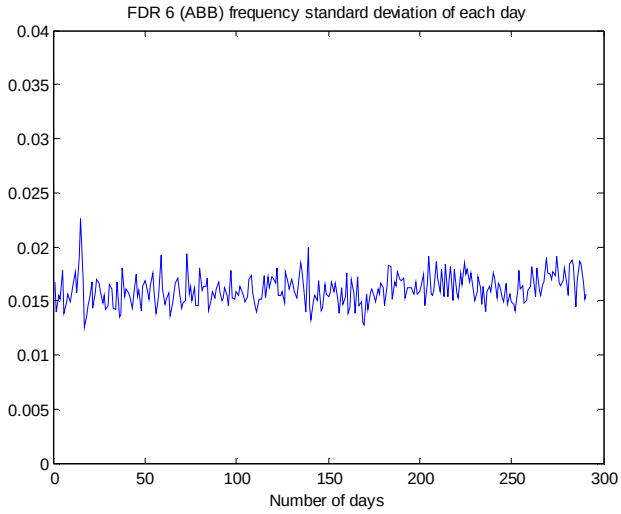
FDR 6 (ABB) frequency standard deviation of each day
Number of days

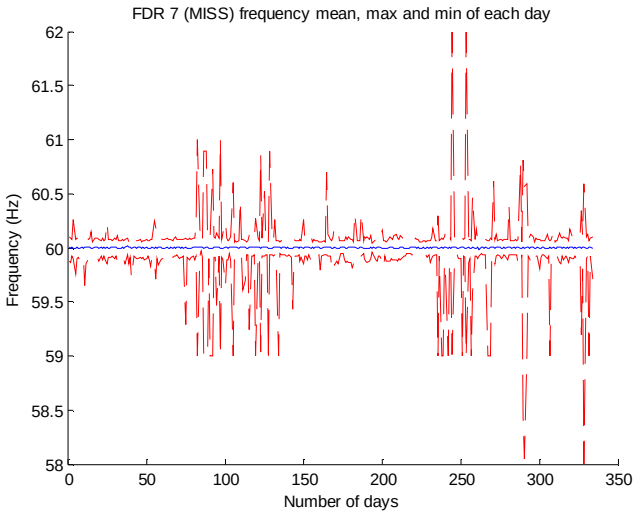
FDR 7 (MISS) frequency mean, max and min of each day
Frequency (Hz)
Number of days

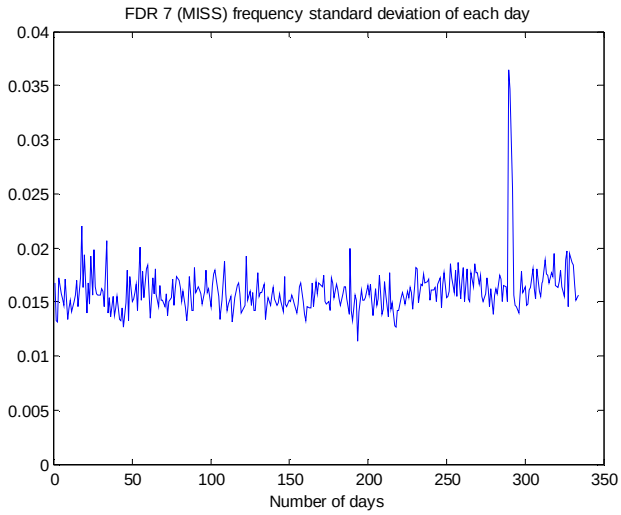
FDR 7 (MISS) frequency standard deviation of each day
Number of days

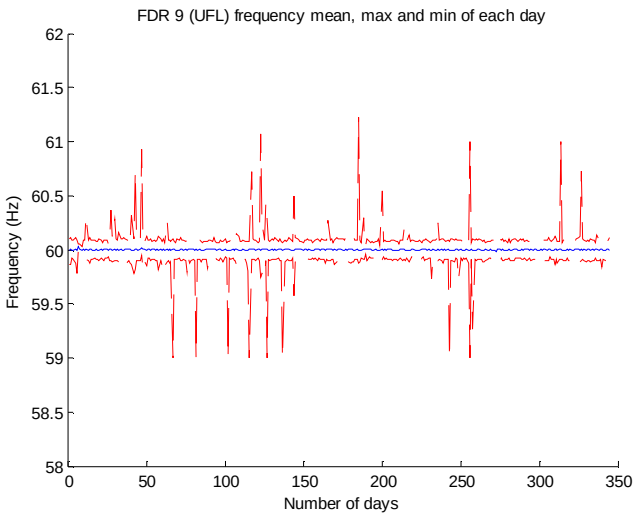
FDR 9 (UFL) frequency mean, max and min of each day
Frequency (Hz)
Number of days

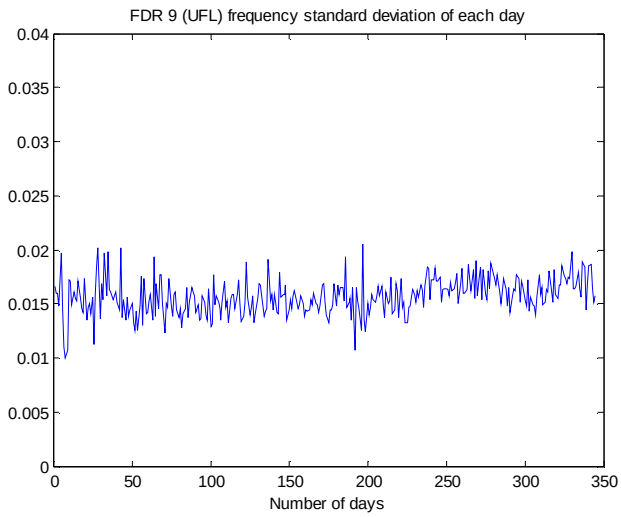
FDR 9 (UFL) frequency standard deviation of each day
Number of days

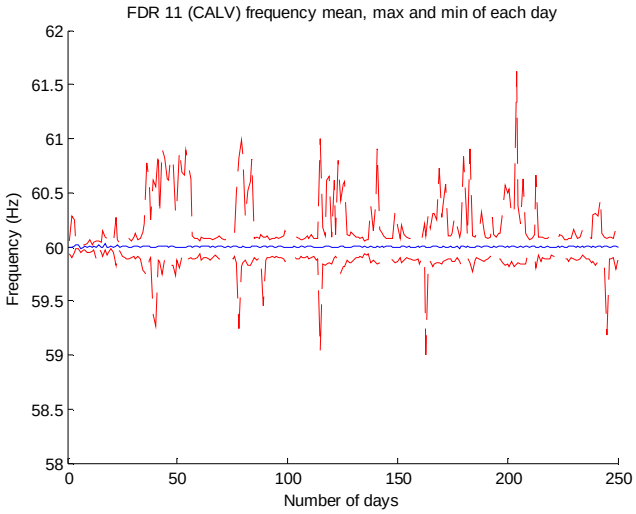
FDR 11 (CALV) frequency mean, max and min of each day
Frequency (Hz)
Number of days

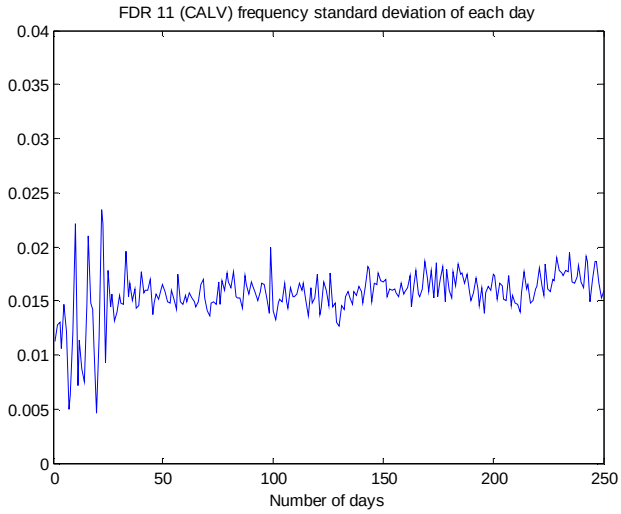
FDR 11 (CALV) frequency standard deviation of each day
Number of days

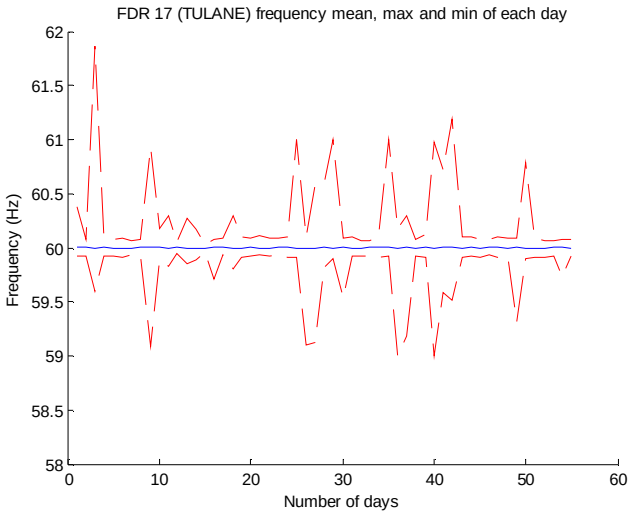
FDR 17 (TULANE) frequency mean, max and min of each day
Frequency (Hz)
Number of days

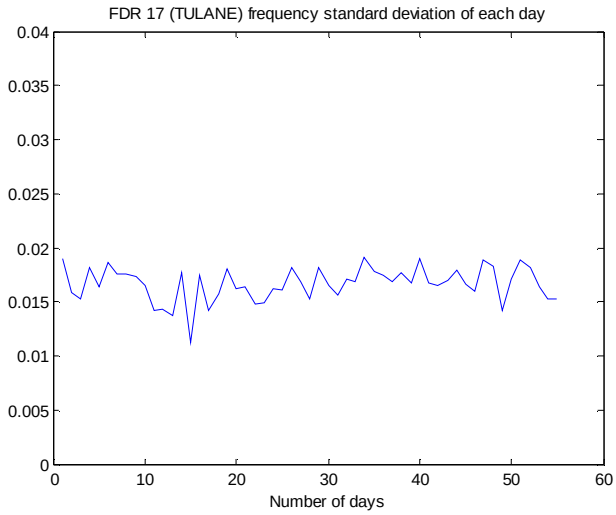
FDR 17 (TULANE) frequency standard deviation of each day
Number of days

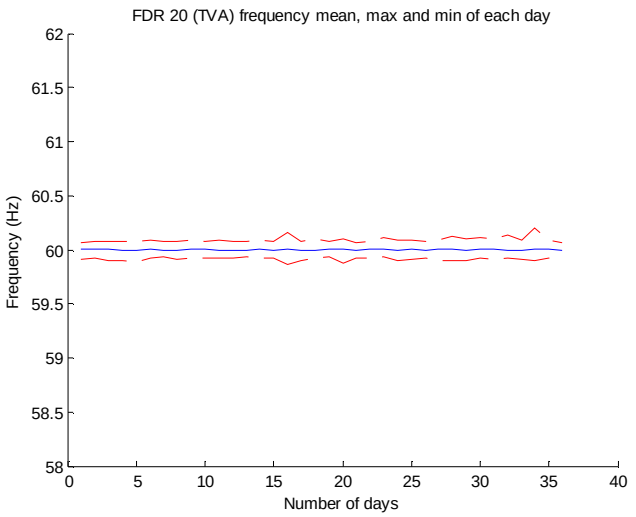
FDR 20 (TVA) frequency mean, max and min of each day
Frequency (Hz)
Number of days

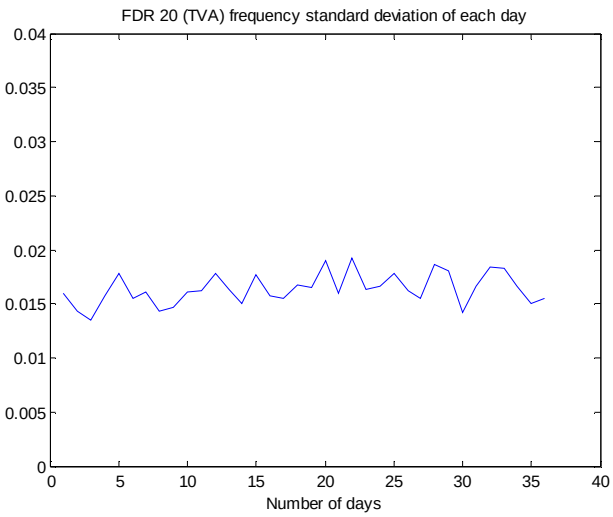
FDR 20 (TVA) frequency standard deviation of each day
Number of days

WECC

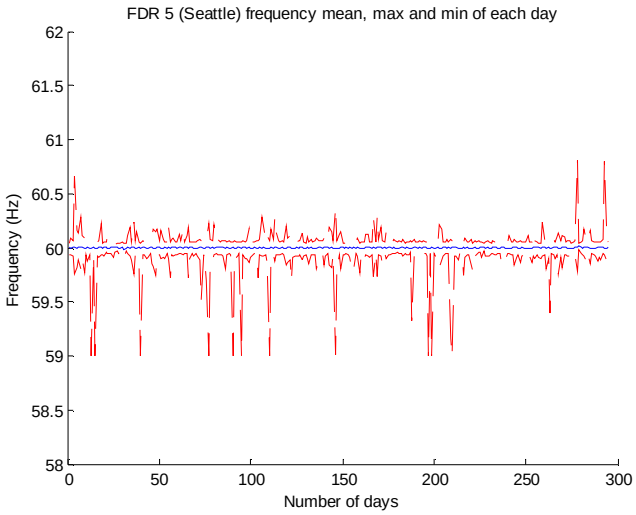
FDR 5 (Seattle) frequency mean, max and min of each day
Frequency (Hz)
Number of days
62
61.5
61
60.5
60
59.5
59
58.5
58
0
50
100
150
200
250
300

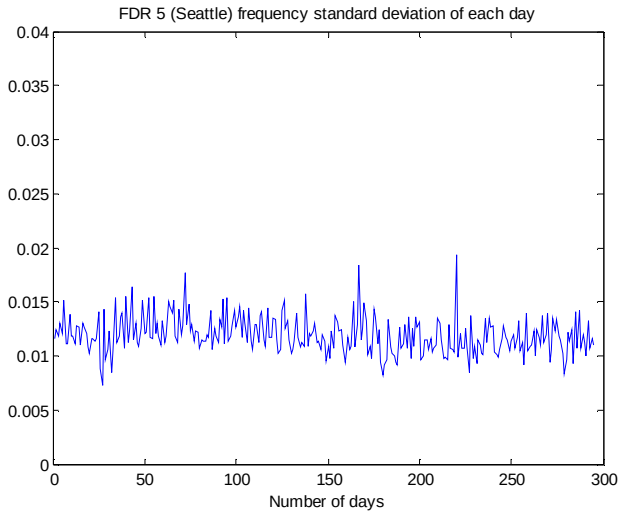
FDR 5 (Seattle) frequency standard deviation of each day
Number of days
0.04
0.035
0.03
0.025
0.02
0.015
0.01
0.005
0
0
50
100
150
200
250
300

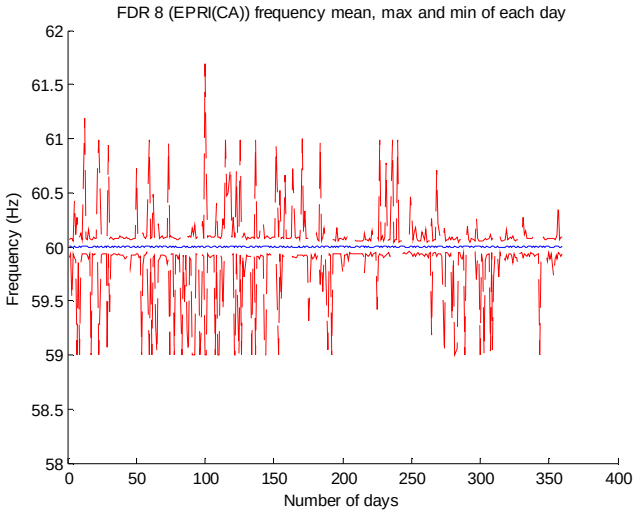
FDR 8 (EPRI(CA)) frequency mean, max and min of each day
Frequency (Hz)
Number of days
62
61.5
61
60.5
60
59.5
59
58.5
58
0
50
100
150
200
250
300
350
400

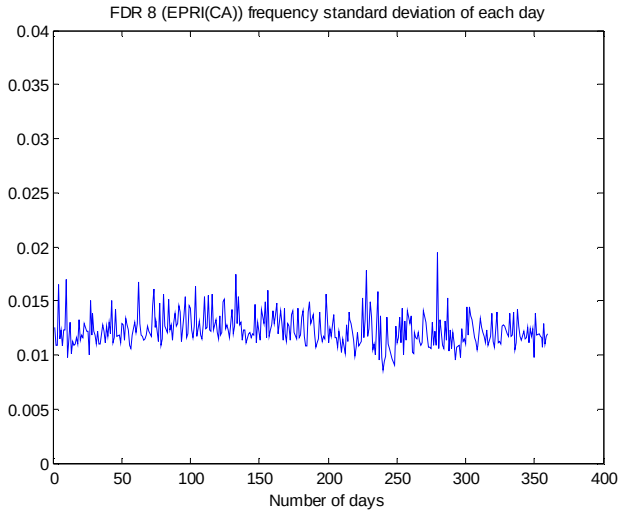
FDR 8 (EPRI(CA)) frequency standard deviation of each day
Number of days
0.04
0.035
0.03
0.025
0.02
0.015
0.01
0.005
0
0
50
100
150
200
250
300
350
400

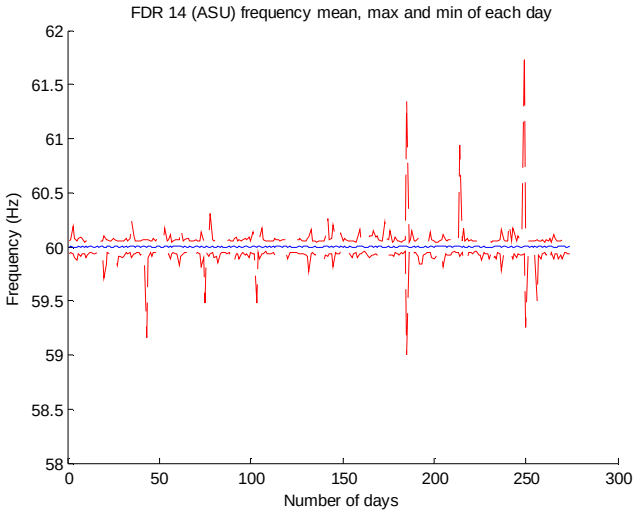
FDR 14 (ASU) frequency mean, max and min of each day
Frequency (Hz)
Number of days
62
61.5
61
60.5
60
59.5
59
58.5
58
0
50
100
150
200
250
300

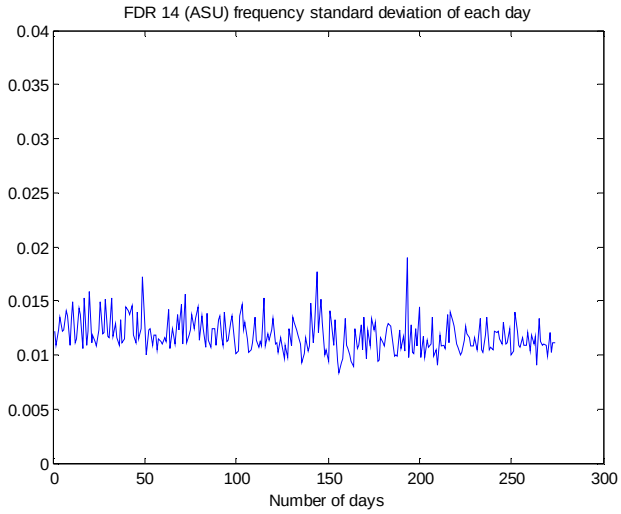
FDR 14 (ASU) frequency standard deviation of each day
Number of days
0.04
0.035
0.03
0.025
0.02
0.015
0.01
0.005
0
0
50
100
150
200
250
300

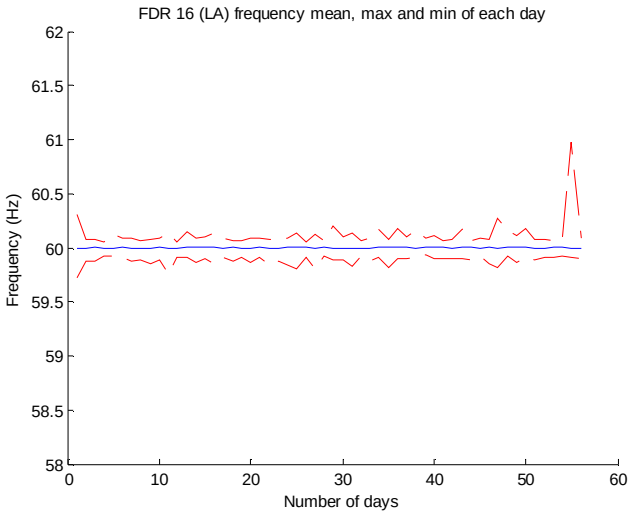
FDR 16 (LA) frequency mean, max and min of each day
Frequency (Hz)
Number of days
62
61.5
61
60.5
60
59.5
59
58.5
58
0
10
20
30
40
50
60

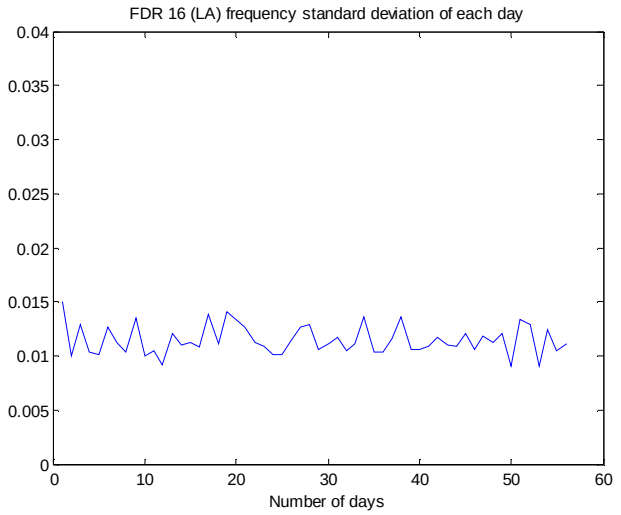
FDR 16 (LA) frequency standard deviation of each day
Number of days
0.04
0.035
0.03
0.025
0.02
0.015
0.01
0.005
0
0
10
20
30
40
50
60

ERCOT

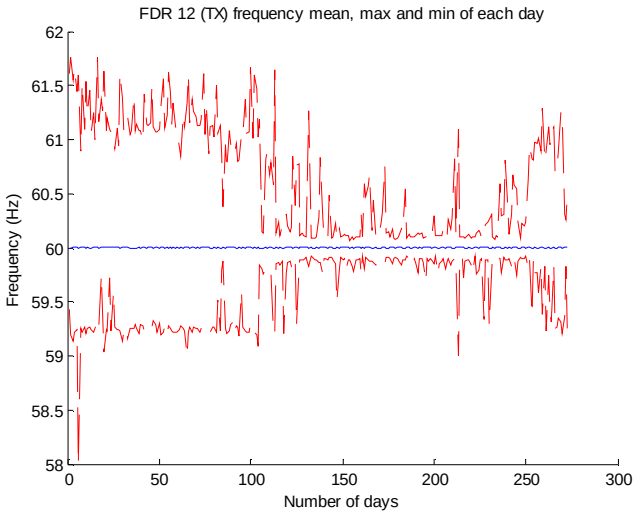
FDR 12 (TX) frequency mean, max and min of each day
Frequency (Hz)
Number of days
62
61.5
61
60.5
60
59.5
59
58.5
58
0
50
100
150
200
250
300

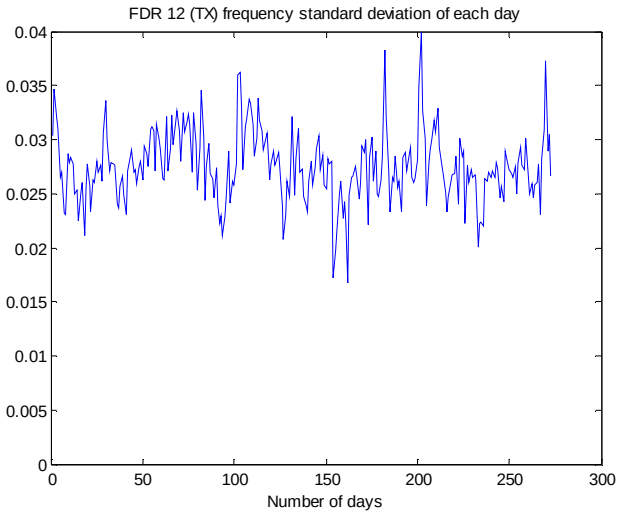
FDR 12 (TX) frequency standard deviation of each day
Number of days
0.04
0.035
0.03
0.025
0.02
0.015
0.01
0.005
0
0
50
100
150
200
250
300

Appendix V Trigger Program Flow Chart

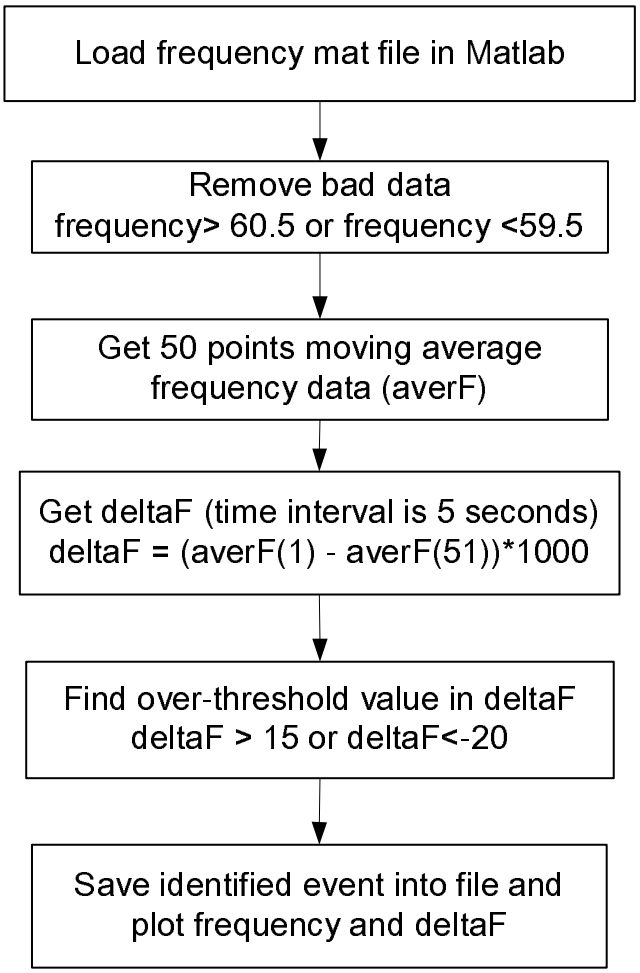

Appendix VI Sample Eastern US System Events from Trigger Program

The following plots show the events identified by the frequency trigger program between April 1, 2004 and April 30, 2005 in EUS. We categorized the cases into 4 types:

- Generator-trip-like events
- load-rejection-like events
- Sharp frequency variation at 2004 Superbowl night
- Misidentified cases

Generator-trip-like or load-rejection-like events:

Total of 67 generator-like events and 3 load-rejection-like events.

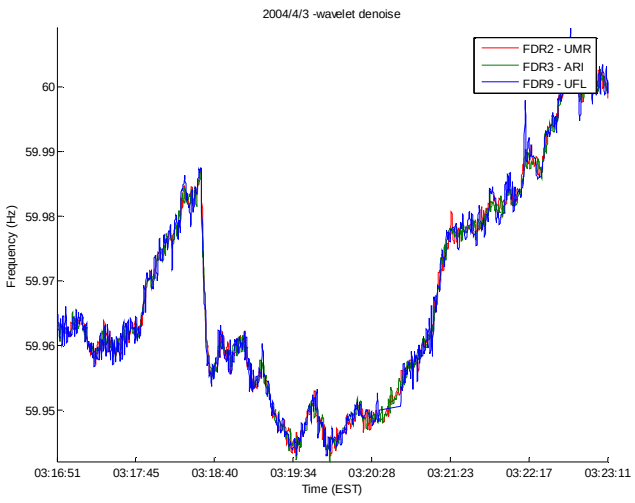

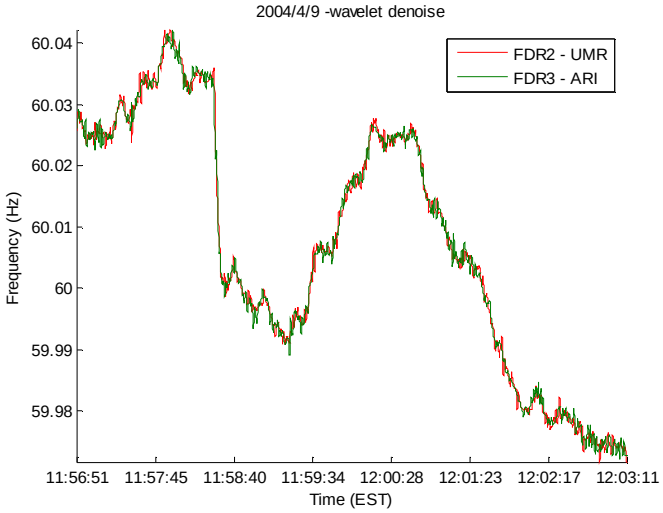

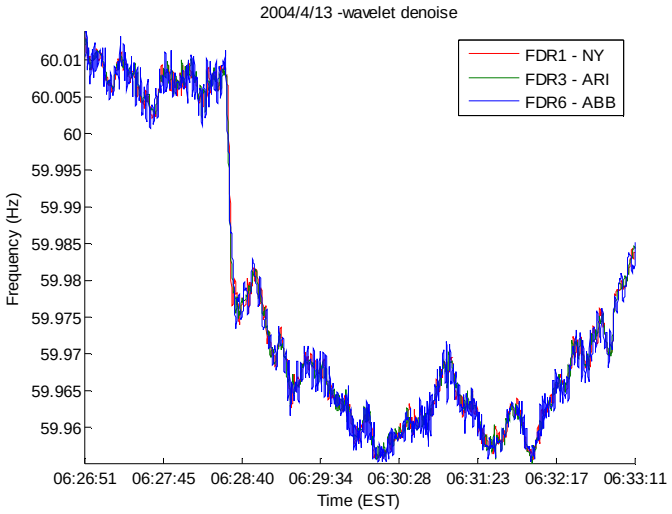
2004/4/13 -wavelet denoise
FDR1 - NY
FDR3 - ARI
FDR6 - ABB
Frequency (Hz)
60.01
60.005
60
59.995
59.99
59.985
59.98
59.975
59.97
59.965
59.96
06:26:51
06:27:45
06:28:40
06:29:34
06:30:28
06:31:23
06:32:17
06:33:11
Time (EST)

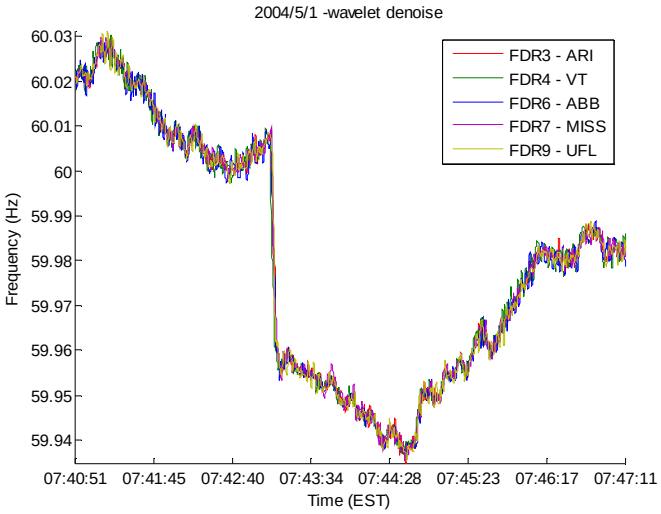
2004/5/1 -wavelet denoise
FDR3 - ARI
FDR4 - VT
FDR6 - ABB
FDR7 - MISS
FDR9 - UFL
Frequency (Hz)
60.03
60.02
60.01
60
59.99
59.98
59.97
59.96
59.95
59.94
07:40:51
07:41:45
07:42:40
07:43:34
07:44:28
07:45:23
07:46:17
07:47:11
Time (EST)

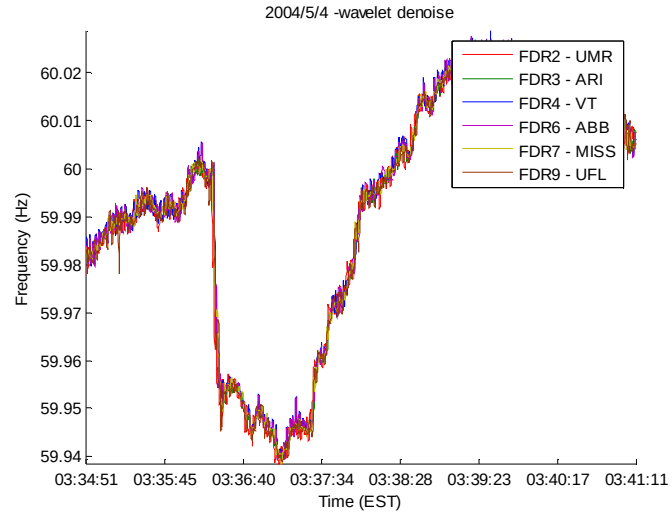
2004/5/4 -wavelet denoise
FDR2 - UMR
FDR3 - ARI
FDR4 - VT
FDR6 - ABB
FDR7 - MISS
FDR9 - UFL
Frequency (Hz)
60.02
60.01
60
59.99
59.98
59.97
59.96
59.95
59.94
03:34:51
03:35:45
03:36:40
03:37:34
03:38:28
03:39:23
03:40:17
03:41:11
Time (EST)

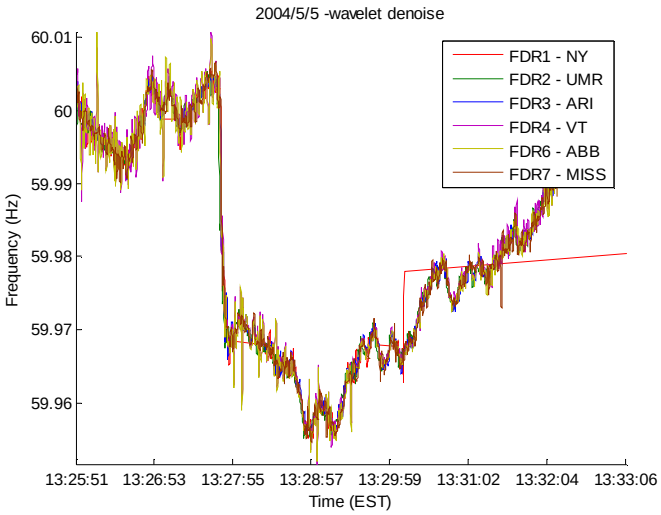
2004/5/5 -wavelet denoise
FDR1 - NY
FDR2 - UMR
FDR3 - ARI
FDR4 - VT
FDR6 - ABB
FDR7 - MISS
Frequency (Hz)
60.01
60
59.99
59.98
59.97
59.96
13:25:51
13:26:53
13:27:55
13:28:57
13:29:59
13:31:02
13:32:04
13:33:06
Time (EST)

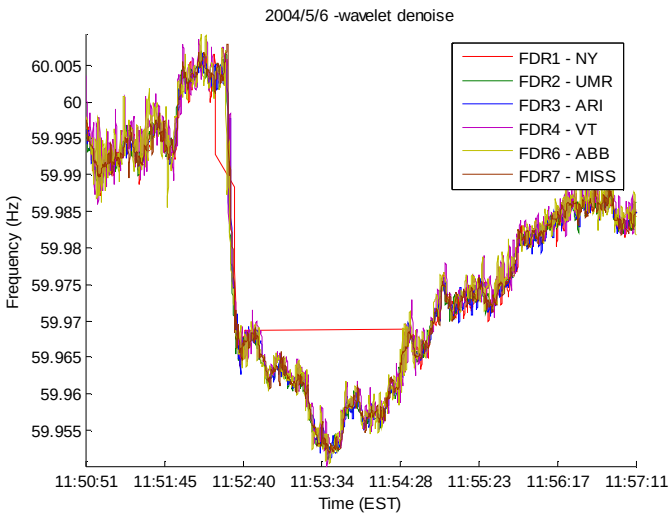
2004/5/6 -wavelet denoise
FDR1 - NY
FDR2 - UMR
FDR3 - ARI
FDR4 - VT
FDR6 - ABB
FDR7 - MISS
Frequency (Hz)
60.005
60
59.995
59.99
59.985
59.98
59.975
59.97
59.965
59.96
59.955
11:50:51
11:51:45
11:52:40
11:53:34
11:54:28
11:55:23
11:56:17
11:57:11
Time (EST)

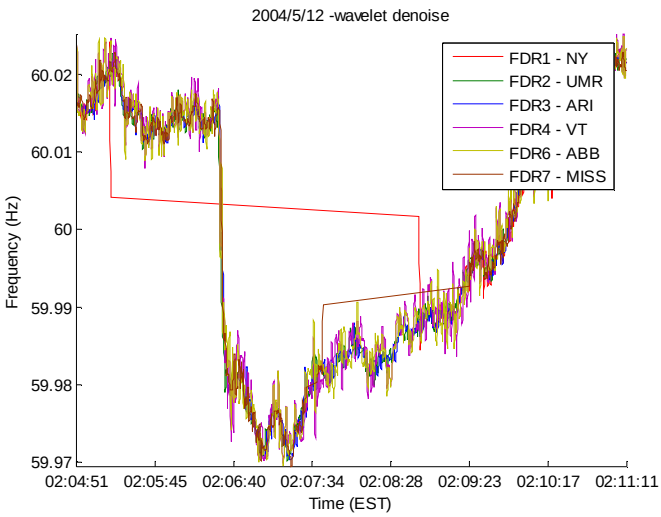
2004/5/12 -wavelet denoise
FDR1 - NY
FDR2 - UMR
FDR3 - ARI
FDR4 - VT
FDR6 - ABB
FDR7 - MISS
Frequency (Hz)
60.02
60.01
60
59.99
59.98
59.97
02:04:51
02:05:45
02:06:40
02:07:34
02:08:28
02:09:23
02:10:17
02:11:11
Time (EST)

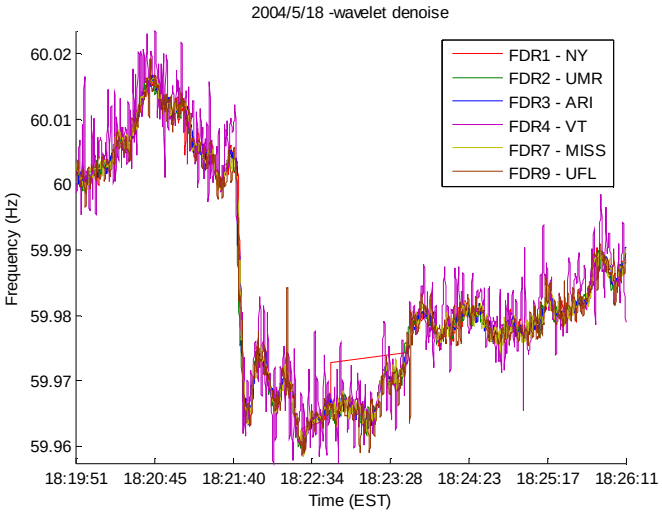
2004/5/18 -wavelet denoise
FDR1 - NY
FDR2 - UMR
FDR3 - ARI
FDR4 - VT
FDR7 - MISS
FDR9 - UFL
Frequency (Hz)
60.02
60.01
60
59.99
59.98
59.97
59.96
18:19:51
18:20:45
18:21:40
18:22:34
18:23:28
18:24:23
18:25:17
18:26:11
Time (EST)

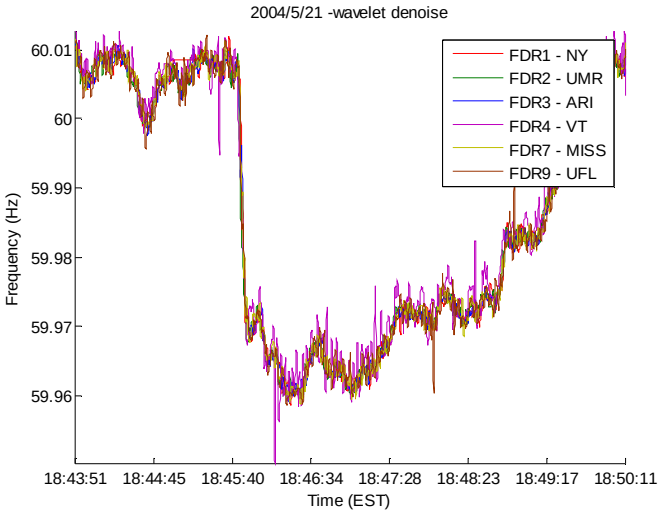
2004/5/21 -wavelet denoise
FDR1 - NY
FDR2 - UMR
FDR3 - ARI
FDR4 - VT
FDR7 - MISS
FDR9 - UFL
Frequency (Hz)
60.01
60
59.99
59.98
59.97
59.96
18:43:51
18:44:45
18:45:40
18:46:34
18:47:28
18:48:23
18:49:17
18:50:11
Time (EST)

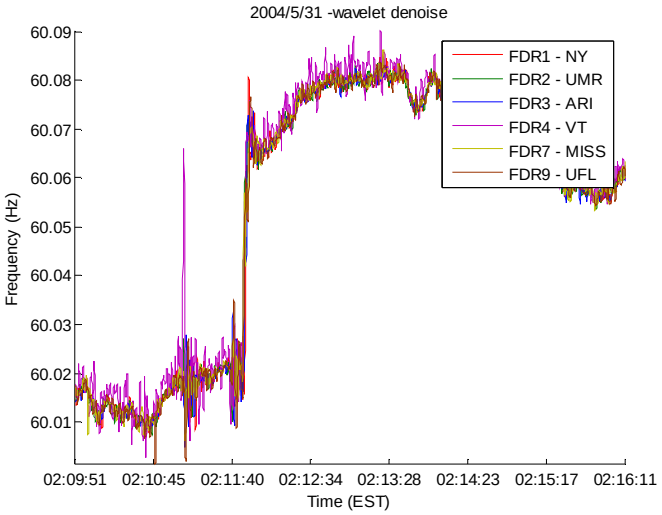
2004/5/31 -wavelet denoise
FDR1 - NY
FDR2 - UMR
FDR3 - ARI
FDR4 - VT
FDR7 - MISS
FDR9 - UFL
Frequency (Hz)
60.09
60.08
60.07
60.06
60.05
60.04
60.03
60.02
60.01
02:09:51
02:10:45
02:11:40
02:12:34
02:13:28
02:14:23
02:15:17
02:16:11
Time (EST)

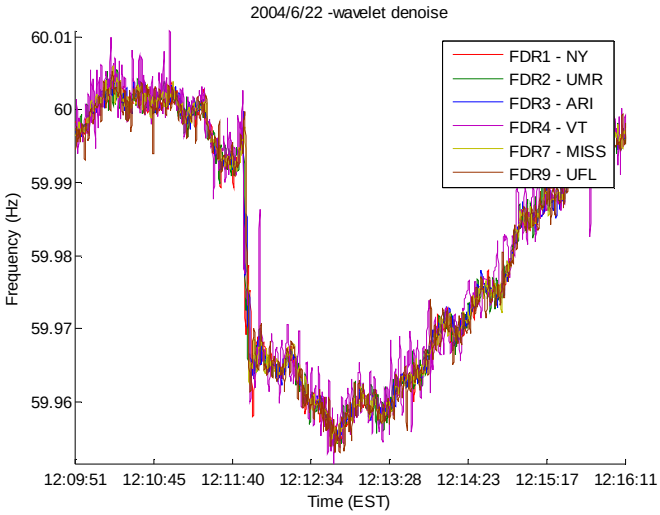
2004/6/22 -wavelet denoise
FDR1 - NY
FDR2 - UMR
FDR3 - ARI
FDR4 - VT
FDR7 - MISS
FDR9 - UFL
Frequency (Hz)
60.01
60
59.99
59.98
59.97
59.96
12:09:51
12:10:45
12:11:40
12:12:34
12:13:28
12:14:23
12:15:17
12:16:11
Time (EST)

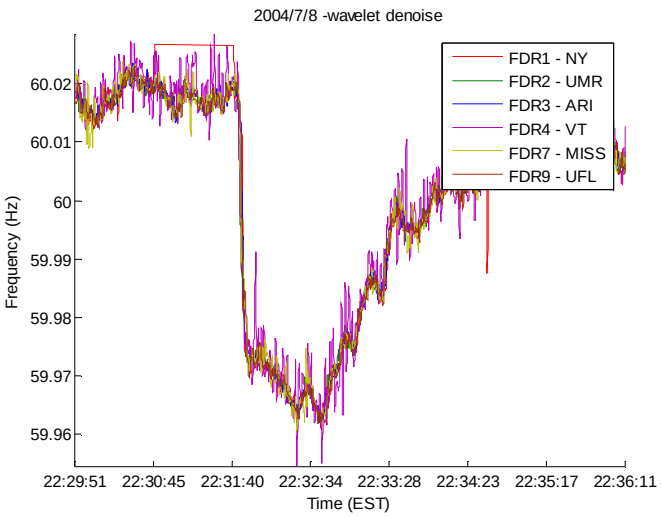
2004/7/8 -wavelet denoise
FDR1 - NY
FDR2 - UMR
FDR3 - ARI
FDR4 - VT
FDR7 - MISS
FDR9 - UFL
Frequency (Hz)
60.02
60.01
60
59.99
59.98
59.97
59.96
22:29:51
22:30:45
22:31:40
22:32:34
22:33:28
22:34:23
22:35:17
22:36:11
Time (EST)

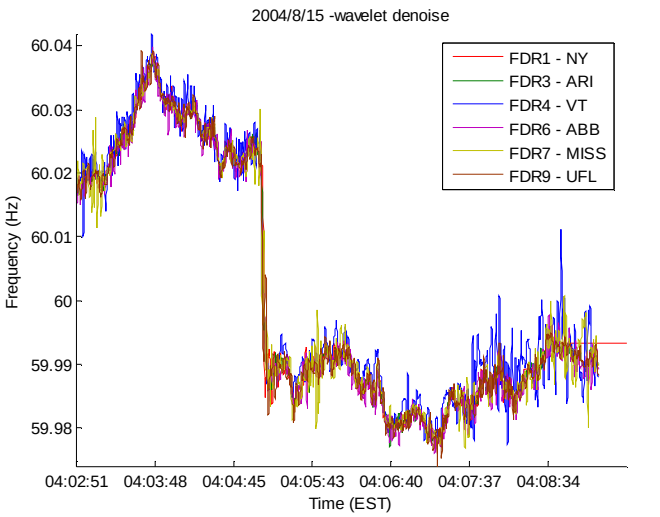
2004/8/15 -wavelet denoise
FDR1 - NY
FDR3 - ARI
FDR4 - VT
FDR6 - ABB
FDR7 - MISS
FDR9 - UFL
Frequency (Hz)
60.04
60.03
60.02
60.01
60
59.99
59.98
04:02:51
04:03:48
04:04:45
04:05:43
04:06:40
04:07:37
04:08:34
Time (EST)

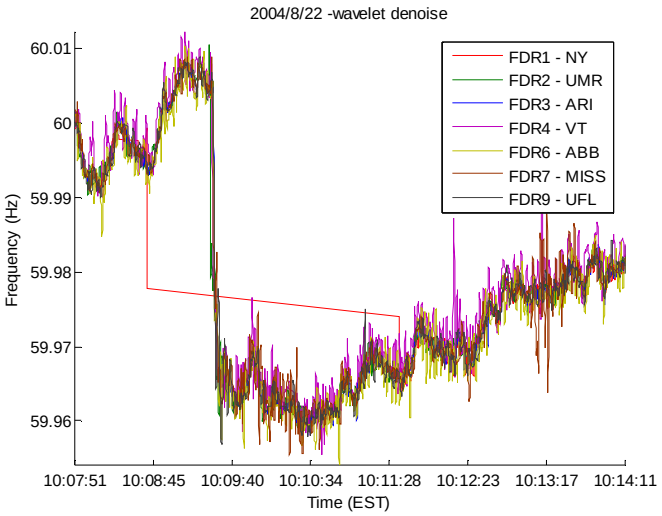
2004/8/22 -wavelet denoise
FDR1 - NY
FDR2 - UMR
FDR3 - ARI
FDR4 - VT
FDR6 - ABB
FDR7 - MISS
FDR9 - UFL
Frequency (Hz)
60.01
60
59.99
59.98
59.97
59.96
10:07:51
10:08:45
10:09:40
10:10:34
10:11:28
10:12:23
10:13:17
10:14:11
Time (EST)

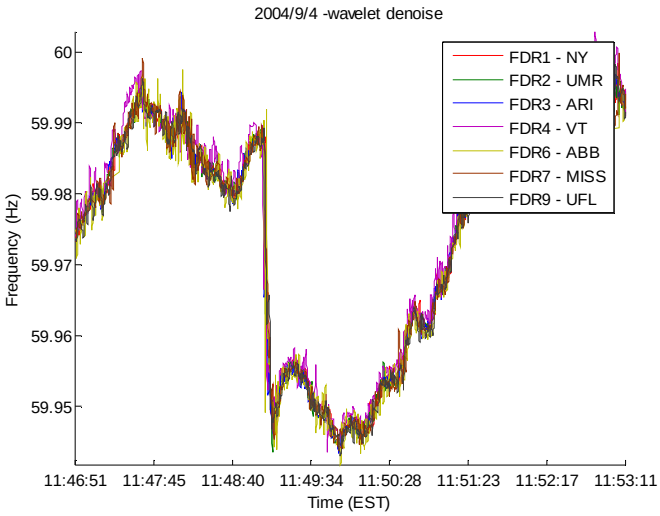
2004/9/4 -wavelet denoise
FDR1 - NY
FDR2 - UMR
FDR3 - ARI
FDR4 - VT
FDR6 - ABB
FDR7 - MISS
FDR9 - UFL
Frequency (Hz)
60
59.99
59.98
59.97
59.96
59.95
11:46:51
11:47:45
11:48:40
11:49:34
11:50:28
11:51:23
11:52:17
11:53:11
Time (EST)

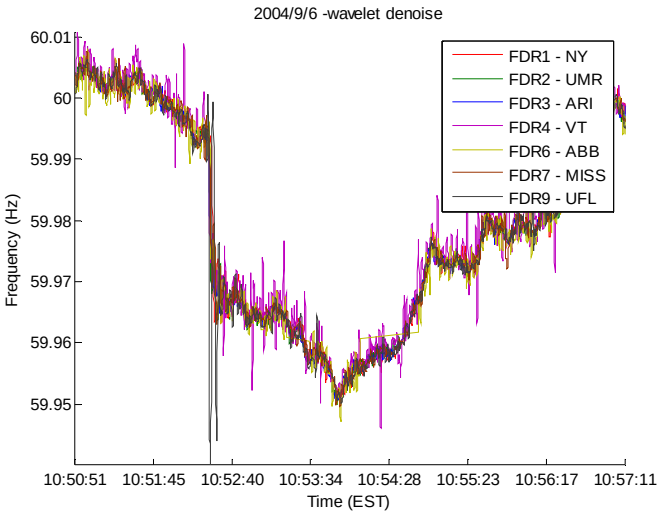
2004/9/6 -wavelet denoise
FDR1 - NY
FDR2 - UMR
FDR3 - ARI
FDR4 - VT
FDR6 - ABB
FDR7 - MISS
FDR9 - UFL
Frequency (Hz)
60.01
60
59.99
59.98
59.97
59.96
59.95
10:50:51
10:51:45
10:52:40
10:53:34
10:54:28
10:55:23
10:56:17
10:57:11
Time (EST)

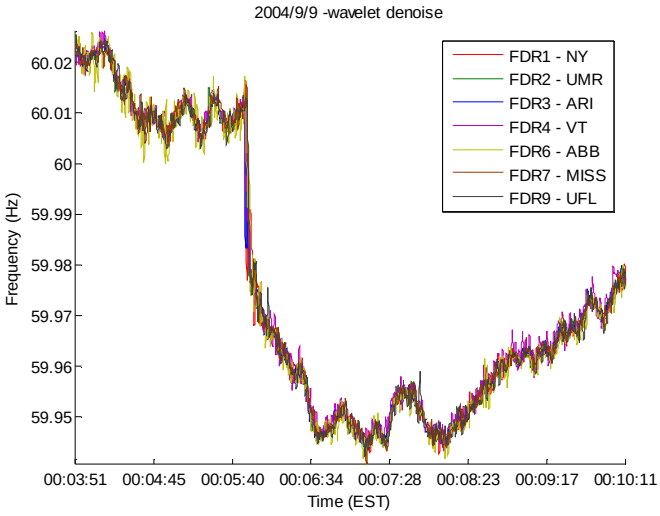
2004/9/9 -wavelet denoise
FDR1 - NY
FDR2 - UMR
FDR3 - ARI
FDR4 - VT
FDR6 - ABB
FDR7 - MISS
FDR9 - UFL
Frequency (Hz)
60.02
60.01
60
59.99
59.98
59.97
59.96
59.95
00:03:51
00:04:45
00:05:40
00:06:34
00:07:28
00:08:23
00:09:17
00:10:11
Time (EST)

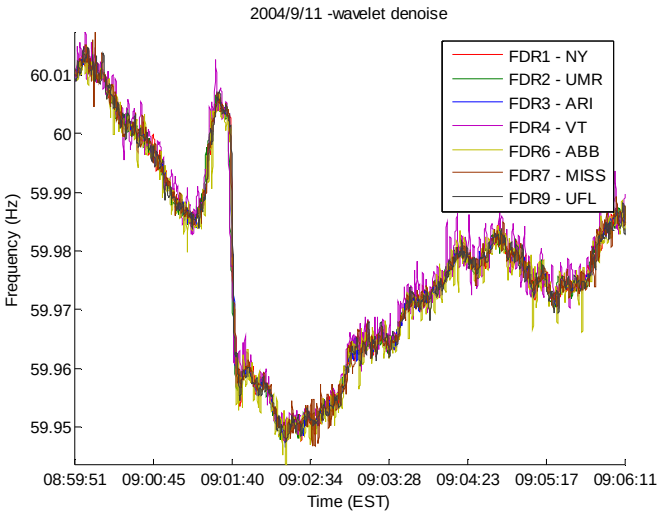
2004/9/11 -wavelet denoise
FDR1 - NY
FDR2 - UMR
FDR3 - ARI
FDR4 - VT
FDR6 - ABB
FDR7 - MISS
FDR9 - UFL
Frequency (Hz)
60.01
60
59.99
59.98
59.97
59.96
59.95
08:59:51
09:00:45
09:01:40
09:02:34
09:03:28
09:04:23
09:05:17
09:06:11
Time (EST)

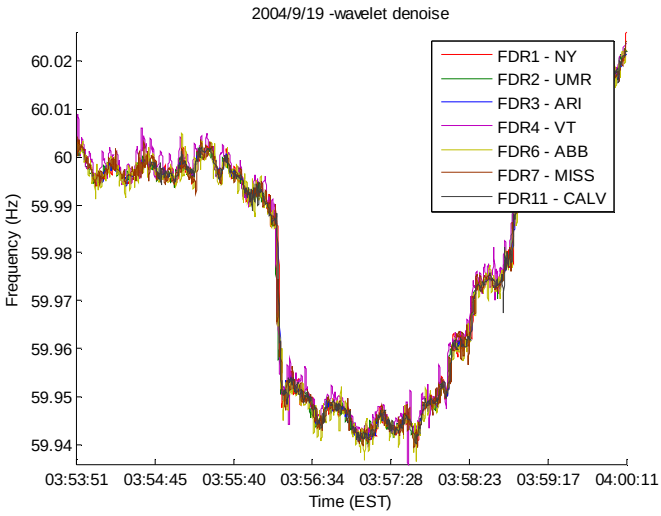
2004/9/19 -wavelet denoise
FDR1 - NY
FDR2 - UMR
FDR3 - ARI
FDR4 - VT
FDR6 - ABB
FDR7 - MISS
FDR11 - CALV
Frequency (Hz)
60.02
60.01
60
59.99
59.98
59.97
59.96
59.95
59.94
03:53:51
03:54:45
03:55:40
03:56:34
03:57:28
03:58:23
03:59:17
04:00:11
Time (EST)

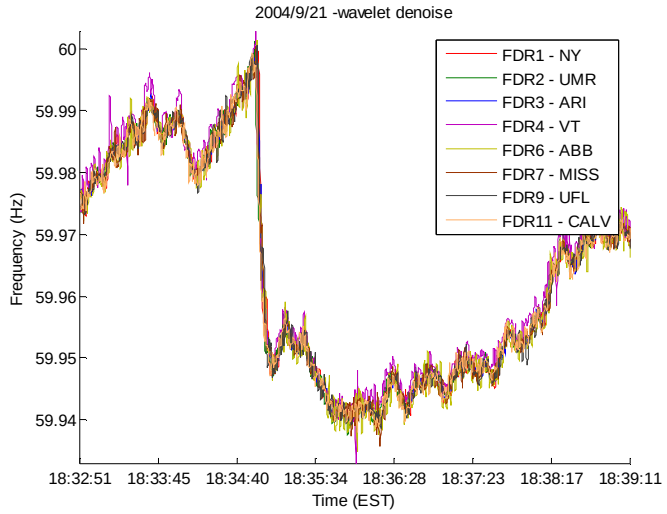
2004/9/21 -wavelet denoise
Frequency (Hz)
Time (EST)
FDR1 - NY
FDR2 - UMR
FDR3 - ARI
FDR4 - VT
FDR6 - ABB
FDR7 - MISS
FDR9 - UFL
FDR11 - CALV

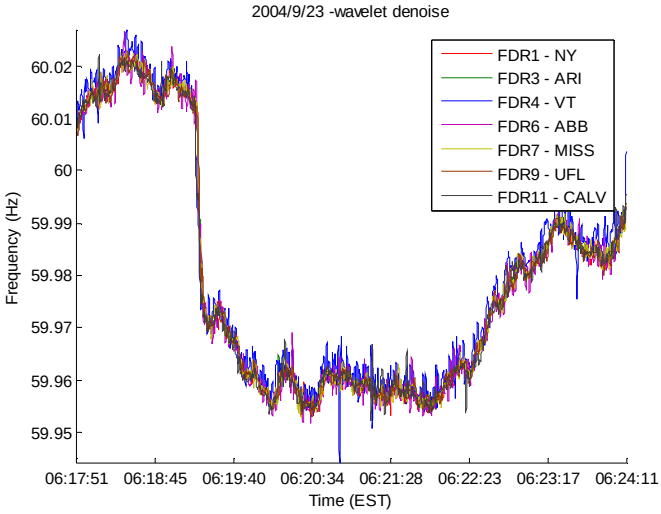
2004/9/23 -wavelet denoise
Frequency (Hz)
Time (EST)
FDR1 - NY
FDR3 - ARI
FDR4 - VT
FDR6 - ABB
FDR7 - MISS
FDR9 - UFL
FDR11 - CALV

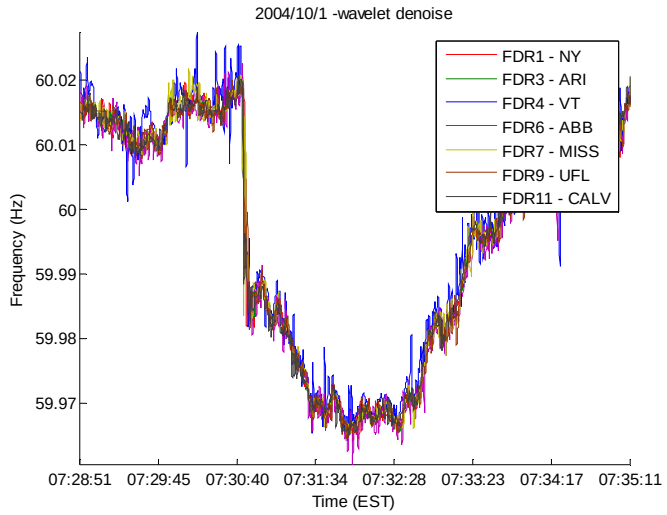
2004/10/1 -wavelet denoise
Frequency (Hz)
Time (EST)
FDR1 - NY
FDR3 - ARI
FDR4 - VT
FDR6 - ABB
FDR7 - MISS
FDR9 - UFL
FDR11 - CALV

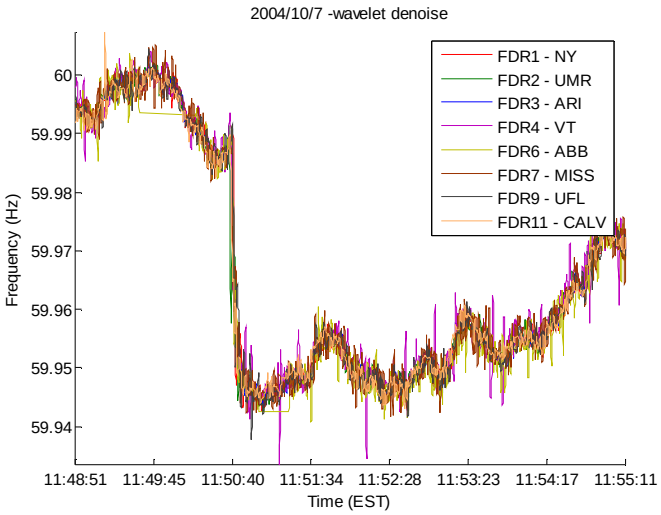
2004/10/7 -wavelet denoise
Frequency (Hz)
Time (EST)
FDR1 - NY
FDR2 - UMR
FDR3 - ARI
FDR4 - VT
FDR6 - ABB
FDR7 - MISS
FDR9 - UFL
FDR11 - CALV

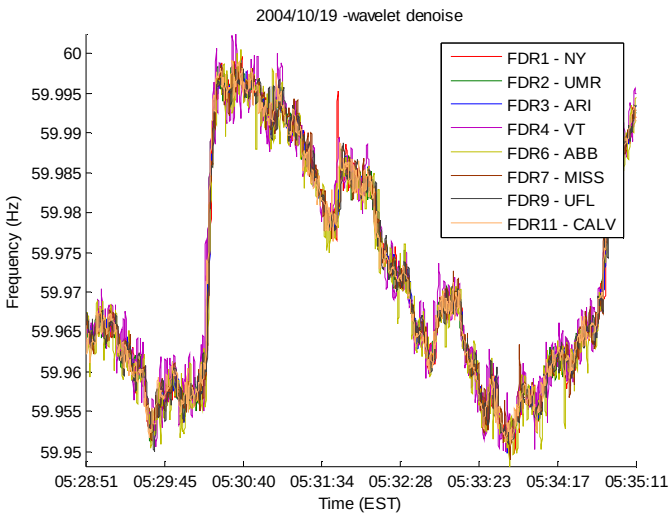
2004/10/19 -wavelet denoise
Frequency (Hz)
Time (EST)
FDR1 - NY
FDR2 - UMR
FDR3 - ARI
FDR4 - VT
FDR6 - ABB
FDR7 - MISS
FDR9 - UFL
FDR11 - CALV

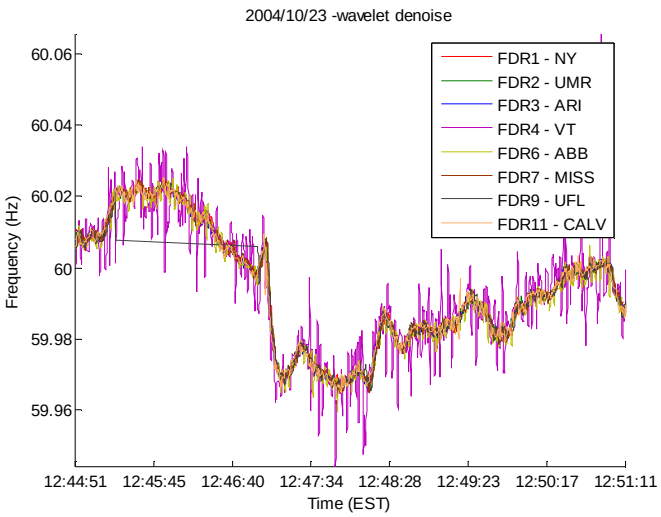
2004/10/23 -wavelet denoise
Frequency (Hz)
Time (EST)
FDR1 - NY
FDR2 - UMR
FDR3 - ARI
FDR4 - VT
FDR6 - ABB
FDR7 - MISS
FDR9 - UFL
FDR11 - CALV

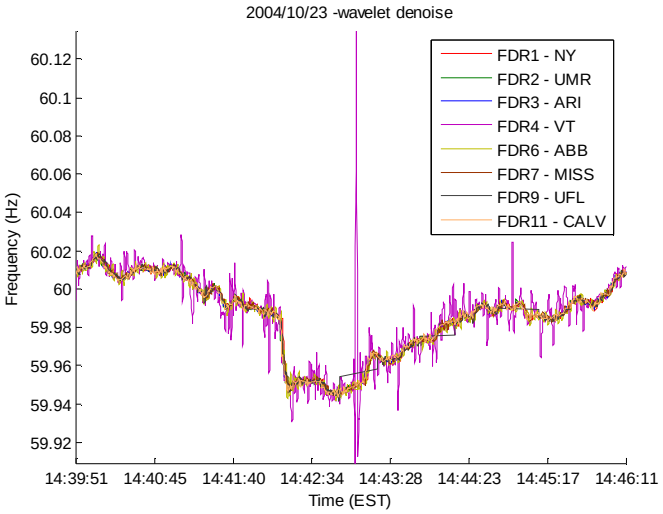
2004/10/23 -wavelet denoise
FDR1 - NY
FDR2 - UMR
FDR3 - ARI
FDR4 - VT
FDR6 - ABB
FDR7 - MISS
FDR9 - UFL
FDR11 - CALV
Frequency (Hz)
60.12
60.1
60.08
60.06
60.04
60.02
60
59.98
59.96
59.94
59.92
14:39:51
14:40:45
14:41:40
14:42:34
14:43:28
14:44:23
14:45:17
14:46:11
Time (EST)

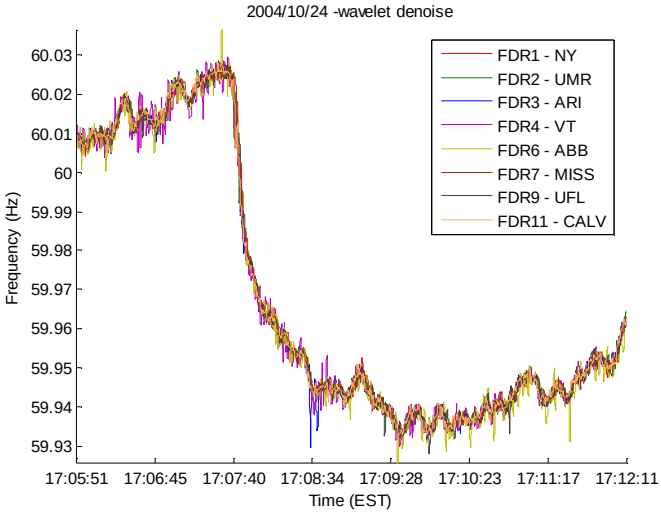
2004/10/24 -wavelet denoise
FDR1 - NY
FDR2 - UMR
FDR3 - ARI
FDR4 - VT
FDR6 - ABB
FDR7 - MISS
FDR9 - UFL
FDR11 - CALV
Frequency (Hz)
60.03
60.02
60.01
60
59.99
59.98
59.97
59.96
59.95
59.94
59.93
17:05:51
17:06:45
17:07:40
17:08:34
17:09:28
17:10:23
17:11:17
17:12:11
Time (EST)

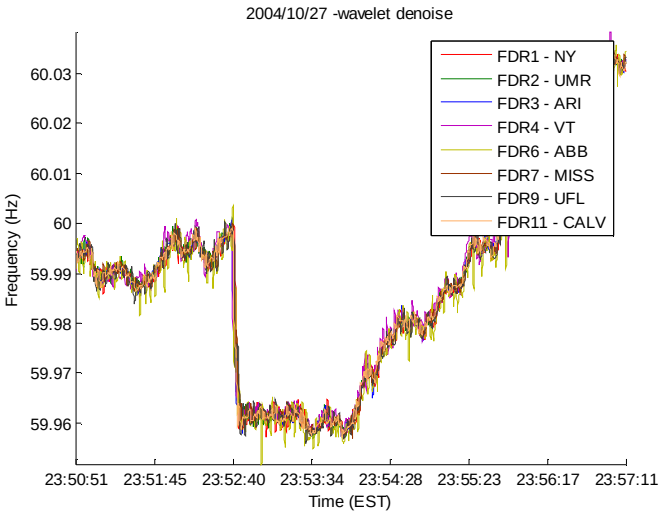
2004/10/27 -wavelet denoise
FDR1 - NY
FDR2 - UMR
FDR3 - ARI
FDR4 - VT
FDR6 - ABB
FDR7 - MISS
FDR9 - UFL
FDR11 - CALV
Frequency (Hz)
60.03
60.02
60.01
60
59.99
59.98
59.97
59.96
23:50:51
23:51:45
23:52:40
23:53:34
23:54:28
23:55:23
23:56:17
23:57:11
Time (EST)

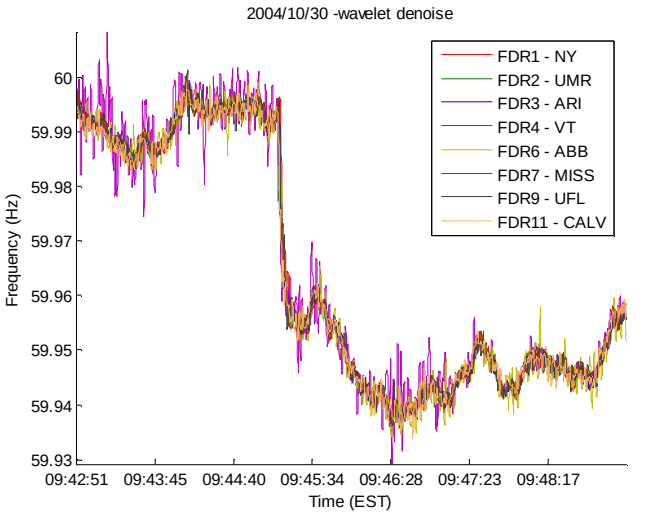
2004/10/30 -wavelet denoise
FDR1 - NY
FDR2 - UMR
FDR3 - ARI
FDR4 - VT
FDR6 - ABB
FDR7 - MISS
FDR9 - UFL
FDR11 - CALV
Frequency (Hz)
60
59.99
59.98
59.97
59.96
59.95
59.94
59.93
09:42:51
09:43:45
09:44:40
09:45:34
09:46:28
09:47:23
09:48:17
Time (EST)

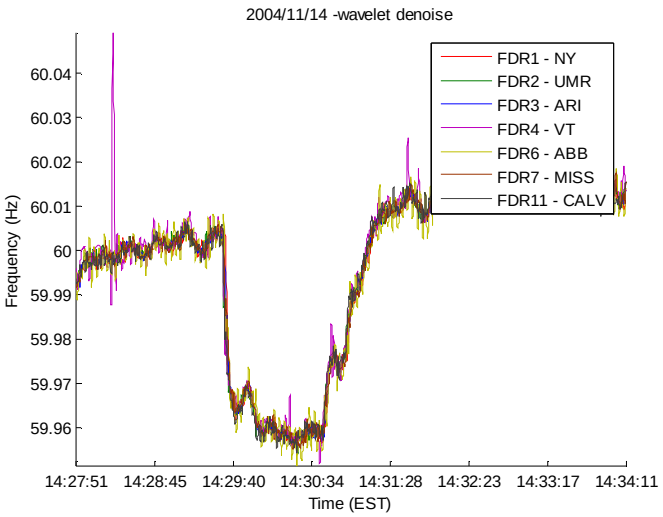
2004/11/14 -wavelet denoise
FDR1 - NY
FDR2 - UMR
FDR3 - ARI
FDR4 - VT
FDR6 - ABB
FDR7 - MISS
FDR11 - CALV
Frequency (Hz)
60.04
60.03
60.02
60.01
60
59.99
59.98
59.97
59.96
14:27:51
14:28:45
14:29:40
14:30:34
14:31:28
14:32:23
14:33:17
14:34:11
Time (EST)

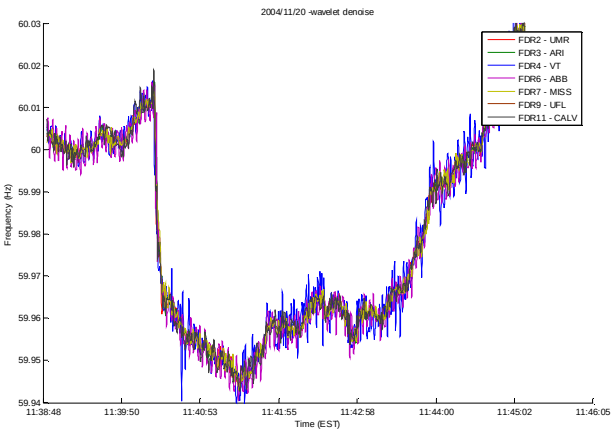
2004/11/20 -wavelet denoise
FDR2 - UMR
FDR3 - ARI
FDR4 - VT
FDR6 - ABB
FDR7 - MISS
FDR9 - UFL
FDR11 - CALV
Frequency (Hz)
60.03
60.02
60.01
60
59.99
59.98
59.97
59.96
59.95
59.94
11:38:48
11:39:50
11:40:53
11:41:55
11:42:58
11:44:00
11:45:02
11:46:05
Time (EST)

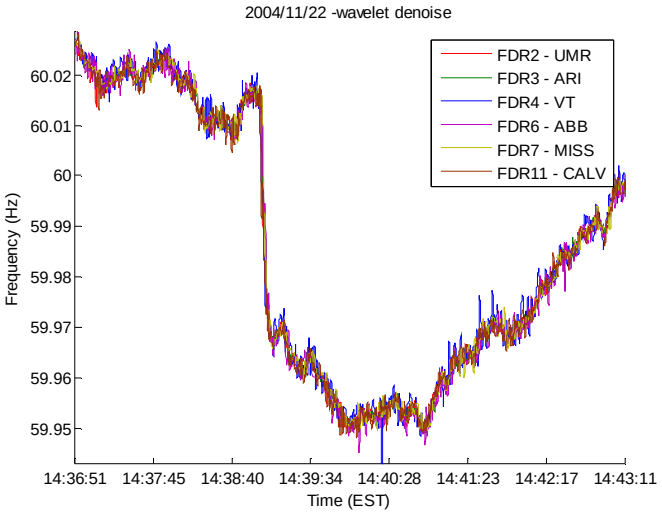
2004/11/22 -wavelet denoise
FDR2 - UMR
FDR3 - ARI
FDR4 - VT
FDR6 - ABB
FDR7 - MISS
FDR11 - CALV
Frequency (Hz)
60.02
60.01
60
59.99
59.98
59.97
59.96
59.95
14:36:51
14:37:45
14:38:40
14:39:34
14:40:28
14:41:23
14:42:17
14:43:11
Time (EST)

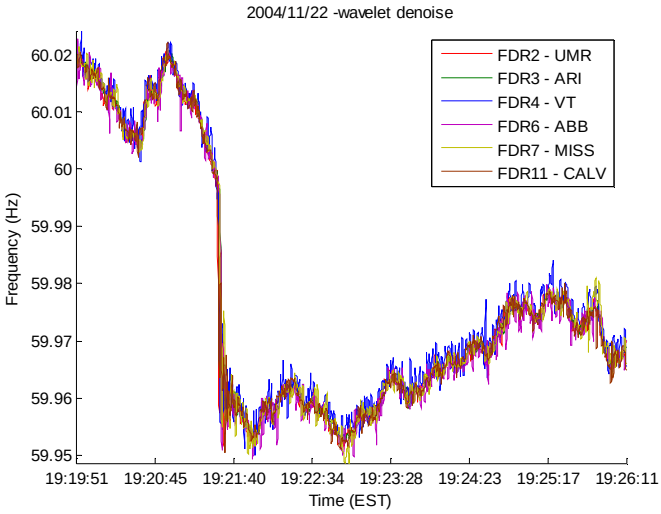
2004/11/22 -wavelet denoise
FDR2 - UMR
FDR3 - ARI
FDR4 - VT
FDR6 - ABB
FDR7 - MISS
FDR11 - CALV
Frequency (Hz)
60.02
60.01
60
59.99
59.98
59.97
59.96
59.95
19:19:51
19:20:45
19:21:40
19:22:34
19:23:28
19:24:23
19:25:17
19:26:11
Time (EST)

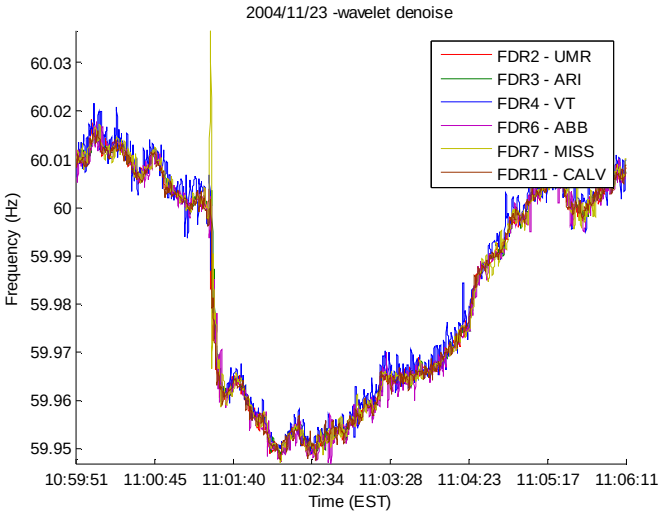
2004/11/23 -wavelet denoise
FDR2 - UMR
FDR3 - ARI
FDR4 - VT
FDR6 - ABB
FDR7 - MISS
FDR11 - CALV
Frequency (Hz)
60.03
60.02
60.01
60
59.99
59.98
59.97
59.96
59.95
10:59:51
11:00:45
11:01:40
11:02:34
11:03:28
11:04:23
11:05:17
11:06:11
Time (EST)

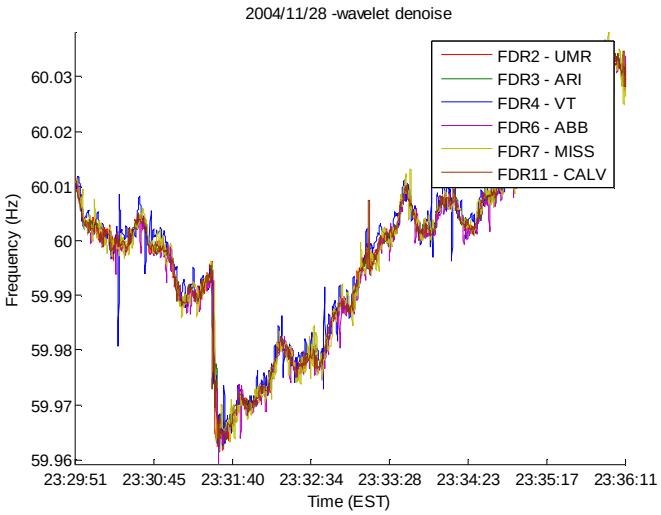
2004/11/28 -wavelet denoise
FDR2 - UMR
FDR3 - ARI
FDR4 - VT
FDR6 - ABB
FDR7 - MISS
FDR11 - CALV
Frequency (Hz)
60.03
60.02
60.01
60
59.99
59.98
59.97
59.96
23:29:51
23:30:45
23:31:40
23:32:34
23:33:28
23:34:23
23:35:17
23:36:11
Time (EST)

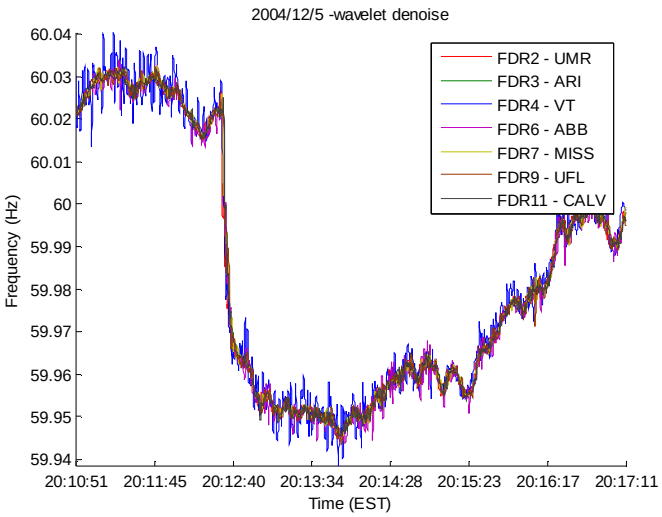
2004/12/5 -wavelet denoise
FDR2 - UMR
FDR3 - ARI
FDR4 - VT
FDR6 - ABB
FDR7 - MISS
FDR9 - UFL
FDR11 - CALV
Frequency (Hz)
60.04
60.03
60.02
60.01
60
59.99
59.98
59.97
59.96
59.95
59.94
20:10:51
20:11:45
20:12:40
20:13:34
20:14:28
20:15:23
20:16:17
20:17:11
Time (EST)

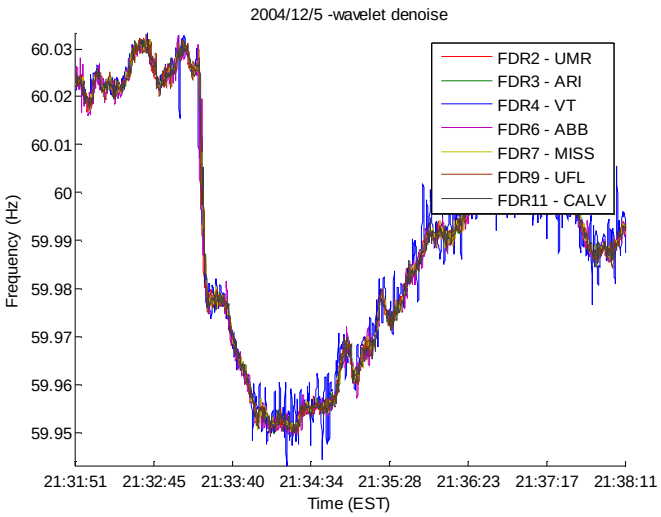
2004/12/5 -wavelet denoise
FDR2 - UMR
FDR3 - ARI
FDR4 - VT
FDR6 - ABB
FDR7 - MISS
FDR9 - UFL
FDR11 - CALV
Frequency (Hz)
60.03
60.02
60.01
60
59.99
59.98
59.97
59.96
59.95
21:31:51
21:32:45
21:33:40
21:34:34
21:35:28
21:36:23
21:37:17
21:38:11
Time (EST)

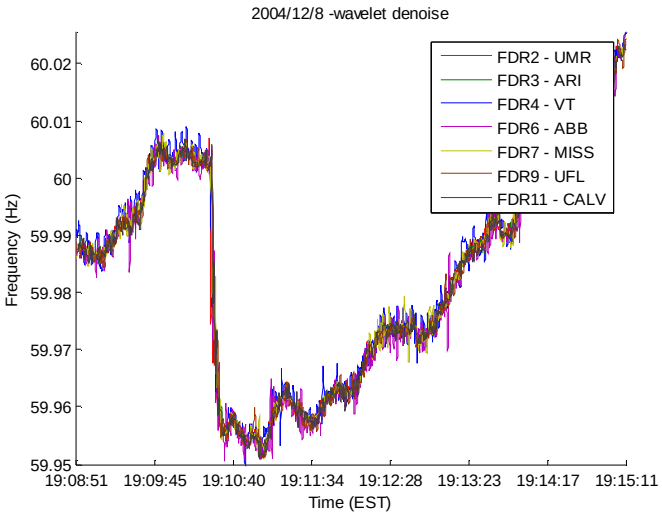
2004/12/8 -wavelet denoise
FDR2 - UMR
FDR3 - ARI
FDR4 - VT
FDR6 - ABB
FDR7 - MISS
FDR9 - UFL
FDR11 - CALV
Frequency (Hz)
60.02
60.01
60
59.99
59.98
59.97
59.96
59.95
19:08:51
19:09:45
19:10:40
19:11:34
19:12:28
19:13:23
19:14:17
19:15:11
Time (EST)

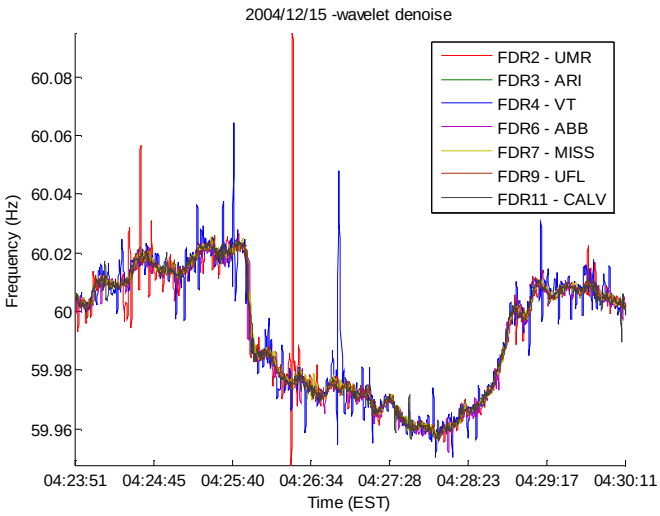
2004/12/15 -wavelet denoise
FDR2 - UMR
FDR3 - ARI
FDR4 - VT
FDR6 - ABB
FDR7 - MISS
FDR9 - UFL
FDR11 - CALV
Frequency (Hz)
60.08
60.06
60.04
60.02
60
59.98
59.96
04:23:51
04:24:45
04:25:40
04:26:34
04:27:28
04:28:23
04:29:17
04:30:11
Time (EST)

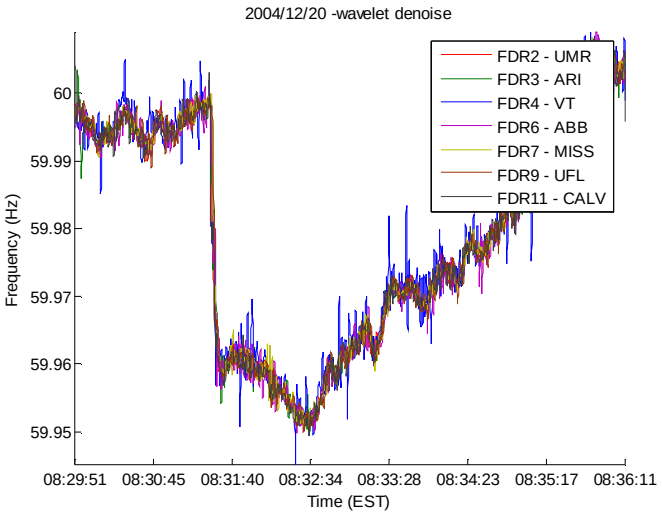
2004/12/20 -wavelet denoise
FDR2 - UMR
FDR3 - ARI
FDR4 - VT
FDR6 - ABB
FDR7 - MISS
FDR9 - UFL
FDR11 - CALV
Frequency (Hz)
60
59.99
59.98
59.97
59.96
59.95
08:29:51
08:30:45
08:31:40
08:32:34
08:33:28
08:34:23
08:35:17
08:36:11
Time (EST)

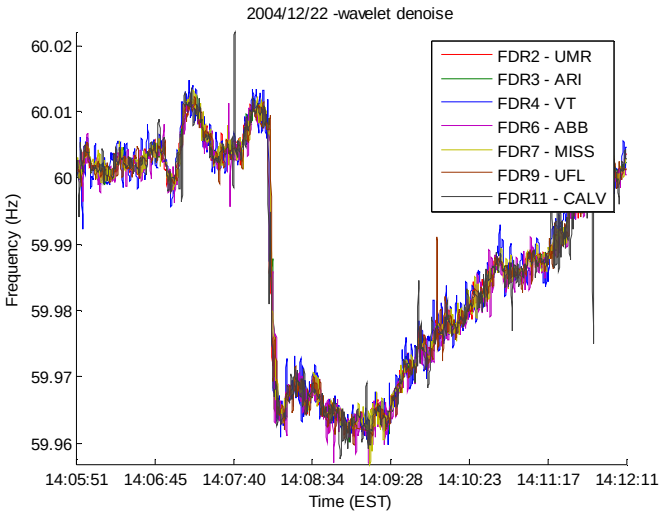
2004/12/22 -wavelet denoise
FDR2 - UMR
FDR3 - ARI
FDR4 - VT
FDR6 - ABB
FDR7 - MISS
FDR9 - UFL
FDR11 - CALV
Frequency (Hz)
60.02
60.01
60
59.99
59.98
59.97
59.96
14:05:51
14:06:45
14:07:40
14:08:34
14:09:28
14:10:23
14:11:17
14:12:11
Time (EST)

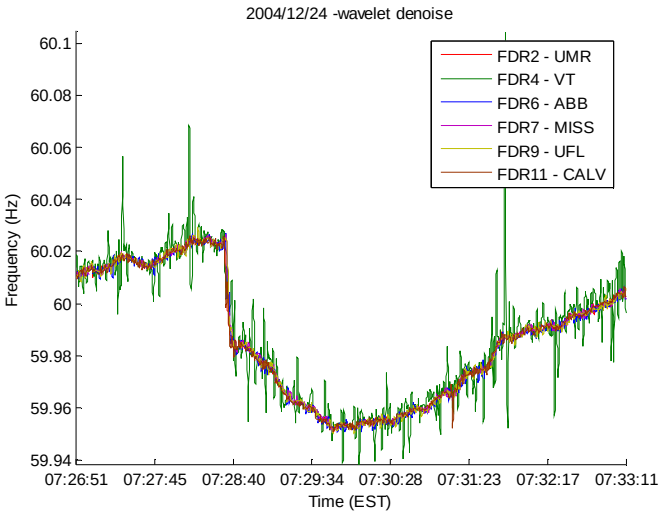
2004/12/24 -wavelet denoise
FDR2 - UMR
FDR4 - VT
FDR6 - ABB
FDR7 - MISS
FDR9 - UFL
FDR11 - CALV
Frequency (Hz)
60.1
60.08
60.06
60.04
60.02
60
59.98
59.96
59.94
07:26:51
07:27:45
07:28:40
07:29:34
07:30:28
07:31:23
07:32:17
07:33:11
Time (EST)

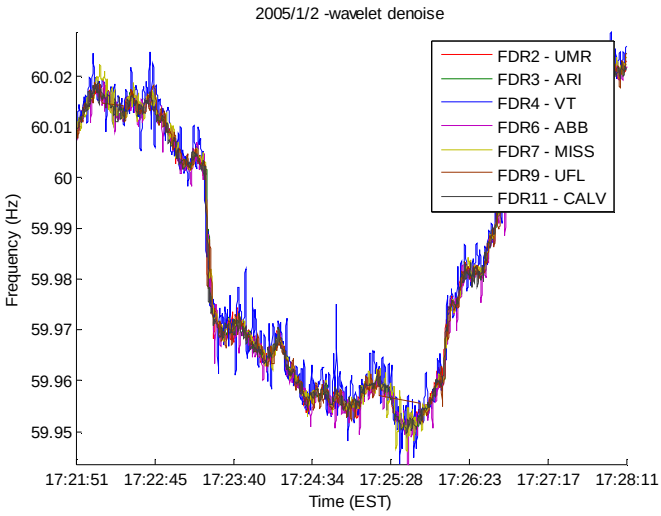
2005/1/2 -wavelet denoise
FDR2 - UMR
FDR3 - ARI
FDR4 - VT
FDR6 - ABB
FDR7 - MISS
FDR9 - UFL
FDR11 - CALV
Frequency (Hz)
60.02
60.01
60
59.99
59.98
59.97
59.96
59.95
17:21:51
17:22:45
17:23:40
17:24:34
17:25:28
17:26:23
17:27:17
17:28:11
Time (EST)

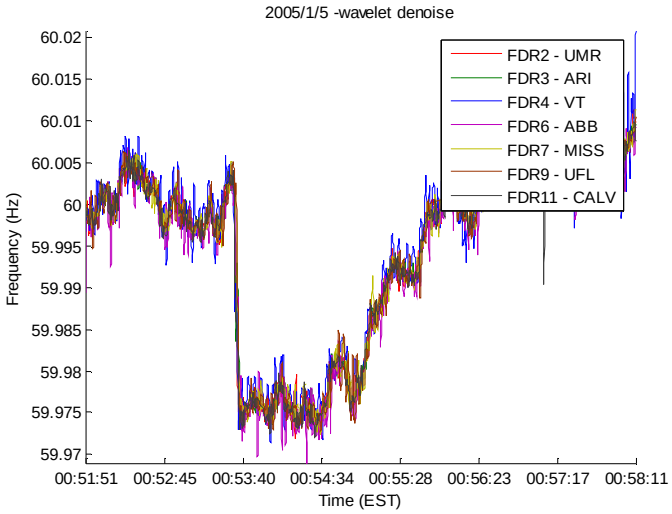
2005/1/5 -wavelet denoise
FDR2 - UMR
FDR3 - ARI
FDR4 - VT
FDR6 - ABB
FDR7 - MISS
FDR9 - UFL
FDR11 - CALV
Frequency (Hz)
60.02
60.015
60.01
60.005
60
59.995
59.99
59.985
59.98
59.975
59.97
00:51:51
00:52:45
00:53:40
00:54:34
00:55:28
00:56:23
00:57:17
00:58:11
Time (EST)

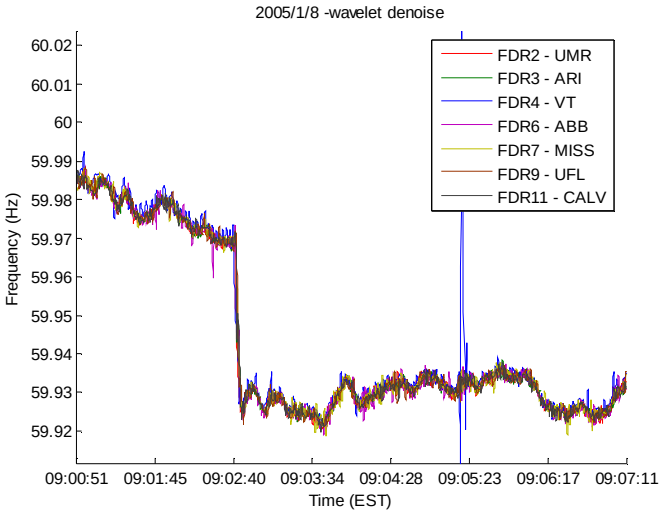
2005/1/8 -wavelet denoise
FDR2 - UMR
FDR3 - ARI
FDR4 - VT
FDR6 - ABB
FDR7 - MISS
FDR9 - UFL
FDR11 - CALV
Frequency (Hz)
60.02
60.01
60
59.99
59.98
59.97
59.96
59.95
59.94
59.93
59.92
09:00:51
09:01:45
09:02:40
09:03:34
09:04:28
09:05:23
09:06:17
09:07:11
Time (EST)

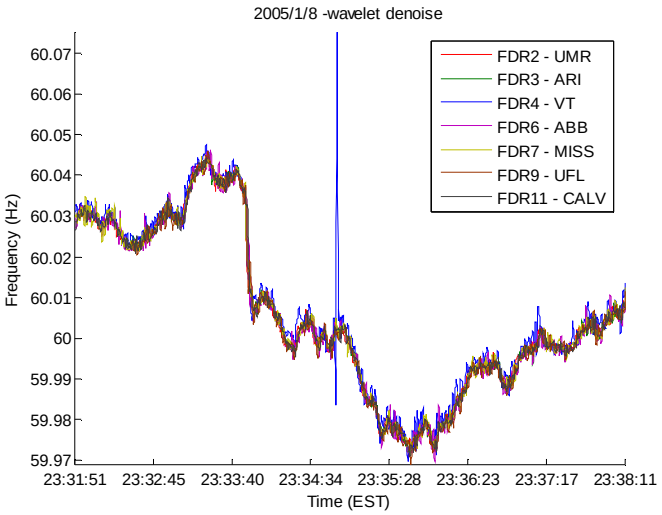
2005/1/8 -wavelet denoise
FDR2 - UMR
FDR3 - ARI
FDR4 - VT
FDR6 - ABB
FDR7 - MISS
FDR9 - UFL
FDR11 - CALV
Frequency (Hz)
60.07
60.06
60.05
60.04
60.03
60.02
60.01
60
59.99
59.98
59.97
23:31:51
23:32:45
23:33:40
23:34:34
23:35:28
23:36:23
23:37:17
23:38:11
Time (EST)

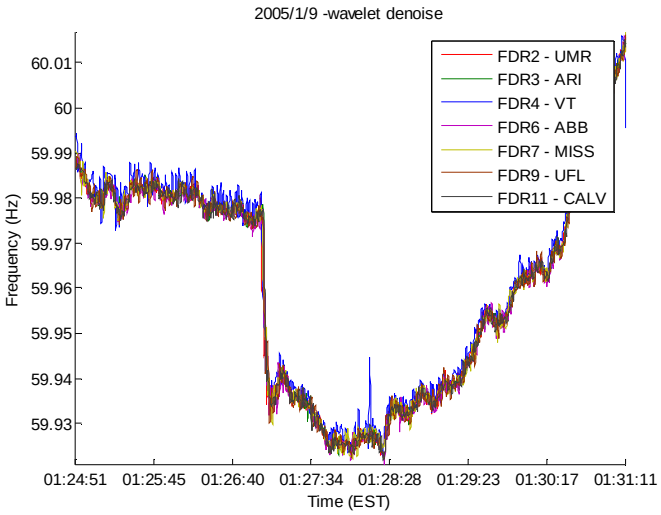
2005/1/9 -wavelet denoise
FDR2 - UMR
FDR3 - ARI
FDR4 - VT
FDR6 - ABB
FDR7 - MISS
FDR9 - UFL
FDR11 - CALV
Frequency (Hz)
60.01
60
59.99
59.98
59.97
59.96
59.95
59.94
59.93
01:24:51
01:25:45
01:26:40
01:27:34
01:28:28
01:29:23
01:30:17
01:31:11
Time (EST)

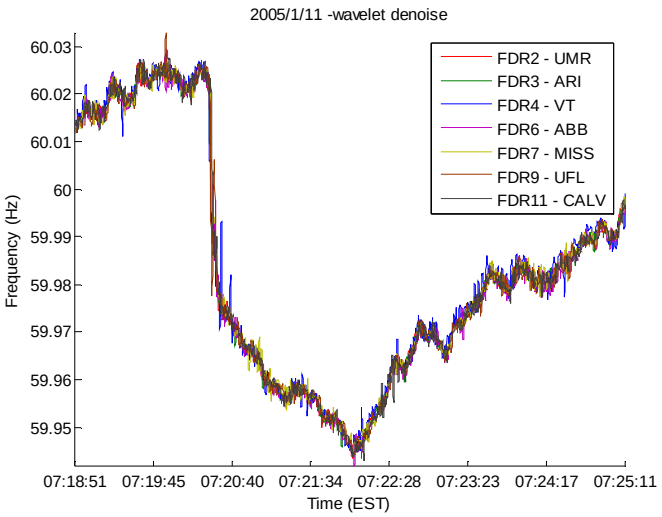
2005/1/11 -wavelet denoise
FDR2 - UMR
FDR3 - ARI
FDR4 - VT
FDR6 - ABB
FDR7 - MISS
FDR9 - UFL
FDR11 - CALV
Frequency (Hz)
60.03
60.02
60.01
60
59.99
59.98
59.97
59.96
59.95
07:18:51
07:19:45
07:20:40
07:21:34
07:22:28
07:23:23
07:24:17
07:25:11
Time (EST)

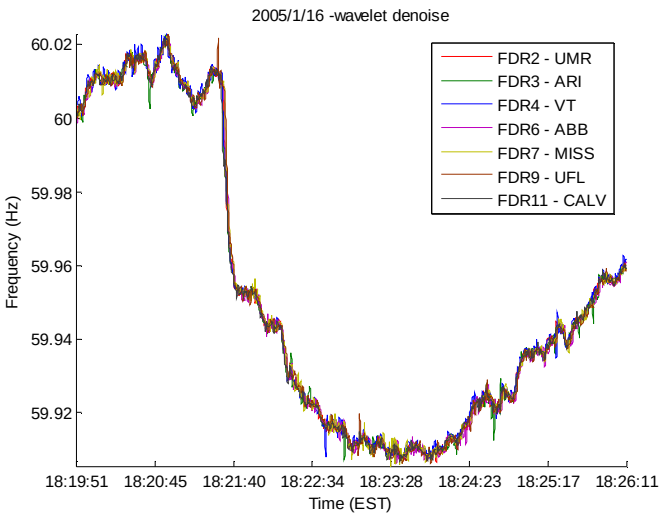
2005/1/16 -wavelet denoise
FDR2 - UMR
FDR3 - ARI
FDR4 - VT
FDR6 - ABB
FDR7 - MISS
FDR9 - UFL
FDR11 - CALV
Frequency (Hz)
60.02
60
59.98
59.96
59.94
59.92
18:19:51
18:20:45
18:21:40
18:22:34
18:23:28
18:24:23
18:25:17
18:26:11
Time (EST)

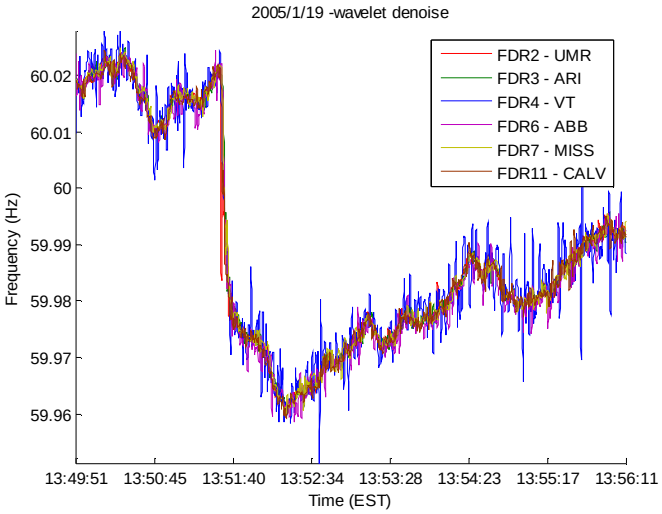
2005/1/19 -wavelet denoise
FDR2 - UMR
FDR3 - ARI
FDR4 - VT
FDR6 - ABB
FDR7 - MISS
FDR11 - CALV
Frequency (Hz)
60.02
60.01
60
59.99
59.98
59.97
59.96
13:49:51
13:50:45
13:51:40
13:52:34
13:53:28
13:54:23
13:55:17
13:56:11
Time (EST)

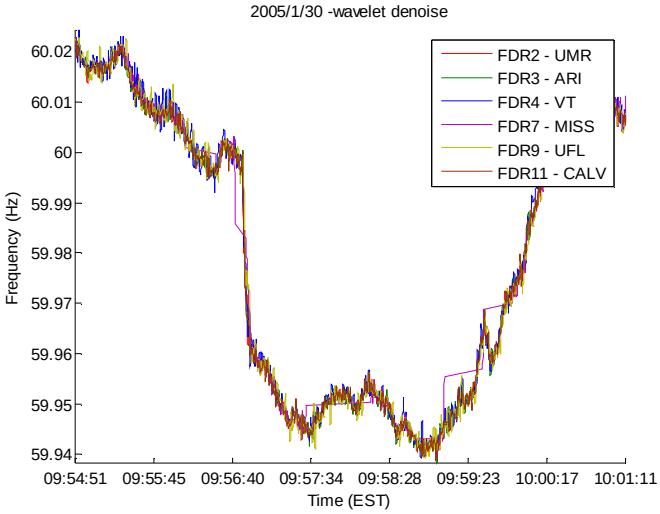
2005/1/30 -wavelet denoise
FDR2 - UMR
FDR3 - ARI
FDR4 - VT
FDR7 - MISS
FDR9 - UFL
FDR11 - CALV
Frequency (Hz)
60.02
60.01
60
59.99
59.98
59.97
59.96
59.95
59.94
09:54:51
09:55:45
09:56:40
09:57:34
09:58:28
09:59:23
10:00:17
10:01:11
Time (EST)

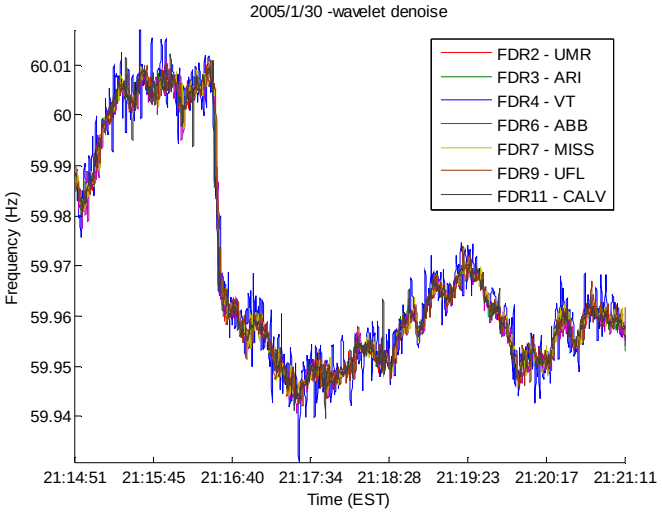
2005/1/30 -wavelet denoise
FDR2 - UMR
FDR3 - ARI
FDR4 - VT
FDR6 - ABB
FDR7 - MISS
FDR9 - UFL
FDR11 - CALV
Frequency (Hz)
60.01
60
59.99
59.98
59.97
59.96
59.95
59.94
21:14:51
21:15:45
21:16:40
21:17:34
21:18:28
21:19:23
21:20:17
21:21:11
Time (EST)

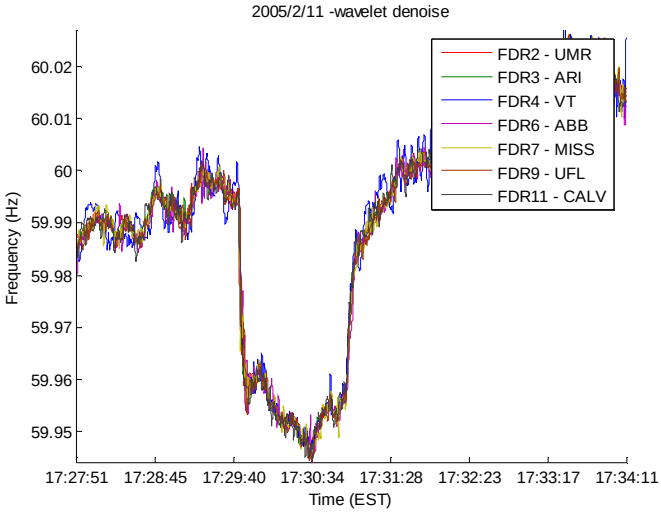
2005/2/11 -wavelet denoise
FDR2 - UMR
FDR3 - ARI
FDR4 - VT
FDR6 - ABB
FDR7 - MISS
FDR9 - UFL
FDR11 - CALV
Frequency (Hz)
60.02
60.01
60
59.99
59.98
59.97
59.96
59.95
17:27:51
17:28:45
17:29:40
17:30:34
17:31:28
17:32:23
17:33:17
17:34:11
Time (EST)

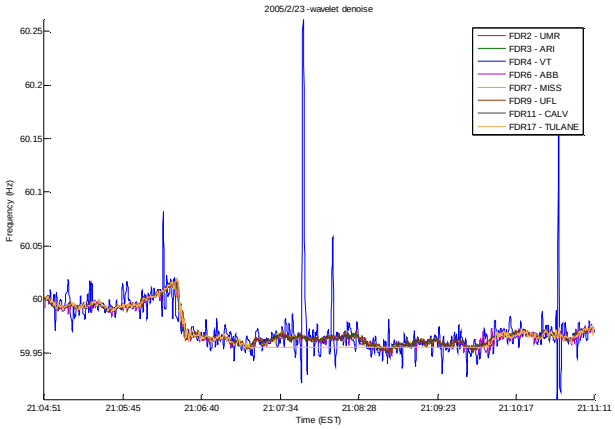
2005/2/23 -wavelet denoise
FDR2 - UMR
FDR3 - ARI
FDR4 - VT
FDR6 - ABB
FDR7 - MISS
FDR9 - UFL
FDR11 - CALV
FDR17 - TULANE
Frequency (Hz)
60.25
60.2
60.15
60.1
60.05
60
59.95
21:04:51
21:05:45
21:06:40
21:07:34
21:08:28
21:09:23
21:10:17
21:11:11
Time (EST)

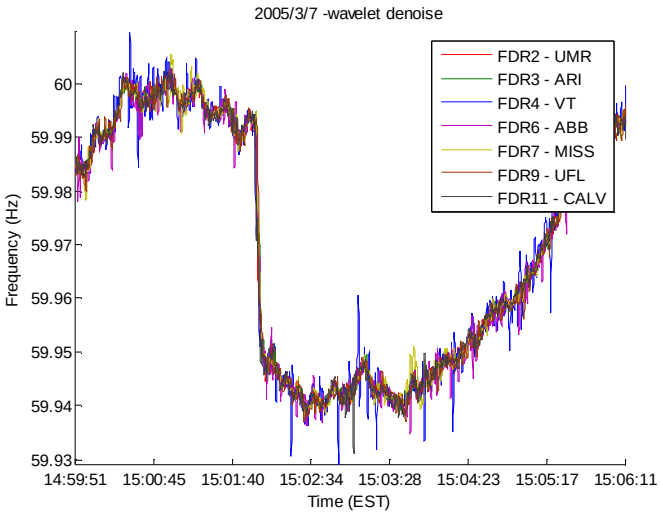
2005/3/7 -wavelet denoise
FDR2 - UMR
FDR3 - ARI
FDR4 - VT
FDR6 - ABB
FDR7 - MISS
FDR9 - UFL
FDR11 - CALV
Frequency (Hz)
60
59.99
59.98
59.97
59.96
59.95
59.94
59.93
14:59:51
15:00:45
15:01:40
15:02:34
15:03:28
15:04:23
15:05:17
15:06:11
Time (EST)

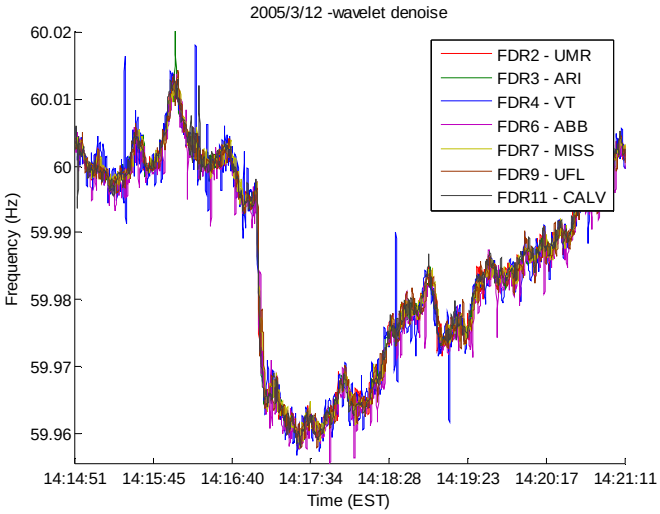
2005/3/12 -wavelet denoise
Frequency (Hz)
Time (EST)
FDR2 - UMR
FDR3 - ARI
FDR4 - VT
FDR6 - ABB
FDR7 - MISS
FDR9 - UFL
FDR11 - CALV

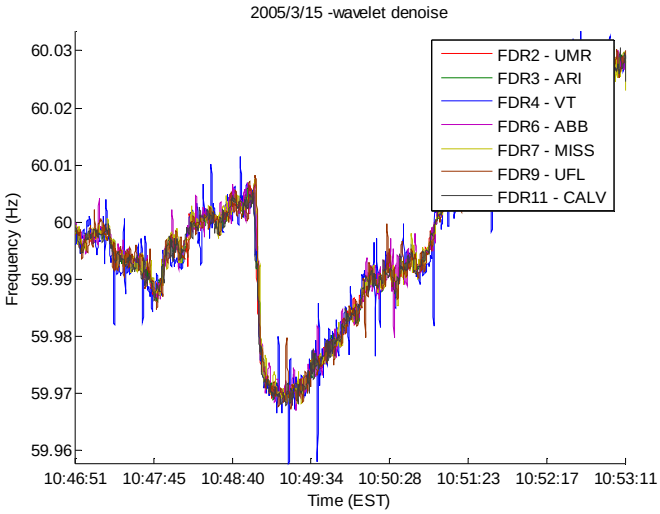
2005/3/15 -wavelet denoise
Frequency (Hz)
Time (EST)
FDR2 - UMR
FDR3 - ARI
FDR4 - VT
FDR6 - ABB
FDR7 - MISS
FDR9 - UFL
FDR11 - CALV

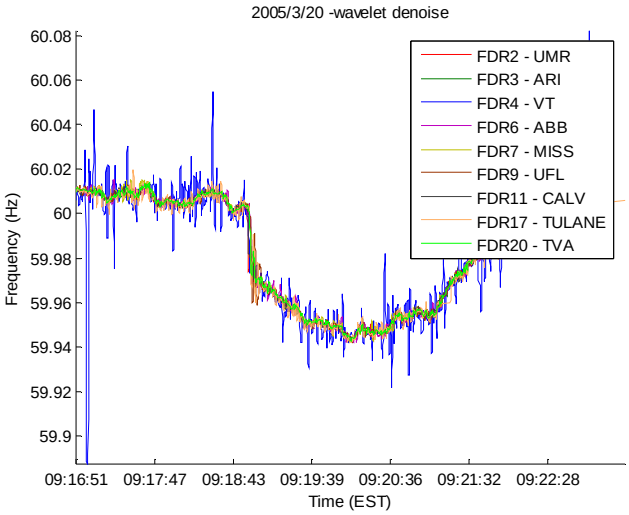
2005/3/20 -wavelet denoise
Frequency (Hz)
Time (EST)
FDR2 - UMR
FDR3 - ARI
FDR4 - VT
FDR6 - ABB
FDR7 - MISS
FDR9 - UFL
FDR11 - CALV
FDR17 - TULANE
FDR20 - TVA

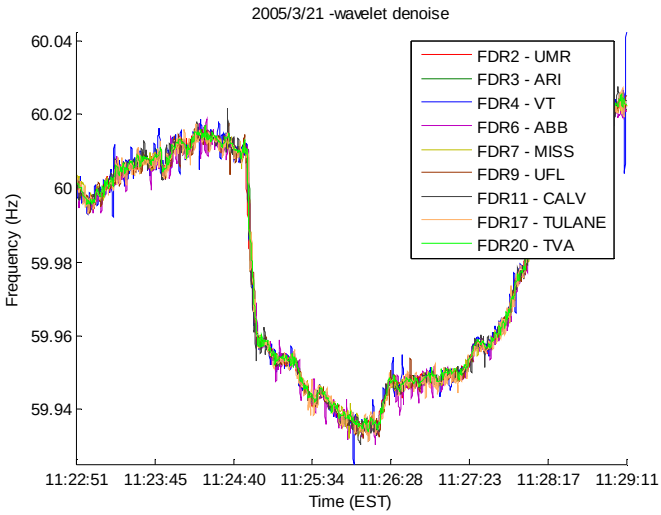
2005/3/21 -wavelet denoise
Frequency (Hz)
Time (EST)
FDR2 - UMR
FDR3 - ARI
FDR4 - VT
FDR6 - ABB
FDR7 - MISS
FDR9 - UFL
FDR11 - CALV
FDR17 - TULANE
FDR20 - TVA

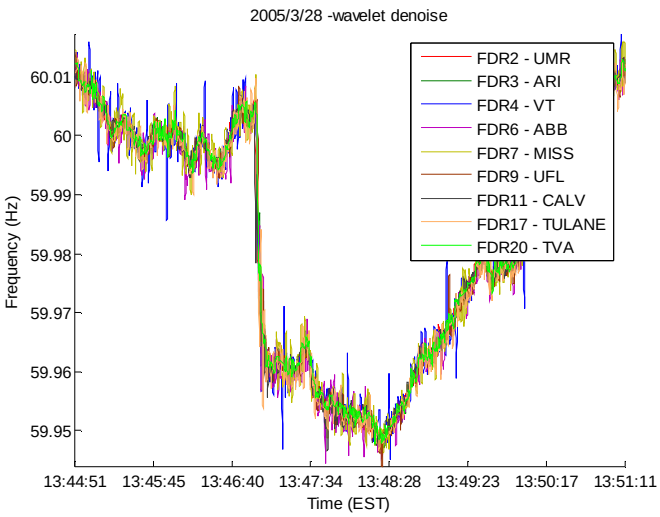
2005/3/28 -wavelet denoise
Frequency (Hz)
Time (EST)
FDR2 - UMR
FDR3 - ARI
FDR4 - VT
FDR6 - ABB
FDR7 - MISS
FDR9 - UFL
FDR11 - CALV
FDR17 - TULANE
FDR20 - TVA

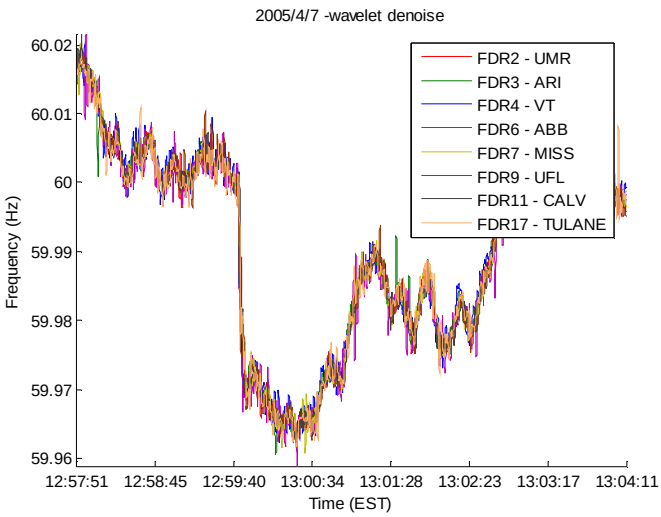
2005/4/7 -wavelet denoise
Frequency (Hz)
Time (EST)
FDR2 - UMR
FDR3 - ARI
FDR4 - VT
FDR6 - ABB
FDR7 - MISS
FDR9 - UFL
FDR11 - CALV
FDR17 - TULANE

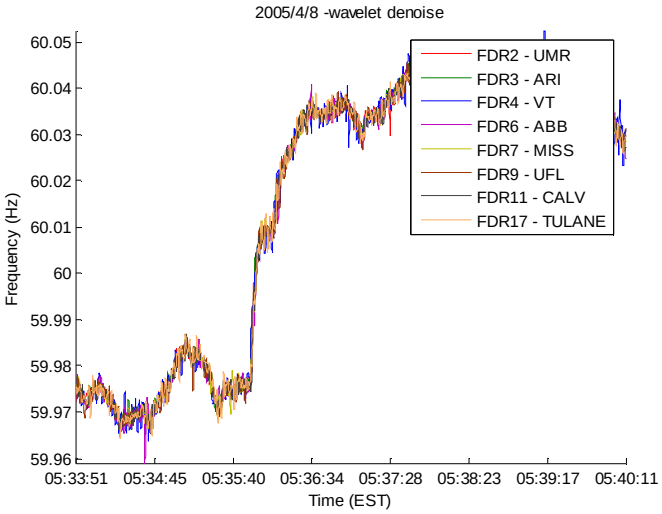
2005/4/8 -wavelet denoise
Frequency (Hz)
Time (EST)
FDR2 - UMR
FDR3 - ARI
FDR4 - VT
FDR6 - ABB
FDR7 - MISS
FDR9 - UFL
FDR11 - CALV
FDR17 - TULANE

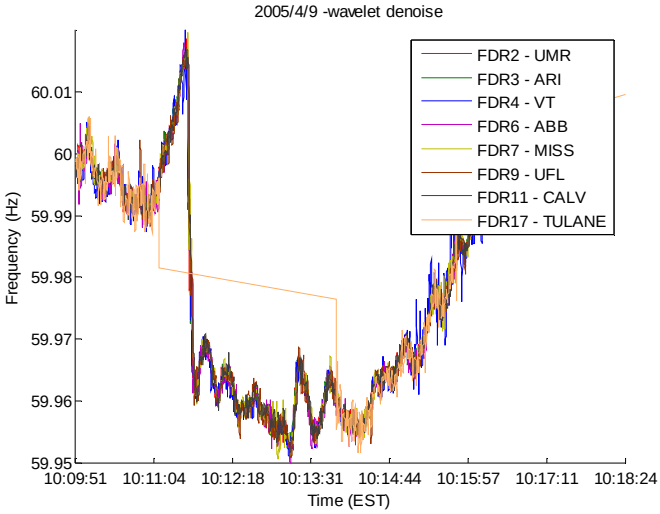
2005/4/9 -wavelet denoise
Frequency (Hz)
Time (EST)
FDR2 - UMR
FDR3 - ARI
FDR4 - VT
FDR6 - ABB
FDR7 - MISS
FDR9 - UFL
FDR11 - CALV
FDR17 - TULANE

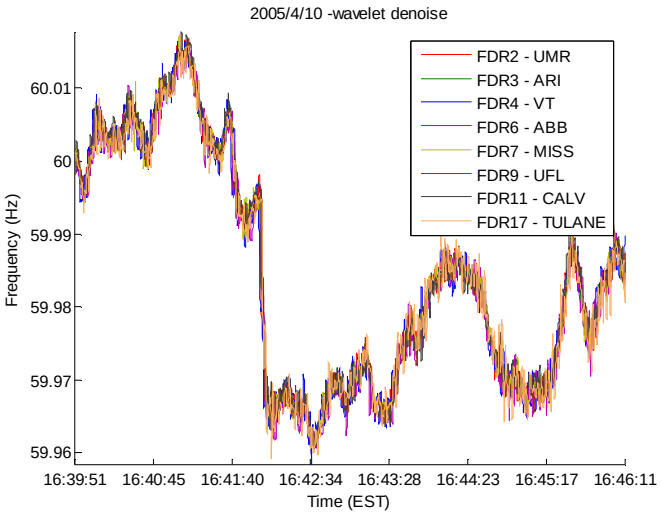
2005/4/10 -wavelet denoise
Frequency (Hz)
Time (EST)
FDR2 - UMR
FDR3 - ARI
FDR4 - VT
FDR6 - ABB
FDR7 - MISS
FDR9 - UFL
FDR11 - CALV
FDR17 - TULANE

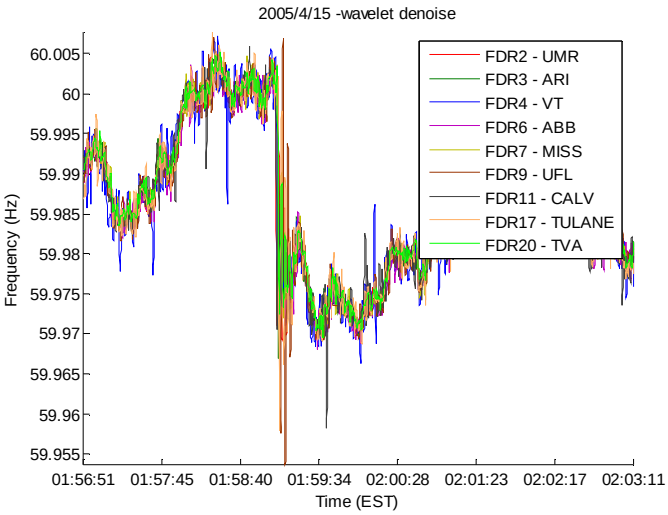
2005/4/15 -wavelet denoise
Frequency (Hz)
Time (EST)
FDR2 - UMR
FDR3 - ARI
FDR4 - VT
FDR6 - ABB
FDR7 - MISS
FDR9 - UFL
FDR11 - CALV
FDR17 - TULANE
FDR20 - TVA

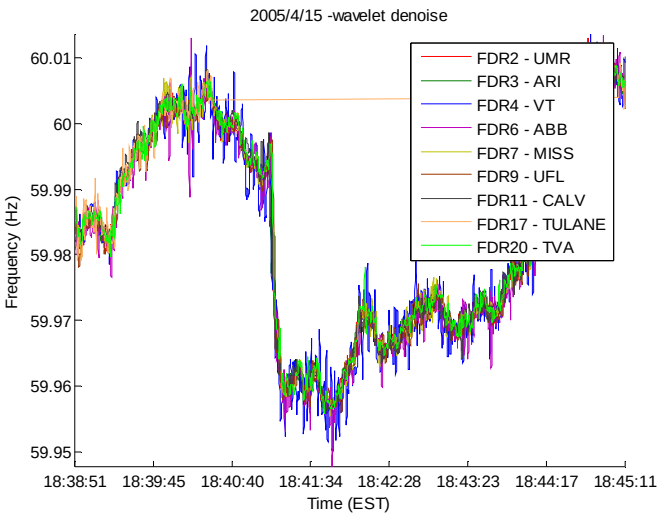
2005/4/15 -wavelet denoise
Frequency (Hz)
Time (EST)
FDR2 - UMR
FDR3 - ARI
FDR4 - VT
FDR6 - ABB
FDR7 - MISS
FDR9 - UFL
FDR11 - CALV
FDR17 - TULANE
FDR20 - TVA

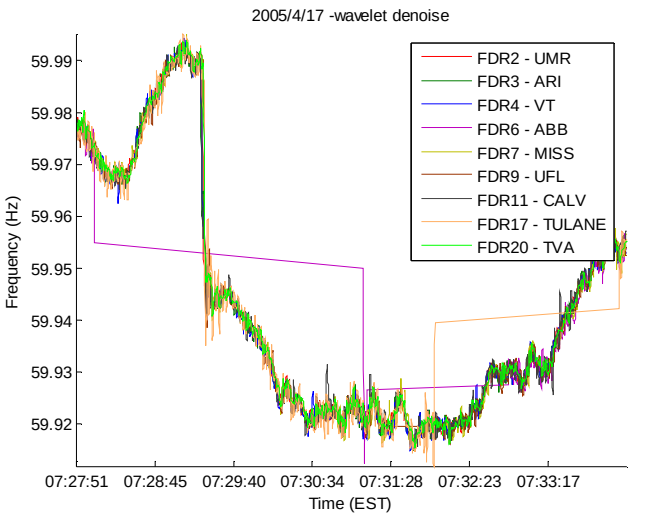
2005/4/17 -wavelet denoise
Frequency (Hz)
Time (EST)
FDR2 - UMR
FDR3 - ARI
FDR4 - VT
FDR6 - ABB
FDR7 - MISS
FDR9 - UFL
FDR11 - CALV
FDR17 - TULANE
FDR20 - TVA

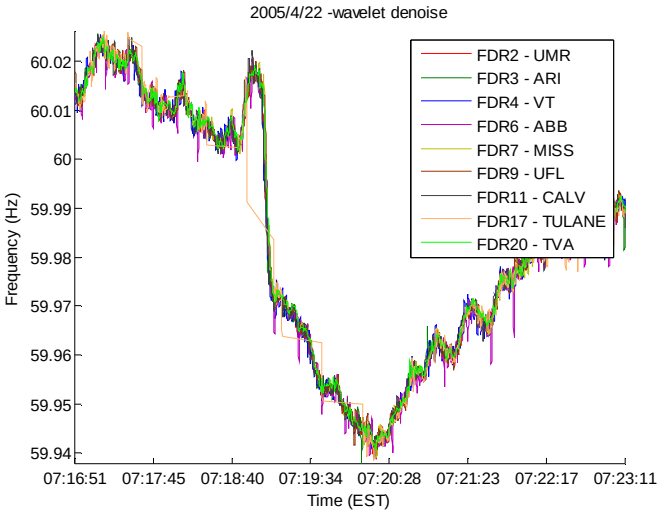
2005/4/22 -wavelet denoise
Frequency (Hz)
60.02
60.01
60
59.99
59.98
59.97
59.96
59.95
59.94
07:16:51
07:17:45
07:18:40
07:19:34
07:20:28
07:21:23
07:22:17
07:23:11
Time (EST)
FDR2 - UMR
FDR3 - ARI
FDR4 - VT
FDR6 - ABB
FDR7 - MISS
FDR9 - UFL
FDR11 - CALV
FDR17 - TULANE
FDR20 - TVA

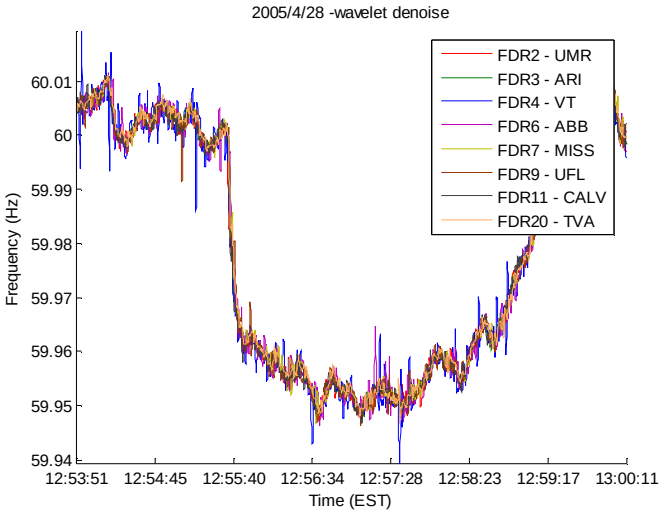
2005/4/28 -wavelet denoise
Frequency (Hz)
60.01
60
59.99
59.98
59.97
59.96
59.95
59.94
12:53:51
12:54:45
12:55:40
12:56:34
12:57:28
12:58:23
12:59:17
13:00:11
Time (EST)
FDR2 - UMR
FDR3 - ARI
FDR4 - VT
FDR6 - ABB
FDR7 - MISS
FDR9 - UFL
FDR11 - CALV
FDR20 - TVA

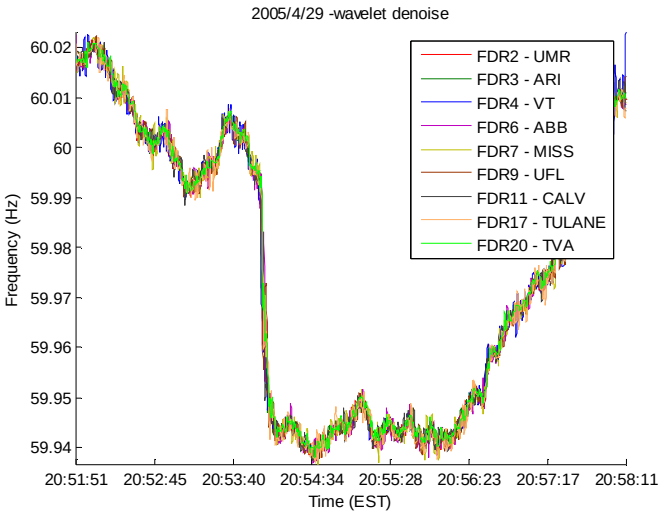
2005/4/29 -wavelet denoise
Frequency (Hz)
60.02
60.01
60
59.99
59.98
59.97
59.96
59.95
59.94
20:51:51
20:52:45
20:53:40
20:54:34
20:55:28
20:56:23
20:57:17
20:58:11
Time (EST)
FDR2 - UMR
FDR3 - ARI
FDR4 - VT
FDR6 - ABB
FDR7 - MISS
FDR9 - UFL
FDR11 - CALV
FDR17 - TULANE
FDR20 - TVA

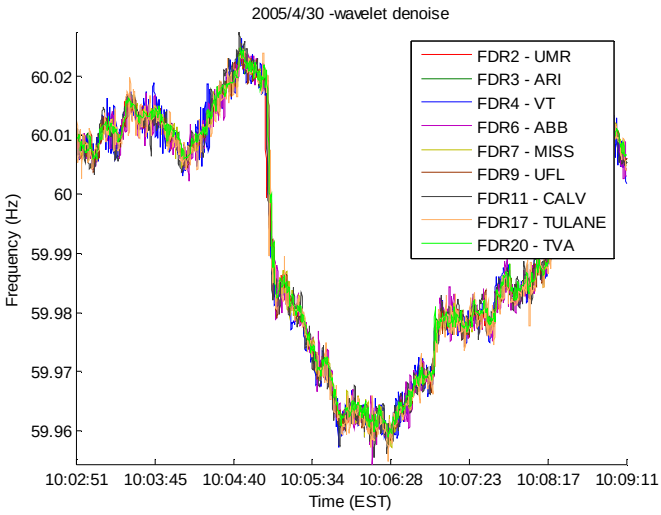
2005/4/30 -wavelet denoise
Frequency (Hz)
60.02
60.01
60
59.99
59.98
59.97
59.96
10:02:51
10:03:45
10:04:40
10:05:34
10:06:28
10:07:23
10:08:17
10:09:11
Time (EST)
FDR2 - UMR
FDR3 - ARI
FDR4 - VT
FDR6 - ABB
FDR7 - MISS
FDR9 - UFL
FDR11 - CALV
FDR17 - TULANE
FDR20 - TVA

Sharp frequency variation at 2004 Superbowl night (February, 06 2005). Total of 9 events.

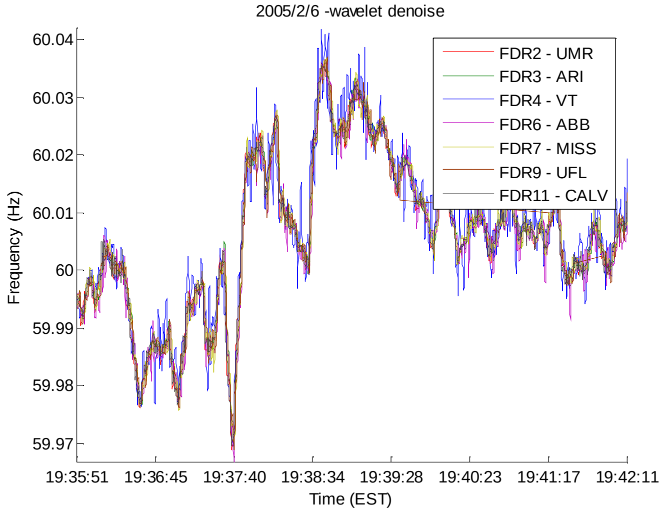

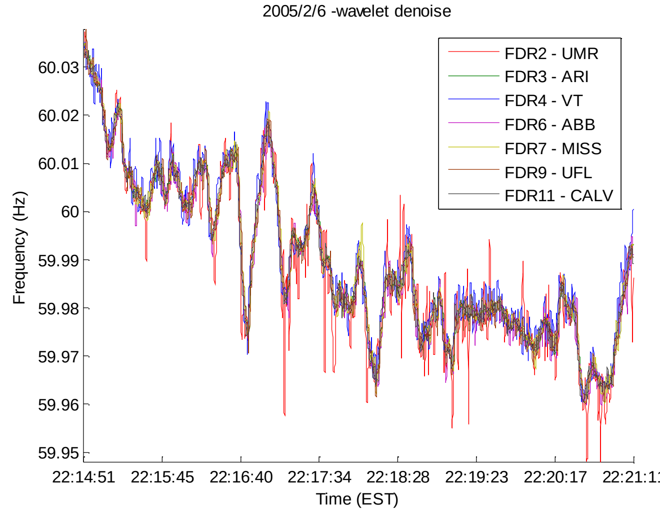

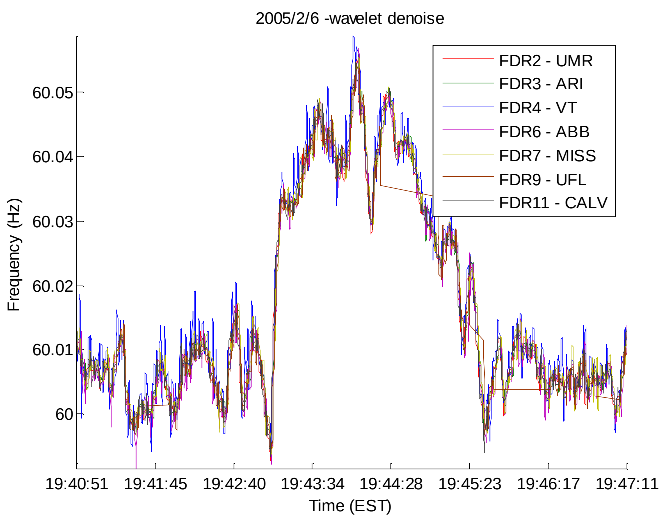

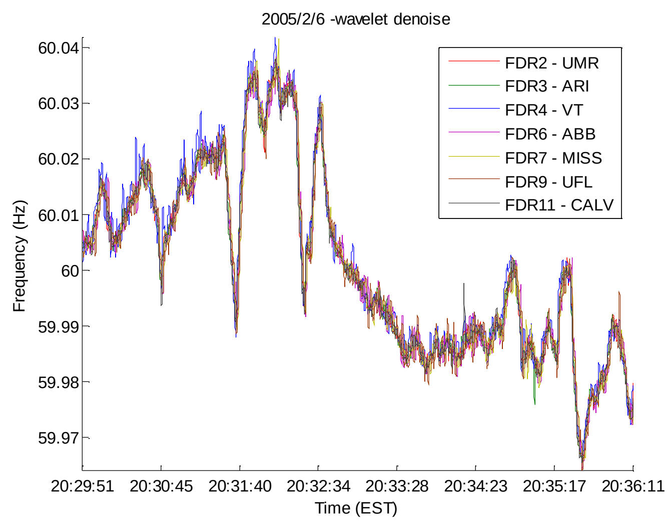

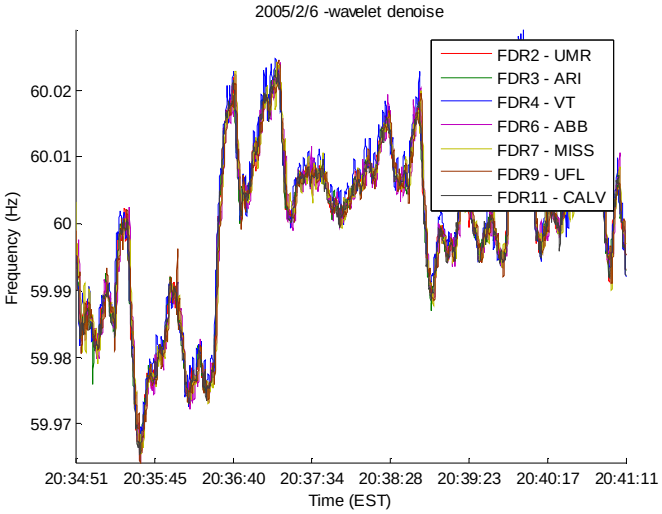
2005/2/6 -wavelet denoise
FDR2 - UMR
FDR3 - ARI
FDR4 - VT
FDR6 - ABB
FDR7 - MISS
FDR9 - UFL
FDR11 - CALV
Frequency (Hz)
60.02
60.01
60
59.99
59.98
59.97
20:34:51
20:35:45
20:36:40
20:37:34
20:38:28
20:39:23
20:40:17
20:41:11
Time (EST)

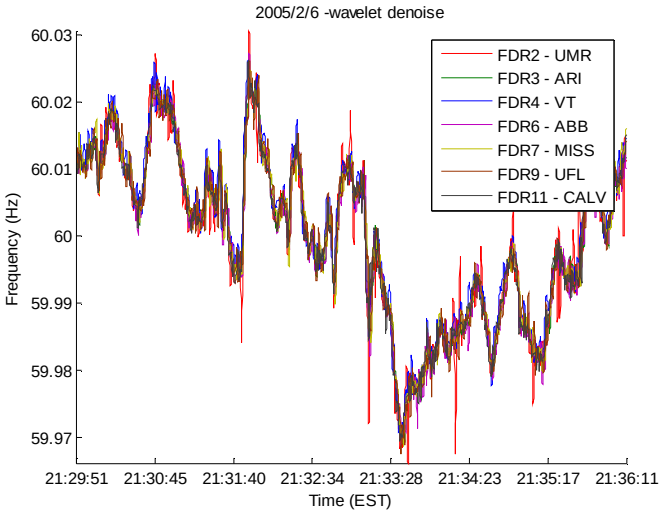
2005/2/6 -wavelet denoise
FDR2 - UMR
FDR3 - ARI
FDR4 - VT
FDR6 - ABB
FDR7 - MISS
FDR9 - UFL
FDR11 - CALV
Frequency (Hz)
60.03
60.02
60.01
60
59.99
59.98
59.97
21:29:51
21:30:45
21:31:40
21:32:34
21:33:28
21:34:23
21:35:17
21:36:11
Time (EST)

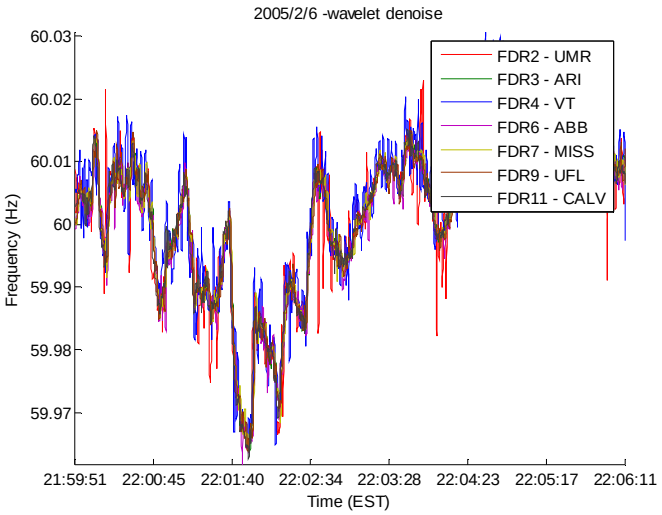
2005/2/6 -wavelet denoise
FDR2 - UMR
FDR3 - ARI
FDR4 - VT
FDR6 - ABB
FDR7 - MISS
FDR9 - UFL
FDR11 - CALV
Frequency (Hz)
60.03
60.02
60.01
60
59.99
59.98
59.97
21:59:51
22:00:45
22:01:40
22:02:34
22:03:28
22:04:23
22:05:17
22:06:11
Time (EST)

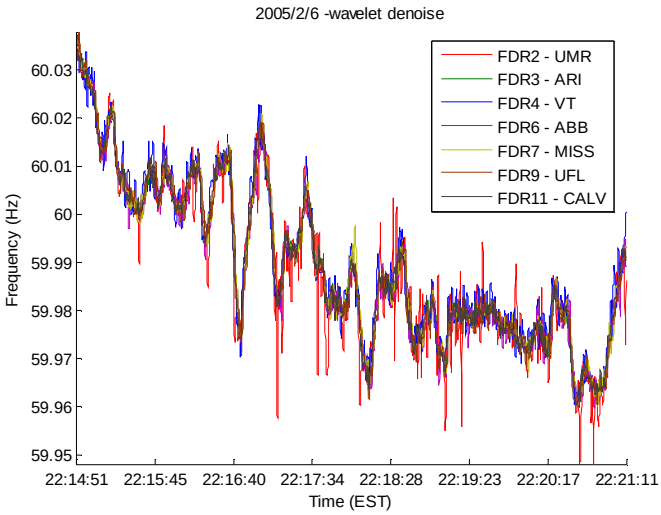
2005/2/6 -wavelet denoise
FDR2 - UMR
FDR3 - ARI
FDR4 - VT
FDR6 - ABB
FDR7 - MISS
FDR9 - UFL
FDR11 - CALV
Frequency (Hz)
60.03
60.02
60.01
60
59.99
59.98
59.97
59.96
59.95
22:14:51
22:15:45
22:16:40
22:17:34
22:18:28
22:19:23
22:20:17
22:21:11
Time (EST)

Misidentified cases due to local frequency spike.

Total of 8 events.

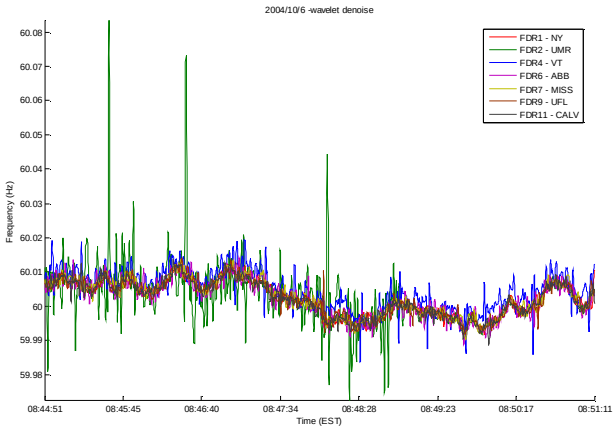

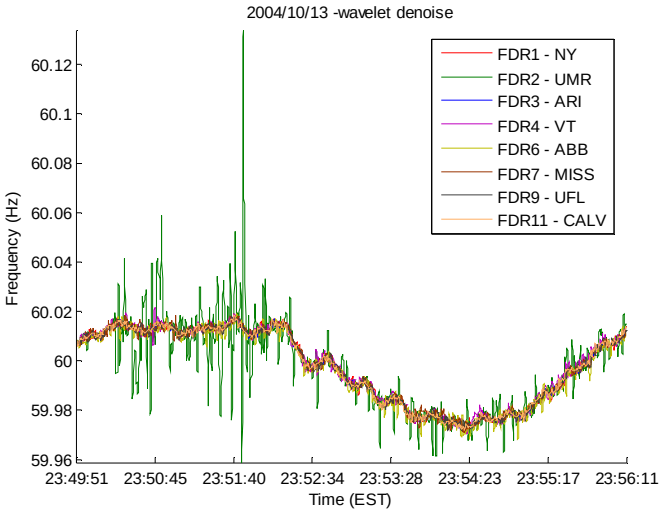

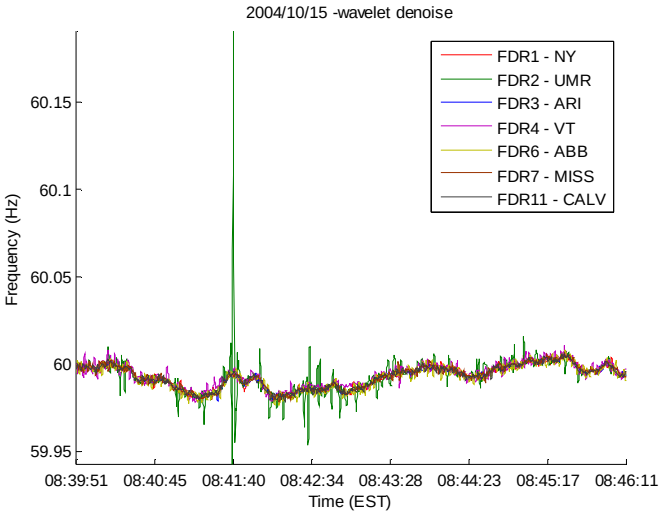

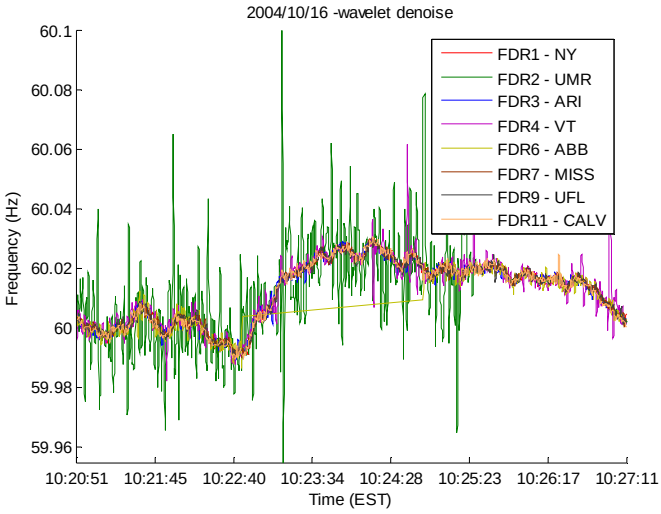

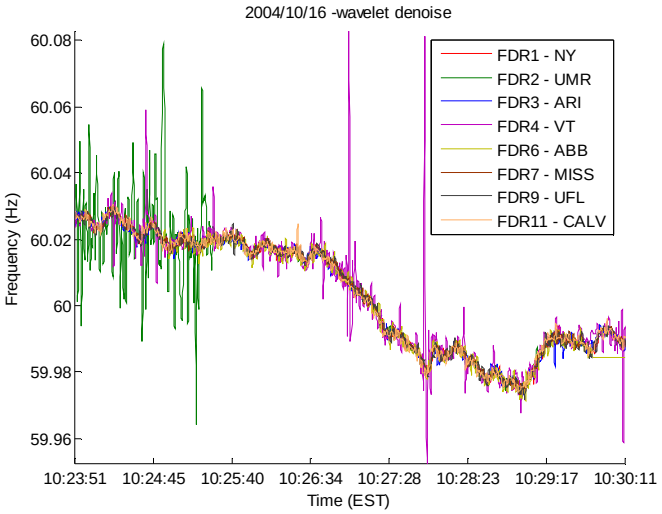
2004/10/16 -wavelet denoise
FDR1 - NY
FDR2 - UMR
FDR3 - ARI
FDR4 - VT
FDR6 - ABB
FDR7 - MISS
FDR9 - UFL
FDR11 - CALV
Frequency (Hz)
60.08
60.06
60.04
60.02
60
59.98
59.96
10:23:51
10:24:45
10:25:40
10:26:34
10:27:28
10:28:23
10:29:17
10:30:11
Time (EST)

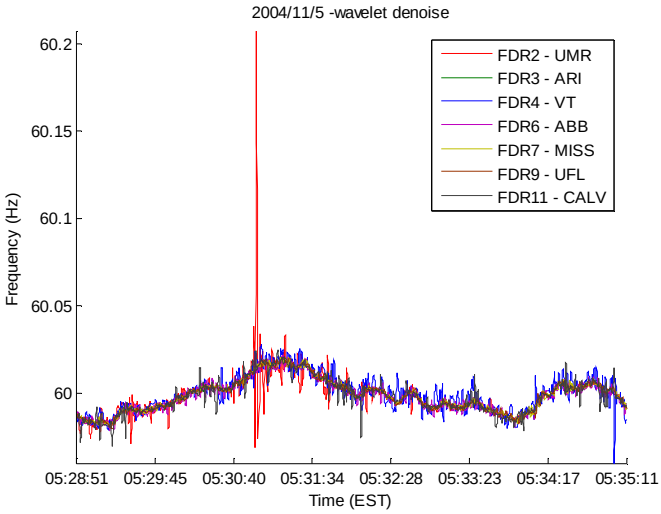
2004/11/5 -wavelet denoise
FDR2 - UMR
FDR3 - ARI
FDR4 - VT
FDR6 - ABB
FDR7 - MISS
FDR9 - UFL
FDR11 - CALV
Frequency (Hz)
60.2
60.15
60.1
60.05
60
05:28:51
05:29:45
05:30:40
05:31:34
05:32:28
05:33:23
05:34:17
05:35:11
Time (EST)

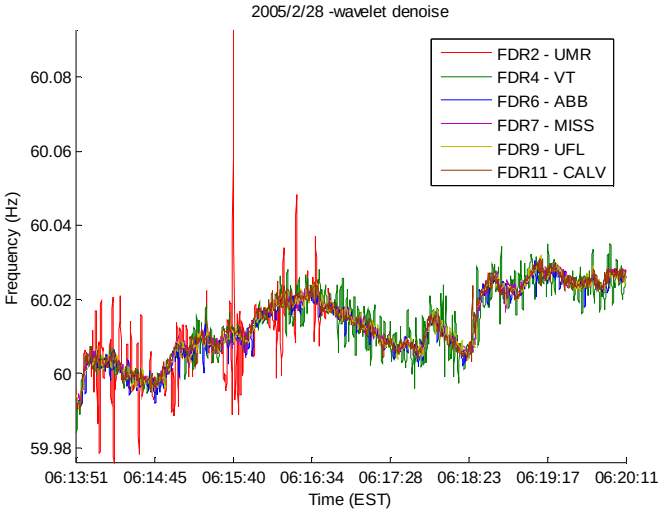
2005/2/28 -wavelet denoise
FDR2 - UMR
FDR4 - VT
FDR6 - ABB
FDR7 - MISS
FDR9 - UFL
FDR11 - CALV
Frequency (Hz)
60.08
60.06
60.04
60.02
60
59.98
06:13:51
06:14:45
06:15:40
06:16:34
06:17:28
06:18:23
06:19:17
06:20:11
Time (EST)

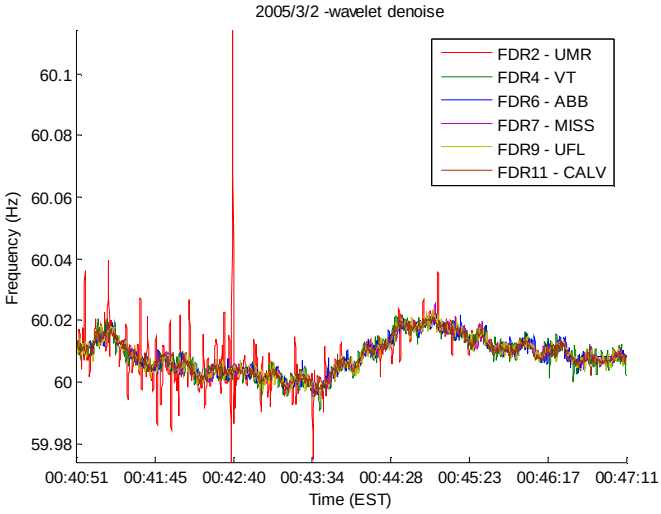
2005/3/2 -wavelet denoise
FDR2 - UMR
FDR4 - VT
FDR6 - ABB
FDR7 - MISS
FDR9 - UFL
FDR11 - CALV
Frequency (Hz)
60.1
60.08
60.06
60.04
60.02
60
59.98
00:40:51
00:41:45
00:42:40
00:43:34
00:44:28
00:45:23
00:46:17
00:47:11
Time (EST)

Vita

Shu-Jen Steven Tsai

E-mail: stsai@vt.edu

Research interests

Power system operation, stability, and protection

Power system wide-area measurement, control and coordination

Power quality investigation and mitigation

FACTS (Flexible AC Transmission System) applications to power system

Power equipment testing, monitoring, and diagnosis

Signal processing

Education background

Ph.D., Virginia Polytechnic Institute and State University (Virginia Tech), Blacksburg, VA, U.S.A.

Department of Electrical and Computer Engineering. August 2005

M.S., Virginia Polytechnic Institute and State University (Virginia Tech), Blacksburg, VA, U.S.A.

Department of Electrical and Computer Engineering. December 2002

M.S., Carnegie Mellon University, Pittsburgh, PA, U.S.A.

Department of Mechanical Engineering, Institute for Complex Engineered Systems, and The Robotics Institute. December 1998

B.S., National Central University, Chungli, TAIWAN

Department of Mechanical Engineering. June 1995

Employment history

Research Assistant, Electric Power IT Laboratory, Electrical Engineering Department, Virginia Tech, Blacksburg, VA, U.S.A. January 2002 – June 2005

Teaching Assistant, Electrical Engineering Department, Virginia Tech, Blacksburg, VA, U.S.A. January 2003 – May 2005

Design Engineer, Advanced Development Laboratory, Quantum Corporation, Shrewsbury, MA, U.S.A. February 1999 - September 2000.

Research Assistant, Institute for Complex Engineered Systems and The Robotics Institute, Carnegie Mellon University, Pittsburgh, PA, U.S.A. January 1998 - December 1998.

Corporal, The Chinese Army Logistics Command, Taoyuan, TAIWAN, August 1995 - July 1997.

Awards/Honors

Member of ΦΚΦ, the honor society for the selective personnel with excellent academic achievement. Virginia Polytechnic Institute and State University (Chapter 25), November 2002.

Top of the Class, National Central University, Mechanical Engineering Department. January 1995

Outstanding Academics Achievement, Taipei Professional Electrical Engineering Association. April 1995

Affiliation

IEEE student member. Member of PES society.

Publications

Journals:

E. D. Ferreira, S.-J. Tsai, C. J. J. Paredis, and H. B. Brown, "Control of the Gyrover: a Single-Wheel Gyroscopically Stabilized Robot," *Advanced Robotics*, pp. 459-75, 2000.

"Modeling Devices With Nonlinear Voltage-Current Characteristics for Harmonic Studies," *IEEE Transactions on Power Delivery*, vol. 19, pp. 1802-11, 2004. (Major contributor)

S.-J. S. Tsai, Y. Liu, and M. Ingram, "Mitigation of Voltage Flicker by Superconducting Synchronous Condenser (SuperVAR)," *Electric Power Quality and Utilization Journal*, vol. 1, no. 1, pp. 41-46, 2005

Z. Zhong, C. Xu, B. J. Billian, S.-J. S. Tsai, R. W. Conners, V. A. Centeno, A.G. Phadke, and Y. Liu, "Power System Frequency Monitoring Network (FNET) Implementation," *IEEE Transactions on Power Systems*, (accepted).

S.-J. S. Tsai, L. Zhang, A. G. Phadke, Y. Liu, M. R. Ingram, S. C. Bell, I. Grant, D. Bradshaw, D. Lubkeman, and L. Tang, "Frequency sensitivity and Electromechanical Propagation Study in Large Power Systems," *IEEE Transactions on Power Systems*, (submitted).

S.-J. S. Tsai, Z. Zhong, J. Zuo, and Y. Liu, "Frequency Analysis of Bulk Power Systems from Wide Area Measurements" (In progress)

Conference Proceedings:

S.-J. Tsai, E. D. Ferreira, and C. J. J. Paredis, "Control of the Gyrover: A Single-Wheel Gyroscopically Stabilized Robot," in Proceedings of the IEEE/RSJ International Conference on Intelligent Robots and Systems (IROS'99), Kyongju, Korea, 1999.

X.-G. Li, D.-M. Xiao, S.-J. Tsai, and Y. Liu, "Electron Ionization, Attachment and Detachment Coefficients in SF6 and Xe Gas Mixtures," in IEEE Power Engineering Society Summer Meeting, Chicago, 2002.

L. Chen, S.-J. S. Tsai, B. Qiu, Y. Liu, B. Yu, A. Wang, and B. Ward, "Finite Element Simulation and Theoretical Analysis of the Partial Discharge Acoustic Wave Propagation inside Power Transformers," in EPRI Substation Equipment Diagnostics Conference, New Orleans, 2003.

S.-J. S. Tsai, B. Yu, L. Chen, A. Wang, Y. Liu, and B. Ward, "Analysis of On-site Transformer Partial Discharge Measurement from Fiber Optic Acoustic Sensors," in EPRI Substation Equipment Diagnostics Conference, New Orleans, 2003.

S.-J. S. Tsai, L. Zhang, A. G. Phadke, Y. Liu, M. R. Ingram, S. C. Bell, I. S. Grant, D. T. Bradshaw, D. Lubkeman, and L. Tang, "Study of Global Frequency Dynamic Behavior of Large Power Systems," in IEEE PES Power System Conference & Exposition, New York, 2004.

S.-J. S. Tsai, J. Zuo, Y. Zhang and Y. Liu, "Frequency Visualization in Large Electric Power Systems," in IEEE Power Engineering Society General Meeting, San Francisco, 2005.

Technical Reports:

L. Chen, S.-J. Tsai, B. Qiu, and Y. Liu, "Computer Simulation and Theoretical Analysis of the Partial Discharge Acoustic Wave Propagation in Power Transformers (Technical report submitted to Electric Power Research Institute (EPRI))," Virginia Polytechnic Institute and State University, Blacksburg Jul. 2002.

S.-J. Tsai, L. Chen, and Y. Liu, "Northfleet West SGT3A 500MVA, 400kV/275kV Transformer On-Site PD Measurement Signal Processing (Technical report submitted to Electric Power Research Institute (EPRI))," Virginia Polytechnic Institute and State University, Blacksburg Jul. 2002.

S.-J. S. Tsai, Y. Liu, L. Zhang, and A. Phadke, "Part II: Frequency Sensitivity and Propagation Speed Study Using Simulations (Technical report submitted to TVA and ABB)," Virginia Polytechnic and State University, Blacksburg Nov. 2003.

L. Zhang, Y. Liu, S.-J. S. Tsai, and A. Phadke, "Part I - Applications of the Wide-Area Power System Dynamic Frequency Monitoring Network (FNET) (Technical report submitted to TVA and ABB)," Virginia Polytechnic Institute and State University, Blacksburg Dec. 2003.